

AD/A-007 225

OH-6A PROPULSION SYSTEM VIBRATION
INVESTIGATION

R. J. Sullivan, et al

Hughes Helicopters

Prepared for:

Army Air Mobility Research and Development
Laboratory

January 1975

DISTRIBUTED BY:

NTIS

National Technical Information Service
U. S. DEPARTMENT OF COMMERCE

EUSTIS DIRECTORATE POSITION STATEMENT

This program was one of three contractual efforts undertaken in an initial attempt to define a better engine-airframe-propulsion installation interface. The long-range goal is to provide adequate design and test methods to insure compatibility of the engine and airframe.

Analytical and experimental work was conducted relative to an assessment of engine/airframe vibratory interface design technology. An analytical finite element model of the airframe produced reasonably satisfactory correlation with laboratory test data.

The technical monitor for this contract was Mr. James Gomez, Jr., Technology Applications Division.

ACCESSION for	
DTIC	White Section <input checked="" type="checkbox"/>
BPC	Ball Section <input type="checkbox"/>
UNCLASSIFIED	<input type="checkbox"/>
JUSTIFICATION	
BY	
DISTRIBUTION AVAILABILITY CODES	
Dist.	AVAIL. CODE OR SPECIAL
A	

DISCLAIMERS

The findings in this report are not to be construed as an official Department of the Army position unless so designated by other authorized documents.

When Government drawings, specifications, or other data are used for any purpose other than in connection with a definitely related Government procurement operation, the United States Government thereby incurs no responsibility nor any obligation whatsoever; and the fact that the Government may have formulated, furnished, or in any way supplied the said drawings, specifications, or other data is not to be regarded by implication or otherwise as in any manner licensing the holder or any other person or corporation, or conveying any rights or permission, to manufacture, use, or sell any patented invention that may in any way be related thereto.

Trade names cited in this report do not constitute an official endorsement or approval of the use of such commercial hardware or software.

DISPOSITION INSTRUCTIONS

Destroy this report when no longer needed. Do not return it to the originator.

UNCLASSIFIED

SECURITY CLASSIFICATION OF THIS PAGE (When Data Entered)

REPORT DOCUMENTATION PAGE		READ INSTRUCTIONS BEFORE COMPLETING FORM	
1. REPORT NUMBER USAAMRDL-TR-74-85	2. GOVT ACCESSION NO.	3. RECIPIENT'S CATALOG NUMBER A D/A - 007225	
4. TITLE (and Subtitle) OH-6A PROPULSION SYSTEM VIBRATION INVESTIGATION		5. TYPE OF REPORT & PERIOD COVERED Final 27 Nov 72 - 15 Jun 74	6. PERFORMING ORG. REPORT NUMBER 369-V-8009(HH 74-114)
		8. CONTRACT OR GRANT NUMBER(s) DAAJ02-73-C-0016	
7. AUTHOR(s) R. J. Sullivan, R. E. Head, G. J. Korkosz, J. R. Neff, and S. J. Soltis and M. A. Gockel(MacNeal-Schwendler Corp.)		10. PROGRAM ELEMENT, PROJECT, TASK AREA & WORK UNIT NUMBERS Task 1G162204AA7201	
9. PERFORMING ORGANIZATION NAME AND ADDRESS Hughes Helicopters Culver City, California 90230		11. CONTROLLING OFFICE NAME AND ADDRESS Eustis Directorate U. S. Army Air Mobility R & D Laboratory Fort Eustis, Virginia 23604	12. REPORT DATE January 1975
14. MONITORING AGENCY NAME & ADDRESS (if different from Controlling Office)		13. NUMBER OF PAGES 216	15. SECURITY CLASS. (of this report) Unclassified
		15a. DECLASSIFICATION/DOWNGRADING SCHEDULE	
16. DISTRIBUTION STATEMENT (of this Report) Approved for public release; distribution unlimited			
17. DISTRIBUTION STATEMENT (of the abstract entered in Block 20, if different from Report)			
18. SUPPLEMENTARY NOTES Reproduced by NATIONAL TECHNICAL INFORMATION SERVICE US Department of Commerce Springfield, VA. 22151 PRICES SUBJECT TO CHANGE			
19. KEY WORDS (Continue on reverse side if necessary and identify by block number) Vibration Helicopters Shafts (Machine Elements) Turbojet Engines Airframe Structures Compatibility			
20. ABSTRACT (Continue on reverse side if necessary and identify by block number) A study was made of means to improve helicopter engine/airframe vibratory interface compatibility. The study was based on the characteristics of the OH-6A helicopter and the T63 engine in order to utilize existing data to validate the methodology produced in the study. Available engine and airframe data was reviewed and used to prepare a vibration spectrum for a typical mission. Airframe mobility data was acquired during a ground shake test.			

UNCLASSIFIED

SECURITY CLASSIFICATION OF THIS PAGE(When Data Entered)

20. **ABSTRACT - continued**

A finite element model of the OH-6A airframe was prepared and was coupled to a model of the T63 engine, which was based on mobility data supplied by the engine manufacturer. The airframe and engine models were combined using a modal coupling technique, and reasonable correlation with test data was obtained. An impedance/mobility coupling technique is recommended where many flexible modes are in the frequency ranges that could be excited by main-rotor-induced vibratory forces.

Based on the study, recommendations were prepared and circulated to engine manufacturers for future engine vibration specification, vibration parameter selection, and data reduction. The results of the survey and the proposed recommendations are presented.

UNCLASSIFIED

SECURITY CLASSIFICATION OF THIS PAGE(When Data Entered)

PREFACE

This is the final report on the Hughes Helicopters project entitled "OH-6A Propulsion System Vibration Investigation." This study was conducted for the U. S. Army Air Mobility Research and Development Laboratory (USAAMRDL), Eustis Directorate, under Contract DAAJ02-73-C-0016 between 27 November 1972 and 30 May 1974.

USAAMRDL technical direction was provided by Mr. James Gomez. The following Hughes personnel participated in this study:

R. J. Sullivan	Project Engineer
R. E. Head	Senior Research Engineer
G. J. Korkosz	Senior Test Engineer
J. R. Neff	Chief of Dynamics
S. J. Soltis	Senior Stress Engineer

Mr. M. A. Gockel, Senior Dynamics Engineer of The MacNeal-Schwendler Corporation, planned and supervised the preparation of the NASTRAN model of the airframe and engine used in this study.

Acknowledgment is made of special contributions on loads and dynamics by Mr. R. A. Wagner, Manager, Research and Development Department.

TABLE OF CONTENTS

	<u>Page</u>
PREFACE	1
INTRODUCTION	14
REVIEW OF EXISTING DATA	16
ANALYSIS OF EXISTING DATA	20
Deduced Mode Shapes	20
Predominant Responding Mode Shapes and Relative Contribution of Airframe and Engine	22
Amplitude Versus Discrete Frequency	27
Comparison With Allowable Vibration Limits	27
Spectrum of Engine Vibration for Typical Mission Operation	27
Transient Load Condition - Hard Landing	30
MOBILITY TESTS	33
Laboratory (Ground) Tests and Flight Tests	33
Test Apparatus and Mobility Measurement Equipment	35
Test Shakedown	40
Test Conditions	43
Test Results	51
ESTIMATED LIMITING ENGINE VIBRATION SPECTRUM	56
Periodic Forces Based on Flight Data	56
Calculated Limiting Engine Vibration Spectrum	60
Influence of Rotor Head Moments	64
AIRFRAME-WITHOUT-ENGINE MODELING	65
Description of Dynamic Models	65
Correlation of Frequency Response	81
ENGINE MODELING	107
Derivation of Modal Parameters	107
Implementation in NASTRAN	116
Correlation of Engine Model with Test Data	117

	<u>Page</u>
Engine Gyroscopic Coupling	117
Correlation of Airframe-Engine Model with Test Data	118
NASTRAN MODEL FORCING FUNCTIONS	143
Main Rotor 4/Rev Loads	143
Tail Rotor 2/Rev Loads	143
Transient Load	145
CORRELATION OF PREDICTED RESPONSE WITH FLIGHT DATA	146
Response to Main Rotor 4/Rev Loads	146
Response to Tail Rotor 2/Rev Loads	149
Response to Hard Landing Loads	151
ENGINE VIBRATION LIMITS AND METHODS OF DATA ANALYSIS	155
SURVEY OF ENGINE MANUFACTURERS	159
Results of Survey	160
Evaluation of Survey	162
SUITABILITY OF IMPEDANCE/MOBILITY COUPLING AND MODAL COUPLING METHODS	164
Cost-Effective Interface Dynamic Modeling	164
Objectivity Versus Reliability of Test Data	164
Choosing Between Impedance/Mobility Coupling and Modal Coupling for the OH-6A	165
Choosing Between Methods for the General Case	167
Development of Impedance/Mobility Coupling Technique . . .	168
Advantages of Acceleration as a Vibration Parameter	173
DEFINITIONS/RECOMMENDATIONS FOR VIBRATION SPECIFICATION METHODOLOGY	175
CONCLUSIONS	176
REFERENCES	177

	<u>Page</u>
APPENDIXES	
A. Test Program	180
B. Description of Unique MacNeal-Schwendler Corporation/NASTRAN Features Used	197
C. Engine Modeling	200
LIST OF SYMBOLS	211

LIST OF ILLUSTRATIONS

<u>Figure</u>		<u>Page</u>
1	Vibration Velocity (Average) Versus Frequency	18
2	T63 Mode Shape - 8 Hertz	23
3	T63 Mode Shape - 32 Hertz	24
4	T63 Mode Shape - 100 Hertz	25
5	T63 Mode Shape - 800 Hertz	26
6	Amplitude vs Discrete Frequency - Compressor Front . .	28
7	Amplitude vs Discrete Frequency - Accessory Gearbox. .	28
8	Amplitude vs Discrete Frequency - Turbine Mid-Split-Line.	28
9	T63 Discrete Frequency Limits Versus Frequency	29
10	Load at Skid for Hard Landing	32
11	OH-6A (SN 65-12945) Suspended for Mobility Tests	36
12	Shaker Arrangement for Excitation of Rotor Hubs	37
13	Shaker Arrangement for Excitation of Engine Shaft at Transmission	37
14	Mockup of Shaker With 90-Degree Bellcrank Installed . .	38
15	Spectral Dynamics Corporation - Automatic Mechanical Impedance Analysis and Recording System, Model SD 1002E-42	39
16	Sample Mobility Graph Paper	41
17	Typical Accelerometer Mounting - Left Engine Mount . .	42
18	Engine Front Compressor - Vertical Mobility in Response to Main Rotor Longitudinal Excitation	52

<u>Figure</u>		<u>Page</u>
19	Engine Front Compressor - Lateral Mobility in Response to Main Rotor Longitudinal Excitation	53
20	Turbine Mid-Split-Line - Vertical Mobility in Response to Main Rotor Longitudinal Excitation	54
21	Rotor Mast Bending Moment Measurement	57
22	Rotor Mast 4/Rev Bending Moments	59
23	Isometric of Bar Elements	66
24	Side View Shear Panels and Selected Elements	66
25	Selects "a Set" Grid Points - Side View	67
26	Selected "a Set" Grid Points - Top View	67
27	Rigid-Body Mode - Longitudinal	70
28	Rigid-Body Mode - Lateral	70
29	Rigid-Body Mode - Vertical	71
30	Rigid-Body Mode - Roll	71
31	Rigid-Body Mode - Pitch	72
32	Rigid-Body Mode - Yaw	72
33	Mode #7 Boom Lateral Bending, 7.92 Hz	73
34	Mode #8 Boom Vertical Bending, 8.59 Hz	73
35	Mode #9 Landing Gear Longitudinal Antisymmetric, 11.76 Hz	74
36	Mode #10 Boom Torsional, 13.87 Hz	74
37	Mode #11 Landing Gear Lateral Symmetric, 15.22 Hz	75
38	Mode #12 Landing Gear Lateral Antisymmetric, 16.26 Hz	75

<u>Figure</u>		<u>Page</u>
39	Mode #13 Main Rotor Mast Longitudinal, 18.51 Hz	76
40	Mode #14 Horizontal Stabilizer Chordwise Bending, 18.79 Hz	76
41	Mode #15 Lower Vertical Stabilizer Chordwise Bending, 20.35 Hz	77
42	Mode #16 Main Rotor Mast Lateral, 22.29 Hz	77
43	Mode #17 Landing Gear, 25.66 Hz	78
44	Mode #18 Landing Gear, 26.49 Hz	78
45	Mode #19 Landing Gear, 27.09 Hz	79
46	Mode #20 Landing Gear, 28.35 Hz	79
47	Mode #21 Upper Vertical Stabilizer Chordwise Bending, 29.09 Hz	80
48	Mode #22 Tail Rotor Drive Shaft Vertical Bending, 33.60 Hz	80
49	Mode #23 Tail Rotor Drive Shaft Lateral Bending, 34.76 Hz	81
50	Direct Mobility - Main Rotor Longitudinal	82
51	Direct Mobility - Main Rotor Lateral	83
52	Direct Mobility - Main Rotor Vertical	84
53	Direct Mobility - Center Mount Perpendicular	85
54	Direct Mobility - Center Mount Normal	86
55	Direct Mobility - Center Mount Parallel	37
56	Direct Mobility - Right-Hand Mount Perpendicular	88
57	Direct Mobility - Right-Hand Mount Normal	89

<u>Figure</u>		<u>Page</u>
58	Direct Mobility - Right-Hand Mount Parallel	90
59	Direct Mobility - Left-Hand Mount Perpendicular	91
60	Direct Mobility - Left-Hand Mount Normal	92
61	Direct Mobility - Left-Hand Mount Parallel	93
62	Direct Mobility - Tail Rotor Longitudinal	94
63	Direct Mobility - Tail Rotor Lateral	95
64	Direct Mobility - Tail Rotor Vertical	96
65	Direct Mobility - Engine/Transmission Coupling Axial . .	97
66	Direct Mobility - Engine/Transmission Coupling Lateral	98
67	Direct Mobility - Engine/Transmission Longitudinal . . .	99
68	Cross Mobility - Center Mount Perpendicular Due to Main Rotor Longitudinal	100
69	Cross Mobility - Center Mount Perpendicular Due to Main Rotor Lateral	101
70	Cross Mobility - Center Mount Perpendicular Due to Main Rotor Vertical	102
71	Cross Mobility - Center Mount Normal Due to Main Rotor Longitudinal	103
72	Cross Mobility - Center Mount Normal Due to Main Rotor Lateral	104
73	Cross Mobility - Center Mount Normal Due to Main Rotor Vertical	105
74	T63 Bending Mode - 127 Hz	109
75	T63 Bending Mode - 145 Hz	110

<u>Figure</u>		<u>Page</u>
76	T63 Bending Mode - 156 Hz	111
77	T63 Bending Mode - 183 Hz	112
78	Engine Drive Shaft Modeling	115
79	Correlation of Engine Model With Test Data	118
80	Direct Mobility, Main Rotor Longitudinal	121
81	Direct Mobility, Main Rotor Lateral	122
82	Direct Mobility, Main Rotor Vertical	123
83	Cross Mobility, Main Rotor Longitudinal Due to Main Rotor Vertical	124
84	Cross Mobility, Center Mount Axial Due to Main Rotor Longitudinal	125
85	Cross Mobility, Center Mount Axial Due to Main Rotor Lateral	126
86	Cross Mobility, Center Mount Axial Due to Main Rotor Vertical	127
87	Cross Mobility, Center Mount Lateral Due to Main Rotor Lateral	128
88	Cross Mobility, Center Mount Vertical (Engine Axis) Due to Main Rotor Longitudinal	129
89	Cross Mobility, Center Mount Vertical (Engine Axis) Due to Main Rotor Vertical	130
90	Cross Mobility, Right Mount Vertical Due to Main Rotor Longitudinal	131
91	Cross Mobility, Right Mount Lateral Due to Main Rotor Lateral	132
92	Cross Mobility, Right Mount Vertical Due to Main Rotor Vertical	133

<u>Figure</u>		<u>Page</u>
93	Cross Mobility, Turbine Mid-Split Lateral Due to Main Rotor Longitudinal	134
94	Cross Mobility, Turbine Mid-Split Lateral Due to Main Rotor Lateral	135
95	Turbine Mid-Split Lateral Due to Main Rotor Vertical.	136
96	Cross Mobility, Turbine Mid-Split Vertical (Engine Axis) Due to Main Rotor Longitudinal	137
97	Cross Mobility, Turbine Mid-Split Vertical (Engine Axis) Due to Main Rotor Lateral	138
98	Cross Mobility, Turbine Mid-Split Vertical (Engine Axis) Due to Main Rotor Vertical	139
99	Forward Compressor Vertical Due to Main Rotor Longitudinal	140
100	Front Compressor Vertical Due to Main Rotor Lateral	141
101	Front Compressor Vertical Due to Main Rotor Vertical	142
102	4/Rev Load Permutations	144
103	Forward Compressor Vertical Response (Engine Axis) Due to Hard Landing Load	152
104	Ignitor Lateral Response Due to Hard Landing Load	153
105	Ignitor Vertical Response Due to Hard Landing Load	154
106	Engine Vibration Specifications	157
107	Typical Engine Test Data	166

<u>Figure</u>		<u>Page</u>
A-1	Mass Calibration of a 20-Pound Steel Bar Suspended as a Ballistic Pendulum	187
A-2	Suspension and Shaker Arrangement - Main Rotor Vertical Excitation	188
A-3	Transducer Locations on Engine	189
A-4	Transducer Locations on Engine Mount Bipods With Engine Removed - Coincide With Shaker Input Force Positions	190
A-5	Transducer Locations on Engine Mounts as They Were Located With Engine Installed - Photograph Taken With Engine Removed for Clarity	191
A-6	Transducer Locations on Engine Shaft at Transmission - Coincide With Shaker Input Force Positions	192
A-7	Shaker Locations for Rotor Excitation	193
A-8	Shaker Locations at Engine and Transmission	194
A-9	Shaker Locations at Engine Mounts	195
A-10	Side Engine Mount Geometry	196
C-1	Engine, Mount, and Rigid Airframe Model	202
C-2	Test Coordinate System - Engine Out	203
C-3	Test Coordinate System - Engine In	204
C-4	Most Likely 4/Rev Rotor Force Configuration	209

LIST OF TABLES

<u>Table</u>		<u>Page</u>
1	Engine Overall Vibration Velocity (Inches per Second Average) for Various Conditions	17
2	Listing of Discrete Frequency Data and Excitation Source	21
3	Excitation Frequency, Mode Shape, and Excitation Source	22
4	Spectrum of Compressor Vibration for Typical Mission Operation	31
5	Test Condition Summary	44
6	Force/Response Directions	49
7	Derivation of Ratio of Test and Measured Mast Moments	58
8	Main Rotor Plus-and-Minus Mast Bending Moments at 4/Rev	61
9	Equivalent Rotor Shear Forces and Calculated Compressor Front Motion	62
10	Comparison of Predicted and Measured Natural Frequencies	69
11	Comparison of Engine Mode Natural Frequencies	119
12	Effect of Load Phasing on Center Mount 4/Rev Response	146
13	Effect of Load Phasing on Turbine Mid-Split 4/Rev Response	147
14	Effect of Rotor RPM Variation on Center Mount Main Rotor 4/Rev Vibration	148

<u>Table</u>	<u>Page</u>
15	Effect of Rotor RPM Variation on Turbine Mid-Split Main Rotor 4/Rev Vibration 148
16	Forward Compressor Response Due to Unit Rotor Forces and Moments at Main Rotor 4/Rev 149
17	Effect of Rotor RPM Variation on Center Mount Tail Rotor 2/Rev Vibration 150
18	Effect of Rotor RPM Variation on Turbine Mid-Split Tail Rotor 2/Rev Vibration 150
19	Effect of Rotor RPM Variation on Forward Compressor Vibration 150
B-1	Rigid-Body Elements 198
C-1	Engine Variable List 201
C-2	Renormalized Mode Shapes 205
C-3	Engine Model Characteristics 206

INTRODUCTION

This study was undertaken to identify means of improving helicopter airframe/engine vibratory compatibility, based on available OH-6A and T63 data. Reports have been published concerning instances when excessive engine vibration was encountered in a helicopter installation (such as described in Reference 1), but the number of such published reports is few (as mentioned in Reference 2). As a result, no general procedure is available in the literature for obtaining acceptable airframe/engine compatibility. This study proposes a methodology involving close cooperation between the airframe and the engine manufacturer.

The elements of the vibration compatibility problem are simple: what environment does the helicopter present to the engine, and what environment can the engine tolerate? (This generalization excludes the possibility of a well-balanced turbine engine noticeably shaking the airframe, as was typical in the reciprocating engine era).

The pioneering work of Balke in Reference 3 is recommended to all those interested in an airframe/engine vibration compatibility problem. Balke presented considerable data on airframe vibration for some typical installations. Of more importance to the airframe manufacturer, he pointed out the "wide variations in the limits which have been established for vibration in the installation of various engines -- in terms of vibration magnitude, frequency range, and methods of measuring and analyzing them." This wide variation observed by Balke was also discussed in Reference 4.

Clearly, the situation presented in Reference 3 was relevant to that time frame (1970 and earlier). During the course of this study (1973-1974), it appeared that engine manufacturers are now beginning to specify vibration limits for their engines that are more consistent than those reported in Reference 3. It is not known whether this is by arbitrary agreement or by independent study that produced the same type of recommendation. This recent trend toward consistency of installed engine vibration limits will be discussed starting on page 155.

It should be noted that the airframe manufacturer must always meet the engine manufacturer's specified installed engine vibration limits, whether these are the same for the several engine companies or not. It is felt to be evident that if engine limits are more alike than different, the airframe manufacturers will more easily develop expertise in meeting such limits and thus avoid the painful and expensive interruptions of flight test and development programs that have occurred in the past.

For this present study, the T63 engine vibration limits were already available, as were certain flight test data on T63 engine vibration in the OH-6A helicopter. An analysis was made of the predicted engine motion, and the results were compared with the permissible vibration. The analysis was based on a finite-element structural model of the OH-6A helicopter. The NASTRAN computer program (mentioned in Reference 4) was used for the airframe. The structural model was correlated with ground shake tests without the engine installed. The dynamic properties of the T63 engine were determined from engine shake test data provided in Reference 5. Based on this data, generalized engine modal properties were deduced and correlated with the engine data to ensure the accuracy of the engine model. Then the airframe-only model and the engine model were combined, using NASTRAN techniques described in Reference 6. The excitation forces at the main and tail rotors were determined and applied to the combined airframe/engine model for the final correlation of predicted and measured engine vibration.

The addition of the T63 engine to the OH-6A airframe using a modal analysis in preference to the impedance/mobility method presented in Reference 4 is also discussed.

The relatively good degree of correlation of predicted and measured engine vibration presented here demonstrates that a methodology is available to permit precise communication between airframe and engine manufacturers. The next step should be an attempt to improve the reliability of the airframe/engine mating. To that end, a better understanding of airframe and engine vibration capabilities and limitations is required (as discussed in References 3 and 4). As a first step, this study included a review of current engine vibration specifications, which led to certain recommendations. These recommendations were presented to six engine manufacturers, and the responses to those recommendations are reviewed herein.

REVIEW OF EXISTING DATA

In order to ensure improved engine/airframe vibratory compatibility, a proposed method of analysis, or methodology, must be devised and substantiated. As a basis for that methodology, the available T63/OH-6A vibration data was assembled; it was found to consist essentially of two reports, References 7 and 8.

Reference 7 is a Detroit Diesel Allison (DDA) report prepared in 1964 for the purpose of evaluation by DDA of the vibration characteristics of the T63 engine installed in the YO6A prototype helicopter. That report included accelerometer and strain-gage readings for a wide variety of flight conditions. It contained overall vibration values at eight locations on the engine, as shown in Table 1 (taken from Table 1 of Reference 7). In addition, discrete frequency vibration values at the critical high-speed cruise condition of Table 1 are given, as shown in Figure 1 (Figure 2 of Reference 7).

At the time of the preparation of Reference 7, the T63 allowable vibration criterion was 2.0 inches per second overall (independent of frequency), and, as can be seen in Table 1, the maximum recorded vibration was 1.7 inches per second overall, leading to the following remarks on page 2 of Reference 7:

Vibration measurements for all test conditions were below the 2.0 in./sec (avg.) limit at all transducer locations. The maximum overall vibration level recorded was 1.7 in./sec (avg.) in the vertical front compressor position at 126 knots in straight flight, 5000 ft. altitude (see Table 1).

The author of Reference 7 reviewed Table 1, located the highest vibration condition, and remarked (on page 2):

Frequency analysis of the 126 knot test point showed a maximum of 1.2 in./sec (avg.) at rotor blade passage frequency (32 cps), and 0.5 in./sec (avg.) at rotor rotational frequency (8 cps) vertically at the front of the compressor.

Table 1 and Figure 1 thus constitute the T63 engine vibration data used in this study.

TABLE 1. ENGINE OVERALL VIBRATION VELOCITY (INCHES PER SECOND AVERAGE) FOR VARIOUS CONDITIONS													
Horse- power	IAS (mph)	Alt (ft)	Bal Cond	Conditions	Maneuver	Vibration Pickup Number and Location							
						1	2	3	4	5	6	7	8
						Comp Vert (Top)	Comp Front Lat (Right)	Acc G/B Vert (Btm Left)	Acc G/B Vert (Right)	Acc G/B Lat (Btm Left)	Acc G/B F&A (Top)	Turb Mid S/L Vert (Top)	Turb Mid S/L Lat (Left)
100	-	Grd	B		Tie-down ground run	0.60	0.50	0.35	0.55	0.45	0.32	0.45	0.45
100	-	Grd	U		Tie-down ground run	0.80	0.50	0.35	0.50	0.38	0.30	0.55	0.40
134	-	Grd	B		Tie-down ground run	0.60	0.50	0.30	0.60	0.35	0.35	0.50	0.40
134	-	Grd	U		Tie-down ground run	0.75	0.50	0.38	0.62	0.42	0.30	0.55	0.38
200	0	5000	B		Hover	0.85	0.83	0.40	0.56	0.47	0.50	0.60	0.55
134	44	5000	B		Hover	0.62	0.60	0.35	0.40	0.45	0.45	0.52	0.47
134	87	5000	B		Straight flight	0.60	0.75	0.33	0.45	0.55	0.50	0.60	0.60
227	120	5000	B		Straight flight	1.3	0.35	0.90	0.65	0.50	0.71	0.65	0.72
224	126	5000	B		Straight flight	1.7	0.82	0.60	0.80	0.52	0.70	0.85	0.65
-	-	100	B		Sideward flight - right	0.92	Δ	Δ	Δ	Δ	Δ	0.63	Δ
-	-	100	B		Sideward flight - left	0.93	Δ	Δ	Δ	Δ	Δ	0.65	Δ
-	0-10	100	B		Pedal turn - right	1.25	Δ	Δ	Δ	Δ	Δ	0.67	Δ
-	0-10	100	B		Pedal turn - left	1.0	Δ	Δ	Δ	Δ	Δ	0.71	Δ
-	-	Grd	B		Engine start to 100% N ₂ rpm	0.68	0.60	0.38	0.95	0.40	0.65	0.50	0.42
-	-	Grd	U		Engine start to 100% N ₂ rpm	0.80	0.60	0.45	0.70	0.47	0.62	0.45	0.45
-	-	Grd	B		Stabilized 100% N ₂ rpm	0.70	0.45	0.40	0.47	0.45	0.58	0.39	0.30
-	-	Grd	U		Stabilized 100% N ₂ rpm	0.80	0.40	0.45	0.30	0.40	0.62	0.35	0.40

B = Normal balance in rotors and drive shaft
U = Maximum allowable imbalance in rotors
Δ = Not recorded during this maneuver

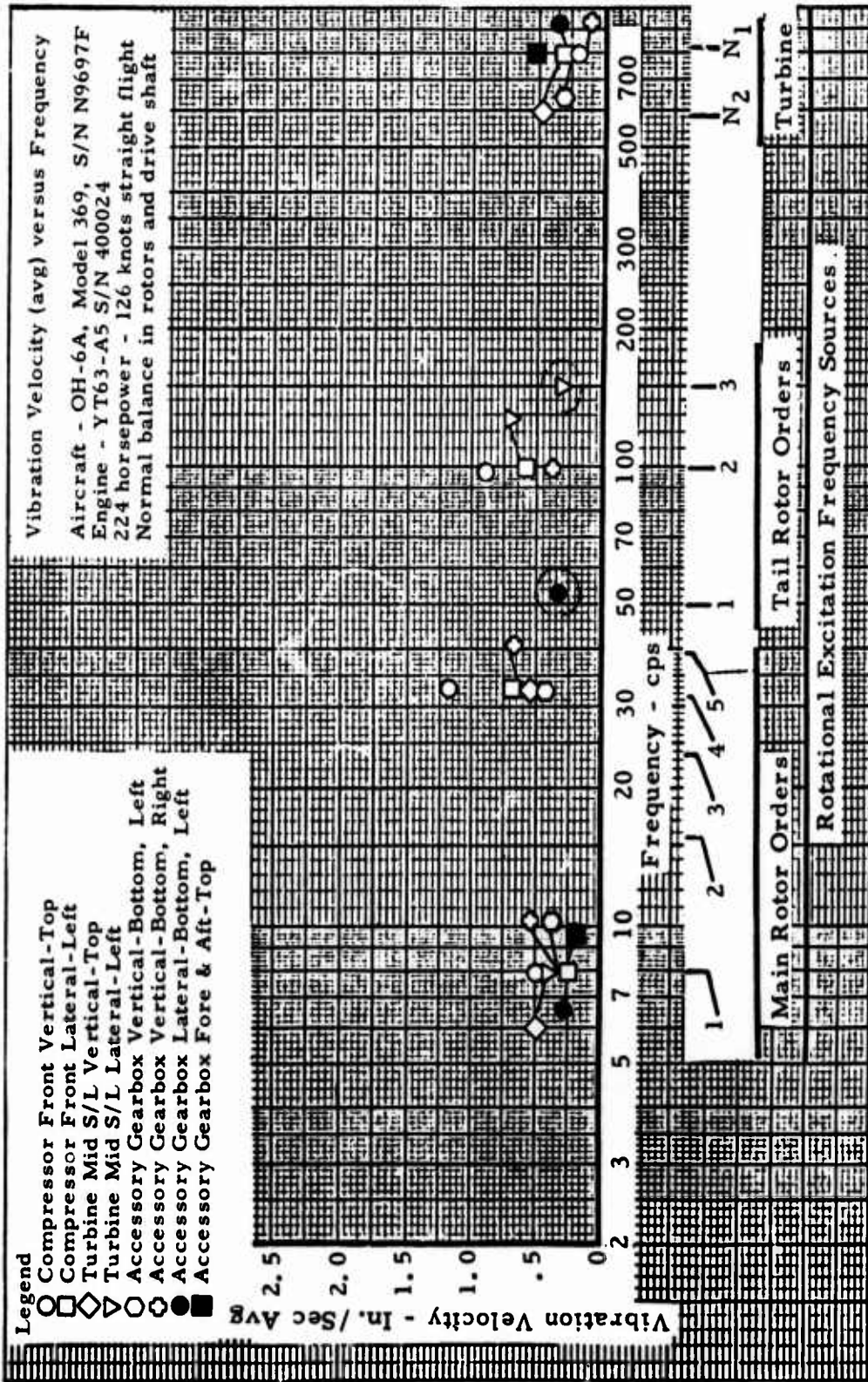


Figure 1. Vibration Velocity (Average) Versus Frequency.

The experimental OH-6A airframe excitation forces that cause engine vibration are determined indirectly. Based on the favorable report for the T63 installation presented in Reference 7, no test work was directed toward obtaining airframe excitation forces as related to engine vibration. These forces were derived from rotor mast data measured during FAA certification, and presented in Reference 8, and from calculations presented in Reference 9. Results are given here in the discussion on page 56.

Toward the conclusion of this present study, some additional T63/OH-6A engine vibration data became available in Reference 10. That report summarized a large amount of vibration data taken on magnetic tape for many locations, including seven engine locations. Because of the volume of data taken (mostly not yet reduced), only peak values were sifted out for mention. It is noted on page 25 of Reference 10 that the highest acceleration recorded during the program was 75g at an engine location (at the fuel nozzle at 832 hertz), and it is further stated that "The source of this fuel nozzle vibration was identified as the engine gas producer." No engine difficulty has ever been observed related to this information. It is suggested that this point, as well as the remainder of the unreduced tape data reported by Reference 10, be the subject of future study.

It should be noted that, in essence, the amount of flight-test data available for this program is limited. This situation is perhaps more typical than unique. Traditionally, the engine installation has been given much less attention than rotor blade aeroelasticity and fuselage vibration reduction, as mentioned in Reference 2. However, with the advanced technology engines available to the UTTAS program, the AAH program, and possibly the ASH program, it may be necessary to plan in advance to acquire, analyze, and evaluate considerably more data than was available for this program to ensure engine/airframe compatibility.

ANALYSIS OF EXISTING DATA

The data presented in References 7 and 8 were analyzed with the goal of identifying the following objectives, which were presented in Reference 4 as significant elements of the engine/airframe compatibility problem:

- Relative contribution of airframe and engine to engine vibration
- Amplitude versus discrete frequency -- from 8 to 800 hertz in high-speed level flight for this study
- Predominant responding mode shapes of the engine -- both rigid body and flexural
- Spectrum of engine vibration for typical mission operation
- Engine response to a hard landing

All of these items are discussed below; because of limited data and interdependence, there will be some repetition.

DEDUCED MODE SHAPES

Figure 1 (from Reference 7) gives engine vibration at eight locations for straight and level flight -- at a calibrated airspeed of 126 knots, an altitude of 5000 feet, and a gross weight of 2180 pounds -- using a YOH-6A helicopter, serial number N9697F. Table 2 lists the values of the measured discrete frequencies, together with the source of excitation at the named frequencies.

The data in Reference 7 was reported without reference to phasing, and the original magnetic tape has since been destroyed. Therefore, engine mode shapes were deduced from inspection of the data in Figure 1 in light of the engine manufacturer's statement in Reference 5 that the lowest frequency free-free bending mode of the engine is 127 hertz. On that premise, it is deduced that frequencies of 8, 32, 50, and 100 hertz are associated with rigid-body modes which are excited by the main and tail rotor (i. e., airframe-related) and that 800 hertz is associated with a flexural mode, excited by the gas generator. (The power turbine operated at 590 hertz, and no vibration data is shown at that frequency in Figure 1.)

TABLE 2. LISTING OF DISCRETE FREQUENCY DATA AND EXCITATION SOURCE

Frequency (Hz)	Excitation Source
8	Main rotor, 1/rev
32	Main rotor, 4/rev
50	Tail rotor, 1/rev
100	Tail rotor, 2/rev; engine shaft 1/rev
150	Tail rotor, 3/rev
800	Gas generator

The data in Figure 1 is shown for the following engine locations:

- Compressor front vertical - top
- Compressor front lateral - left
- Turbine mid-split-line-vertical - top
- Turbine mid-split-line-lateral - left
- Accessory gearbox vertical - bottom, left
- Accessory gearbox vertical - bottom, right
- Accessory gearbox lateral - bottom, left
- Accessory gearbox fore and aft - top

These eight transducer locations are seen to be placed at the following engine stations, relative to the engine mount plane:

<u>Location</u>	<u>Engine Fore and Aft Station (inches)</u>
Compressor front	-10.5
Engine mount plane	0
Accessory gearbox	3.0
(Engine center of gravity)	(5.0)
Turbine mid-split-line	12.8

The data in Figure 1 were plotted in Figures 2 through 5, at the engine stations shown on those figures, for 8, 32, 100, and 800 hertz, respectively. (Only a single point is given for 50 hertz, so no mode shape estimation is possible.) Then, on the premise that the lower frequencies are rigid body frequencies, an estimated polarity was given to the data, and mode shapes were drawn as shown (for both vertical and lateral motion where data permitted). Mode shapes were also drawn for 800 hertz in Figure 5, using straight lines to connect the available data, but higher order modes could be present which would not be disclosed by only three fore and aft data stations.

PREDOMINANT RESPONDING MODE SHAPES AND RELATIVE CONTRIBUTION OF AIRFRAME AND ENGINE

Based on Figures 2 through 5, it is concluded that the predominant responding modes are rigid-body modes, chiefly in the vertical direction. Evidence of translation, pitch, and a combination of pitch/translation is seen for the lowest three modes. The data on the highest mode (800 hertz) is inconclusive. The data in Figures 2 through 5 are summarized in Table 3.

TABLE 3. EXCITATION FREQUENCY, MODE SHAPE, AND EXCITATION SOURCE			
Figure	Excitation Frequency (Hz)	Predominant Mode Shape (Vertical)	Relative Contribution - Airframe or Engine
2	8	Rigid translation	Airframe: main rotor, 1/rev
3	32	Rigid pitch	Airframe: main rotor, 4/rev
4	100	Rigid translation/pitch	Airframe: tail rotor, 2/rev; engine drive shaft
5	800	Flexural	Engine: gas generator

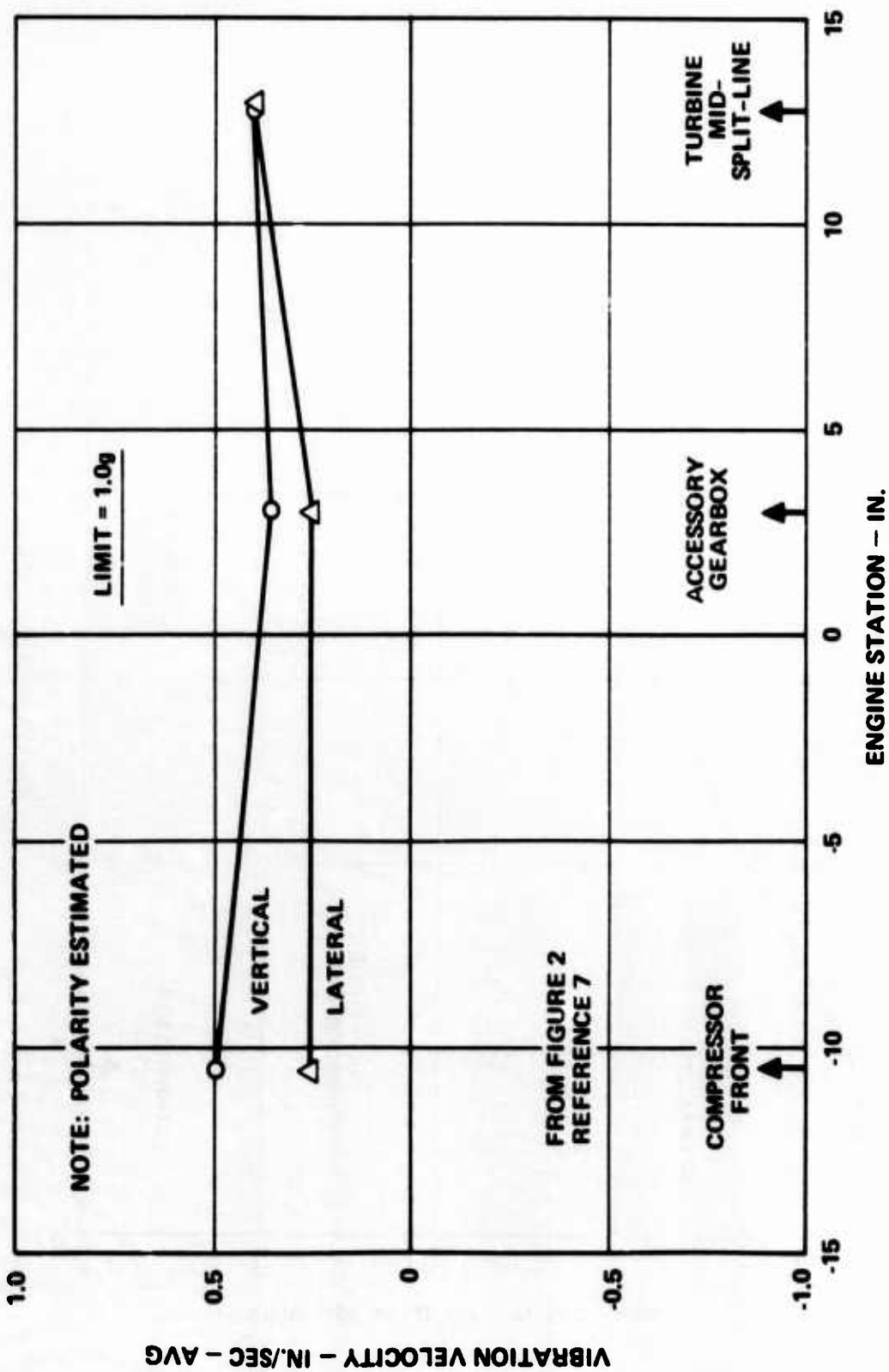


Figure 2. T63 Mode Shape - 8 Hertz.

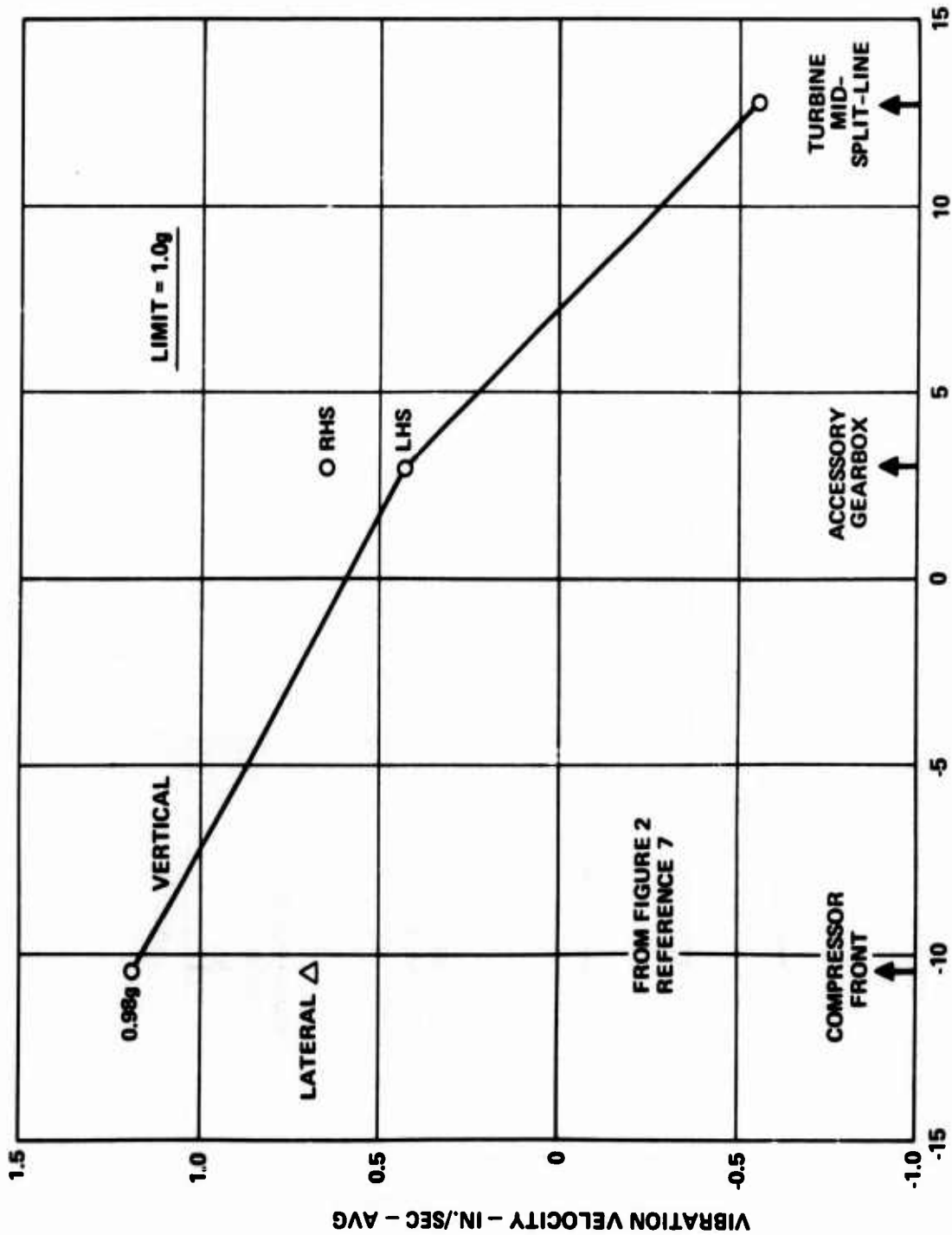


Figure 3. T63 Mode Shape - 32 Hertz.

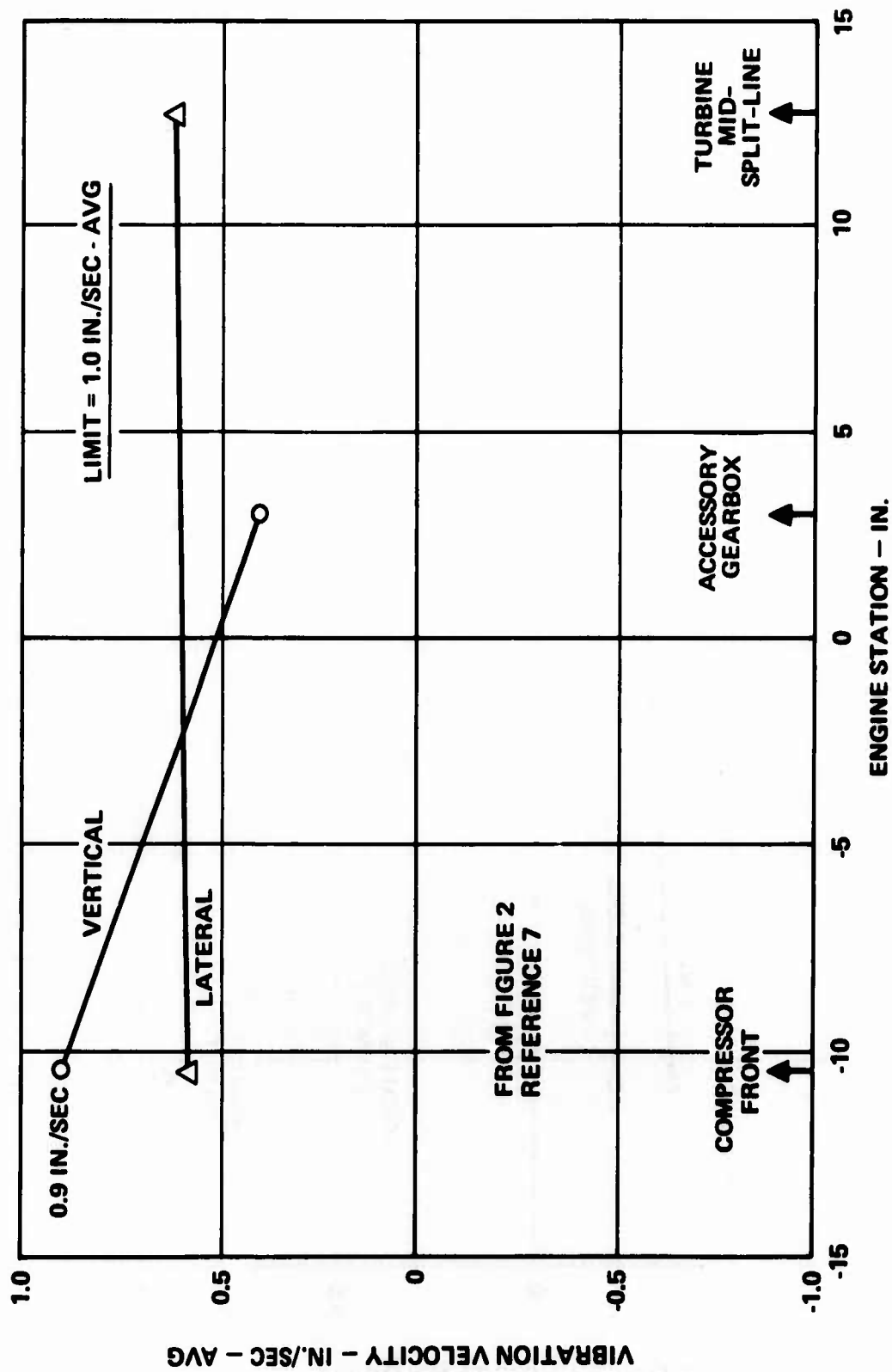


Figure 4. T63 Mode Shape - 100 Hertz.

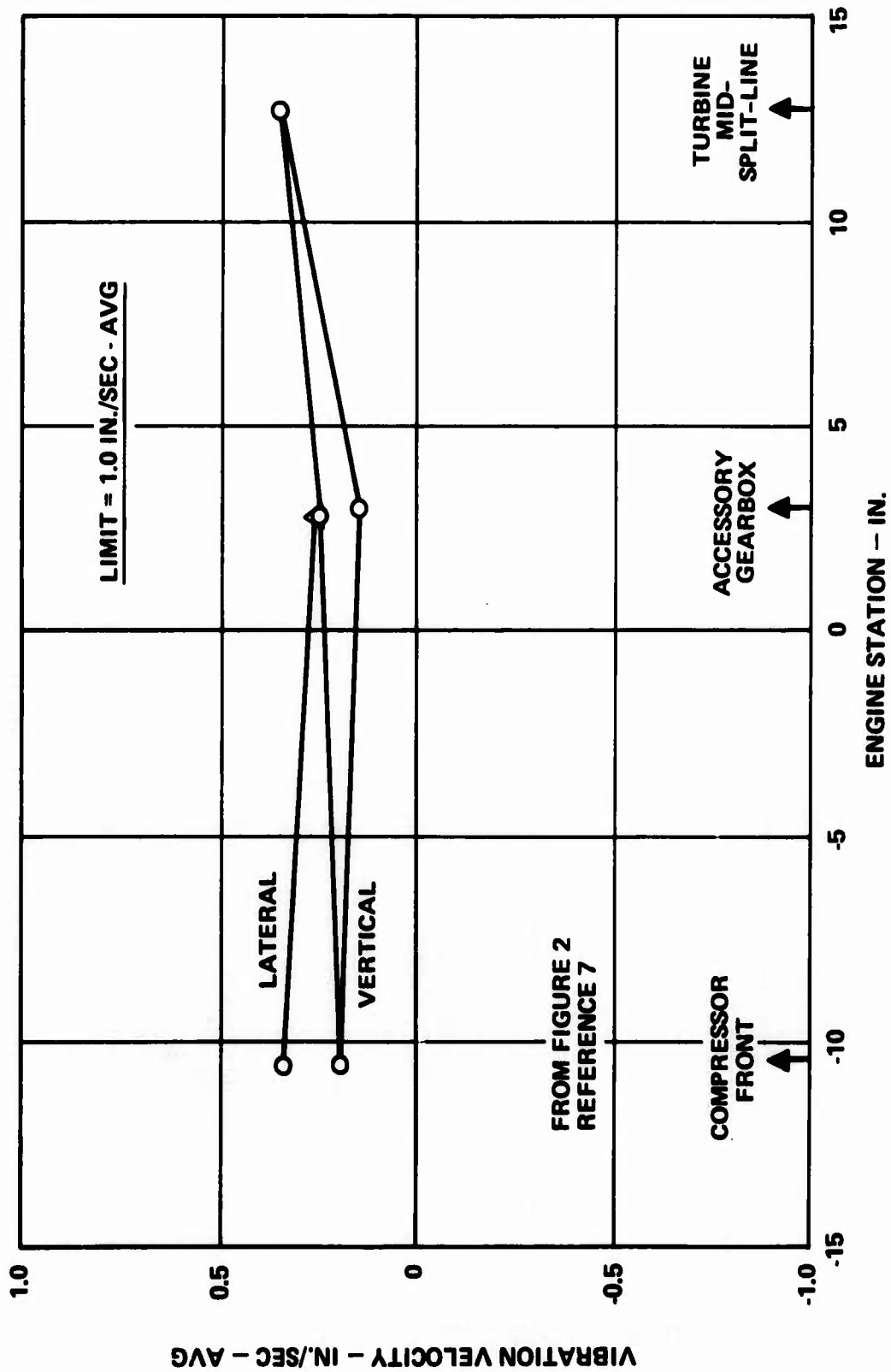


Figure 5. T63 Mode Shape - 800 Hertz.

AMPLITUDE VERSUS DISCRETE FREQUENCY

With the estimated polarities shown above, amplitude of vibration versus discrete frequency is shown for the compressor front, accessory gearbox, and turbine mid-split-line, for vertical and lateral motion, in Figures 6, 7, and 8. The prominent vertical motion of the compressor front at 32 and 100 hertz is noted. Vertical motion generally exceeds lateral motion for 8 and 32 hertz; the reverse is noted at 800 hertz, and data is incomplete at 100 hertz.

COMPARISON WITH ALLOWABLE VIBRATION LIMITS

Figure 9 shows the T63 discrete frequency vibration limits, as established in Reference 11. The limit is 1.0 inch per second (average) from 40 to 2000 hertz, and 1.0g below 40 hertz. The vertical motion of the top front of the compressor is seen to be 1.2 inches per second (average) at 32 hertz on Figures 3 and 6. This value corresponds to 0.98g, which is very nearly the 1.0g vibration limit at 32 hertz on Figure 9. Also, the vertical motion of the top front of the compressor is seen to be 0.9 inch per second (average) at 100 hertz on Figures 4 and 6. This value is nearly the 1.0-inch-per-second (average) limit at 100 hertz on Figure 9.

The limits from Figure 9 were placed on Figures 2 through 5, as applicable, for reference. The comparison noted here points out that significant engine motion exists at 32 hertz, caused by main rotor four-per-revolution (4/rev) excitation; the predominant responding mode is a rigid-body pitch mode. Appreciable engine motion exists at 100 hertz, caused by tail rotor 2/rev excitations; the predominant responding mode is a rigid-body pitch/translation mode.

SPECTRUM OF ENGINE VIBRATION FOR TYPICAL MISSION OPERATION

The spectrum of engine vibration for mission operation is primarily a function of the mission under consideration. No standard mission is available for reference. However, Reference 8 contains the vibratory flight load spectrum used for the FAA Type Inspection Authorization (TIA) for the OH-6A helicopter. Approximately 20 flight conditions are contained in the load spectrum in Reference 8. Discrete frequency data is available in Figure 1 for only a single flight condition. Therefore, it was decided to use the load spectrum in Reference 8 to calculate engine motion for the multiple flight conditions found in typical mission operation.

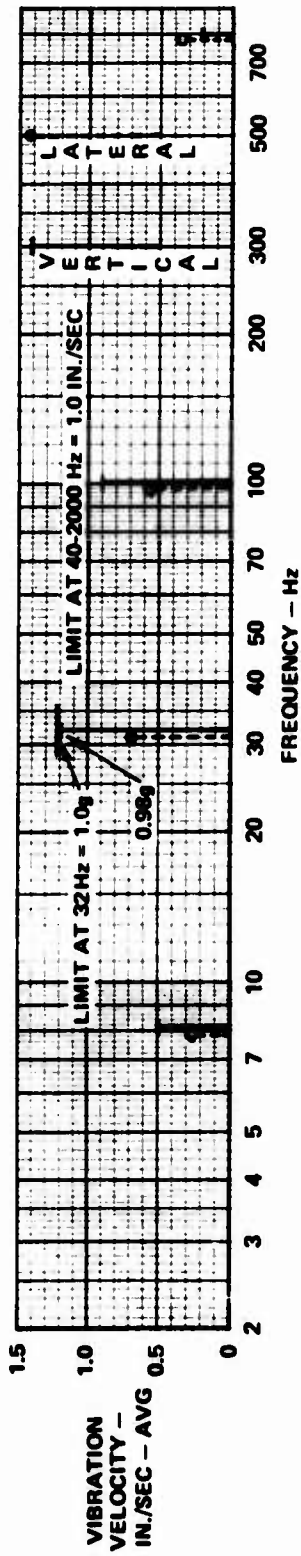


Figure 6. Amplitude vs Discrete Frequency - Compressor Front.

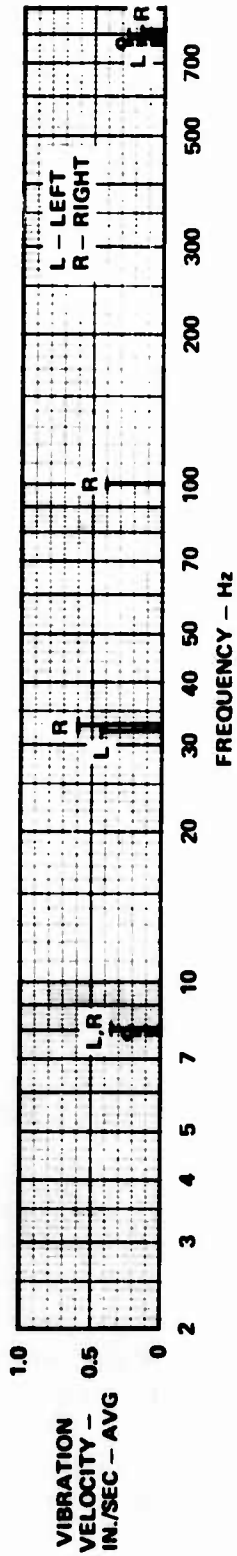


Figure 7. Amplitude vs Discrete Frequency - Accessory Gearbox.

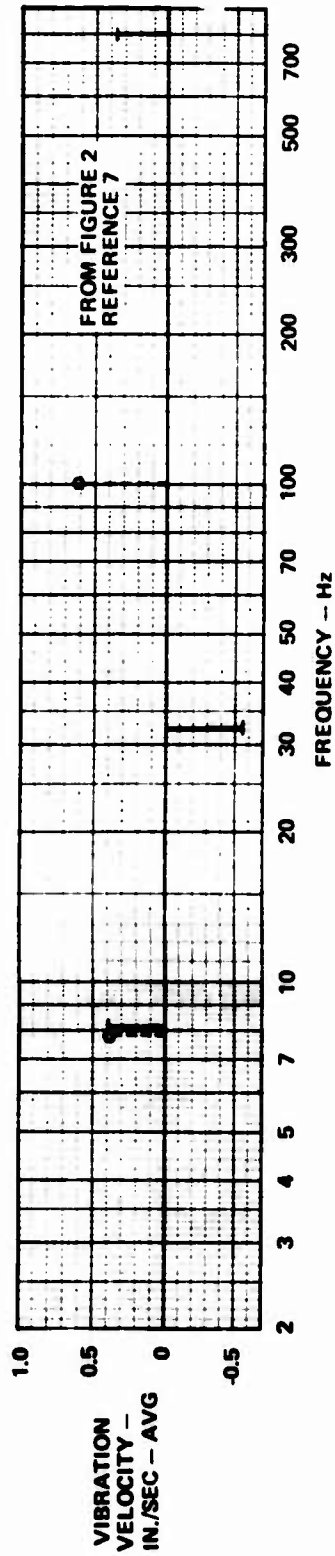
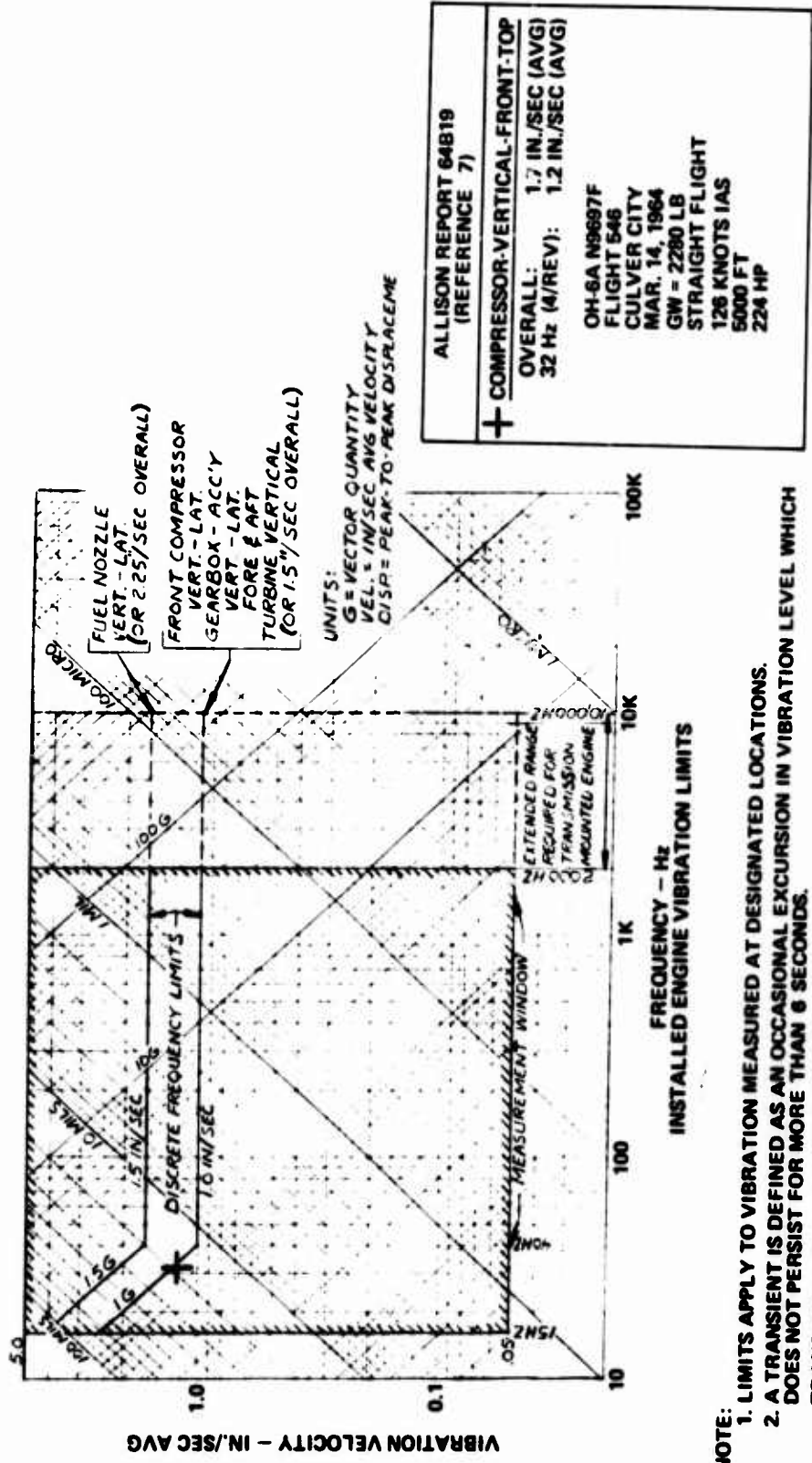


Figure 8. Amplitude vs Discrete Frequency - Turbine Mid-Split-Line.



- NOTE:**
1. LIMITS APPLY TO VIBRATION MEASURED AT DESIGNATED LOCATIONS.
 2. A TRANSIENT IS DEFINED AS AN OCCASIONAL EXCURSION IN VIBRATION LEVEL WHICH DOES NOT PERSIST FOR MORE THAN 6 SECONDS.
TRANSIENT LIMIT - 2 X STEADY-STATE LIMIT.
 3. LIMITS APPLY TO NORMAL FLIGHT OPERATING ENVELOPE.

Figure 9. T63 Discrete Frequency Limits Versus Frequency.

This discussion above indicates that vibration at the compressor top front in cruise flight is the most significant vibration at that condition. To illustrate a spectrum of engine motion, Table 4 was prepared using the compressor front as an example (see page 31). Table 4 presents the several maneuvers in the TIA tests and the percentage of total time expected to be spent in them. The individual time elements do not add up to 100 percent -- a 4-percent "miscellaneous" allowance is included.

It should be noted that none of the steady-state conditions listed in Table 4 shows calculated compressor motion in excess of the allowable limit value shown in Figure 9. Two transient conditions (level flight control reversal, 130 knots, and autorotation approach to landing) are shown to have calculated motion greater than the permissible steady-state value, based on the most adverse phasing of the rotor excitation forces used to prepare Table 4. In general, the calculated values in Table 4 agree with the measured values in Table 1. However, a review of the voluminous data made available during the flight tests reported in Reference 10 may be used. (It should be noted that Table 4 is based on main rotor 4/rev (32 hertz) for illustration.)

TRANSIENT LOAD CONDITION - HARD LANDING

Flight test data is not available for the influence of a hard landing on the engine motion. It is expected that the lower frequency modes are involved in a hard landing. In addition, Reference 3 shows that a hard landing causes the highest engine motion for the cases studied in Reference 3, although the percentage of occurrence is so low as to be included in the "Miscellaneous" condition in Table 4.

Therefore, engine motion during a landing has been calculated using the NASTRAN structural model. The impulse shown in Figure 10, which is based on flight data analysis, was applied to the landing gear of the NASTRAN model (at the rear oleo), and the resulting engine motion was calculated (see page 151).

TABLE 4. SPECTRUM OF COMPRESSOR VIBRATION*
FOR TYPICAL MISSION OPERATION

Flight Condition	Percent Time	Calculated Compressor Motion** (in. /sec)
Hover		
Steady	2	0.21
Control reversal	1	0.28
Level flight		
30 knots	3	0.36
75 knots	21	0.41
100 knots	26	0.40
130 knots	17	0.83
Level flight, 2g turn		
50 knots	2	0.93
130 knots	2	0.63
2g pull-up, 100 knots	2	0.56
Level flight control reversal,		
130 knots	3	1.70
Lateral flight	1	0.33
Maximum climb, 60 knots	6	0.43
Dive, 140 knots	1	0.97
Enter autorotation, 75 knots	1	0.31
Autorotation, 60 knots	3	0.59
Autorotation approach to landing	2	1.55
Autorotation turn		
40 knots	1	0.27
75 knots	1	0.60
120 knots	1	0.59
Hard landing***	-	-
Miscellaneous	4	-
	100	

*At 32 Hz (main rotor, 4/rev).

**Most adverse phase angle is assumed.

***Included in "Miscellaneous" (see p. 151).

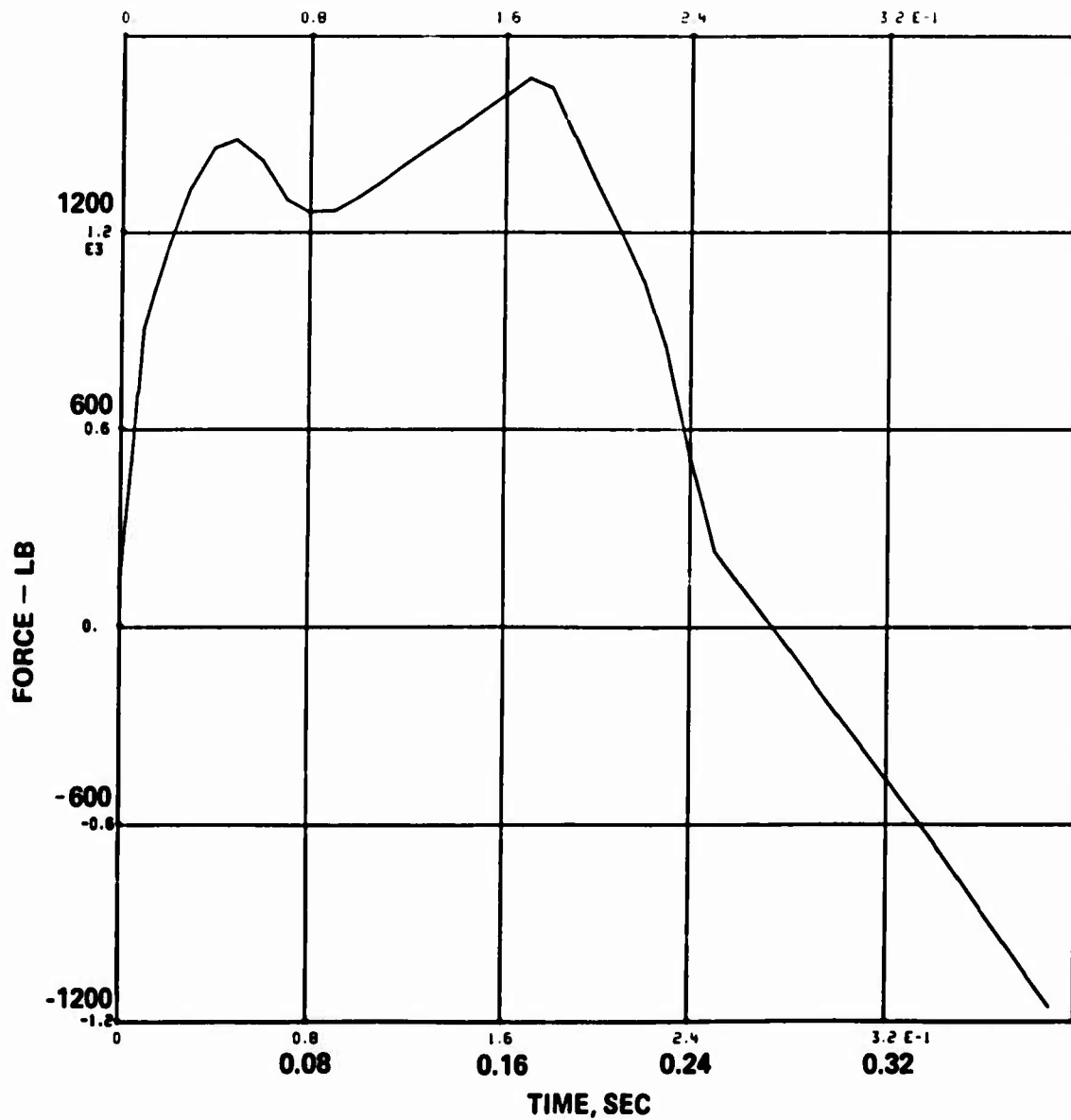


Figure 10. Load at Skid for Hard Landing.

MOBILITY TESTS

LABORATORY (GROUND) TESTS AND FLIGHT TESTS

Test work conducted for this program involved laboratory tests only. The necessary flight data was taken from appropriate tests performed under previous programs. The ground tests were performed in order to acquire additional data to validate the properties of the NASTRAN structural model.

Test Configuration

The laboratory tests were conducted on a bailed U. S. Army OH-6A helicopter, serial number 65-12945, which was the 30th production helicopter. The tests were conducted in two phases:

- Phase I - engine removed
- Phase II - engine installed, but not running

As the intent of the test was to determine vibratory characteristics, crew weights were not simulated because the human body has a low impedance at the frequencies under consideration.

Fuel also was left out to prevent the amplitude - dependent dynamic properties of this material from obscuring the behavior of the structure. The loading, then, is typical of a flight with fuel expended.

All doors (engine access, cargo compartment, and crew compartment) have nonlinear structural characteristics due to free play in hinges and latching mechanisms. Because these doors are nonstructural and are relatively light, they were removed to improve repeatability of test data.

The following equipment and materials were removed from the helicopter from the Phase I and II tests:

- All doors: pilot, copilot, both cargo, both engine access
- All flight instruments and radio equipment
- All fuel
- Main rotor: blades, hub, main rotor drive shaft
- Tail rotor: blades, hub, swashplate, bellcrank

The following additional equipment was removed for Phase I tests only:

- Engine assembly, including exhaust ducts
- Engine/transmission drive shaft

Aircraft Weight

The following weights were added to simulate the mass of the above items deleted for the tests:

- Radio weight* = 87 pounds (simulated by lead shot bags located in the positions vacated by the radio equipment)
- Instrument weight* = 21 pounds (simulated by a piece of aluminum plate 3/16 by 10 by 15 inches, bolted to the instrument panel -- lead pieces added to simulate the instrument weights)
- Simulated main rotor system, including 5/8** blade mass = 142.5 pounds
- Simulated tail rotor system = 12.5 pounds
- Weight added to cargo floor: Phase I = 408 pounds; Phase II = 268 pounds (simulated by weights on a piece of 3/4-inch plywood bolted to the cargo tiedown points on the floor; lead weights placed on the plywood caused the suspended helicopter to hang in a level attitude and ballasted it to the 1331-pound weight discussed below)

The weight configuration of the test aircraft was selected to match, as closely as practical, the weight of an instrumented helicopter test-flown in 1964. That aircraft's gross weight was 2280 pounds. The mobility-test helicopter did not have the following items installed:

● Pilot and observer	400 pounds
● Fuel	380 pounds
● Doors	31 pounds
● Engine	<u>138</u> pounds
Total	949 pounds

Hence, the 2280-pound weight of the 1964 aircraft was reduced by this 949 pounds, and the total aircraft weight was held at 1331 pounds throughout

*Simulates weight of equipment used in YOH-6A flight tests in 1964.

**The actual main and tail rotor assemblies were removed so that mobility data could be obtained without being complicated by hub and blade resonances (nonrotating) that are not present in the flight mode. The 5/8 blade mass was chosen as a practical value for simulating effective dynamic blade mass.

the program. During Phase II, when the engine was installed, 138 pounds was removed from the cargo floor weights to make up for the engine weight.

TEST APPARATUS AND MOBILITY MEASUREMENT EQUIPMENT

A general description of the apparatus and equipment used in the mobility tests is given here. More details may be found in Appendix A.

Aircraft Test Setup

The helicopter was mounted in the static test rig using one of two suspension systems, depending on the type of test:

- For all except main rotor vertical excitation tests, the helicopter was suspended by a cable from a torsion-bar-type spring. This gave the aircraft a rigid-body vertical natural frequency of 1.29 hertz.
- Main rotor vertical excitation tests required additional isolation plus positioning of the shaker directly above the rotor hub. A series/parallel spring arrangement (Figure 11) accomplished this with a vertical natural frequency of 1.39 hertz.

An electrodynamic shaker (50-pound force capability) was mounted on a hydraulic lift that positioned it for applying the oscillating forces to the main and tail rotors and to the engine shaft at the transmission (Figures 12 and 13). Excitations in the engine area required that the shaker be mounted on a smaller hydraulic lift by means of a universal rotary table with horizontal cross slides for orientation at the proper angles (Figure 13). The shaker mount was always configured so that its fundamental vibratory mode was below the lowest test frequency.

Shaker Equipment

Vibratory forces were applied to the aircraft by an MB Model EA 1500 Electrodynamic Shaker (50-pound force capacity) in one of two configurations:

- A conventional model for applying forces at easily accessible points
- A modified model as shown in Figure 14. This incorporated a flexure-mounted bellcrank to change the direction of force application by 90 degrees and make it easier to reach the more inaccessible points.

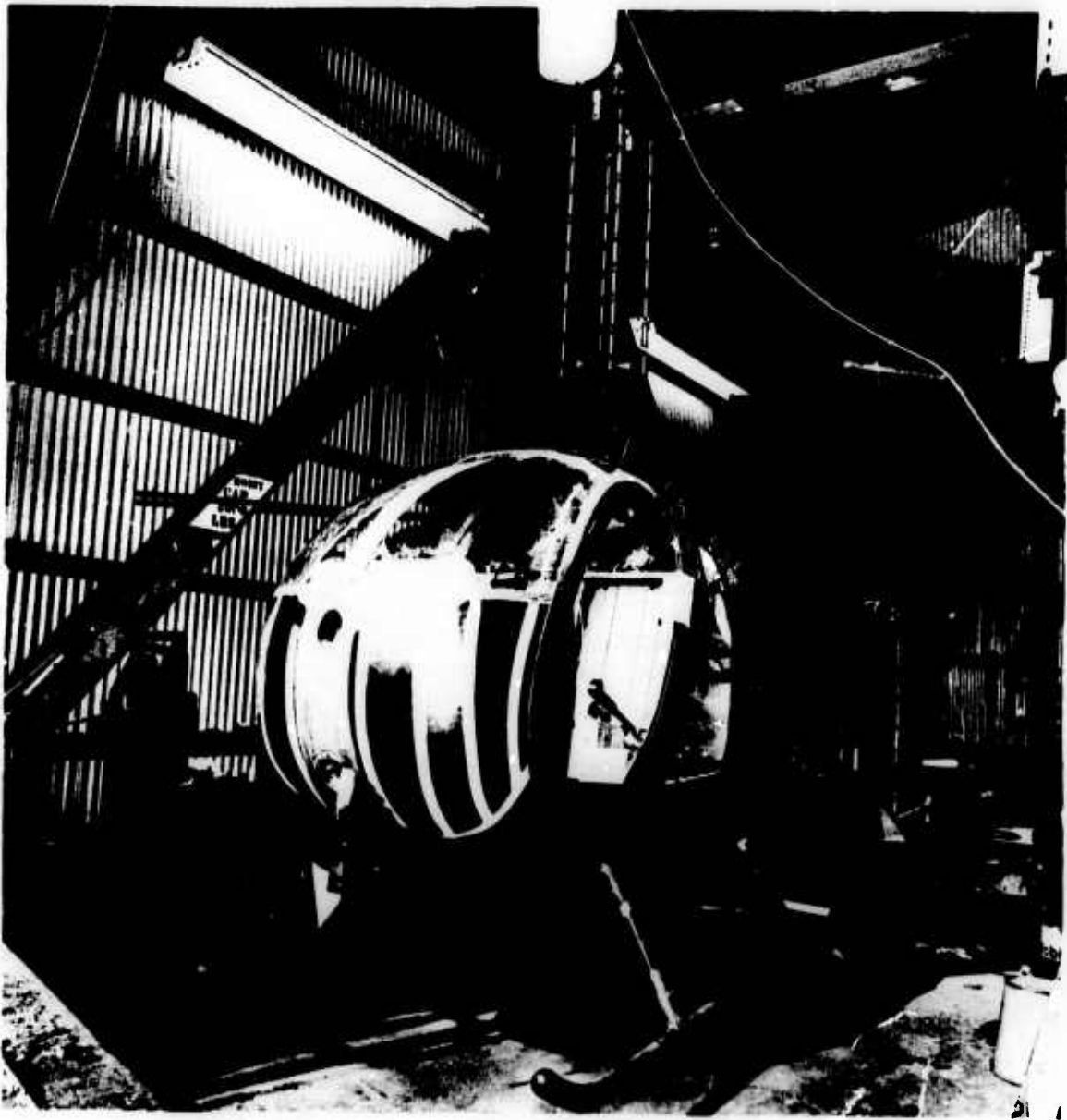
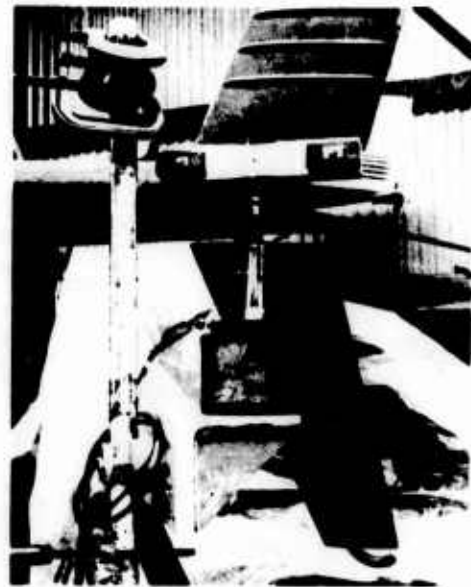


Figure 11. OH-6A (SN 65-12945) Suspended for Mobility Tests.



**Main Rotor Longitudinal
Force Input**



Tail Rotor Vertical Force Input

Figure 12. Shaker Arrangement for Excitation of Rotor Hubs.



**Figure 13. Shaker Arrangement for Excitation of Engine Shaft
at Transmission.**

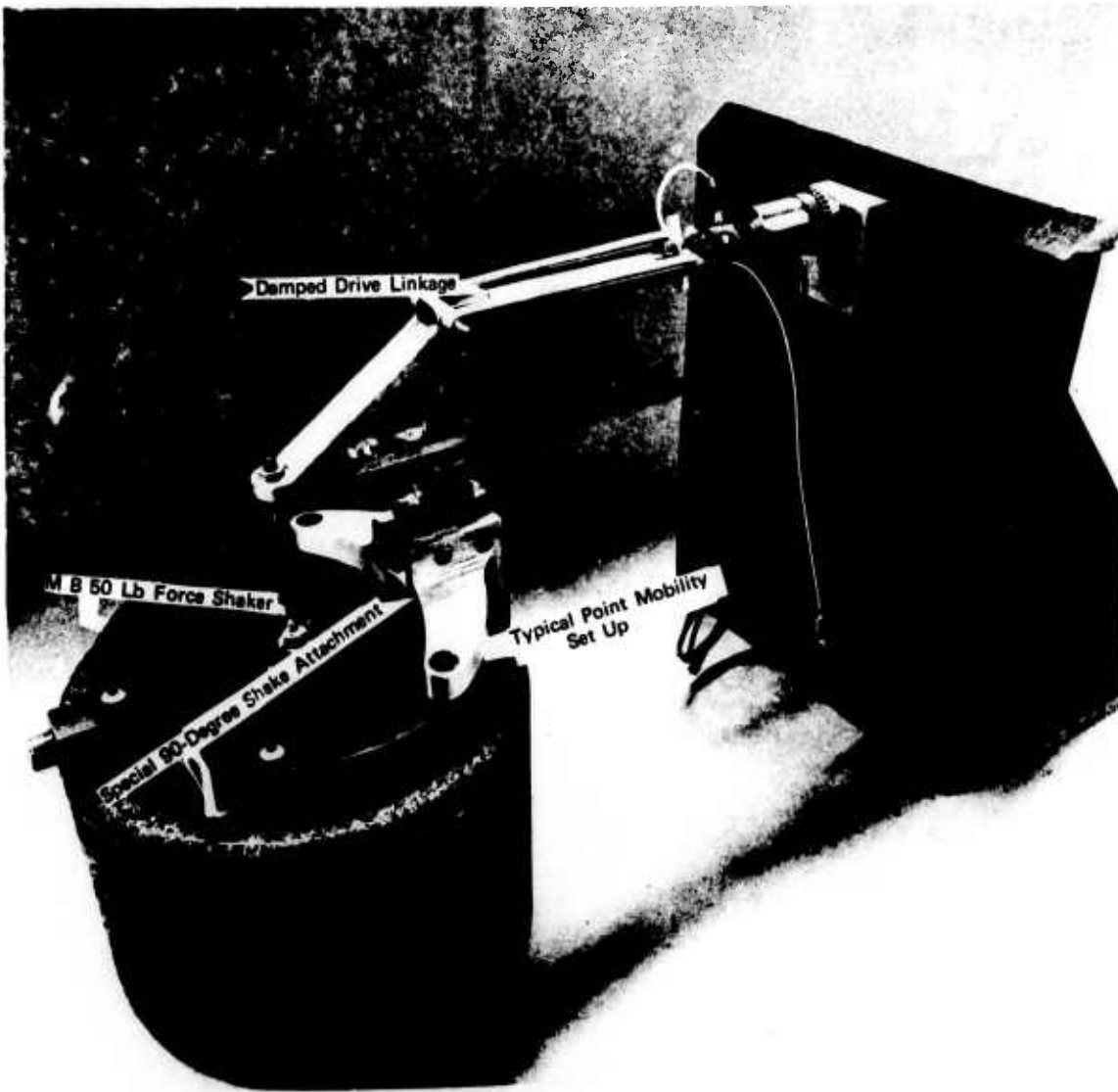


Figure 14. Mockup of Shaker With 90-Degree Bellcrank Installed (Coaxial Drive Linkage and Preloading Elastic Bands Connected to Bellcrank and Impedance Head Transducers; This Method of Attachment Typical for All Shake Points).

Mobility Measuring Equipment

The following equipment was used to measure and record the mobility data:

- Bruel and Kjaer Uni-Gain Accelerometer, Model 4338 (SN 267585)
- Wilcoxon Impedance Head, Model Z-12 (SN 48)
- MB Electronics Zero Drive Amplifiers, Model N400 (SN 708, 711, 1578)
- MB Line Drivers (associated with the N400 Amplifiers), two voltage types and one charge type
- Spectral Dynamics Corporation Mechanical Impedance System, Model SD 1002E-42 (SN 173), Figure 15

The equipment used for these tests is capable of dynamic measurements between frequencies of 5 and 10,000 hertz. It was calibrated with respect to force, acceleration, and frequency through techniques traceable to National Bureau of Standards benchmarks.

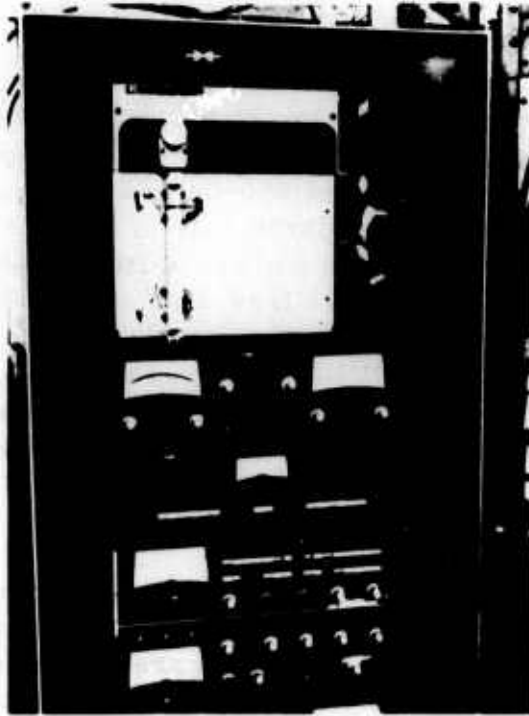


Figure 15. Spectral Dynamics Corporation - Automatic Mechanical Impedance Analysis and Recording System, Model SD 1002E-42.

Special graph paper was designed for recording the engine/airframe mobility data. A sample is shown in Figure 16. A mobility scale from 0.001 to 100 inches per second per pound and a frequency scale from 5 to 5000 hertz were chosen to cover the range of interest for the OH-6A.

Scales for effective mass and stiffness are superimposed. The lines of these scales are basically the solution to the equation of the fundamental response of a single-degree-of-freedom spring-mass system:

$$\left(\omega = \sqrt{\frac{K}{M}} \right)$$

Any point on the grid yields a frequency, a stiffness, and a mass that satisfy the above equation.

The value of having these mass and stiffness lines on the paper is apparent when studying the mobility plot of a structure. For instance, at low frequencies, the effective mass of the item being shaken is indicated when the mobility plot follows a mass line that slopes down to the right. Conversely, if the mobility follows a line that slopes upward to the right, the system is behaving in a spring-like manner, and the force effect of the mass involved is insignificant. The value of stiffness can be read directly from the graph.

The top decade of the mobility scale is seldom entered by the mobility trace and is a convenient place to locate the phase information associated with the mobility plot. It is divided into 90-degree segments corresponding to the 0-, 90-, 180-, 270-, and 360-degree points of phase relationship between force and velocity. The parameter of force is the reference parameter; velocity is plotted as the amount of its lag behind the force. The phase data is plotted linearly. In a free-free system with no spring, the vibratory velocity phase relative to the vibratory force input is plotted on this paper at the 90-degree position. In the same system with a spring between the mass and the force generator, and the system operating above the first resonant frequency, the phase is plotted at the 270-degree point.

TEST SHAKEDOWN

The test helicopter was mounted in the test fixture shown in Figure 11 with the shaker attached through the impedance head shown at the right in Figure 14. Typical accelerometer mountings are indicated in Figure 17. The Spectral Dynamics Corporation impedance/mobility measuring system was very reliable and trouble-free, but there were initially some problems with the peripheral equipment. (See discussion in Appendix A.)



LATERAL



LONGITUDINAL



VERTICAL

Figure 17. Typical Accelerometer Mounting - Left Engine Mount.

TEST CONDITIONS

The helicopter was vibrated by the shaker at a number of locations, one at a time, and the mobility of many points around the engine and its mounts was recorded during frequency sweeps from 8 to 2000 hertz. Table 5 summarizes the conditions tested. These included oscillating force inputs at the following points:

- Main rotor hub - longitudinal, lateral, vertical
- Tail rotor hub - longitudinal, lateral, vertical
- Left engine mount - parallel, perpendicular, normal
- Right engine mount, parallel, perpendicular, normal
- Center engine mount - parallel, perpendicular, normal
- Engine/transmission coupling at transmission - axial, longitudinal, lateral
- Engine power pad - lateral, axial, vertical
- Turbine mid-split - lateral, vertical

The points at which the mobilities were measured were as follows:

- Main rotor hub - longitudinal, lateral, vertical
- Tail rotor hub - longitudinal, lateral, vertical
- Left engine mount - parallel, perpendicular, normal
- Right engine mount - parallel, perpendicular, normal
- Center engine mount - parallel, perpendicular, normal
- Engine/transmission shaft - longitudinal, lateral, axial
- Engine rear power pad - lateral, axial, vertical
- Engine compressor front - lateral, vertical
- Engine gearbox bottom
 - Left - vertical, lateral
 - Right - vertical, lateral
- Engine gearbox top - axial
- Engine turbine mid-split - lateral, vertical

Table 6 describes the sense of the force input direction and point response directions for all the conditions tested.

TABLE 5. TEST CONDITION SUMMARY

MATRIX I

Excitations	MOTION MEASURED														
	Left Engine Mount			Right Engine Mount			Center Engine Mount			Engine / Transmission Coupling at Transmission					
	Parallel	Perpendicular	Normal	Parallel	Perpendicular	Normal	Parallel	Perpendicular	Normal	Parallel	Perpendicular	Normal	Axial	Lateral	Longitudinal
Left Engine Mount	1*	2	3	4	5	6	7	8	9	10	11	12			
	13	14	15	16	17	18	19	20	21	22	23	24			
	25	26	27	28	29	30	31	32	33	34	35	36			
Right Engine Mount	37	38	39	40	41	42	43	44	45	46	47	48			
	49	50	51	52	53	54	55	56	57	58	59	60			
	61	62	63	64	65	66	67	68	69	70	71	72			
Center Engine Mount	73	74	75	76	77	78	79	80	81	82	83	84			
	85	86	87	88	89	90	91	92	93	94	95	96			
	97	98	99	100	101	102	103	104	105	106	107	108			
Engine / Transmission Coupling at Transmission	109	110	111	112	113	114	115	116	117	118	119	120			
	121	122	123	124	125	126	127	128	129	130	131	132			
	133	134	135	136	137	138	139	140	141	142	143	144			

*Numbers in this table refer to mobility plot numbers in Volume II (see page 51).

TABLE 5 - Continued

MATRIX 2

Shake Location	MOTION MEASURED														
	Tail Rotor			Left Engine Mount			Right Engine Mount			Center Engine Mount			Shaft Transmission/Engine		
	Lateral	Longitudinal	Vertical	Parallel	Perpendicular	Normal	Parallel	Perpendicular	Normal	Parallel	Perpendicular	Normal	Longitudinal	Lateral	Axial
Tail Rotor Lateral	1	2	3	4	5	6	7	8	9	10	11	12	37	48	36
Tail Rotor Longitudinal	13	14	15	16	17	18	19	20	21	22	23	24	40	41	42
Tail Rotor Vertical	25	26	27	28	29	30	31	32	33	34	35	36	43	44	45

MATRIX 3

Shake Location	MOTION MEASURED														
	Main Rotor			Left Engine Mount			Right Engine Mount			Center Engine Mount			Engine/Transmission Shaft		
	Lateral	Longitudinal	Vertical	Parallel	Perpendicular	Normal	Parallel	Perpendicular	Normal	Parallel	Perpendicular	Normal	Longitudinal	Lateral	Axial
Main Rotor Lateral	1	2	3	4	5	6	7	8	9	10	11	12	13	14	15
Main Rotor Longitudinal	16	17	18	19	20	21	22	23	24	25	26	27	28	29	30
Main Rotor Vertical	31	32	33	34	35	36	37	38	39	40	41	42	43	44	45

TABLE 5 - Continued

MATRIX 4

← RESPONSES →

Excitations	Relative to Airframe						Relative to Engine																
	Main Rotor		Left Engine Mount		Right Engine Mount		Center Engine Mount		(Engine Shaft) Rear Power Pad		Front Compressor		Gearbox Bottom		Gearbox Top	Turbine Mid-Split							
	L	V	L	V	L	V	L	V	A	V	L	V	L	V	L	V	A	V					
L O E A N R T I G I	1	2	3	4	5	6	7	8	9	10	11	12	13	14	15	16	17	18	19	20	21	22	23
L O E A N R T I G I	24	25	26	27	28	29	30	31	32	33	34	35	36	37	38	39	40	41	42	43	44	45	46
L O E A N R T I G I	47	48	49	50	51	52	53	54	55	56	57	58	59	60	61	62	63	64	65	66	67	68	69

**Boxes refer to tests reported in Figures 18, 19, and 20.

TABLE 5 - Continued

MATRIX 5

Excitations		Relative to Airframe						Relative to Engine																
		Left Engine Mount		Right Engine Mount		Center Engine Mount		(Engine Shaft) Rear Power Lead		Front Compressor		Gearbox Bottom		Gearbox Top		Turbine Mid-Split								
		L	V	L	V	L	V	L	V	L	V	L	V	L	V	L	V	L	V					
L	V	L	V	L	V	L	V	A	V	L	V	L	V	L	V	L	V	L	V					
O	E	O	E	O	E	O	E	N	E	N	E	N	E	N	E	N	E	N	E					
A	N	A	N	A	N	A	N	A	N	A	N	A	N	A	N	A	N	A	N					
T	G	T	G	T	G	T	G	I	I	I	I	I	I	I	I	I	I	I	I					
Tail Rotor Lateral		1	2	3	4	5	6	7	8	9	10	11	12	13	14	15	16	17	18	19	20	21	22	23
Tail Rotor Longitudinal		24	25	26	27	28	29	30	31	32	33	34	35	36	37	38	39	40	41	42	43	44	45	46
Tail Rotor Vertical		47	48	49	50	51	52	53	54	55	56	57	58	59	60	61	62	63	64	65	66	67	68	69

TABLE 5 - Continued

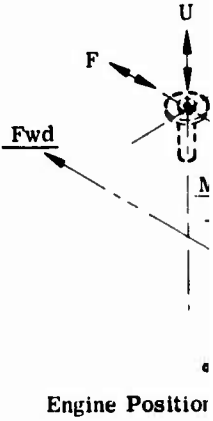
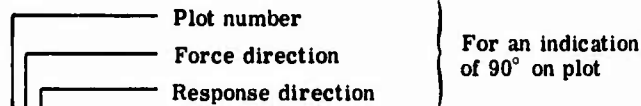
MATRIX 6

← RESPONSES →

Excitations	Relative to Airframe				Relative to Engine				Turbine Mid-Split											
	Left Engine Mount		Right Engine Mount		Center Engine Mount		(Engine Shaft) Rear Power Pad			Front Compressor	Gearbox Bottom		Gearbox Right							
	L	V	L	V	L	V	L	V			Left	Right								
L A T I G T	1	2	3	4	5	6	7	8	9	10	11	12	13	14	15	16	17	18	19	20
O E R T I G T	21	22	23	24	25	26	27	28	29	30	31	32	33	34	35	36	37	38	39	40
V	41	42	43	44	45	46	47	48	49	50	51	52	53	54	55	56	57	58	59	60
Lateral	61	62	63	64	65	66	67	68	69	70	71	72	73	74	75	76	77	78	79	80
Power Pad	81	82	83	84	85	86	87	88	89	90	91	92	93	94	95	96	97	98	99	100
Vertical																				

Lateral on turbine is fourth belt position from vertical, measured counter-clockwise when viewing engine from rear (burner) end. Force vector passes thru center of engine.

TABLE 6. FORCE/RESPONSE DIRECTIONS



Matrix 1

1 γ v	2 γ Δ	3 ν ρ	4 γ β	5 γ Δ	6 γ λ	7 γ a	8 γ r	9 γ u	10 γ a	11 γ l	12 γ d
13 ν β	14 ν v	15 ν ρ	16 ν β	17 ν Δ	18 ν λ	19 ν a	20 ν r	21 ν u	22 ν a	23 ν l	24 ν d
25 λ β	26 λ Δ	27 λ λ	28 λ β	29 λ Δ	30 λ λ	31 λ a	32 λ r	33 λ u	34 λ a	35 λ l	36 λ d
37 γ β	38 γ Δ	39 γ ρ	40 γ γ	41 γ Δ	42 γ λ	43 γ a	44 γ r	45 γ u	46 γ a	47 γ l	48 γ d
49 ν β	50 ν Δ	51 ν ρ	52 ν β	53 ν v	54 ν λ	55 ν a	56 ν r	57 ν u	58 ν a	59 ν l	60 ν d
61 ρ β	62 ρ Δ	63 ρ ρ	64 ρ β	65 ρ Δ	66 ρ ρ	67 ρ a	68 ρ r	69 ρ u	70 ρ a	71 ρ l	72 ρ d
73 f β	74 f Δ	75 f ρ	76 f β	77 f Δ	78 f λ	79 f a	80 f r	81 f u	82 f a	83 f l	84 f d
85 λ β	86 λ Δ	87 λ ρ	88 λ β	89 λ Δ	90 λ λ	91 λ a	92 λ r	93 λ u	94 λ a	95 λ l	96 λ d
97 d β	98 d Δ	99 d ρ	100 d β	101 d Δ	102 d λ	103 d a	104 d r	105 d u	106 d a	107 d l	108 d d
109 f β	110 f Δ	111 f ρ	112 f β	113 f Δ	114 f λ	115 f a	116 f r	117 d u	118 d a	119 d l	120 d d
121 r β	122 r Δ	123 r ρ	124 r β	125 r Δ	126 r λ	127 r a	128 r r	129 r u	130 r a	131 r l	132 r d
133 u β	134 u Δ	135 u ρ	136 u β	137 u Δ	138 u λ	139 u a	140 u r	141 u u	142 u a	143 u l	144 u d

Matrix 2

1RR	2RF	3RU	4R β	5R Δ	6R ρ	7R β	8R Δ	9R λ	10Ra	11Rr	12Ru	37Rd	38Rl	39R
13AL	14AA	15AU	16A β	17A Δ	18A ρ	19A β	20A Δ	21A λ	22Aa	23Ar	24Au	40Ad	41Al	42A
25DL	26DF	27DU	28D β	29D Δ	30D ρ	31D β	32D Δ	33D λ	34Da	35Dr	36Du	43Dd	44Dl	45D

Matrix 3

1LL	2LF	3LU	4L β	5L Δ	6L ρ	7L β	8L Δ	9L λ	10La	11Lr	12Lu	13La	14Ll	15L
16AL	17AA	18AU	19A β	20A Δ	21A ρ	22A β	23A Δ	24A λ	25Aa	26Ar	27Au	28Aa	29Al	30L
31DL	32DF	33DU	34D β	35D Δ	36D ρ	37D β	38D Δ	39D λ	40Da	41Dr	42Du	43Da	44Dl	45E

Matrix 4

1LL	2LF	3LU	4Ll	5La	6Lu	7Lr	8La	9Lu	10Ll	11La	12Ld	13Ll	14La	15L
24AL	25AA	26AU	27Al	28Aa	29Au	30Ar	31Aa	32Au	33Al	34Aa	35Ad	36Al	37Aa	38A
47DL	48DF	49DU	50Dl	51Da	52Du	53Dr	54Da	55Du	56Dl	57Da	58Da	59Dl	60Da	61E

Matrix 5

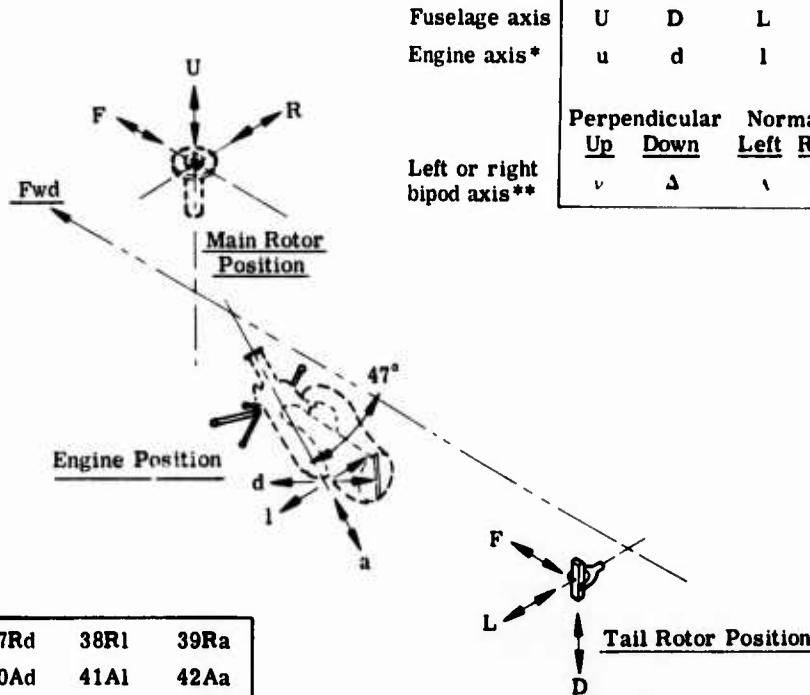
1RR	2RF	3RD	4Rl	5Ra	6Ru	7Rr	8Ra	9Ru	10Rl	11Ra	12Rd	13Rl	14Ra	15R
24AL	25AA	26AU	27Al	28Aa	29Au	30Ar	31Aa	32Au	33Al	34Aa	35Ad	36Al	37Aa	38A
47UL	48UA	49UU	50Ul	51Ua	52Uu	53Ur	54Ua	55Uu	56Ul	57Ua	58Ud	59Ul	60Ua	61U

Matrix 6

1rl	2ra	3ru	4rr	5ra	6ru	7rl	8ra	9rd	10rr	11ra	12rd	13ru	14rr	15r
21fl	22fa	33fu	24fr	25fa	26fu	27fl	28fa	29fd	30fl	31ff	32fd	33fu	34fr	35f
41ul	42ua	43uu	44ur	45ua	46uu	47ul	48ua	49ud	50ul	51ua	52uu	53uu	54ur	55u
61rl	62ra	63ru	64rr	65ra	66ru	67rl	68ra	69rd	70rl	71ra	72rd	73ru	74rr	75r
81dl	82da	83du	84dr	85da	86du	87dl	88da	89dd	90dl	91da	92dd	93du	94dr	95d

TABLE 6. FORCE/RESPONSE DIRECTIONS

DIRECTION LEGEND					
Vertical		Lateral		Longitudinal	
Up	Down	Left	Right	Forward	Aft
U	D	L	R	F	A
Engine axis*					
u	d	l	r	f	a
(axial)					
Perpendicular		Normal		Parallel	
Up	Down	Left	Right	Forward	Aft
v	Δ	λ	ρ	γ	β



8yr	9yu	10ya	11yl	12yd
10vr	21vu	22va	23vl	24vd
12lr	33lu	34la	35ll	36ld
14yr	45yu	46ya	47yl	48yd
16vr	57vu	58va	59vl	60vd
18pr	69pu	70pa	71pl	72pd
10fr	81fu	82fa	83fl	84fd
12lr	93lu	94la	95ll	96ld
14dr	105du	106da	107dl	108dd
16fr	117du	118da	119dl	120dd
18rr	129ru	130ra	131rl	132rd
10ur	141uu	142ua	143ul	144ud

8RΔ	9Rλ	10Ra	11Rr	12Ru	37Rd	38Rl	39Ra
10AΔ	21Aλ	22Aa	23Ar	24Au	40Ad	41Al	42Aa
2DΔ	33Dλ	34Da	35Dr	36Du	43Dd	44Dl	45Da

8LΔ	9Lλ	10La	11Lr	12Lu	13La	14Ll	15Ld
3AΔ	24Aλ	25Aa	26Ar	27Au	28Aa	29Al	30Ld
8DΔ	39Dλ	40Da	41Dr	42Du	43Da	44Dl	45Dd

*Center engine mount considered on engine axis for all tests.

**Phase 1 only (engine removed) matrices 1, 2, and 3.

***Boxes refer to tests reported in Figures 18, 19, and 20.

8La	9Lu	10Ll	11La	12Ld	13Ll	14La	15Ld	16Lu***	17Lr	18Ld	19Ll	20Ld	21La	22Ll	23Lu
1Aa	32Au	33Al	34Aa	35Ad	36Al	37Aa	38Ad	39Au	40Ar	41Ad	42Al	43Ad	44Aa	45Al	46Au
4Da	55Du	56Dl	57Da	58Da	59Dl	60Da	61Dd	62Du	63Dr	64Dd	65Dl	66Dd	67Da	68Dl	69Du

8Ra	9Ru	10Rl	11Ra	12Rd	13Rl	14Ra	15Rd	16Ru	17Rr	18Rd	19Rl	20Rd	21Ra	22Rl	23Ru
1Aa	32Au	33Al	34Aa	35Ad	36Al	37Aa	38Ad	39Au	40Ar	41Ad	42Al	43Ad	44Aa	45Al	46Au
4Ua	55Uu	56Ul	57Ua	58Ud	59Ul	60Ua	61Ud	62Uu	63Ur	64Ud	65Ul	66Ud	67Ua	68Ul	69Uu

8ra	9rd	10rr	11ra	12rd	13ru	14rr	15rd	16rl	17rd	18ra	19rl	20ru
8fa	29fd	30fl	31ff	32fd	33fu	34fr	35fd	36fl	37fd	38fa	39fl	40fu
8ua	49ud	50ul	51ua	52uu	53uu	54ur	55ud	56ul	57ud	58ua	59ul	60uu
8ra	69rd	70rl	71ra	72rd	73ru	74rr	75rd	76rl	77rd	78ra	79rr	80ru
8da	89dd	90dl	91da	92dd	93du	94dr	95dd	96dl	97dd	98da	99dl	100dd

TEST RESULTS

The result of this series of tests is a compilation of 472 mobility plots. This complete set of experimental data is contained in a separate Volume II in the form of microfiche. Interested parties may write to Eustis Directorate, Fort Eustis, Va., for a copy of the microfiche.

Three typical plots are shown here in Figures 18, 19, and 20, which show the mobility of the front of the engine compressor case, vertically and laterally, and the vertical mobility of the turbine mid-split-line in response to main rotor longitudinal force input. The lower curve in each case is the mobility of the point in question, i. e., its velocity in inches per second resulting from a 1-pound exciting force as a function of the frequency of the exciting force. It may be seen that the 1/rev main rotor exciting frequency (8 hertz), the vertical mobility is quite low (Figure 18); at the 4/rev frequency (32 hertz), the vertical mobility (Figure 18) is low, but the lateral mobility (Figure 19) is close to a peak.

The upper curves in these figures show the phase relationship of the velocity of the test point relative to the force input. Table 6 indicates that in the case of the vertical response (Figure 18), a 90-degree phase relationship results when the longitudinal force at the rotor hub is aft and the test point moves up. Therefore, at 8 hertz the phase angle is 90 degrees and the compressor front velocity is upward when the force is directed aft.

In the case of lateral mobility (Figure 19), the phase angle for both 8 and 32 hertz is 270 degrees, which indicates that the transducer velocity is to the left when the main rotor hub force is directed aft.

The data on Figures 18 and 20 discloses an extremely interesting situation. Both figures show a relatively low mobility (0.006 and 0.002, respectively) at 32 hertz and a much higher mobility (0.06) at approximately 28 hertz. In other words, at a frequency only a few hertz below the major excitation frequency of main rotor 4/rev, an engine resonance is indicated with an amplification of at least 10. In addition, this resonance can be identified as a rigid-body pitching motion.

The phase angle at 28 hertz at the front of the compressor (Figure 18) is approximately 120 degrees, and the phase angle at 28 hertz at the turbine mid-split-line (Figure 20) is approximately 300 degrees. Therefore, the front and rear of the engine are moving 180 degrees out of phase. It was mentioned earlier that the engine acts as a rigid body at frequencies below 100 hertz. Consequently, the engine is experiencing a pitch mode at 28 hertz.

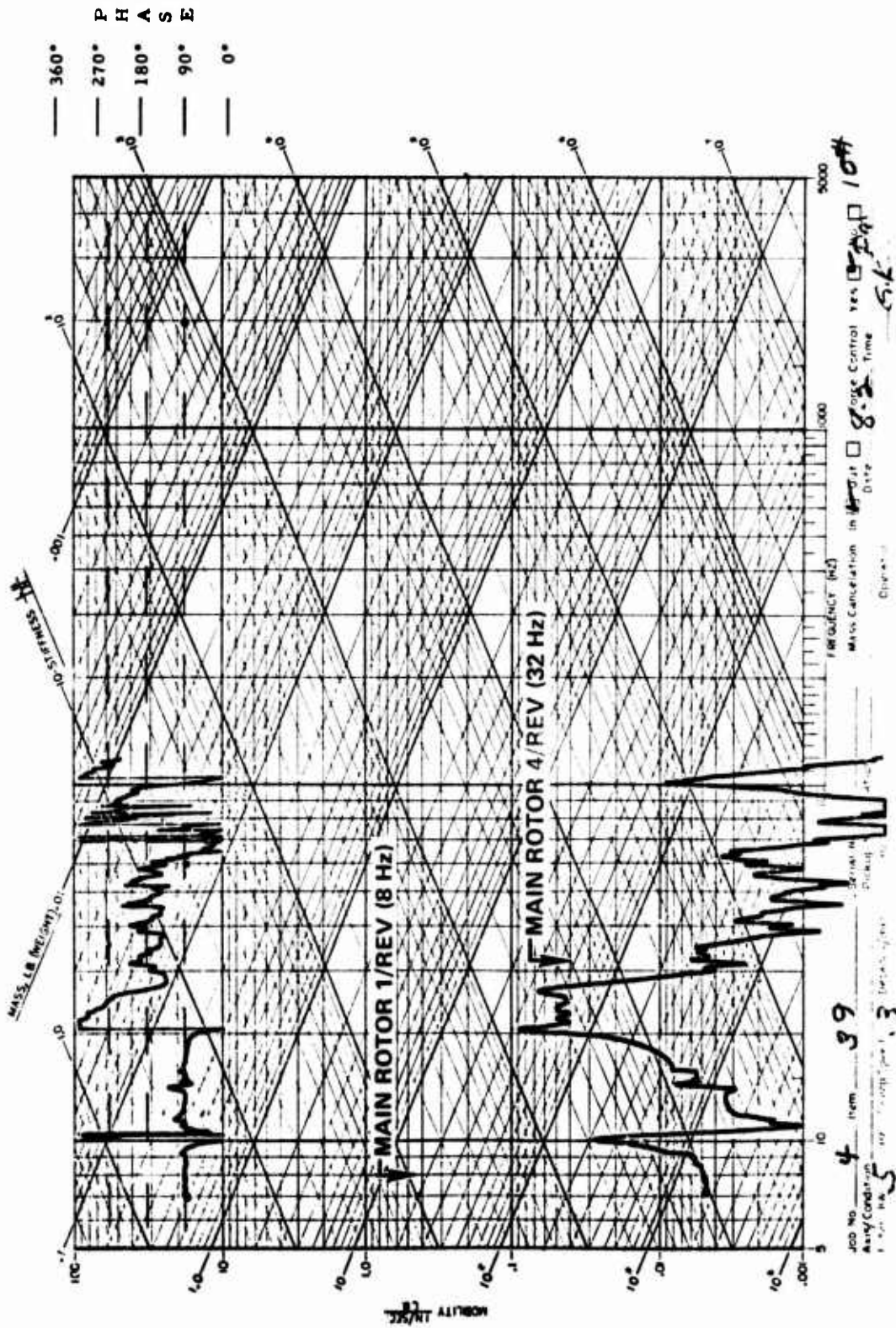


Figure 18. Engine Front Compressor - Vertical Mobility in Response to Main Rotor Longitudinal Excitation.

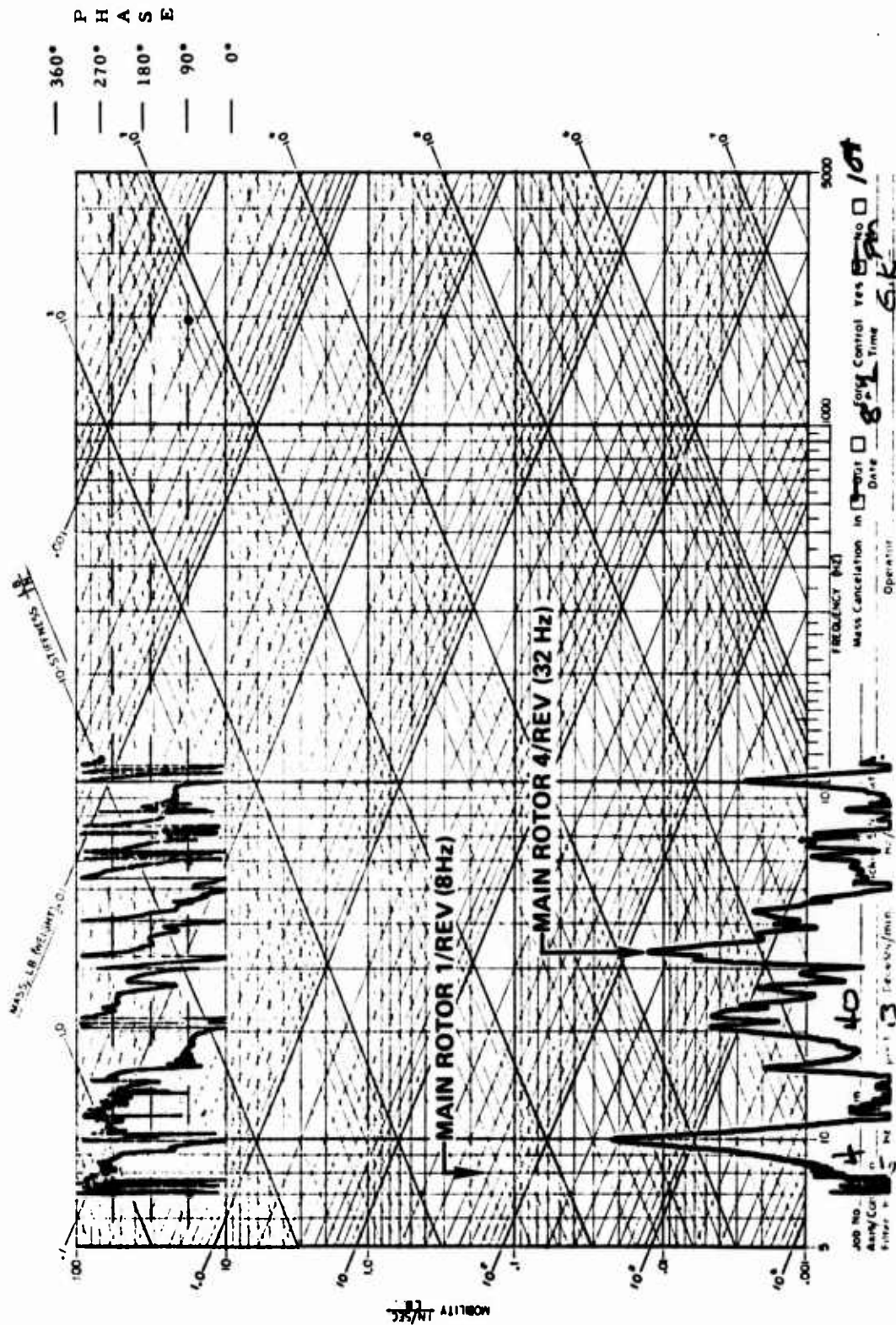


Figure 19. Engine Front Compressor - Lateral Mobility in Response to Main Rotor Longitudinal Excitation.

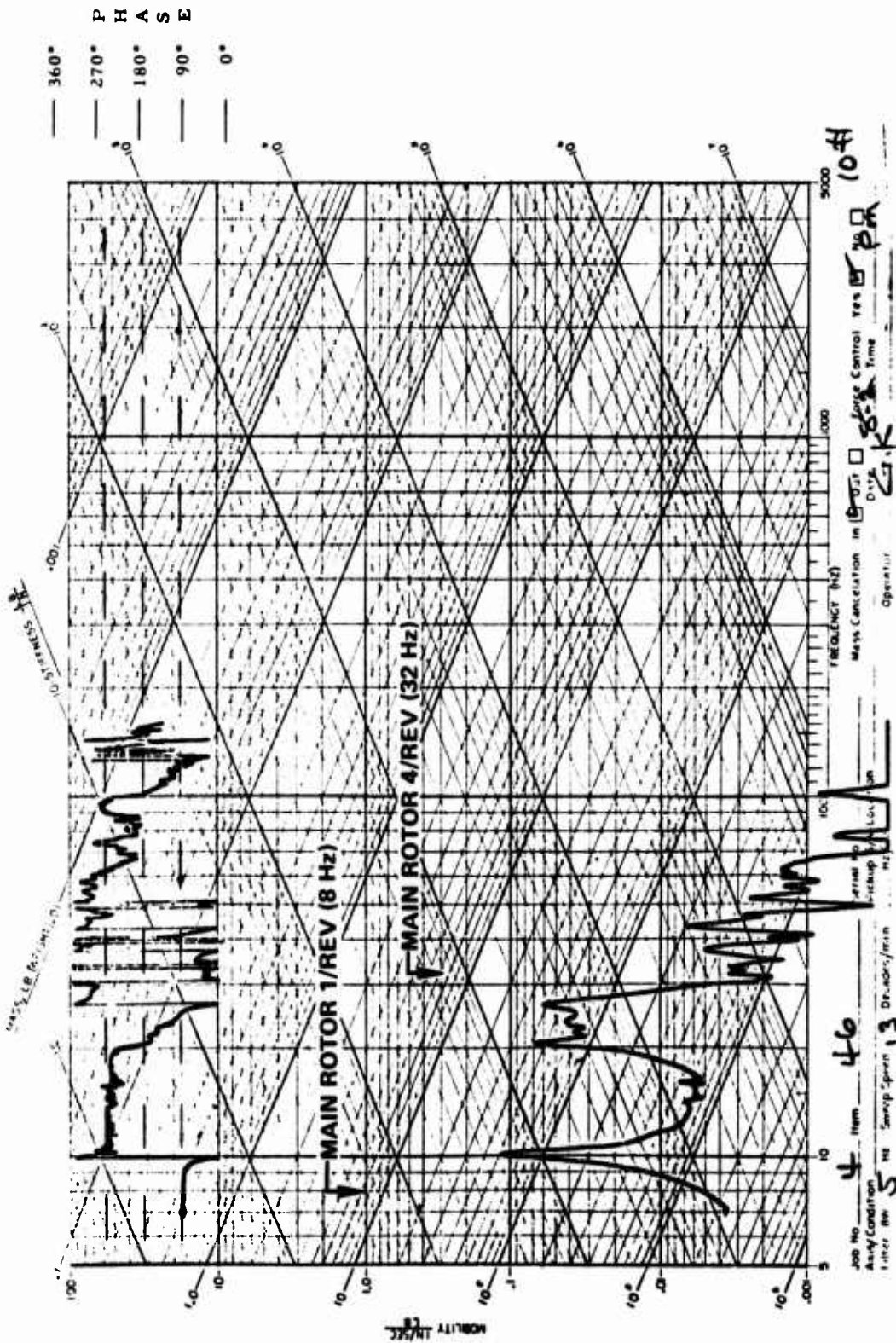


Figure 20. Turbine Mid-Split-Line - Vertical Mobility in Response to Main Rotor Longitudinal Excitation.

It was noted in Figure 9 that engine motion is occurring in cruise flight which is at the limit set by the engine manufacturer. More than 3,000,000 flight-hours have been accumulated on OH-6A helicopters with hard-mounted T63 engines without encountering any engine problems. It is clear that if the engine mounting system pitch resonance frequency were only 15 percent higher, the engine motion would probably be considerably higher and therefore would exceed the allowable velocity. This difficulty did not occur because the rigid-body pitching frequency of the installed T63 is below 32 hertz in the OH-6A (that is, below 4/rev of the main rotor).

Another example of placement of engine rigid-body modes below n/rev , where n is the number of main rotor blades, is reported on Figure 8 of Reference 2 for a three-bladed rotor and a "hard-mounted" T55 engine. A peak in engine yaw response is seen there between the $1/\text{rev}$ and $3/\text{rev}$ frequencies, and acceptable engine vibration characteristics were achieved.

These experiences with two different engines indicate that turbine engines may be hard-mounted to the structure provided that care is taken to separate rigid-body engine modes from primary rotor excitation at $1/\text{rev}$ or n/rev .

ESTIMATED LIMITING ENGINE VIBRATION SPECTRUM

It was pointed out on pages 20, 27, and 30 that a goal of this report would be to present a spectrum of engine vibration for typical mission operation, and that that spectrum would be based on Reference 8. Table 4 shows that spectrum. The manner in which Table 4 was prepared is discussed in this section.

Reference 8 reports flights of the Number 3 prototype YOH-6 (SN N9697F). Among other quantities, the helicopter's instrumentation measured lateral and longitudinal bending moments in the nonrotating main rotor mast.

A separate flight program was conducted on this same helicopter with accelerometers installed on the engine by the engine manufacturer to measure in-flight engine vibration characteristics. These engine vibration characteristics are shown in Table 1 and Figure 1 from Reference 7. (This aircraft was not available for the mobility tests of this study.)

The flight-test data discussed here and the mobility-test data discussed on page 33 were measured on two structurally different aircraft: prototype YOH-6 for flight and production OH-6A for mobility. There were numerous structural changes between the prototype and production helicopters that could be responsible for significant differences in their dynamic characteristics. This point will be discussed again later.

PERIODIC FORCES BASED ON FLIGHT DATA

Representative applied periodic forces at the main rotor hub are derived from a combination of rotor hub forces determined by calculation and mast bending moments measured in the Reference 8 TIA tests. An analytical prediction of the influence of the pendular dampers that the OH-6A uses to minimize 3/rev and 5/rev force and moments from the rotor is reported in Reference 9. Table 4 of that reference lists the calculated 3/rev and 5/rev horizontal shear forces on the rotor hub. (Vertical 3/rev and 5/rev oscillatory forces are neglected because the pendular dampers substantially reduce them. The residual vertical forces introduce a small moment, discussed on page 64.

The data from Table 4 of Reference 9 leads to the following alternating shear forces for the standard tuned pendulum weights (location = 2.25 inches):

- Calculated lateral shear $F_y = 2(-15 \sin 4\psi - 27 \cos 4\psi)$ (1)
- Calculated longitudinal shear $F_x = 2(-15 \sin 4\psi + 13 \cos 4\psi)$ (2)
- Amplitude of calculated resultant lateral shear = ± 62 pounds
- Amplitude of calculated longitudinal shear = ± 40 pounds

In the TIA tests, main rotor longitudinal and lateral mast* bending moments were measured at two locations, as indicated in Figure 21.

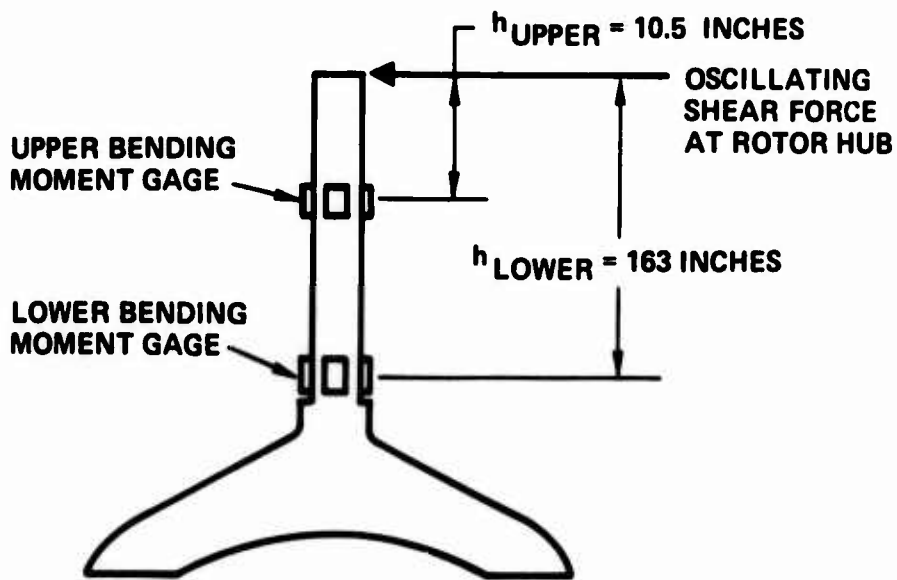


Figure 21. Rotor Mast Bending Moment Measurement.

*The OH-6A rotor mast is a nonrotating tube containing bearings at its upper end to which the rotor head is fastened. The rotor head is turned by the rotor shaft which transmits only torque. Lateral and longitudinal rotor head moments are transmitted to the rotor mast.

- 10.5 inches below the hub
 - 16.3 inches below the hub
- } average = 13.4 inches

At these moment arms, the calculated bending moments are as follows:

- Lateral, upper = 10.5 x (±62) = ±650 inch-pounds
- Lateral, lower = 16.3 x (±62) = ±1030 inch-pounds
- Longitudinal, upper = 10.5 x (±40) = ±420 inch-pounds
- Longitudinal, lower = 16.3 x (±40) = ±660 inch-pounds

The flight-measured bending moments were recorded on an oscillograph and showed themselves to be almost pure 4/rev traces. They were read as plus-and-minus so many inch-pounds of moment at the 4/rev frequency (approximately 32 hertz). The 4/rev mast moments over a range of flight speeds, plotted in Figure 22, are proportionally corrected to 1g because the tests were flown at load factors greater than 1g. There is no vertical force input data available from the flight tests because the helicopter was not instrumented to measure such forces.

The case for which the shears are calculated in Reference 9 corresponds to 112 knots at 1g ($\mu = 0.288$). Table 7 gives the comparable values for calculated and measured moments at this speed.

TABLE 7. DERIVATION OF RATIO OF TEST AND MEASURED MAST MOMENTS								
	Mast Moment (in. /lb)							
	Longitudinal				Lateral			
	Upper	Lower	Avg	Ratio (Test/ Cal)	Upper	Lower	Avg	Ratio (Test/ Cal)
Calculated	±420	±660	±540	4.90	±650	±1030	±840	2.75
Test	±1900	±3400	±2650		±1800	±2800	±2300	

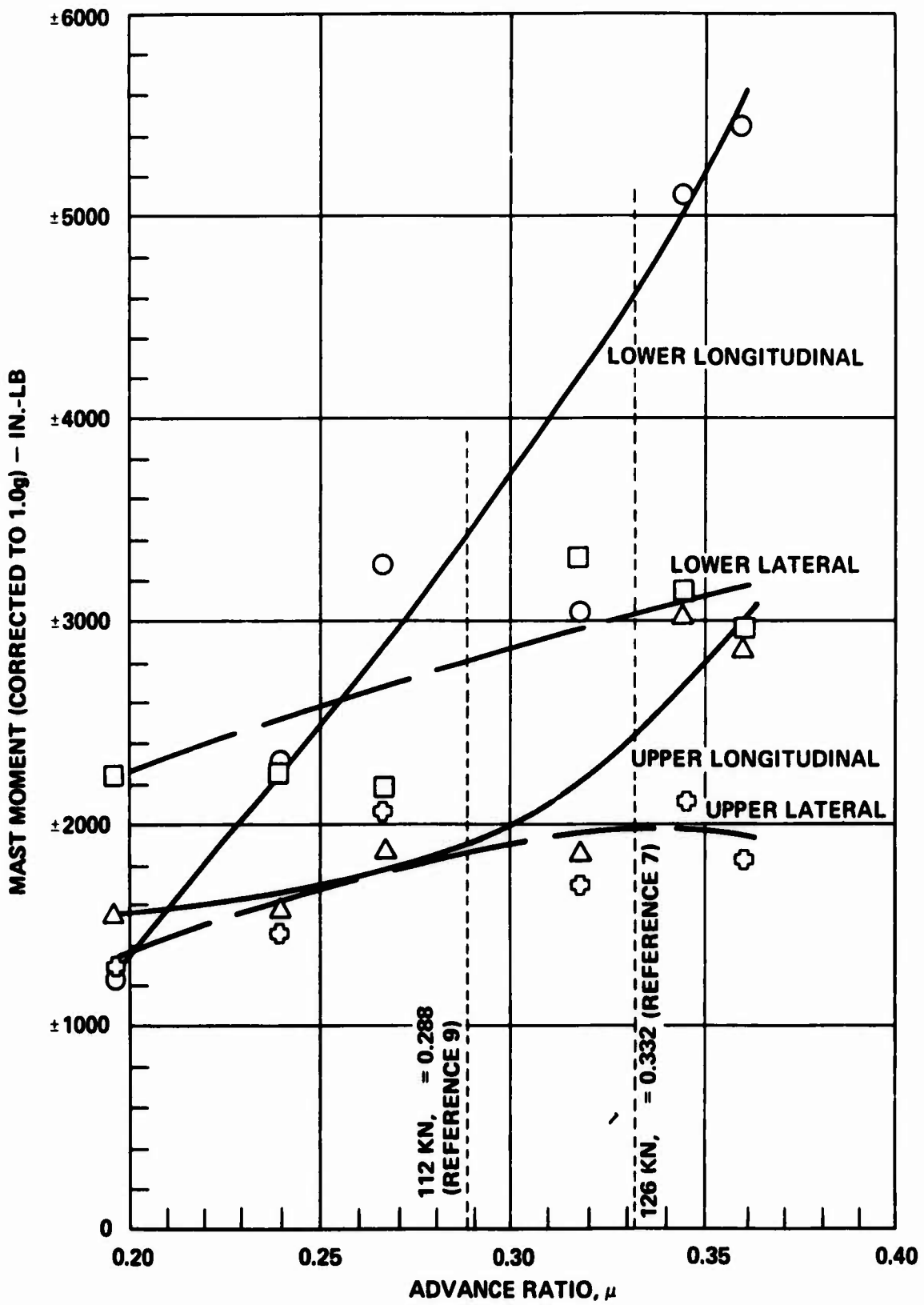


Figure 22. Rotor Mast 4/Rev Bending Moments.

Multiplying the average moment arm by the above ratios gives the following factors for converting from measured bending moments (average at the two stations) to horizontal shear at the rotor hub:

$$\text{Longitudinal factor} = 4.90 \times 13.4 \approx 66$$

$$\text{Lateral factor} = 2.75 \times 13.4 \approx 37$$

This method is demonstrated for the test point at which the engine vibration was measured (Reference 7). Here the airspeed was 126 knots. From Figure 22, the equivalent 4/rev moments and shear forces are as follows:

$$\text{Average longitudinal moment} = \pm \frac{4600 + 2400}{2} = \pm 3500 \text{ inch-pounds}$$

$$\text{Average lateral moment} = \pm \frac{3000 + 2000}{2} = \pm 2500 \text{ inch-pounds}$$

$$\text{Longitudinal shear} = \pm \frac{3500}{66} = \pm 53 \text{ pounds}$$

$$\text{Lateral shear} = \pm \frac{2500}{37} = \pm 68 \text{ pounds}$$

CALCULATED LIMITING ENGINE VIBRATION SPECTRUM

Based on this procedure, the main rotor mast bending moment test data from the TIA flight load spectrum of Reference 8 was compiled in Table 8 and converted to the equivalent shear forces as above. The resulting equivalent longitudinal and lateral shear forces are presented in Table 9.

These equivalent in-plane shear forces, multiplied by the appropriate mobility values, * will give the engine velocity measurements. To do this properly, the phase relationship between lateral and longitudinal inputs should be included, but complete correlation has not been achieved. As an alternate, the limiting engine vibration may be indicated by the sum and difference of the lateral and longitudinal responses. For instance, with engine mobility coefficients as follows,

*Take values at 32 hertz, 4/rev frequency, from Volume II.

TABLE 8. MAIN ROTOR PLUS-AND-MINUS MAST BENDING MOMENTS AT 4/REV*

Flight Condition	Percent Time	Longitudinal		Lateral	
		Upper	Lower	Upper	Lower
Hover					
Steady	2	1000	1050	1050	1600
Control reversal	1	1200	1900	1350	1750
Level flight					
30 knots	3	1450	2250	1600	2450
75 knots	21	1750	2850	1450	3000
100 knots	26	1700	2850	1750	2300
130 knots	17	2850	5150	1900	3000
Level flight, 2g turn					
50 knots	2	3650	4900	4650	7100
130 knots	2	3300	5500	3050	1900
2g pull-up, 100 knots	2	3750	2600	2550	3400
Level flight control reversal, 130 knots	3	12600	14800	4650	7300
Lateral flight	1	1900	2100	1200	2000
Maximum climb					
60 knots	6	1850	2550	2050	2850
Dive, 140 knots	1	4350	6600	4600	5700
Enter autorotation					
75 knots	1	1850	2300	1000	1600
Autorotation, 60 knots	3	2700	5400	1800	2900
Autorotation approach to landing	2	11200	13650	3700	5450
Autorotation turn.					
40 knots	1	1650	2400	800	1200
75 knots	1	2200	2800	5100	3000
120 knots	1	4450	4150	1650	2700
Hard landing	-				

*Data averaged from Reference 8 tests; level flight data adjusted to 1g.

TABLE 9. EQUIVALENT ROTOR SHEAR FORCES AND
CALCULATED COMPRESSOR FRONT MOTION

	Percent Time	Longitudinal Shear (lb)	Lateral Shear (lb)	Vertical Shear (lb)	Calculated Compressor Front Motion (in. /sec)
Hover					
Steady	2	15.5	35.8		0.21
Control reversal	1	23.5	41.9		0.28
Level flight,					
30 knots	3	28.0	54.7		0.36
75 knots	21	34.8	60.1		0.41
100 knots	26	34.5	54.7		0.40
130 knots	17	60.6	66.2	69**	0.83*
Level flight, 2g turn,					
50 knots	2	64.8	158.8		0.93
130 knots	2	66.7	66.9		0.63
2g pull-up, 100 knots	2	48.1	80.4		0.56
Level flight control					
reversal, 130 knots	3	207.6	161.5		1.70
Lateral flight	1	30.3	43.2		0.33
Maximum climb,					
60 knots	6	33.3	66.2		0.43
Dive, 140 knots	1	83.0	139.2		0.97
Enter autorotation,					
75 knots	1	31.4	35.1		0.31
Autorotation, 60 knots	3	61.4	63.5		0.59
Autorotation approach to landing	2	188.2	123.6		1.55
Autorotation turn,					
40 knots	1	30.7	27.0		0.27
75 knots	1	37.9	109.4		0.60
120 knots	1	65.2	58.8		0.59
Hard landing	-	-	-		-
Miscellaneous	4	-	-		-

*For level flight, 130 knots, vertical compressor motion is
 $(0.0060 \times 60.6) + (0.0034 \times 66.2) + (0.0035 \times 69.0) = 0.83 \text{ in. /sec.}$

**Calculated value at 4/rev.

$$M_{\text{compressor front, vertical}} = 0.0060 \text{ in./sec/lb (longitudinal)}$$

$$M_{\text{compressor front, vertical}} = 0.0034 \text{ in./sec/lb (lateral)}$$

the limiting engine vibration velocity is

$$V_{\text{compressor front, vertical}} = (0.0060 \times 53) \pm (0.0034 \times 68)$$

$$= 0.32 \pm 0.23$$

$$= 0.55, 0.09 \text{ in./sec}$$

Figure 1 and Figure 3 indicates that $V_{\text{compressor front, vertical}}$ should be 1.2 inches per second (average), or 1.88 inches per second (peak). Figure 1 and Figure 3 also indicates that $V_{\text{turbine mid split line vertical}}$ should be 0.55 inches per second (average), or 0.86 inches per second (peak), at 4/rev (32 Hz).

It is apparent that the magnitude of in-plane forces derived here is not sufficient to obtain correlation between predicted and measured engine motion. The effect of vertical 4/rev forces was therefore sought. No flight-test data was available for these forces, so a calculation of 4/rev forces at a typical case of 130 knots was made and is included as noted in Table 9. The appropriate engine mobility coefficient was taken from Volume II.

$$M_{\text{compressor front, vertical}} = 0.0035 \text{ in./sec/lb (vertical)}$$

The effect of this vertical 4/rev force is given in the note on Table 9, and the predicted engine motion is increased to 0.83 inch per second, compared to 0.59 inch per second without this vertical force. Clearly, this parameter should be included; however, at this time, only this single instance can be shown.

Therefore, using the available in-plane forces only, the predicted spectrum of engine motion at the representative compressor top front locations was calculated, as shown in Table 9. This result is summarized in Table 4.

INFLUENCE OF ROTOR HEAD MOMENTS

The 4/rev rotor head moments due to residual 3/rev and 5/rev vertical forces calculated in Reference 9 are as follows:

$$M_x = 22 \cos 4\psi + 319 \sin 4\psi \quad (3)$$

$$M_y = -187 \cos 4\psi - 44 \sin 4\psi \quad (4)$$

Test equipment was not available during mobility tests to acquire moment mobility data, which could lead to calculation of an added increment of predicted engine motion. However, satisfactory correlation of the NASTRAN model has been achieved (see pages 146 and 147). Therefore, it is possible to obtain a predicted moment mobility. At 4/rev (32 hertz), the following is noted:

$$M_{\text{long}} = 8.72 \times 10^{-4} \frac{\text{in./sec}}{\text{in.-lb}}$$

$$M_{\text{lat}} = 2.86 \times 10^{-5} \frac{\text{in./sec}}{\text{in.-lb}}$$

The product of moment and mobility, without regard to phase (as employed above), leads to the incremented engine motion:

$$\Delta v = 0.18 \text{ in./sec}$$

It therefore appears that the influence of rotor head moment on engine motion is minor for the OH-6A.

AIRFRAME-WITHOUT-ENGINE MODELING

The purpose of developing a finite-element model of the airframe was to aid in the simulation of a typical design cycle of an airframe/engine interface. It is necessary to prescribe the dynamic criteria for installation before any airframe hardware is available for testing to determine its dynamic characteristics. The only feasible method to determine these characteristics is by use of an analytical model of some sort. For this program, a NASTRAN model of the OH-6A helicopter was prepared. (See Reference 12.)

The participants in this research project were also engaged in an actual design project at the same time, using a similar approach. A subjective opinion, with hindsight, is that the simulation of the design analysis process was realistic.

The major conflict in this simulation was between performing within the constraints of typical design processes and using all of the data available for this aircraft. The OH-6A is a mature aircraft with millions of flight-hours. However, the OH-6A was developed before large-scale finite-element methods were accepted practice, so there was no available model to work from. As the causes of vibration problems tend not to be local with a component such as an engine, it was necessary to develop a complete airframe model. Presumably such models are developed today as part of the airframe design effort and do not need development for airframe/engine interface investigations only.

DESCRIPTION OF DYNAMIC MODELS

The airframe was modeled using the capabilities of the MacNeal-Schwendler Corporation/NASTRAN* system. Its topology is shown in Figures 23 through 26. The tail boom, which is circular in cross section, and the empennage are modeled as beams. The remainder of the airframe is modeled with finite elements following the contours of the actual structure. The scope of modeling is indicated by an element count:

*See Appendix B.

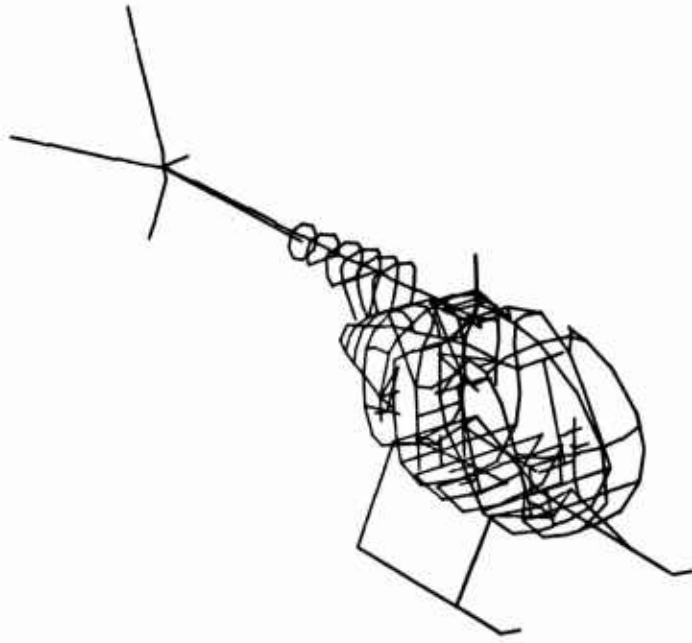


Figure 23. Isometric of Bar Elements.

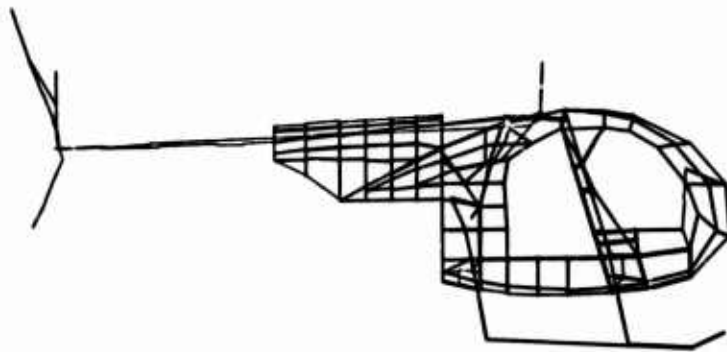


Figure 24. Side View Shear Panels and Selected Elements.

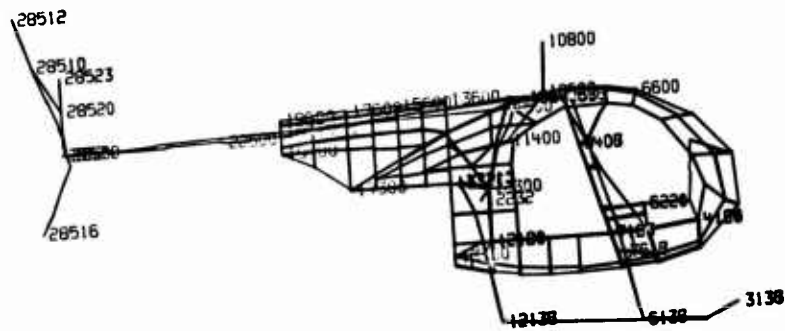


Figure 25. Selected "a Set" Grid Points - Side View.

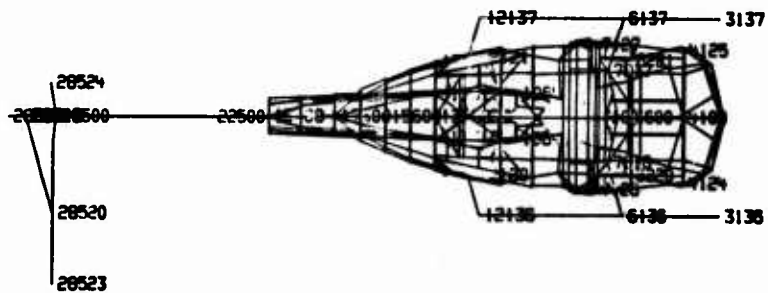


Figure 26. Selected "a Set" Grid Points - Top View
(Same Elements as Side View).

Structure

440 bar elements

586 rod elements

290 shear panels

73 triangular membrane elements

8 assorted plate and scalar elements

20 multipoint constraint equations simulating rigid connections

1417 TOTAL

Mass

Structural mass on most of the elements, plus 126 concentrated mass points (NASTRAN CONM2 CARDS)

There are 442 grid and scalar points in the model, with an average of 4.5 independent static degrees of freedom (NASTRAN "f set") per grid point. The Guyan reduction technique was used to define 145 dynamic degrees of freedom (NASTRAN "a set").

There are two mass distributions discussed below. Two ballasting configurations were required during ground vibration tests to prevent adverse center-of-gravity shifts between the engine-in and engine-out configurations.

As the intent was to use the NASTRAN model methods for dynamic response, the first milestone of modeling was to develop a dynamic model with a reasonable correlation of natural frequency and mode shape with available test data. The first phase of the development process consists of applying static loads to the model, inspecting internal loads for plausibility of distribution, and remodeling where indicated. There were five of these iterations. When a good statics model was developed, there were three iterations of mode shape calculations to match known mode natural frequencies. The model was then used to produce mobility plots, which were correlated against test mobility plots. One more model iteration was made based on the results of this correlation.

Computed mode natural frequencies versus test results are shown in Table 10. Significant mode shapes of this final model are shown in Figures 27 through 49. The dynamic degrees of freedom can be identified from the rigid-body mode shapes, where constant-length vectors appear at the "a set" points.

**TABLE 10. COMPARISON OF PREDICTED AND MEASURED
NATURAL FREQUENCIES**

Mode Number	<u>Natural Frequency (Hz)</u>				Name
	Test*	<u>Analysis</u>			
		Engine Out	Engine In		
1-6	-	0	0		Rigid-body
7	8.9	7.92	7.66		Boom lateral bending
8	8.35	8.59	8.32		Boom vertical bending
9	ND**	11.76	11.69		LG antisymmetric
10	13.5	13.87	13.84		Boom torsion
11	ND	15.22	15.21		LG symmetric
12	ND	16.26	16.27		LG antisymmetric
13	21.0	18.51	16.77		Main rotor mast longitudinal
14	ND	18.79	18.83		Horizontal stabilizer chord bending
15	ND	20.35	19.81		Lower vertical stabilizer chord bending
16	-	22.29	21.45		Main rotor mast lateral bending
	17.4	-	21.80		Engine "rigid-body" vertical
	ND	-	23.23		Engine "rigid-body" lateral
17	ND	25.66	26.97		LG antisymmetric
18	ND	26.49	26.81		LG symmetric
19	ND	27.09	27.29		LG symmetric
20	ND	28.35	28.81		LG antisymmetric
21	ND	29.09	29.02		Upper vertical stabilizer chord bending
22	ND	33.60	32.66		Tail rotor drive shaft vertical bending
23	ND	34.76	34.73		Tail rotor drive shaft lateral bending
	35.1	-	-		Mast lateral
	38.5	-	38.82		Engine "rigid-body" longitudinal

*Source: Reference 13 and tests reported herein.

**ND = Not determined in test.

Table 10 lists the predicted frequencies for modes 1 through 23 shown in Figures 27 through 49 for the engine-out (airframe-only) configuration. The predicted frequencies for modes 7, 8, and 10 show excellent agreement with the measured frequencies for boom lateral bending, boom vertical bending, and boom torsion. The predicted frequency for mode 13 shows reasonable agreement with the measured frequency for main rotor mast longitudinal bending.

Based on the correlation for the engine-out configuration as reported for modes 7, 8, and 10, further calculations were made as reported in later sections for the engine-in configuration. The results of these calculations are also shown in Table 10 for convenience as the "Engine In" column. It is seen that the frequencies of modes 7, 8, and 10 are only slightly influenced by the inclusion of the engine; the calculated frequency for mode 13 drops about 10 percent when the engine is included.

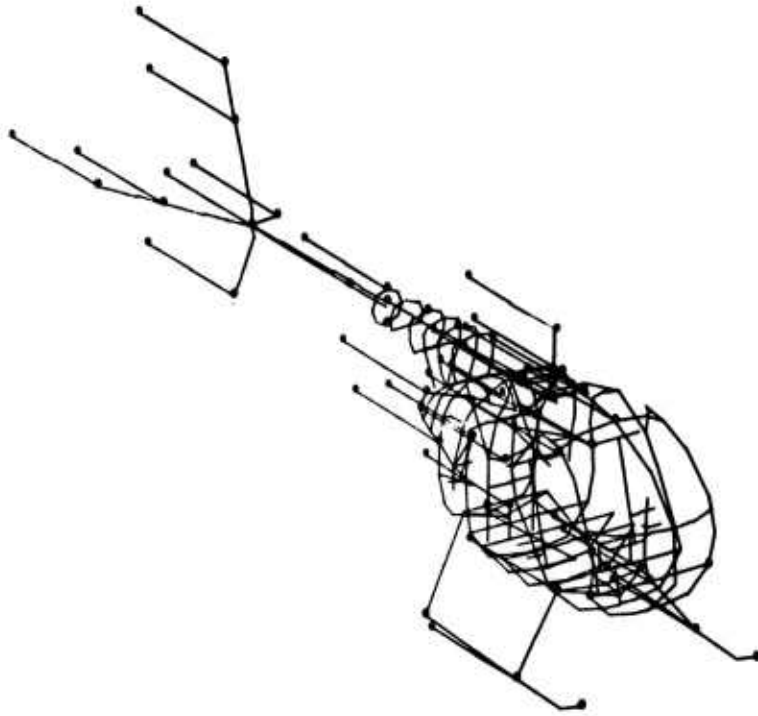


Figure 27. Rigid-Body Mode - Longitudinal.

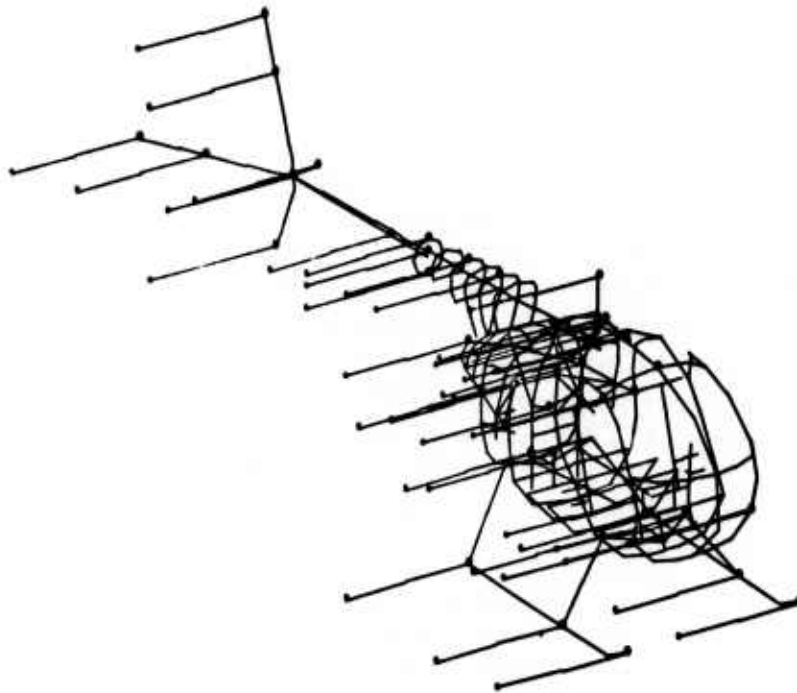


Figure 28. Rigid-Body Mode - Lateral.

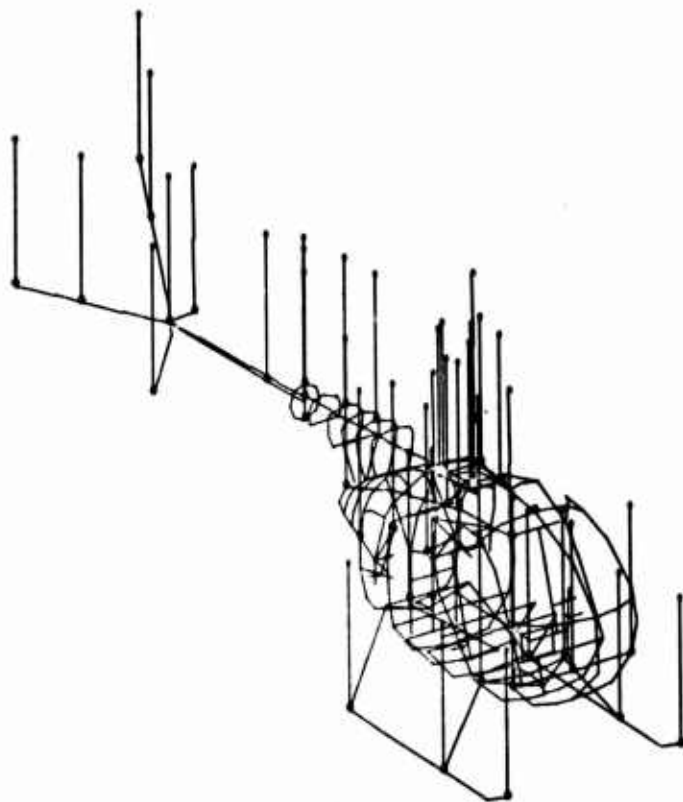


Figure 29. Rigid-Body Mode - Vertical.

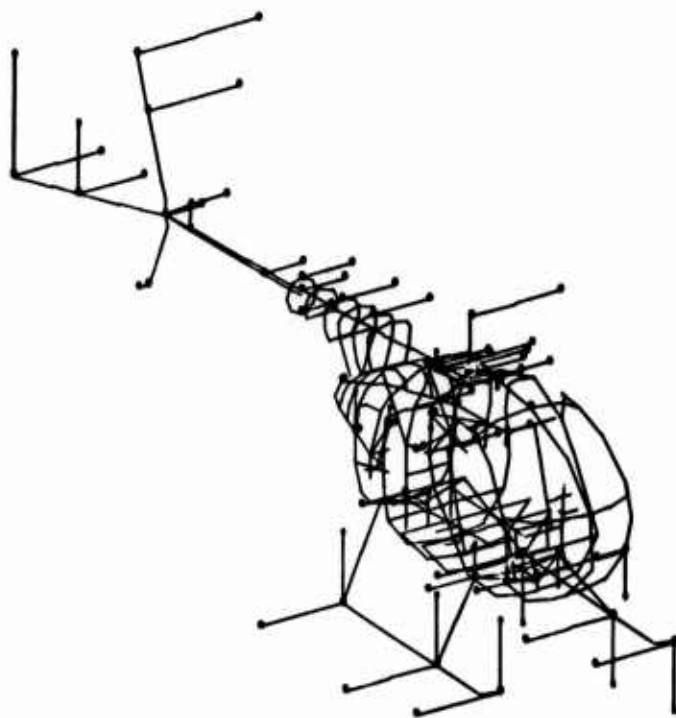


Figure 30. Rigid-Body Mode - Roll.

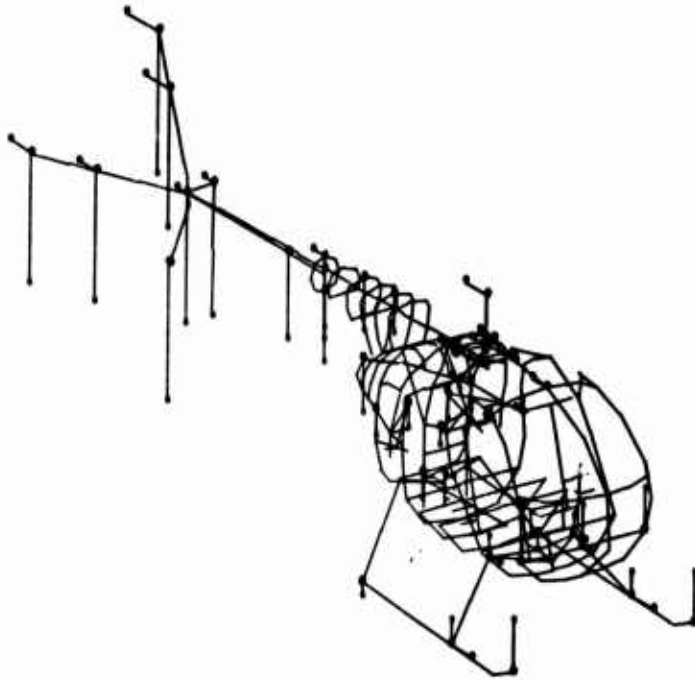


Figure 31. Rigid-Body Mode - Pitch.

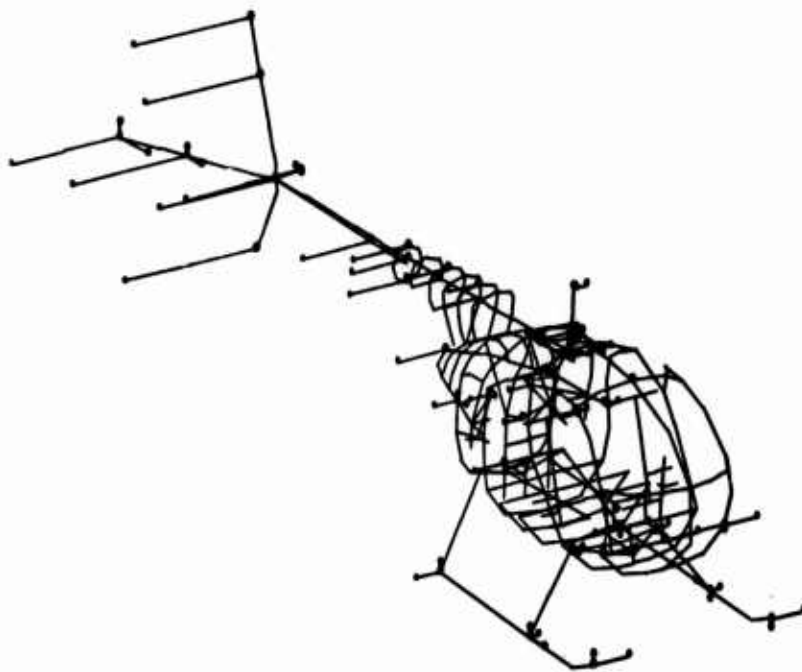


Figure 32. Rigid-Body Mode - Yaw.

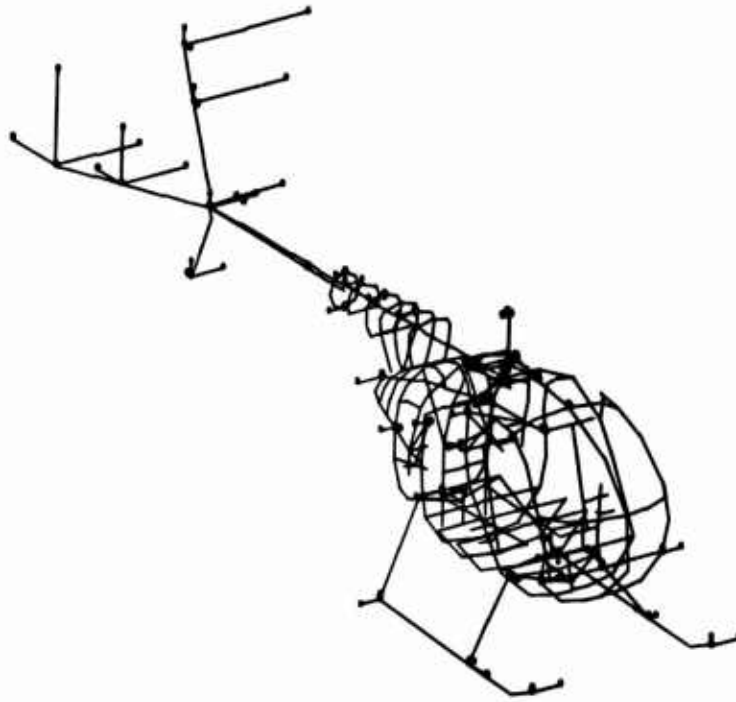


Figure 33. Mode #7 Boom Lateral Bending, 7.92 Hz.

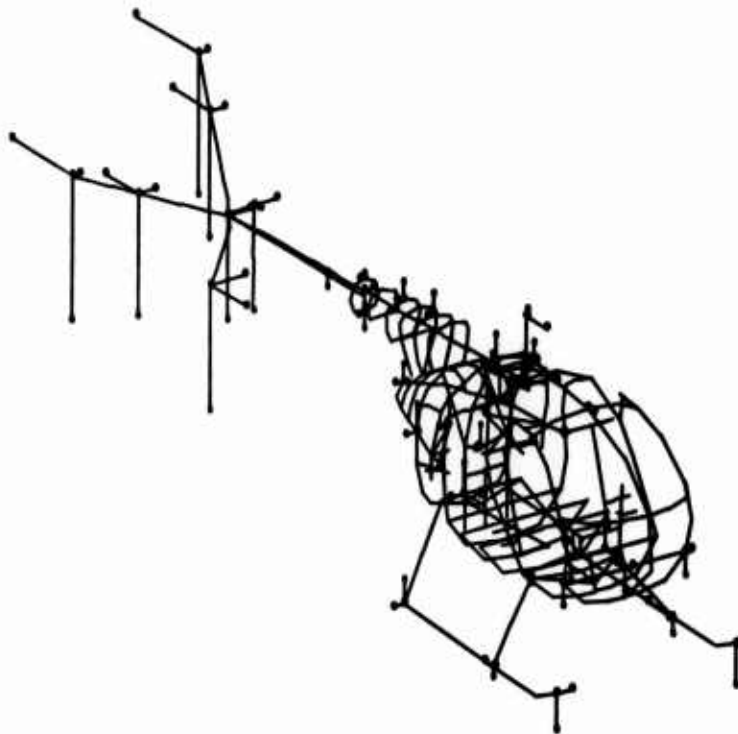


Figure 34. Mode #8 Boom Vertical Bending, 8.59 Hz.

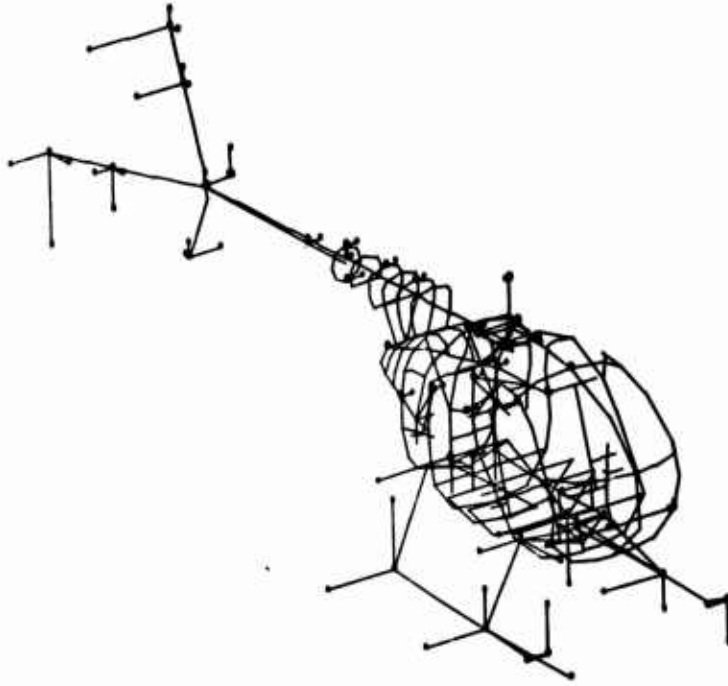


Figure 35. Mode #9 Landing Gear Longitudinal Antisymmetric, 11.76 Hz.

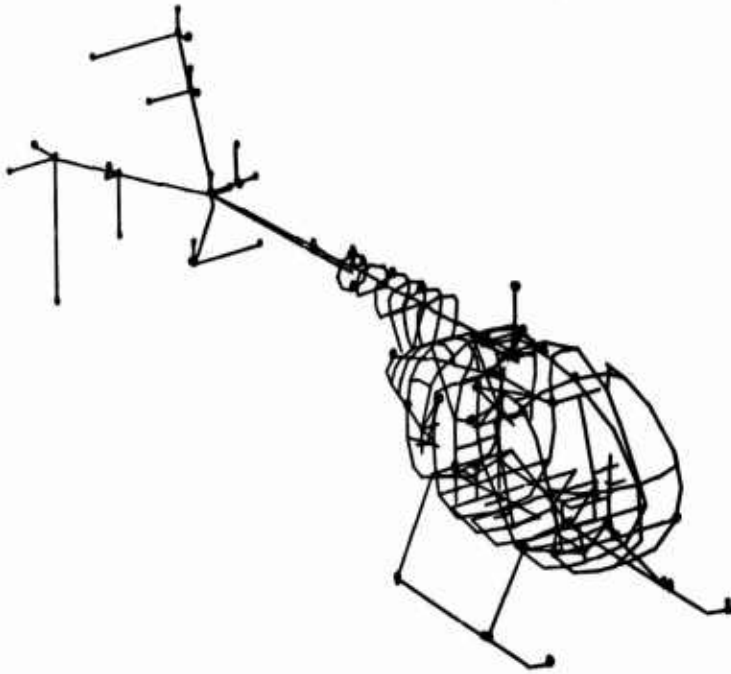


Figure 36. Mode #10 Boom Torsional, 13.87 Hz.

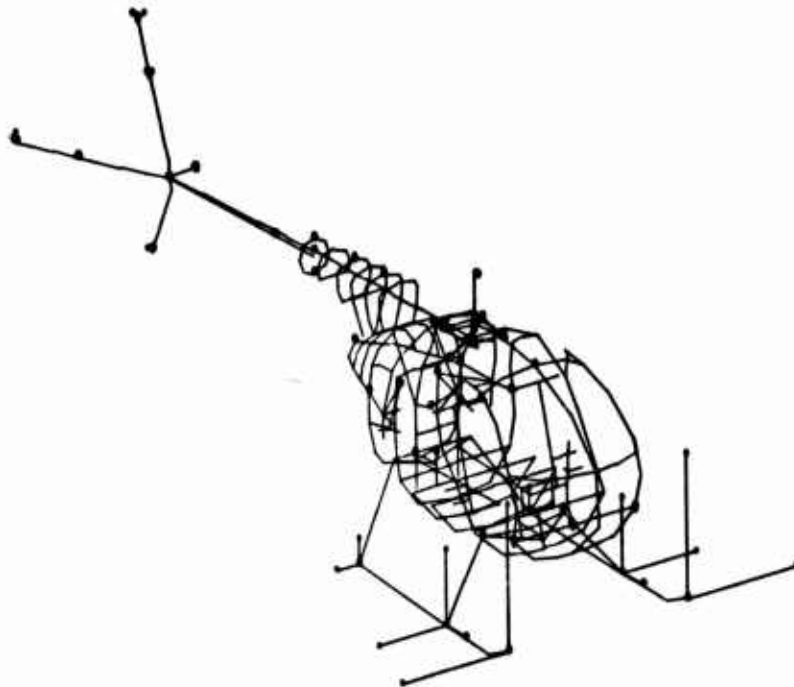


Figure 37. Mode #11 Landing Gear Lateral Symmetric, 15.22 Hz.

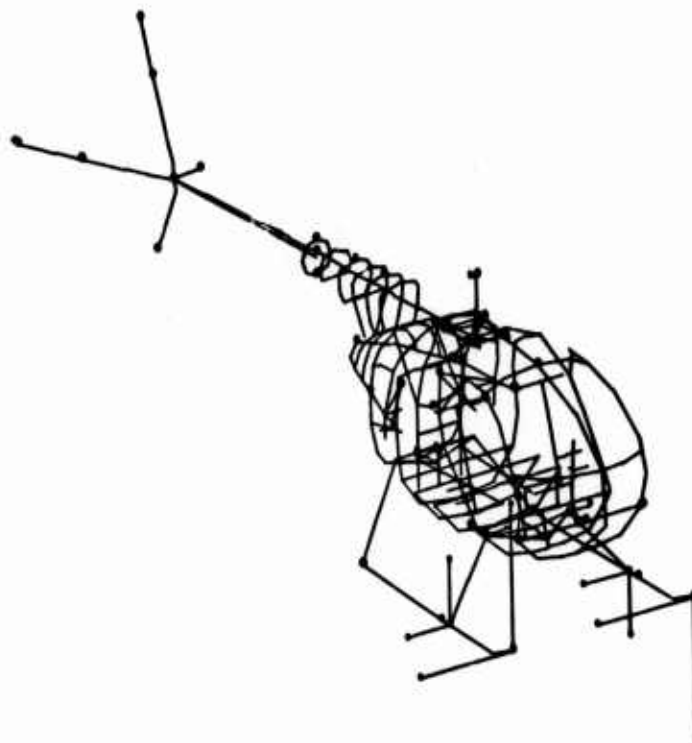


Figure 38. Mode #12 Landing Gear Lateral Antisymmetric, 16.26 Hz.

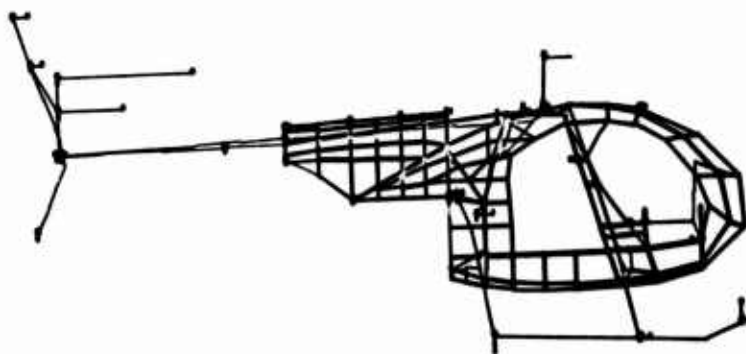


Figure 39. Mode #13 Main Rotor Mast Longitudinal, 18.51 Hz.

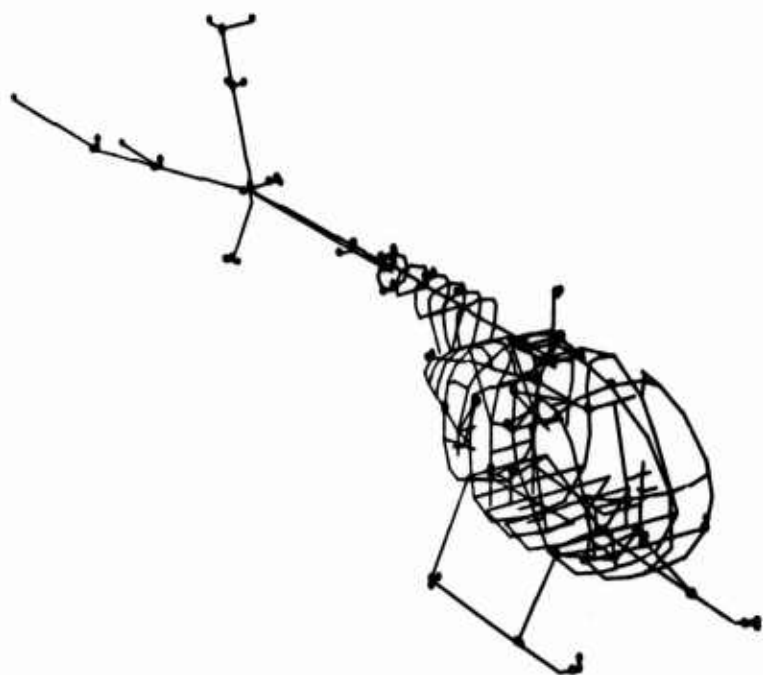


Figure 40. Mode #14 Horizontal Stabilizer Chordwise Bending, 18.79 Hz.

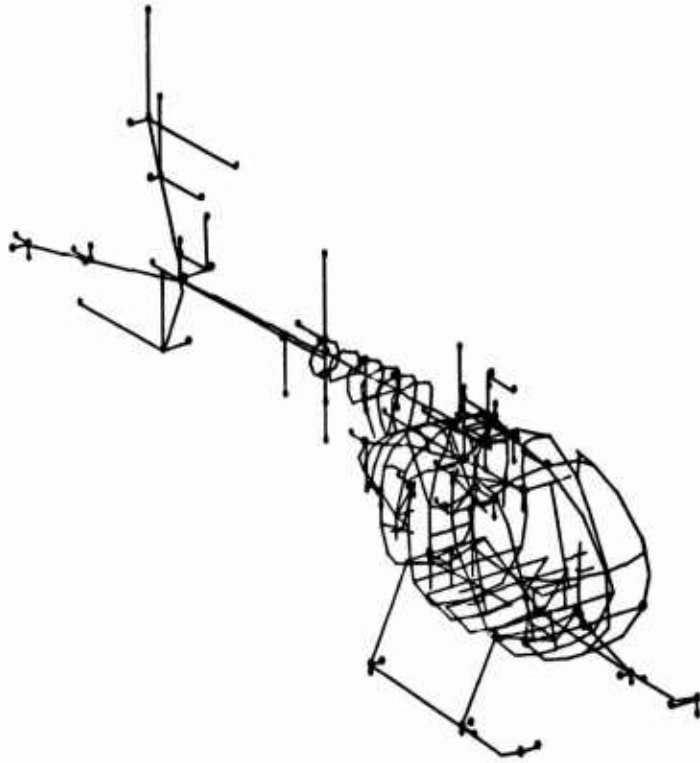


Figure 41. Mode #15 Lower Vertical Stabilizer Chordwise Bending, 20.35 Hz.

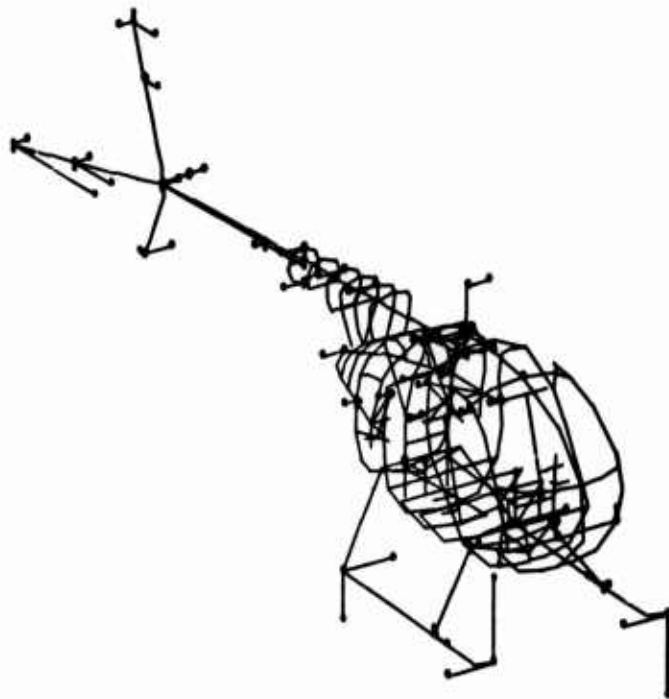


Figure 42. Mode #16 Main Rotor Mast Lateral, 22.29 Hz.

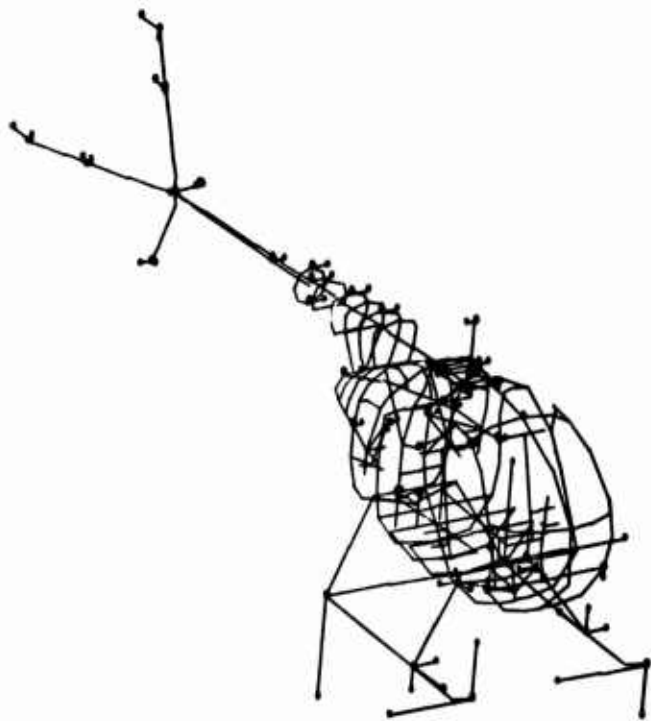


Figure 43. Mode #17 Landing Gear, 25.66 Hz.

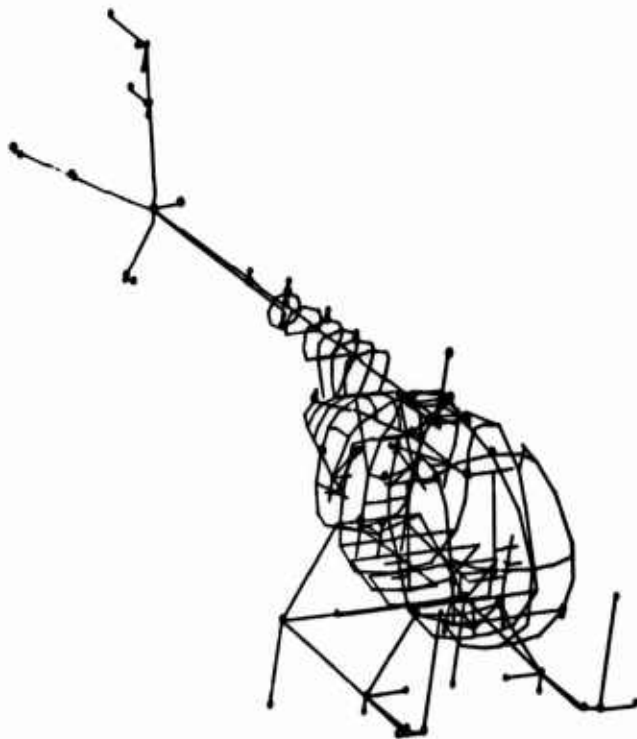


Figure 44. Mode #18 Landing Gear, 26.49 Hz.

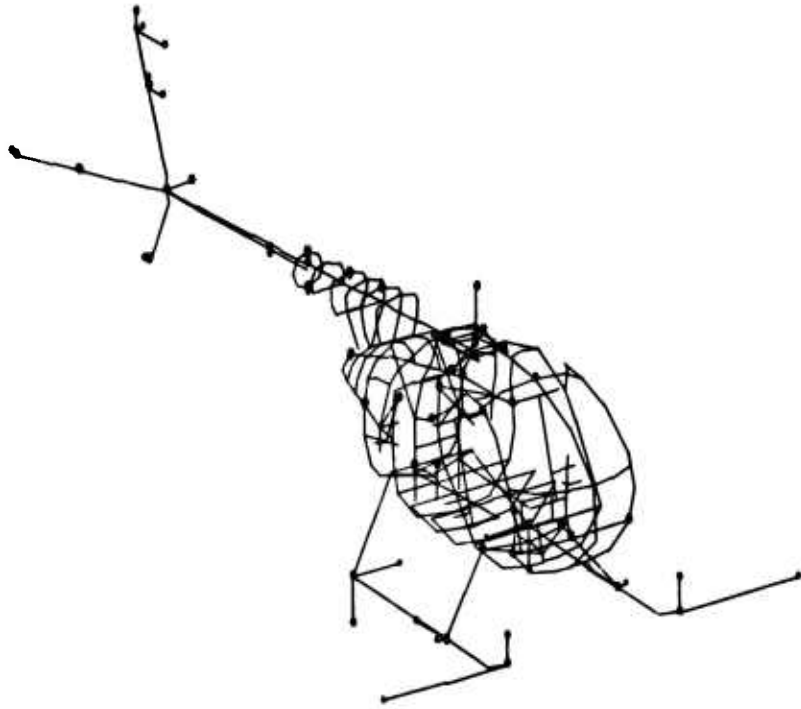


Figure 45. Mode #19 Landing Gear, 27.09 Hz.

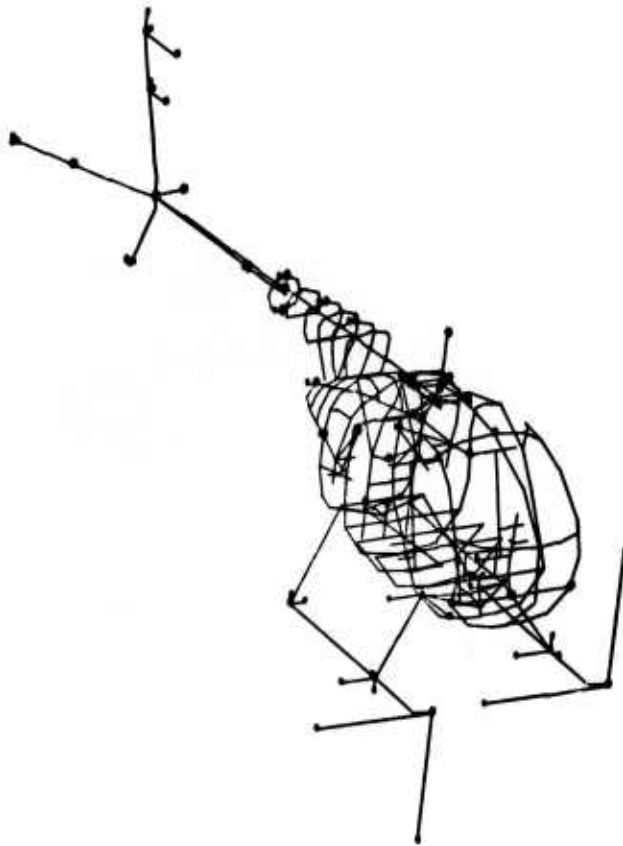


Figure 46. Mode #20 Landing Gear, 28.35 Hz.

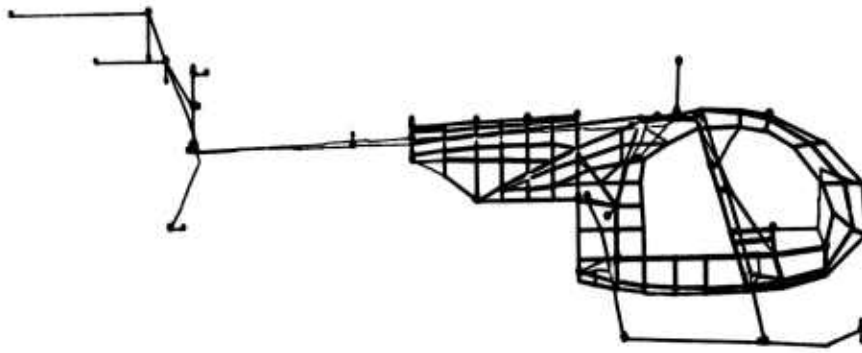


Figure 47. Mode #21 Upper Vertical Stabilizer
Chordwise Bending, 29.09 Hz.

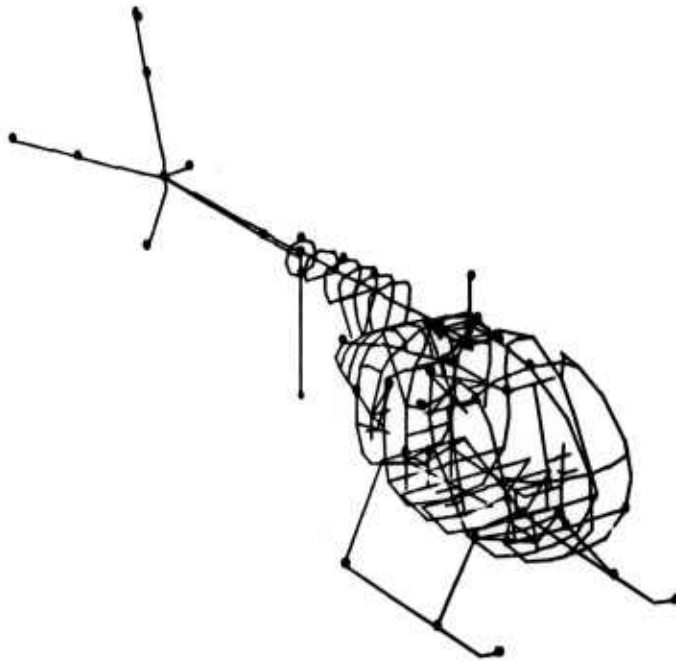


Figure 48. Mode #22 Tail Rotor Drive Shaft
Vertical Bending, 33.60 Hz.

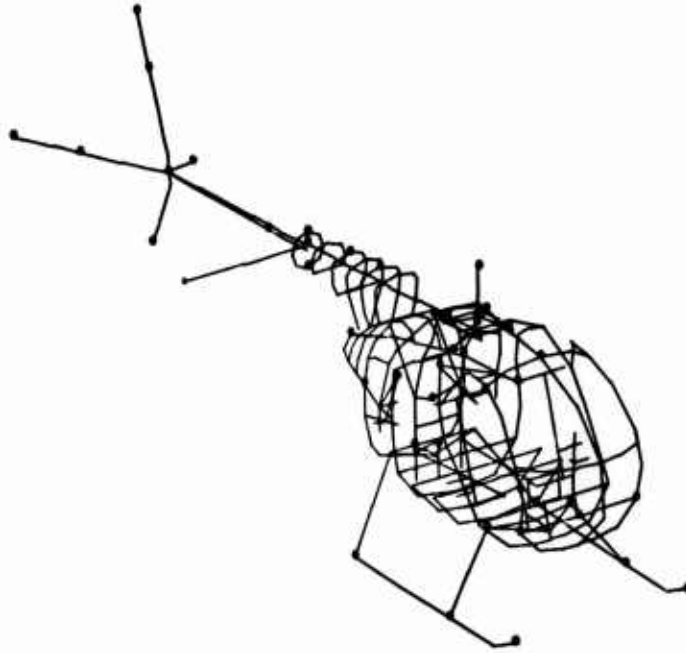


Figure 49. Mode #23 Tail Rotor Drive Shaft
Lateral Bending, 34.76 Hz.

CORRELATION OF FREQUENCY RESPONSE

As mentioned earlier, after the NASTRAN model for the airframe-only had been adjusted to obtain the correlation of measured and predicted frequencies mentioned above, this model was used to produce mobility plots. "Mobility" as used here is the velocity of a point on the structure in response to a force shaking the structure. Mobility therefore has the dimensions of inches per second per pound. If the motion is measured at the point where the force is applied, the mobility is labeled "direct mobility". If the mobility is measured at a point remote from the point where the force is applied, the mobility is called "cross mobility".

Direct-mobility calculations were made for the main rotor hub, the tail rotor hub, the three engine mount locations, and the engine/transmission coupling. These calculations are shown in Figures 50 through 67 (solid lines). Typical cross-mobility calculations for center-engine-mount motion due to shaking at the main rotor in various directions are shown in Figures 68 through 73.

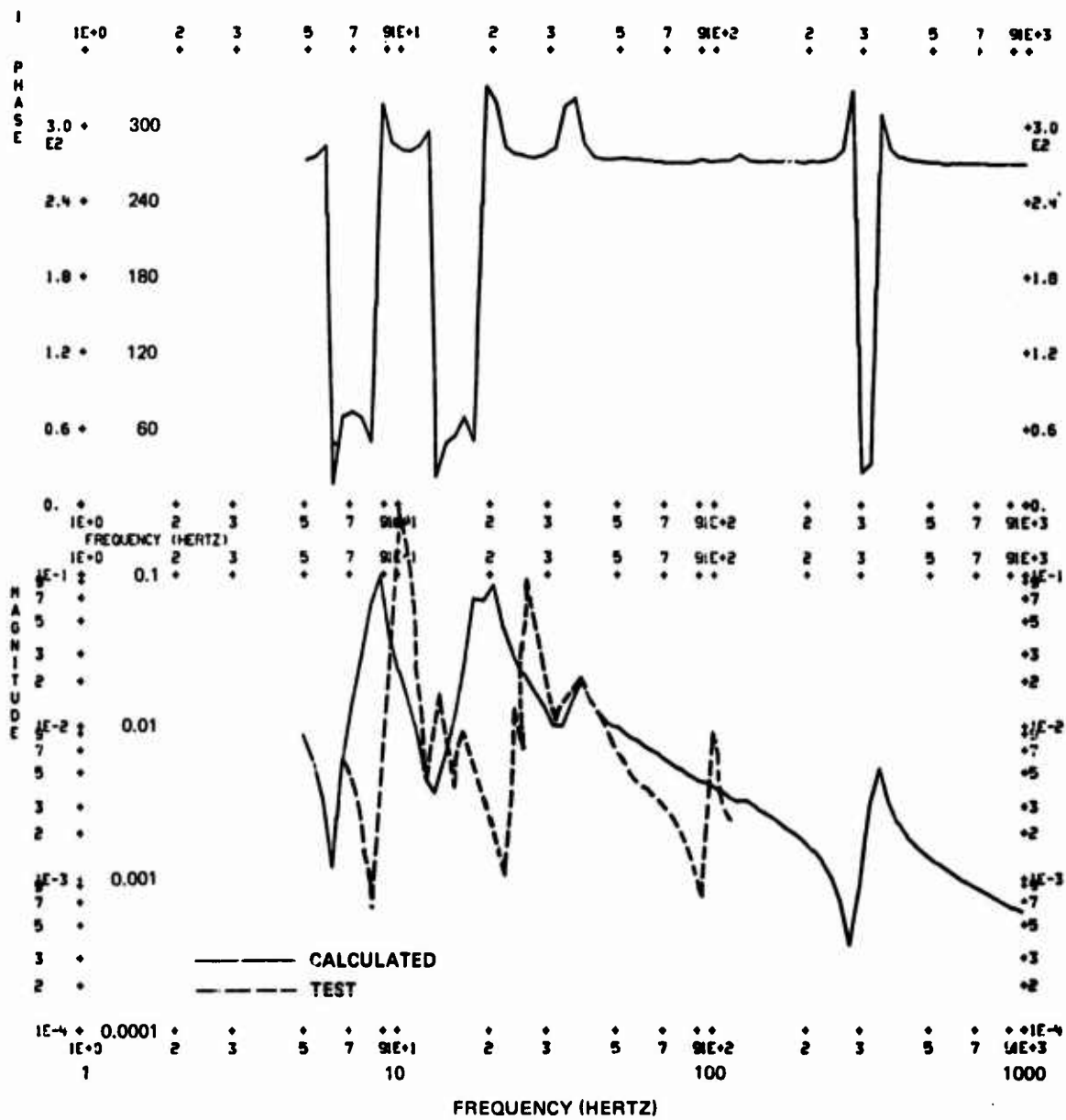


Figure 50. Direct Mobility - Main Rotor Longitudinal.

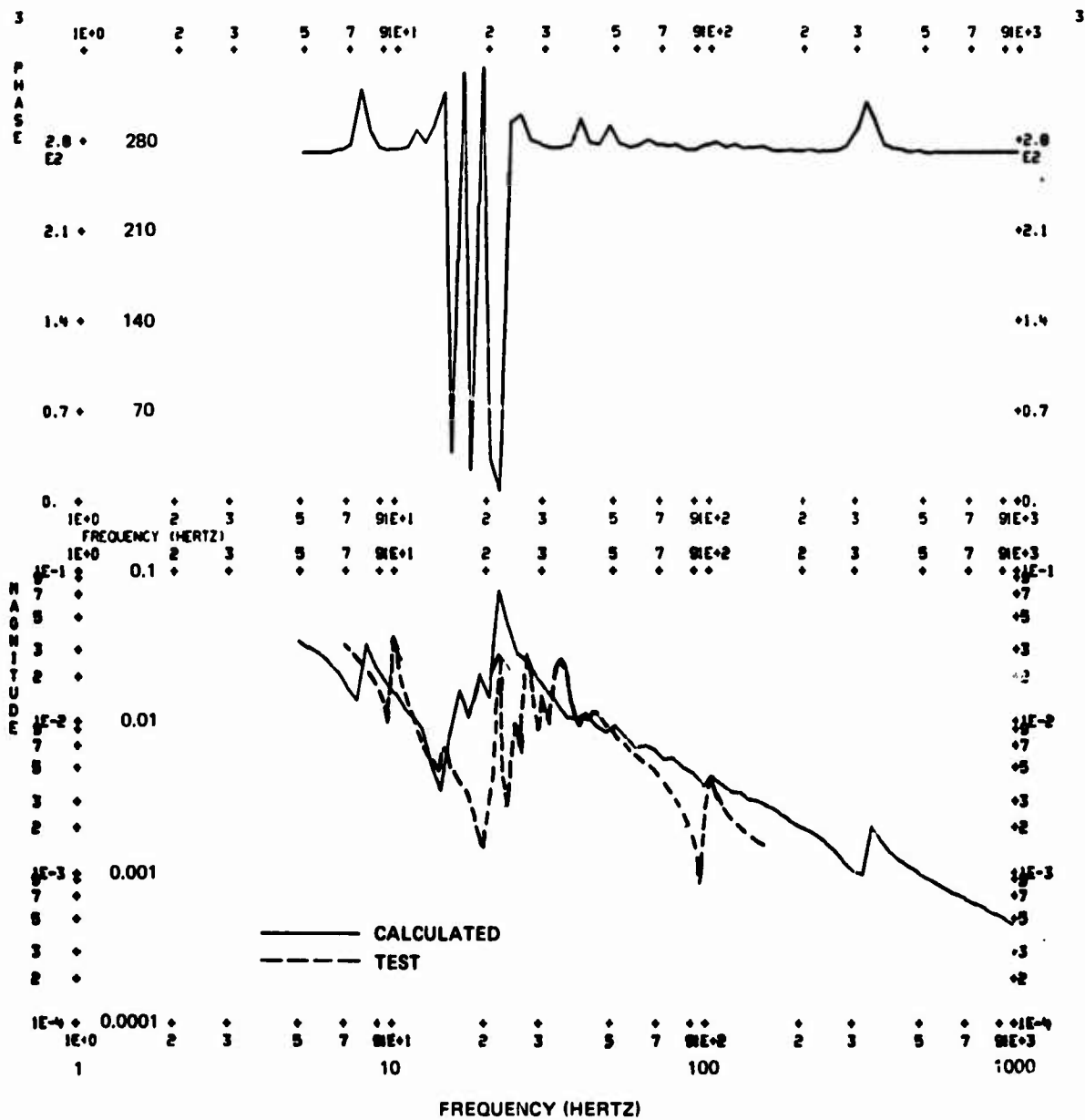


Figure 51. Direct Mobility - Main Rotor Lateral.

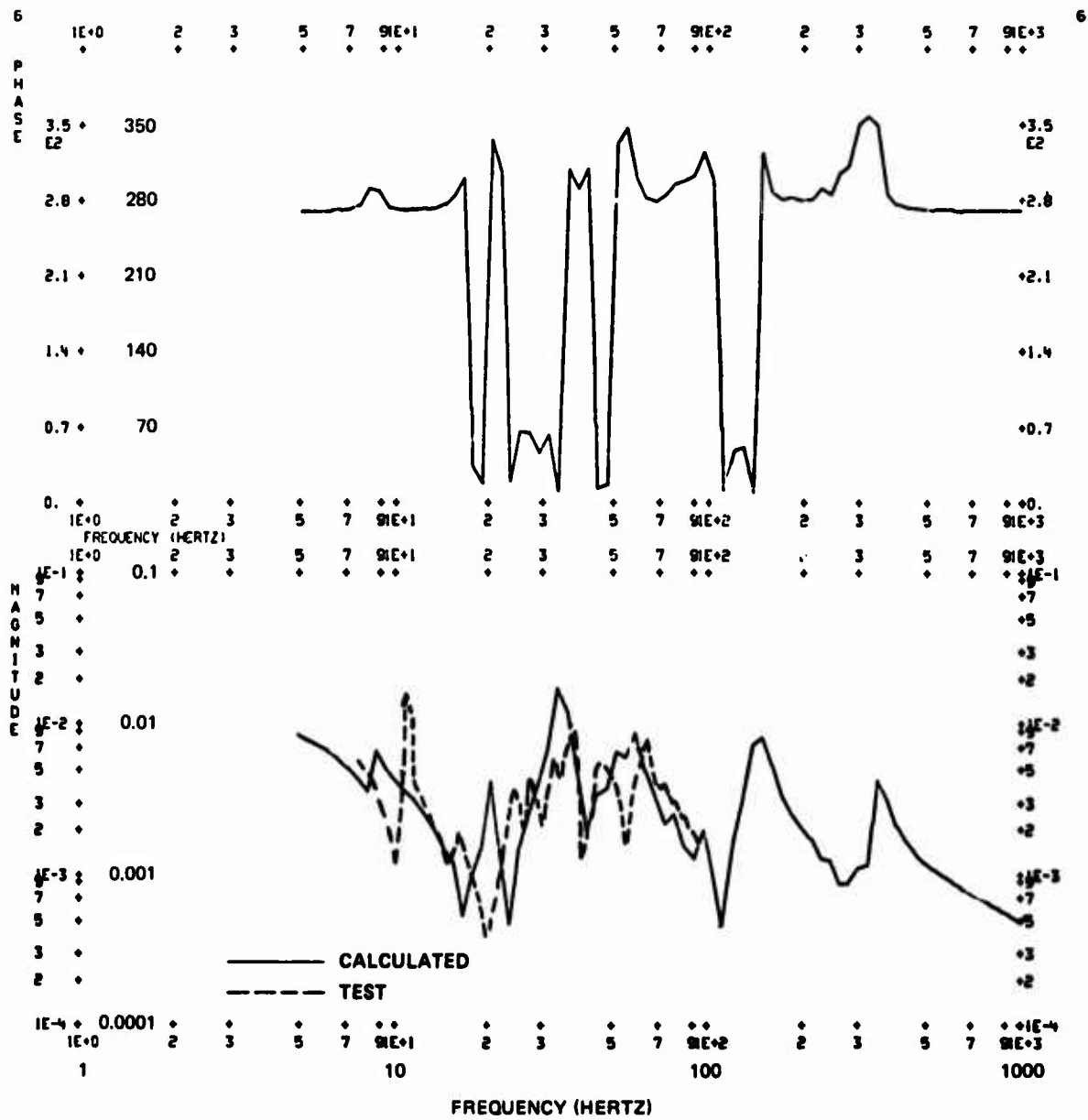


Figure 52. Direct Mobility - Main Rotor Vertical.

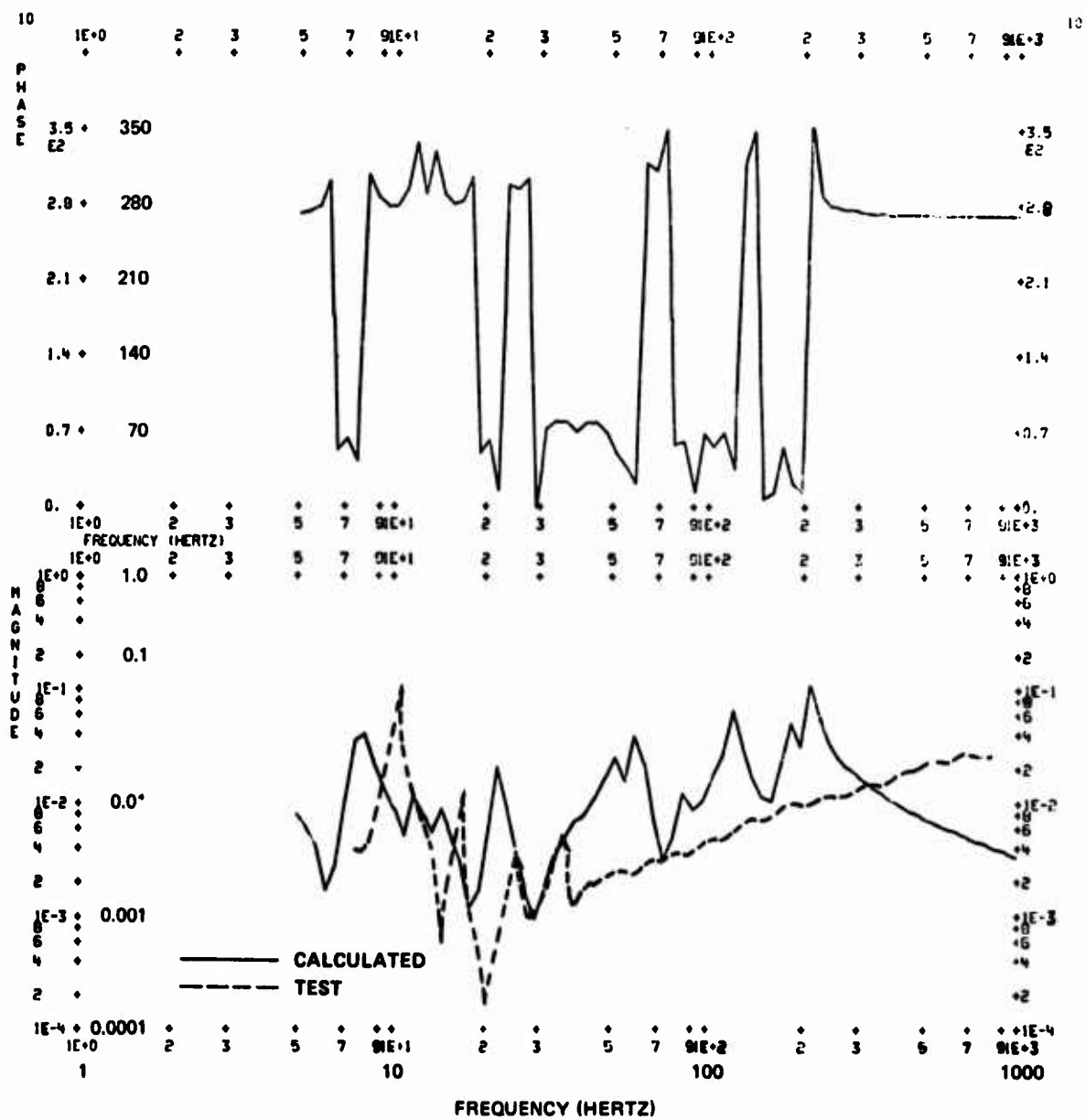


Figure 53. Direct Mobility - Center Mount Perpendicular.

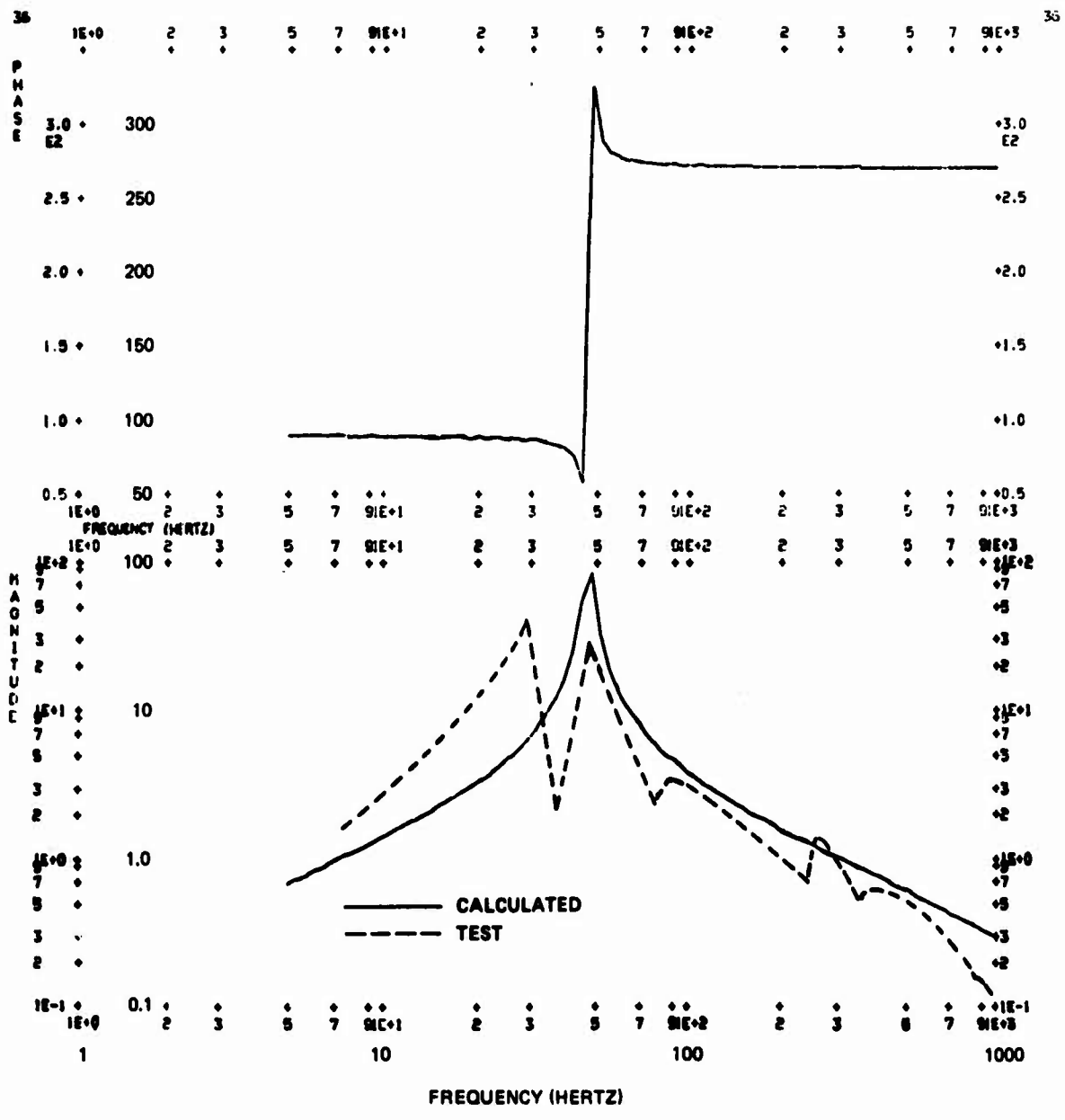


Figure 57. Direct Mobility - Right-Hand Mount Normal.

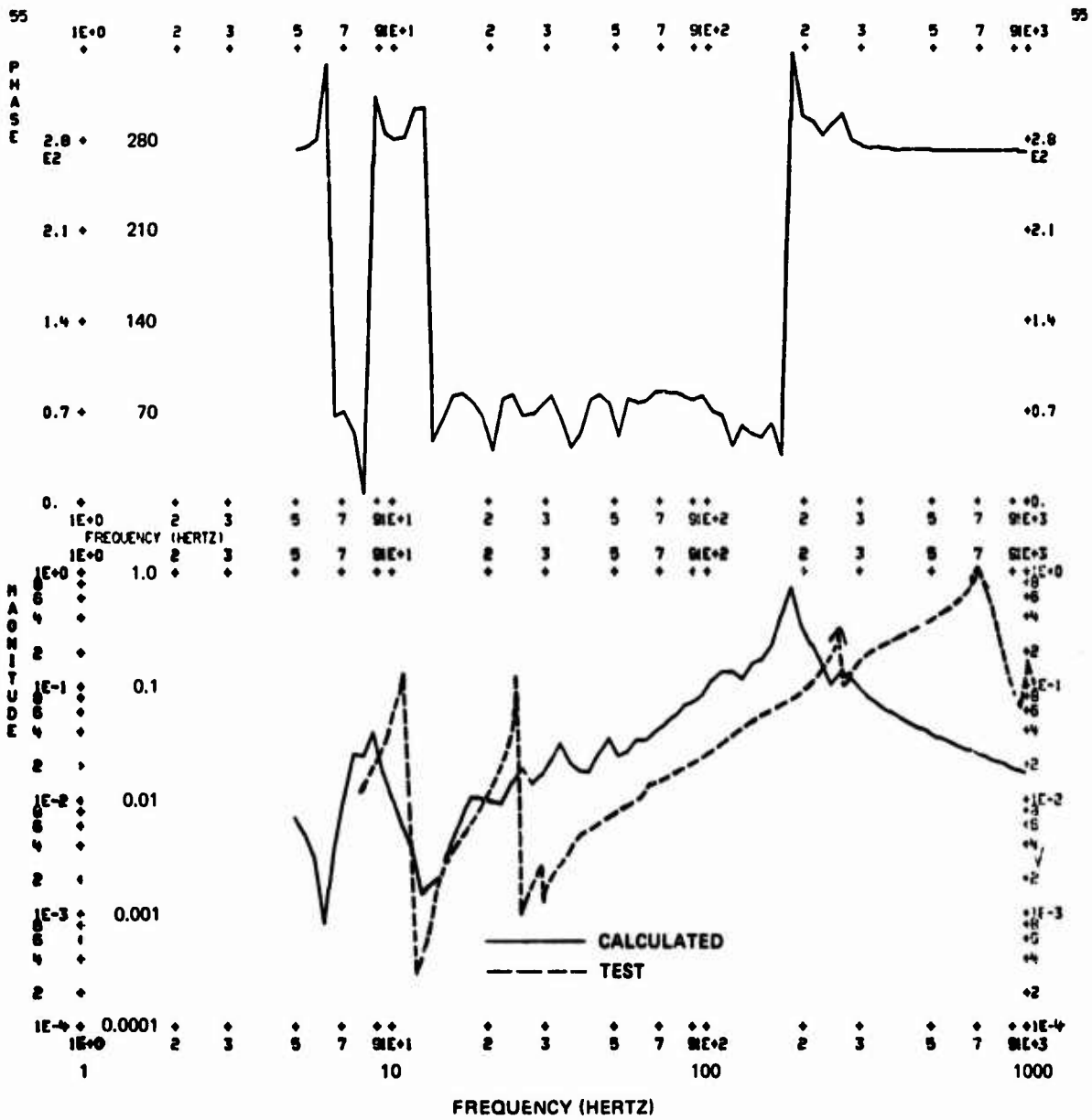


Figure 59. Direct Mobility - Left-Hand Mount Perpendicular.

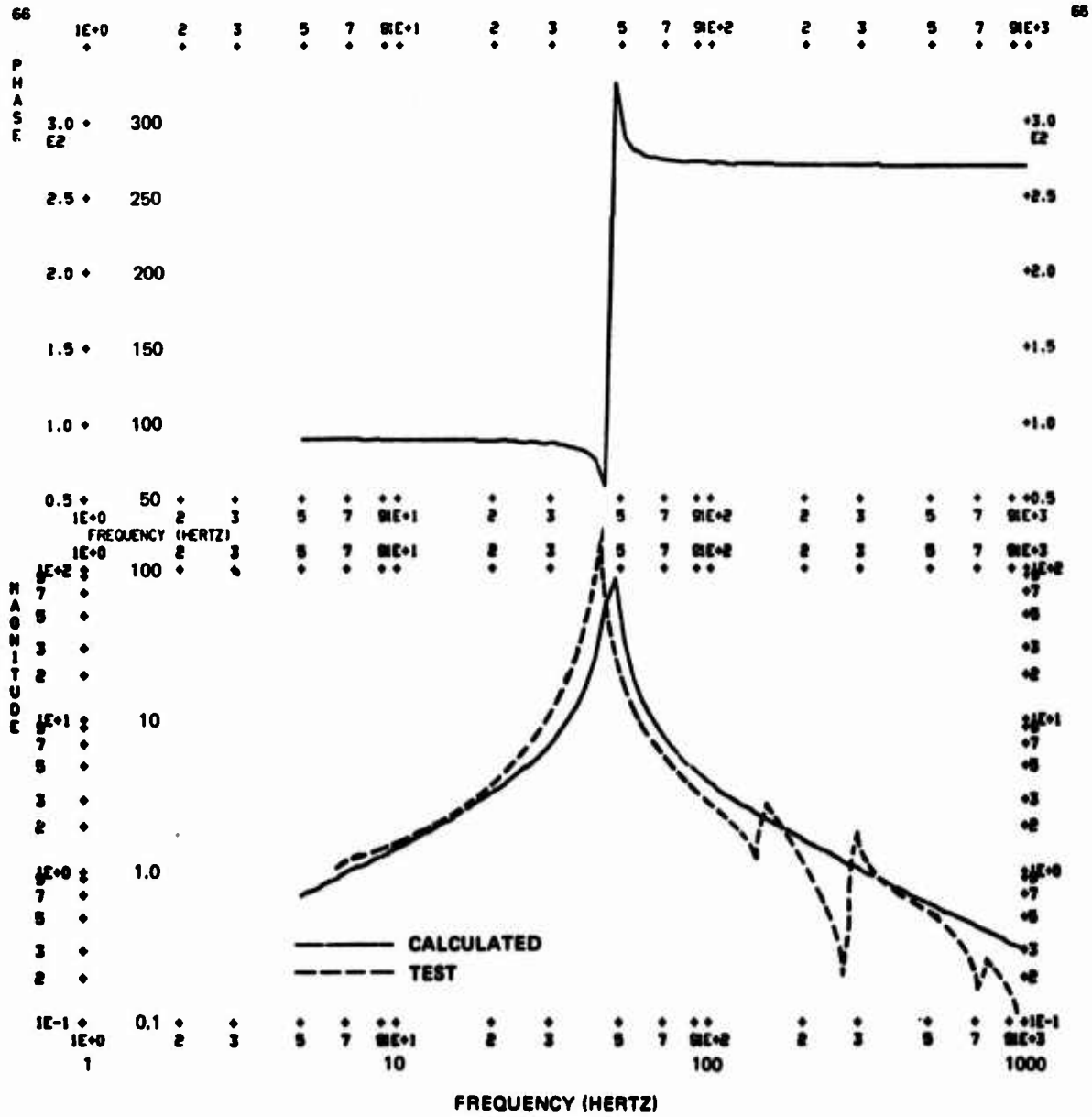


Figure 60. Direct Mobility - Left-Hand Mount Normal.

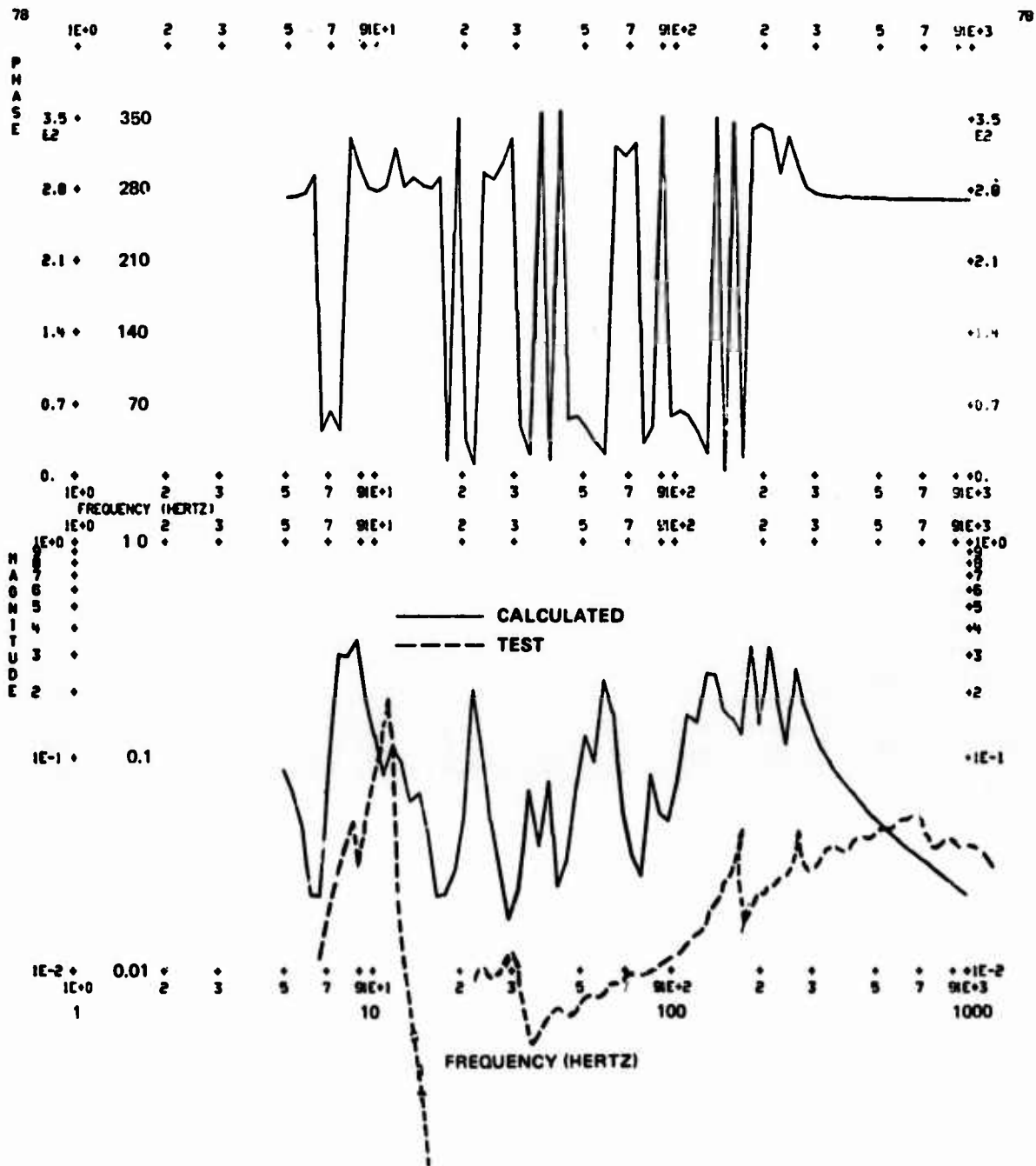


Figure 61. Direct Mobility - Left-Hand Mount Parallel.

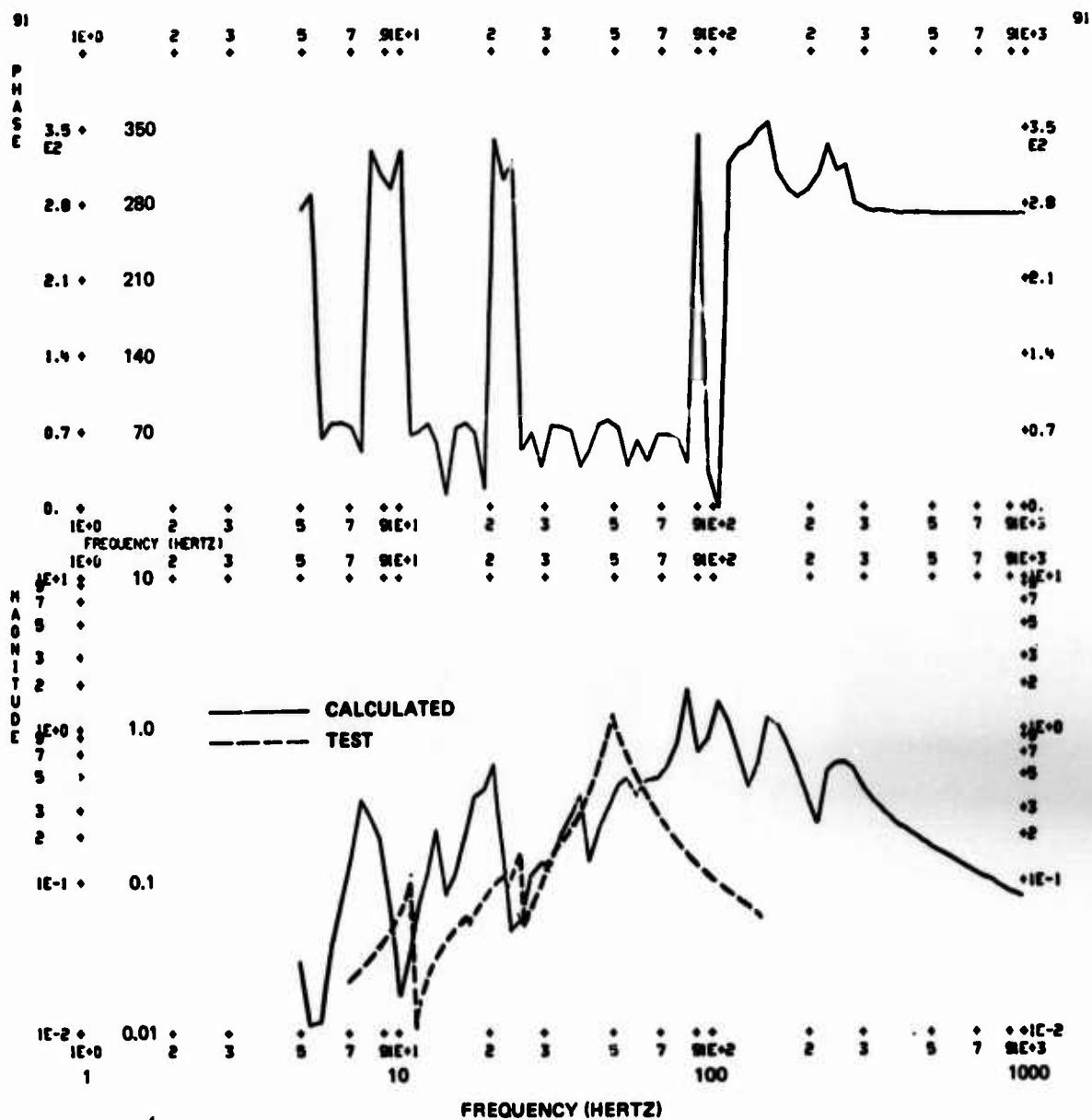


Figure 62. Direct Mobility - Tail Rotor Longitudinal.

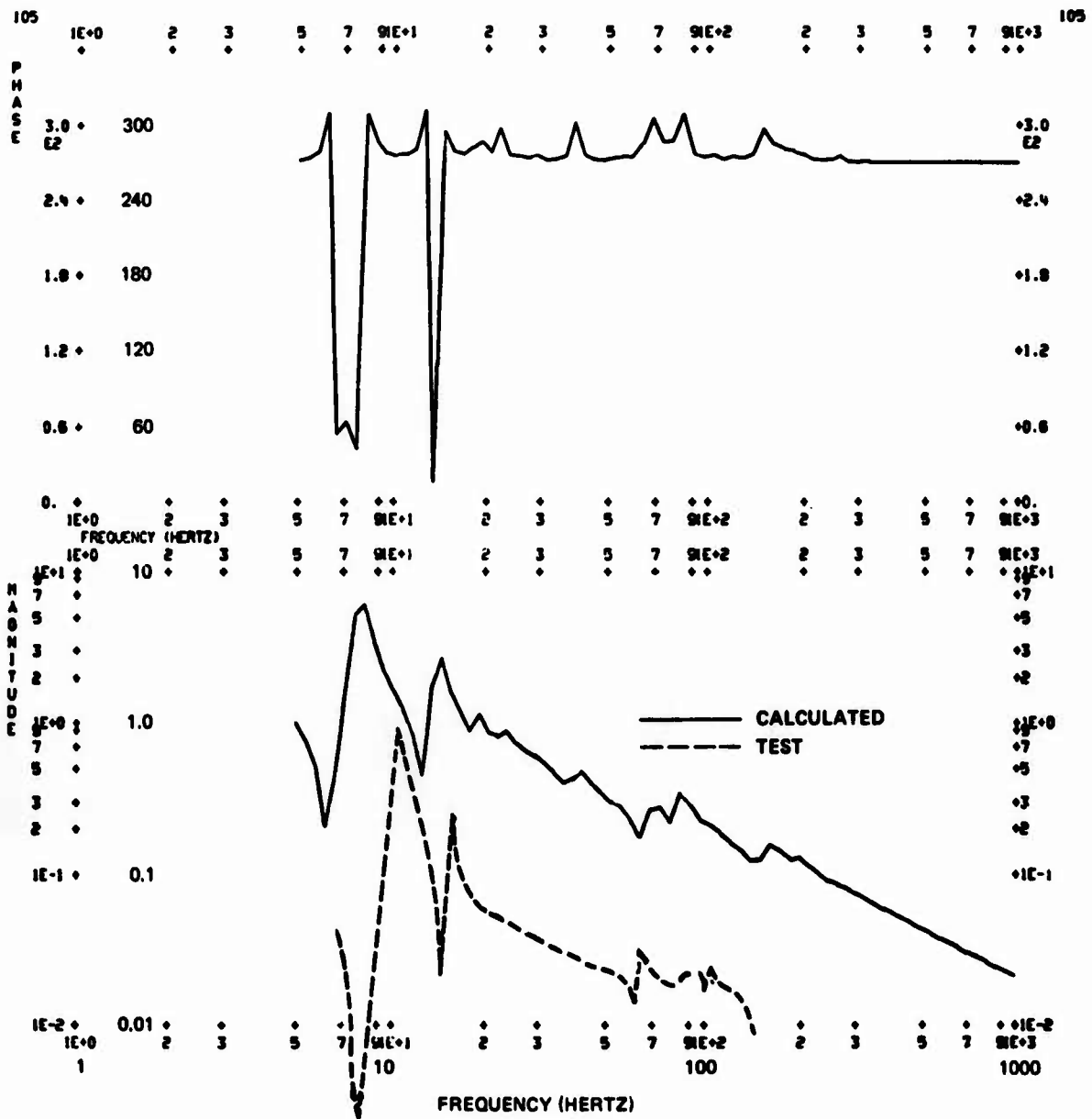


Figure 63. Direct Mobility - Tail Rotor Lateral.

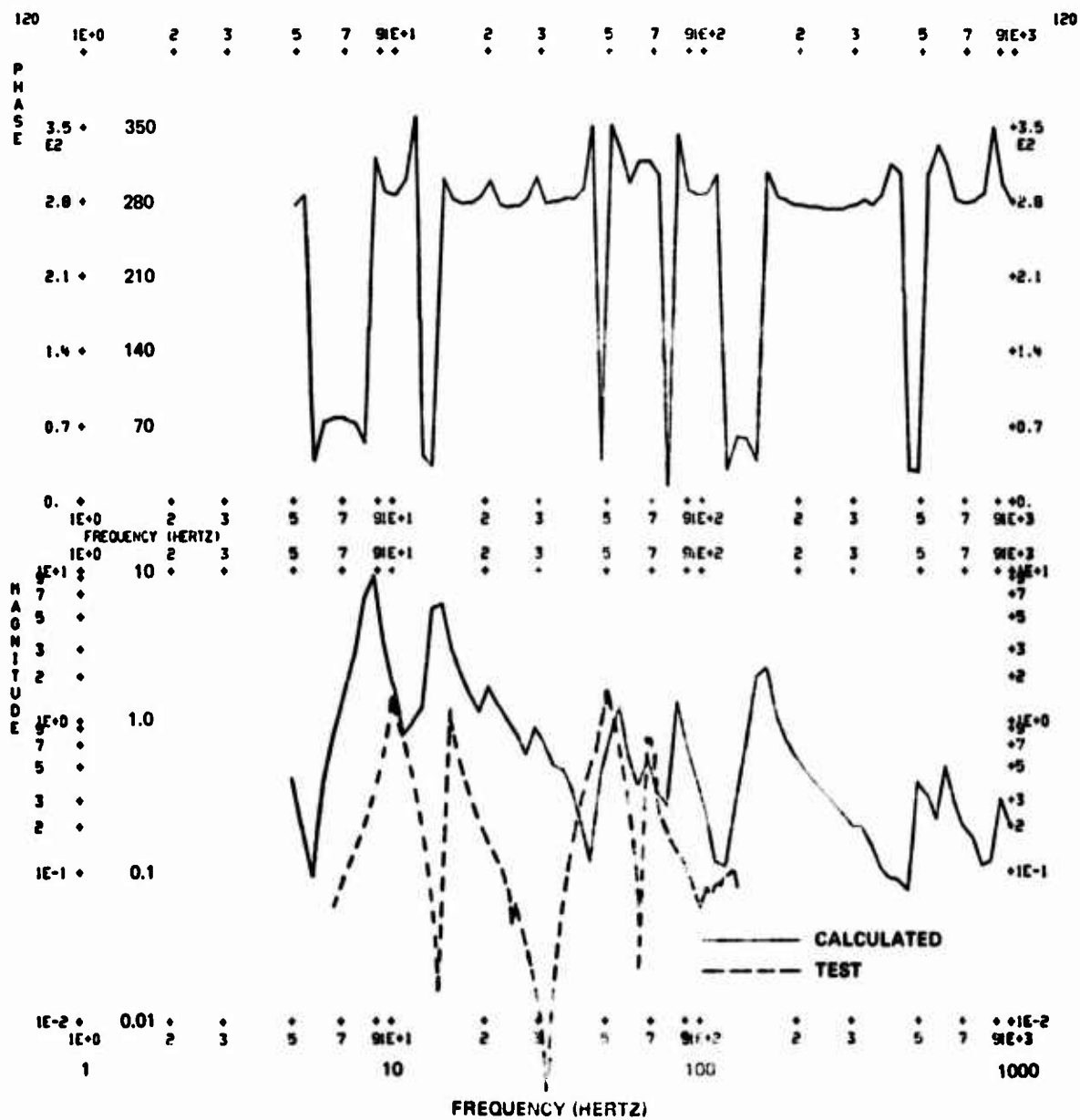


Figure 64. Direct Mobility - Tail Rotor Vertical.

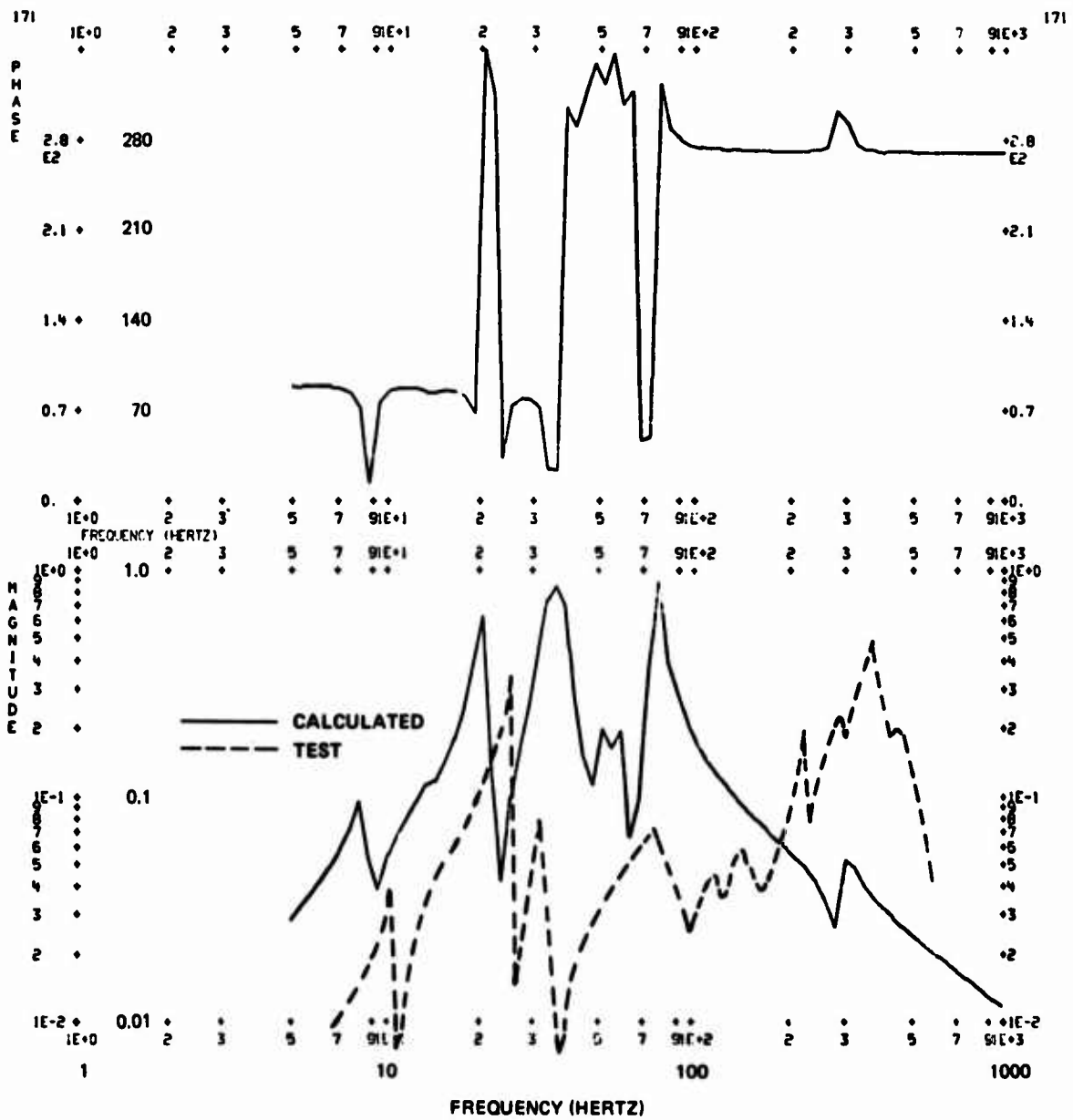


Figure 67. Direct Mobility - Engine/Transmission Longitudinal.

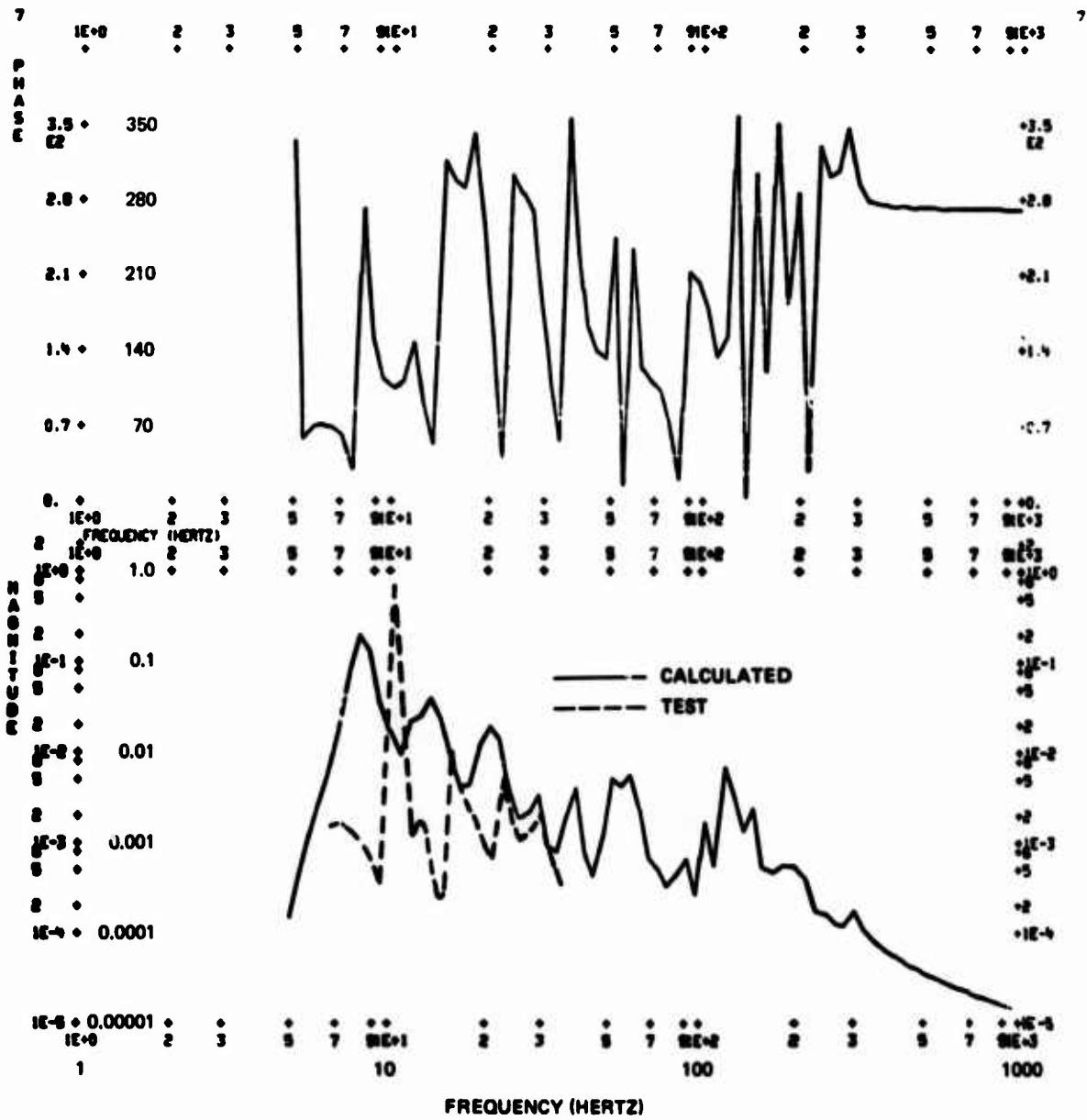


Figure 68. Cross Mobility - Center Mount Perpendicular Due to Main Rotor Longitudinal.

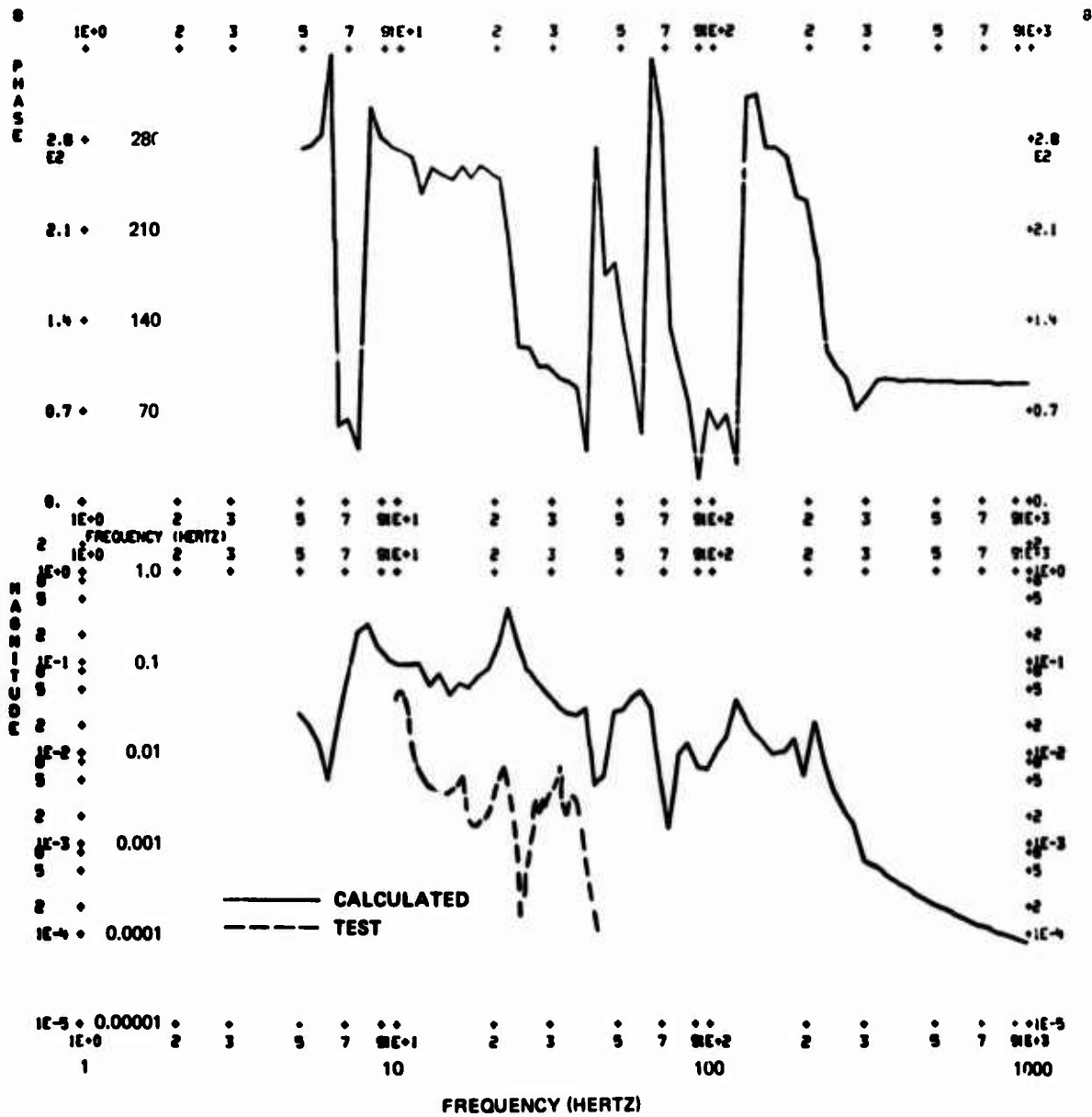


Figure 69. Cross Mobility - Center Mount Perpendicular Due to Main Rotor Lateral.

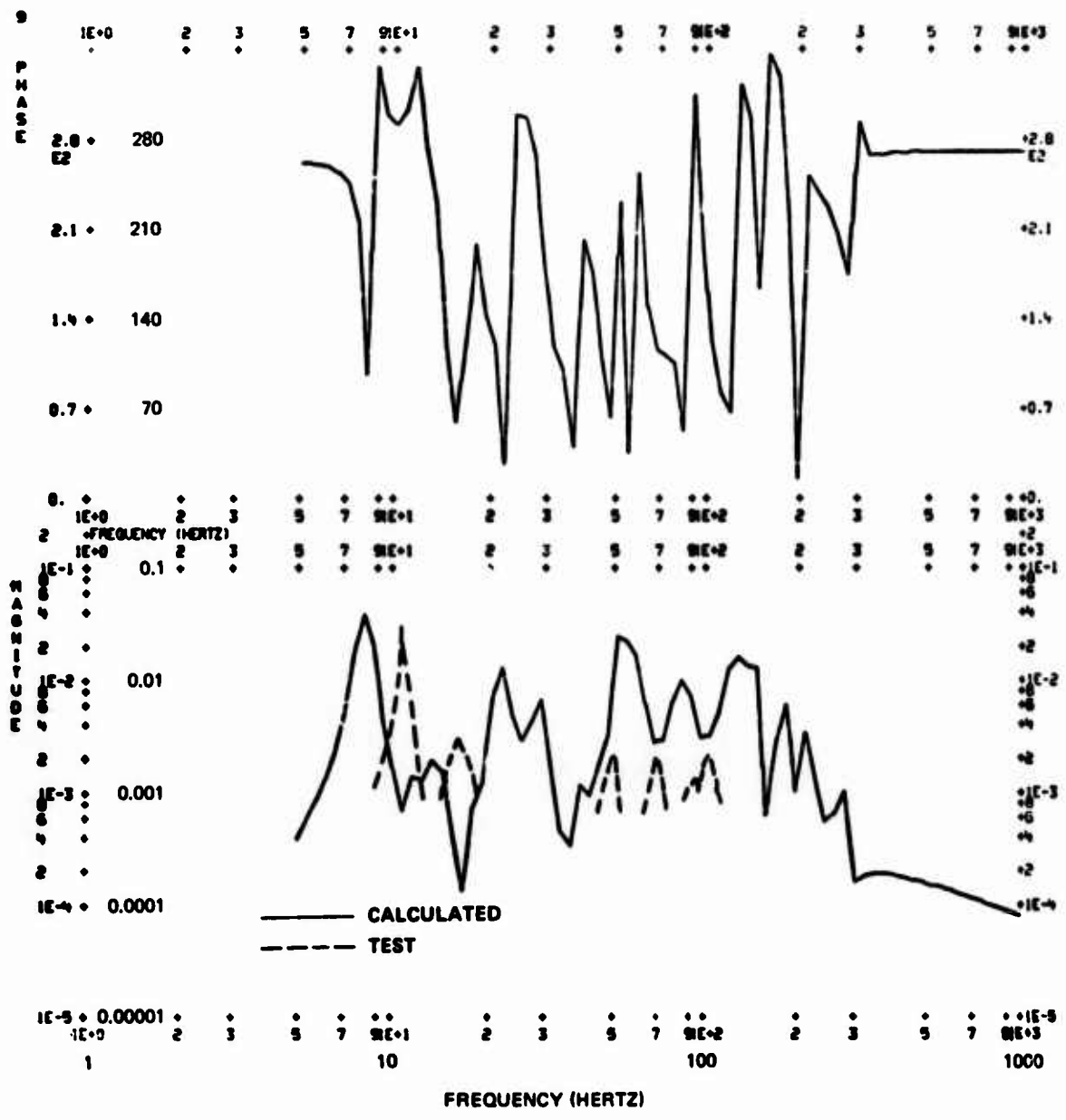


Figure 70. Cross Mobility - Center Mount Perpendicular Due to Main Rotor Vertical.

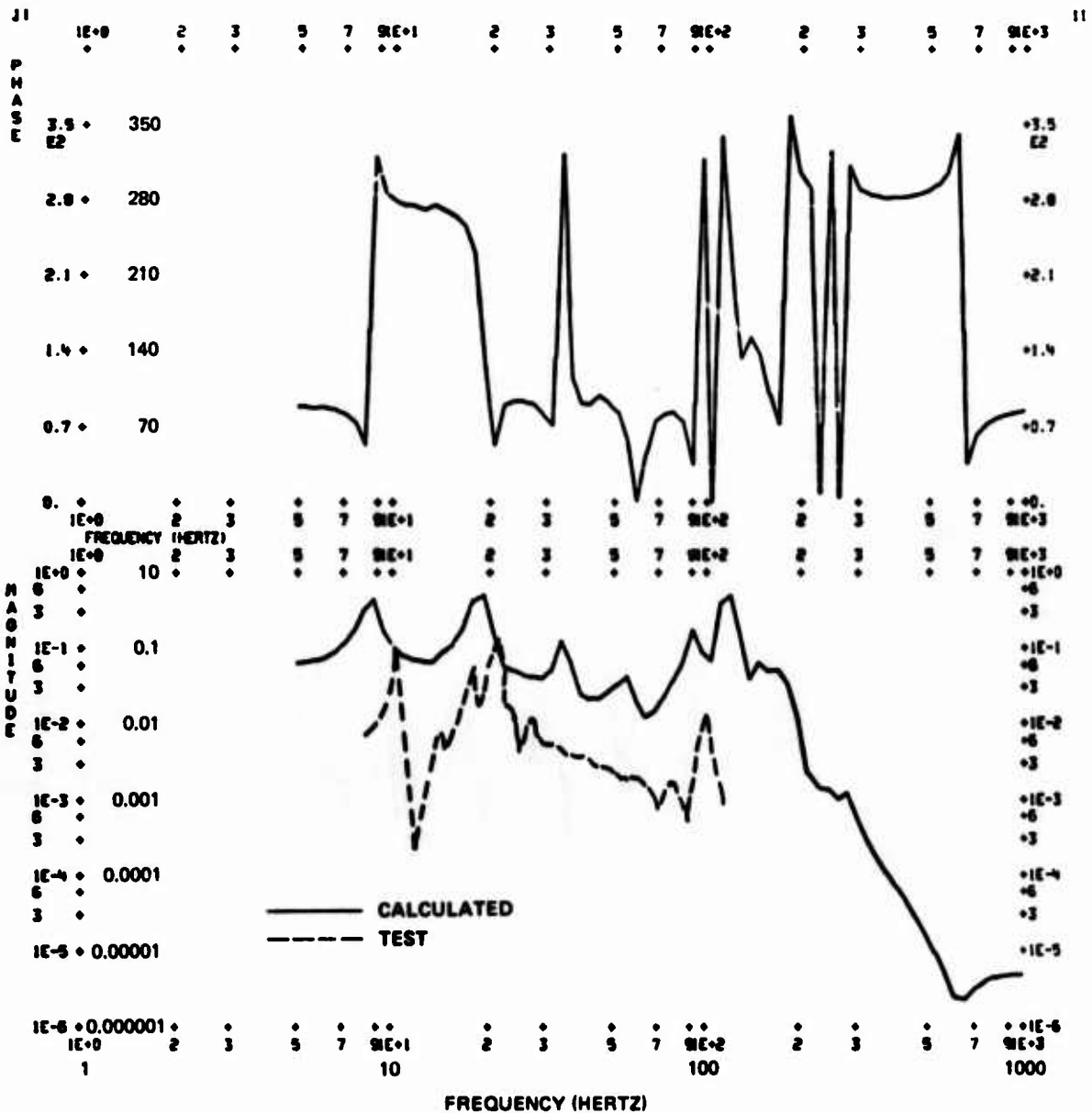


Figure 71. Cross Mobility - Center Mount Normal Due to Main Rotor Longitudinal.

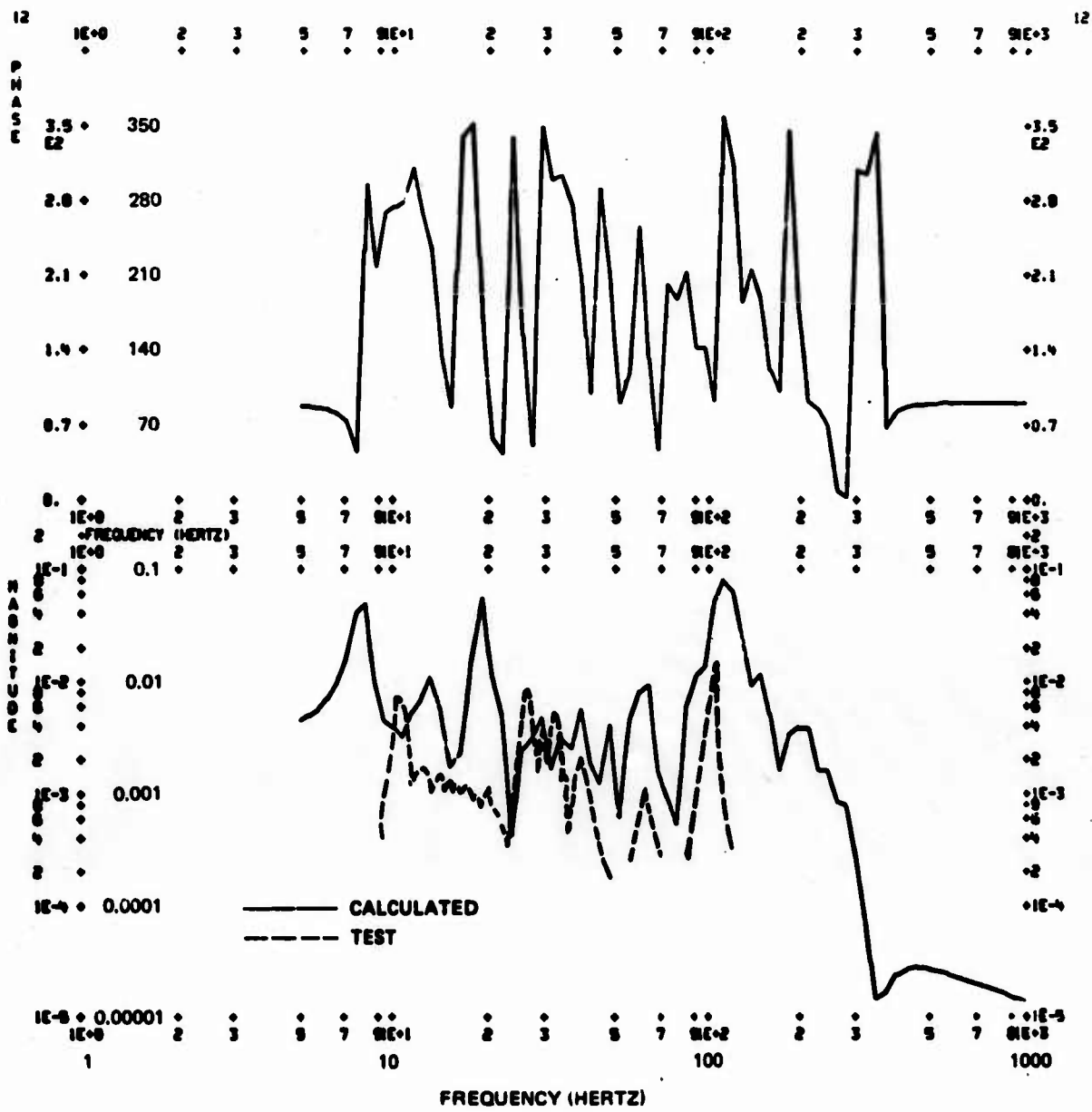


Figure 72. Cross Mobility - Center Mount Normal Due to Main Rotor Lateral.

The measured mobility is shown in Figures 50 through 73 (dashed lines) for frequencies from 7 to 200 Hz. The magnitudes of the direct mobilities at the rotor head agree well with the test data (Figures 50, 51, 52); so do the center mount perpendicular and parallel (Figures 53, 55), the right- and left-hand mounts for perpendicular and normal (Figures 56, 57, 59, 60), the tail rotor longitudinal and vertical (Figures 62, 64), and the engine/transmission coupling axial (Figure 65).

There is noticeable disagreement in magnitudes for the center mount normal (Figure 54), right and left mount parallel (Figures 58, 61), tail rotor lateral (Figure 63), and engine/transmission coupling lateral (Figure 66). These differences indicate that the use of mobility measuring equipment and the application of NASTRAN structural models require more experience for achieving a higher level of correlation. However, the degree of correlation shown here is considered to be quite good, and it is felt that even better correlation can be achieved in the future with these two powerful techniques of impedance measurement and finite element structural dynamics (NASTRAN) modeling.

Agreement between experimental and calculated cross mobility is less satisfactory. The greater amount of intervening structure between applied force and measured motion may explain the greater disagreement between measured and calculated cross mobility.

With respect to frequency correlation, the analytical model is generally softer than the actual aircraft. For instance, in Figure 50, test mobility peaks (dashed lines) are seen at about 10 Hz and about 28 Hz. The calculated (solid line) peaks are seen at about 9 Hz and about 21 Hz. This is due to the fact that half-effective skin in shear and "30 t" in tension (effective area equal to 30 times the product of thickness and width) were used in modeling the double-curvature skin panels in the aft body and tail cone. This indicates that the curved skin panels are more effective for the low loads used in the vibration test than for the loads typical of stress calculations. Use of higher values of skin effectivity on the model would raise the natural frequencies and improve correlation.

ENGINE MODELING

The features of the OH-6A airframe-without-engine NASTRAN model were described in the previous section. The modal component coupling techniques described in section 14.1 of the NASTRAN Theoretical Manual (Reference 6) will be used to add an engine model to this airframe model.

Methods to extract modal coefficients from the engine mobility test data and geometrical data (Reference 5) are described. A means of coupling the engine and airframe degrees of freedom is discussed. The approach used to input these modal and constraint equations on NASTRAN bulk data cards is described. Results of concept checkout on a small-scale model are given.

The engine-airframe model derived here will be used in later sections to compute frequency response plots ("mobility curves") and transient response due to hard landings.

DERIVATION OF MODAL PARAMETERS

Engine test data is available for all of the connection coordinates with the aircraft free (that is, disconnected). In the notation of Reference 6, its equation of motion is

$$(m_i p^2 + b_i p + k_i) \xi_i = \left\{ \phi_{ci} \right\}^T \left\{ f_c \right\} \quad (5)$$

The motion of the physical coordinates $\left\{ u_c \right\}$ in the engine basis (prescript 1) can be related to the modal variables ξ_i by the eigenvectors of the engine modes

$$\left\{ u_c \right\} = \left[\phi_{ci} \right] \left\{ \xi_i \right\} \quad (6)$$

where $\left\{ \xi_i \right\}$ is the set of ξ_i terms. The rigid-body modal parameters will be developed from weight and geometrical data. The flexible mode parameters will be developed from the test data.

Engine Rigid-Body Modes

The rigid-body modes will be defined as unit translations and rotations of the engine center of gravity. The translation component of the rigid-body mode shape at the kth mount, for instance, is then

$$1 \begin{bmatrix} \phi_{ci} \end{bmatrix}_k = \begin{bmatrix} 1 & 0 & 0 & 0 & k_z & -k_y \\ 0 & 1 & 0 & -k_z & 0 & k_x \\ 0 & 0 & 1 & k_y & -k_x & 0 \end{bmatrix} \quad (7)$$

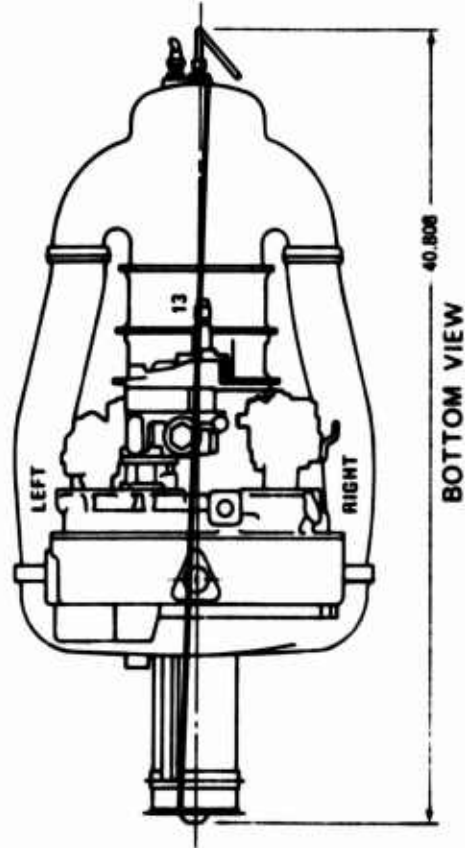
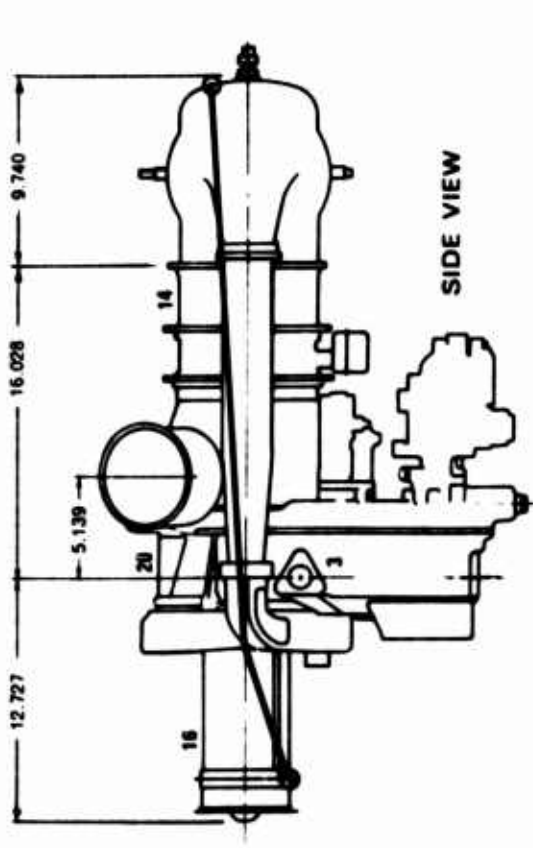
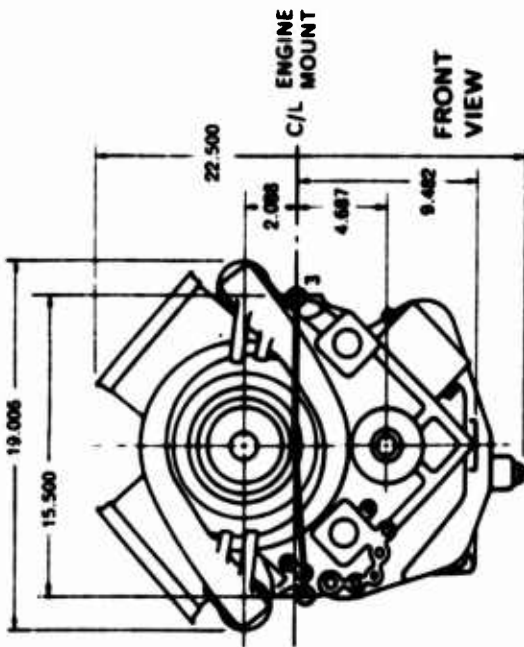
where k_x , k_y , and k_z are the distances in the x, y, and z directions from the center of gravity to the kth mount. As there are three mounts and four other stations where test data is available, there are seven such submatrices.

The damping and stiffness terms of the modal variables are zero. The mass terms are described later in this report.

Flexible Mode Modeling

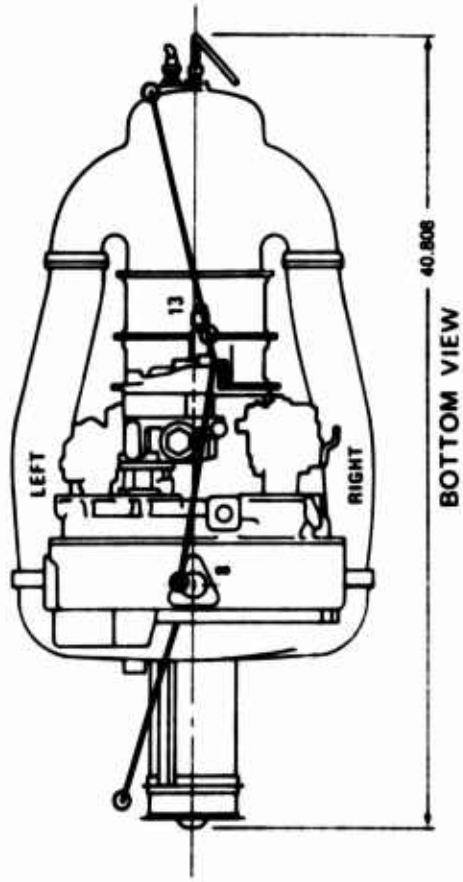
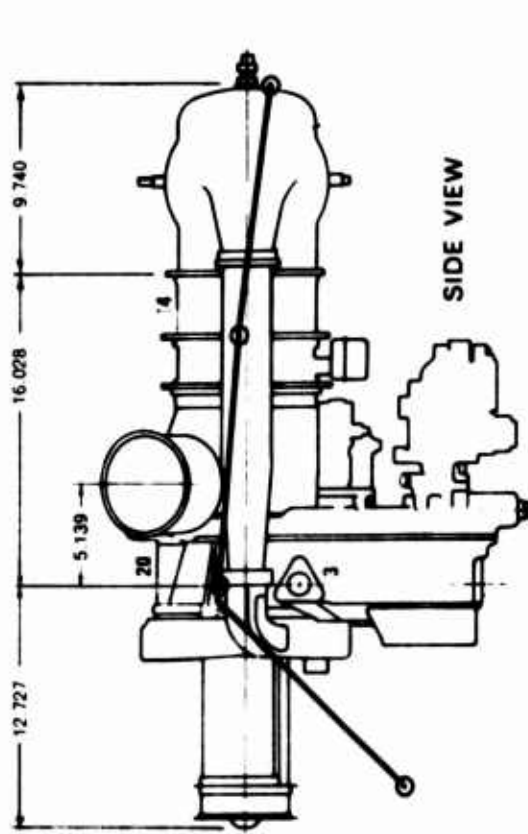
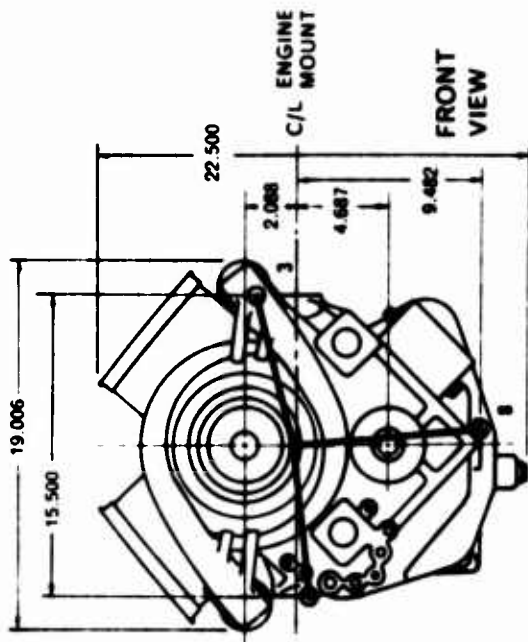
Identification of modal parameters from test data where mode natural frequencies are closely spaced is difficult. Automated methods now being developed (see References 14 through 18) or tedious hand iterative techniques must be used. The four lowest free-free flexible modes of the engine are closely spaced in frequency (see Appendix C). There are two "pitch bending" modes at 127 and 145 hertz and two "yaw bending" modes at 156 and 183 hertz (see Figures 74 through 77), so the fourth mode is only 40 percent higher in frequency than the first. However, the lowest mode is at four times the natural frequency of the main excitation force (main rotor 4/rev at 32.0 hertz). As extensive manipulation of this test data is beyond the scope of this research topic, and is hardly warranted due to the large separation between the main excitation frequency and the natural frequency, only a rough cut will be made at quantifying the parameters for the first two modes. The modeling techniques demonstrated for implementation in NASTRAN are applicable for any number of closely spaced modes.

If the response at the mode natural frequency is approximated as primarily due to rigid-body response and response in the resonant mode, with other modal contributions ignored, and a value of modal damping assumed, the modal parameters can be approximated from the mobility values.



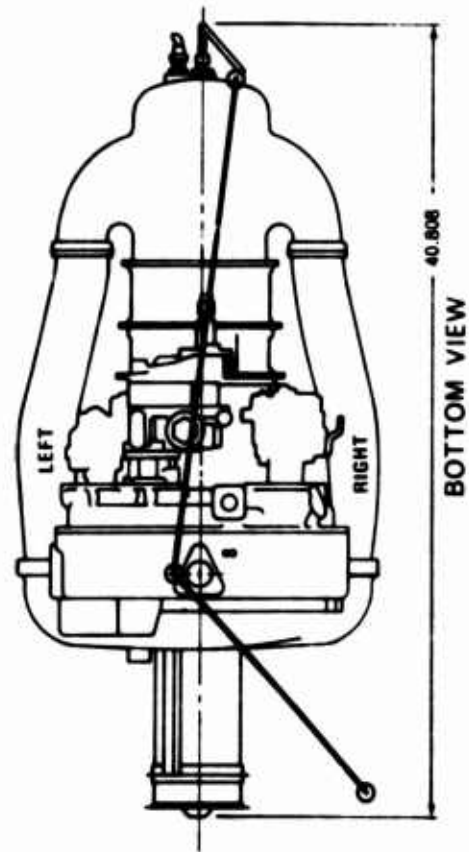
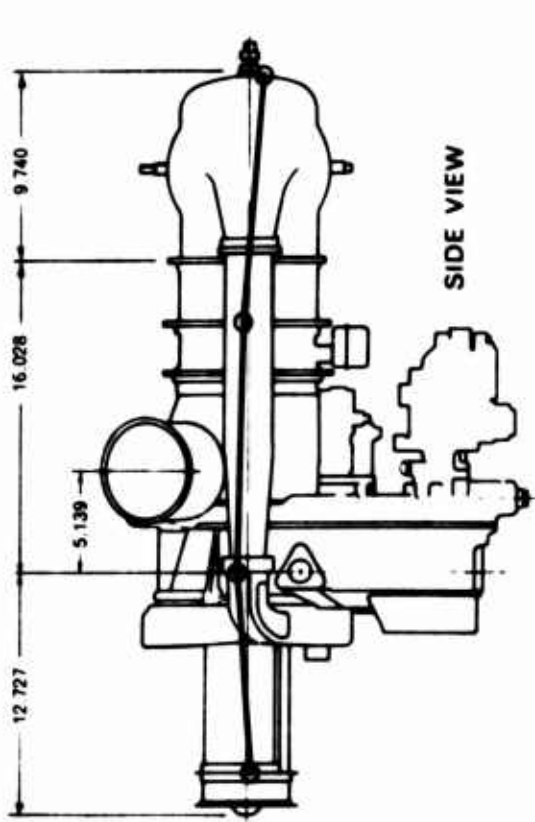
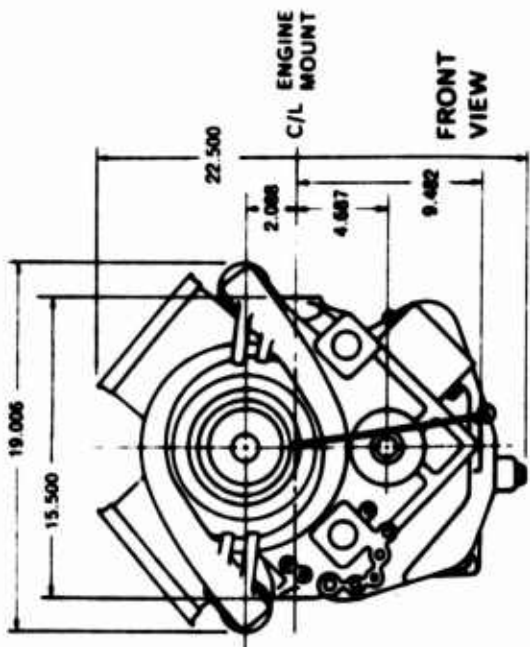
f	#	G	φ	G/cosφ
127	3	.0021	-18.57	.00199
	9	.0019	-8.21	.00188
	14	.0104	-201.61	-.00967
	16	.0355	-118.96	-.01719
	18	.0218	28.62	.01913
	20	.0033	-26.25	.00296
	5	.0012	47.49	.00081
	8	.0002	-110.76	-.00007
	13	.0037	-26.28	.0033
	15	.0093	73.36	.00266
	17	.0046	145.27	-.00378
	2	.0010	-133.09	-.00068
▼	6	.0033	133.03	.00225

Figure 74. T63 Bending Mode - 127 Hz.



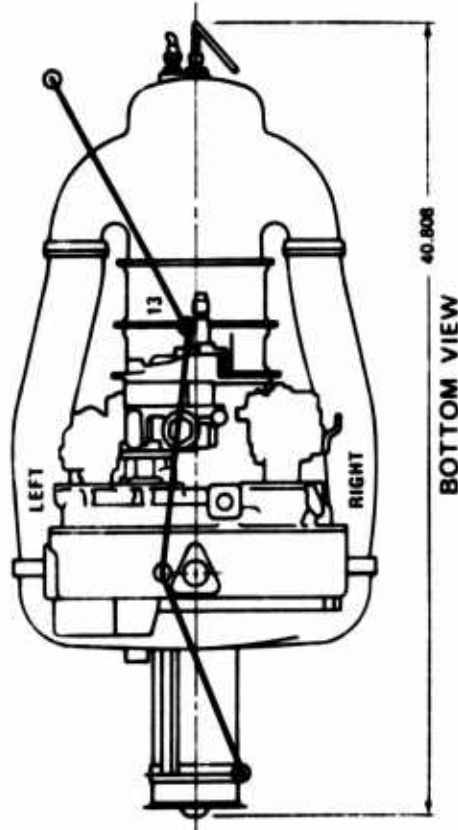
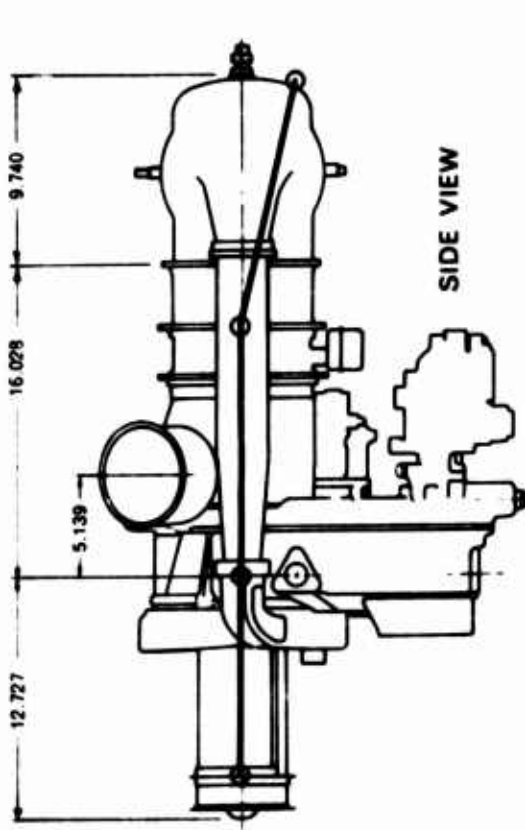
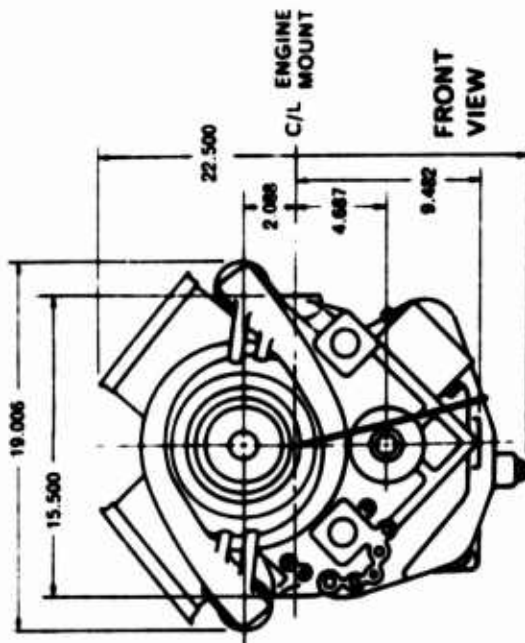
f	#	/G/	ϕ	/G/cos ϕ
1+5	3	.0225	-42.64	.01655
	9	.0072	-20.76	.00860
	14	.0041	-10.58	.0040
	16	.065	-177.36	-.06495
	18	.0157	127.7	-.0006
	20	.010	-41.3	.0075
	2	.0087	133.73	-.00553
	5	.0077	-46.14	.00533
	8	.0051	-0.44	.0051
	13	.0084	140.67	-.00649
	15	.0683	-51.96	.04208
	17	.0218	-33.29	.01822
	3	.0225	-42.64	.01655
	6	.0059	56.72	.00323
▼	8	.0051	-0.44	.0051

Figure 75. T63 Bending Mode - 145 Hz.



f	#	/G/	ϕ	/G/cos ϕ
156	3	-	-	-
	9	.0058	-21.89	.00538
	14	.0045	-8.04	.00445
	16	.0480	92.96	-.00248
	18	.0060	-120.07	-.00300
	20	.0045	22.77	.00415
	2	-	-	-
	5	.0118	-26.1	.0106
	8	.0095	-11.47	.0093
	13	.0013	-67.0	.0005
	15	.0946	134.85	-.0667
	17	.0179	148.6	-.01527
	6			

Figure 76. T63 Bending Mode - 156 Hz.



f	#	/G/	ϕ	/G/ cos ϕ
183	3	-	-	-
	9	.0001	-20.47	.0000936
	14	.0013	-56.55	.0007165
	16	.0019	91.24	-.000041
	18	.0072	127.80	-.00441
	20	.0006	31.49	.0005
	2	-	-	-
	5	.0038	-57.10	.00206
	8	.0058	-40.78	.00439
	13	.0010	-42.58	.000736
	15	.0123	108.02	-.0038
	17	.0148	47.72	.0099
	6			

Figure 77. T63 Bending Mode - 183 Hz.

Rearranging terms of equation (5),

$$\ddot{z}_i = \frac{\phi_c(k, i) f_{ck}}{(m_i p^2 + b_i p + k_i)} \quad (8)$$

$$v_{cj} = p u_{cj} \quad (9)$$

$$u_{cj} = \phi_c(j, i) \ddot{z}_i \quad (10)$$

Combining the above equations,

$$\frac{v_{cj}}{f_{ck}} = \sum_{i=1}^{\# \text{ modes}} \frac{p \phi_c(j, i) \phi_c(k, i)}{(m_i p^2 + b_i p + k_i)} \quad (11)$$

For the rigid-body modes, the stiffness and damping terms are zero. At the flexible mode natural frequency, the mass and stiffness terms cancel, so for a one-flexible-mode approximation,

$$\text{Re} \left[\frac{v_{cj}}{f_{ck}} (p = i_{r, 1}) \right] = \frac{\phi_c(j, 1) \phi_c(k, 1)}{b_i} \quad (12)$$

$$\text{Imag} \left[\frac{v_{cj}}{f_{ck}} (p = i_{r, 1}) \right] = \sum_{i=1}^6 \frac{\phi_c(j, i) \phi_c(k, i)}{i_{r, 1} m_i} \quad (13)$$

That is, the imaginary part of the velocity response is due to rigid-body response, while the real part is primarily due to the resonating mode.

It will be assumed that the engine modes have 3 percent of critical damping, that is, $\xi = 0.03$. Critical damping is related to the modal damping parameter by the equation

$$b_i = 2c_{d_i} m_i \quad (14)$$

where

$$c_{d_i}^2 = \frac{k_i}{m_i} \quad (15)$$

The eigenvectors can be normalized to an arbitrary value. For convenience, they are normalized so that the direct impedance point has a value of unity.

Then

$$R_e \left[\frac{v_{cj}}{f_{cj}} (p = i\omega_i) \right] = \frac{1}{b_i} \quad (16)$$

$$m_i = \frac{b_i}{2(0.03 \omega_i)} \quad (17)$$

$$k_i = \omega_i^2 m_i \quad (18)$$

The assumed value of 3 percent of critical damping is consistent with structures of this nature. It is stressed that this technique is being used to derive a plausible set of values. The low resolution of the test data and the close proximity of other modes make "half-power point" or measurement of the derivative of phase shift with frequency described in References 5, 6, 19, and 20 unlikely to produce more realistic values of modal damping without extensive iteration.

The remaining terms of the eigenvector can be derived from the phase and magnitude readings provided on the engine manufacturer's experimental mode shape data. Returning to equation (12),

$$R_e \left[\frac{v_{ck}}{f_{cj}} (p = i\omega_i) \right] = \frac{1\phi_c(k, i)}{b_i} \quad (19)$$

That is, the eigenvector term at the k th station can be determined from the real part of the cross-impedance value and the modal damping term.

Engine Drive Shaft Modeling

A consistent mass matrix is used to model the engine shaft and couplings. The bending stiffness of the couplings is ignored.

The couplings are considered as point masses at each end of the shaft. The shaft is of uniform mass distribution. Its mass matrix is illustrated in Figure 78. The actual mass values and means of implementation are given in Appendix C.

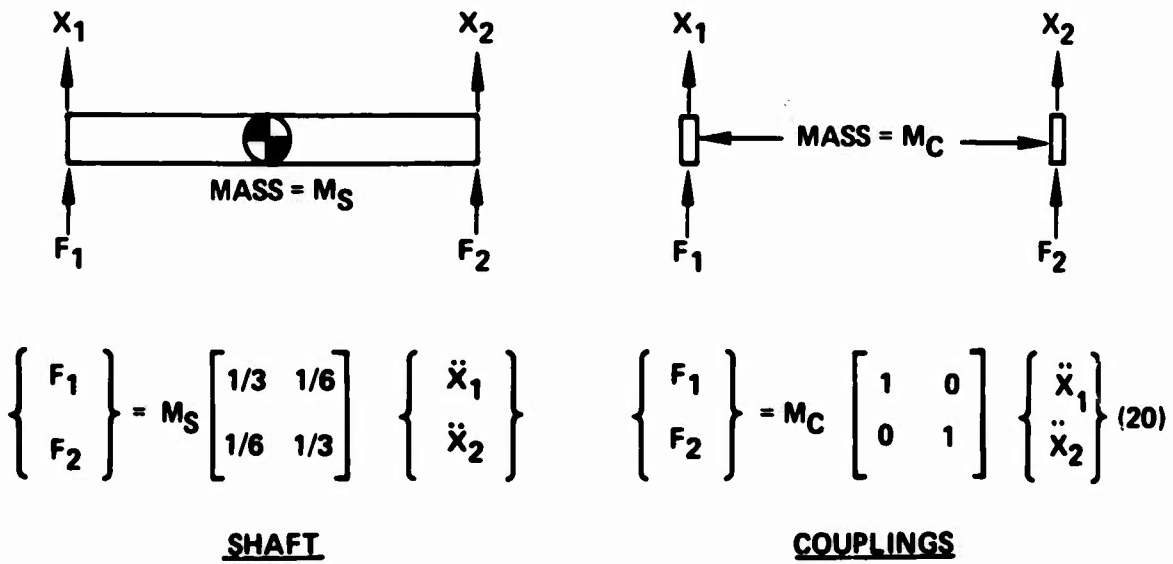


Figure 78. Engine Drive Shaft Modeling.

Damping Terms

A uniform damping of 3 percent of critical damping will be used on all flexible modes for airframe and engine.

Modal Mass Terms

Fuselage masses are described elsewhere. The scalar terms with significant mass are the modal displacement variables:

$M_{\text{translations}}$ = engine mass

$M_{\text{rotations}}$ = corresponding moments of inertias as measured about engine center of gravity

$$M_7 = \frac{b_7}{2 (0.03)}$$

$$M_8 = \frac{b_8}{2 (0.03)}$$

where b_7 is the mobility value at engine test station 9 at 127 hertz, and b_8 at 145 hertz.

IMPLEMENTATION IN NASTRAN

The airframe model described starting on page 61 was modified to account for the reduction in cargo mass, to realign the engine mount variables in line with the test axes, and to add the modal engine to the airframe.

The modal rigid-body displacement variables are modeled with one grid point, and the flexible mode variables with scalar points (SPOINT bulk data cards). The engine mode shapes are described as multipoint constraints (MPC cards), and the modal mass and stiffnesses by scalar elements (CMASS2 and CELAS2 cards).

A list of the variables, and tables and illustrations of the engine model, are given in Appendix C along with a listing of the actual cards used.

CORRELATION OF ENGINE MODEL WITH TEST DATA

The engine model described above was assembled in a NASTRAN model and then used to produce mobility plots. Correlation of the model with test data is shown in Figure 79 (from Reference 5). The correlation is considered to be very good from 8 Hz (main rotor 1/rev) to 145 Hz (second engine bending mode). The engine acts as a rigid body to about 100 Hz. The engine model was then coupled to a collection of rigid elements that have the mass properties of the OH-6A. Ground springs were added so that the system has both rigid and flexible modes. The only other flexible elements are the three bipod mounts that join the airframe to the engine. This gives an indication of where the engine rigid-body modes are when the mounts are attached to a rigid airframe. The natural frequencies of this system are given in Table 11 for the cases of engine flexible modes present and not present.

The effect of adding the two "pitch bending" modes of the engine is to raise the engine rigid-body pitch mode 10 percent in frequency and to lower the uncoupled engine bending frequency 7 percent. The effect on other mode frequencies is less than 5 percent.

ENGINE GYROSCOPIC COUPLING

Gyroscopic coupling effects due to engine turbine rotation are considered negligible for the low angular rates typical of vibratory response, but may be significant for transient response. The terms derived below are added only to the transient response model and not to the frequency response model.

The gyroscopic terms are added to the engine rigid-body variables as shown:

$$\begin{Bmatrix} \dot{M}_{\text{pitch}} \\ \dot{M}_{\text{yaw}} \end{Bmatrix} = \begin{bmatrix} 0 & -\bar{J} \\ +\bar{J} & 0 \end{bmatrix} \begin{Bmatrix} \dot{\theta}_{\text{pitch}} \\ \dot{\theta}_{\text{yaw}} \end{Bmatrix} \quad (21)$$

where

$$\bar{J} = \sum_i I_{pi} \Omega_i$$

I_{pi} = Polar moment of inertia of components on shaft i

Ω_i = Angular velocity of i shaft

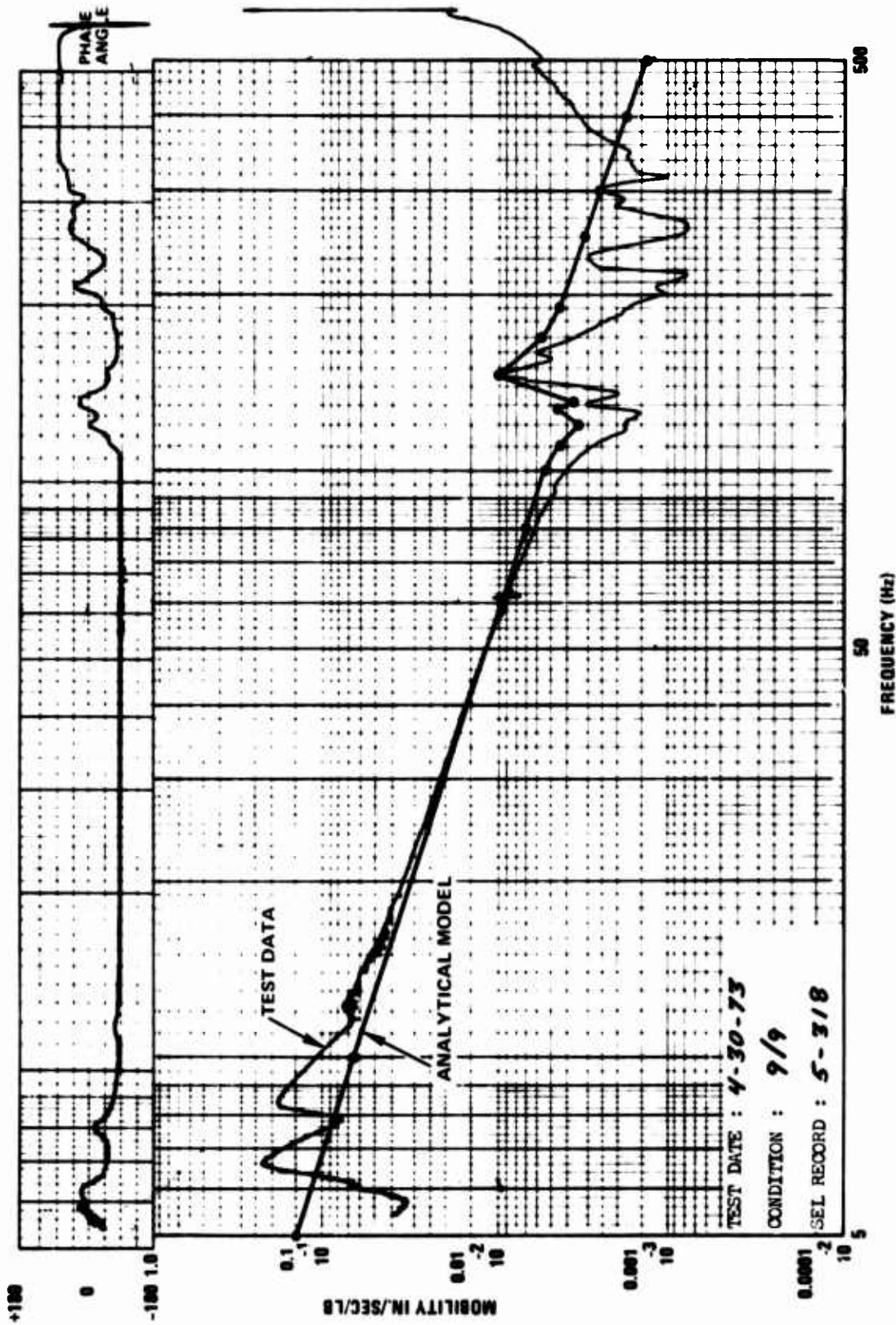


Figure 79. Correlation of Engine Model With Test Data.

TABLE 11. COMPARISON OF ENGINE MODE NATURAL FREQUENCIES

Mode Name	Without Engine Flexible Modes	With Engine Flexible Modes	Flexible Aircraft, Flexible Engine
Aircraft vertical	7.609	7.606	-
Aircraft lateral	9.525	9.518	-
Engine vertical/pitch	31.45	31.43	21.8
Engine lateral	38.01	37.87	23.23
Engine longitudinal	85.27	81.70	38.82
127 Hz uncoupled engine bending mode	-	126.32	127.53
145 Hz uncoupled engine bending mode	-	136.81	139.24
Engine pitch	155.43	170.85	48.80
Engine yaw	182.29	182.21	38.88
Engine roll	290.42	290.79	174.73

CORRELATION OF AIRFRAME-ENGINE MODEL WITH TEST DATA

The airframe-engine model described above with the laboratory (ground) vibration test mass configuration was used to calculate mobility plots corresponding to the ground vibration test data.

Calculated points for 90 percent, 100 percent, and 110 percent of main rotor rpm are plotted on test curves in the region near main rotor 4/rev. Direct mobility points are shown in Figures 80 through 82. Selected cross-mobility plots are shown in Figures 83 through 101.

The calculated direct-mobility points show very good correlation with the test data in Figures 80 through 82. This result is to be expected. Of more importance are the cross-mobility comparisons for the installed engine, because these are the most lengthy to calculate. The comparison of calculation and measurement is good in Figures 83, 84, 86, 87, 88, 89, 90, 91, 92, 94, 96, 98, 99, and 101; it is not good in Figures 85, 93, 95, 97, and 100. In general, this second group of figures involves the most dissymmetry; i. e., forces in the main plane of the helicopter and motion out of the main plane, such as Figure 93, which is turbine mid-split line

lateral motion due to main rotor longitudinal. It is considered that additional study could improve the correlation of items in this second group.

Figures 96, 98, 99, and 101 show vertical mobility of the turbine mid-split line and of the forward compressor, due to main rotor vertical and main rotor longitudinal forces. Correlation in these figures of calculated mobility is very good, particularly at 100 percent rpm (32 Hz). That is important, because vertical motion of the forward compressor and turbine mid-split line shows prominently on the flight test data of Figure 1.

The next sections of this report will be directed toward a correlation of the measured overall engine motion using the elements of the motion as correlated satisfactorily in figures such as 96, 98, 99, and 101.

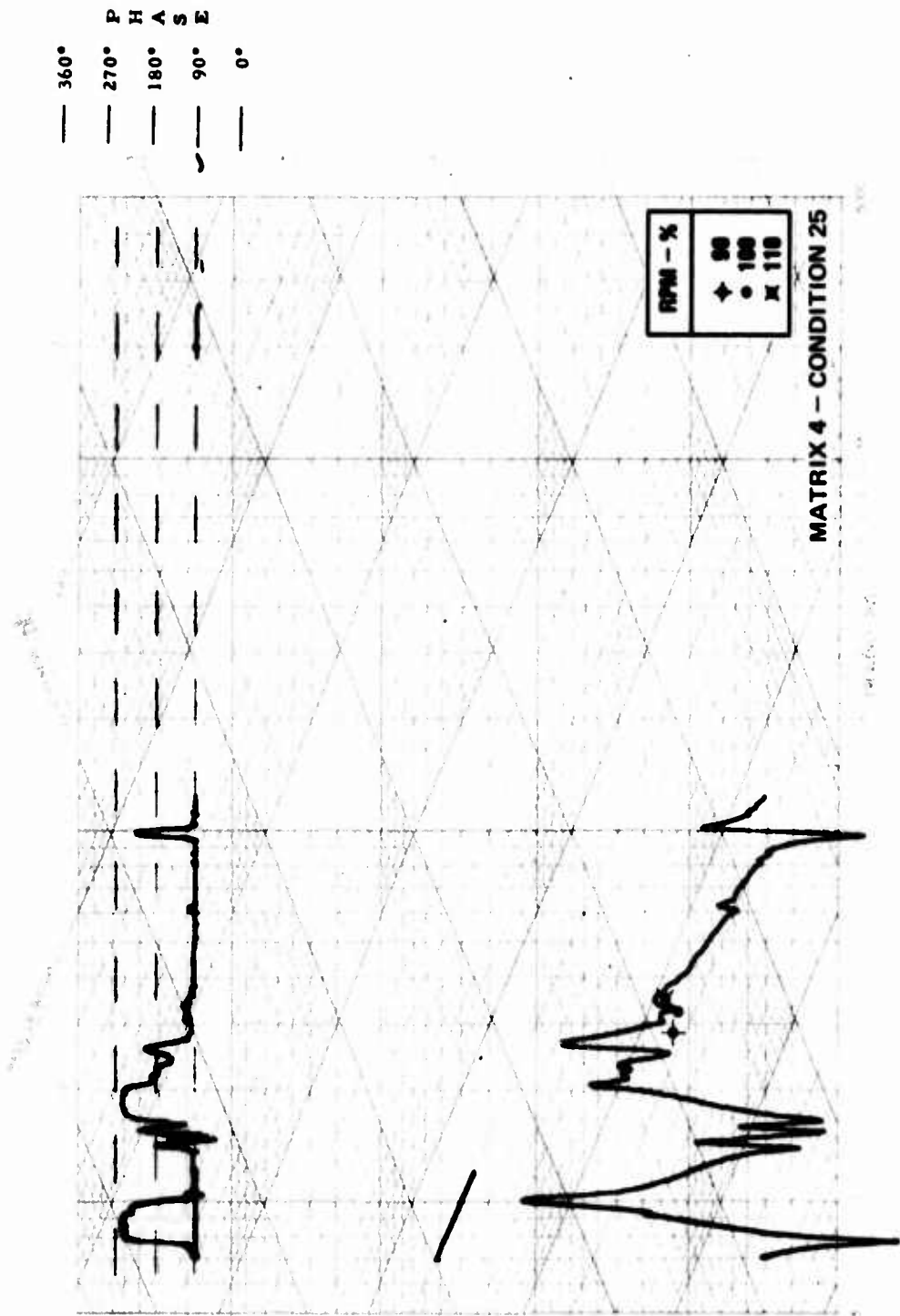


Figure 80. Direct Mobility, Main Rotor Longitudinal.

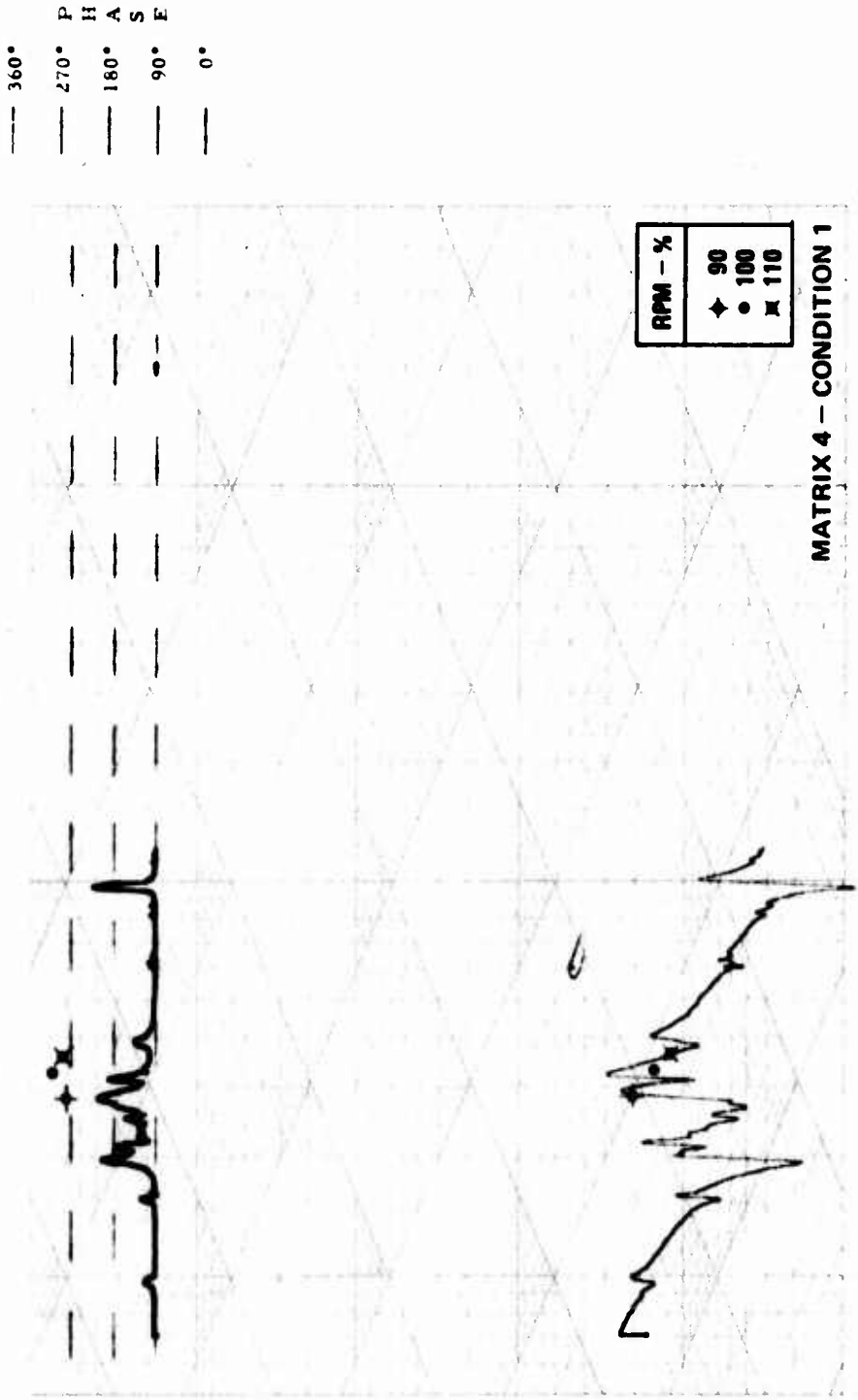


Figure 81. Direct Mobility, Main Rotor Lateral.

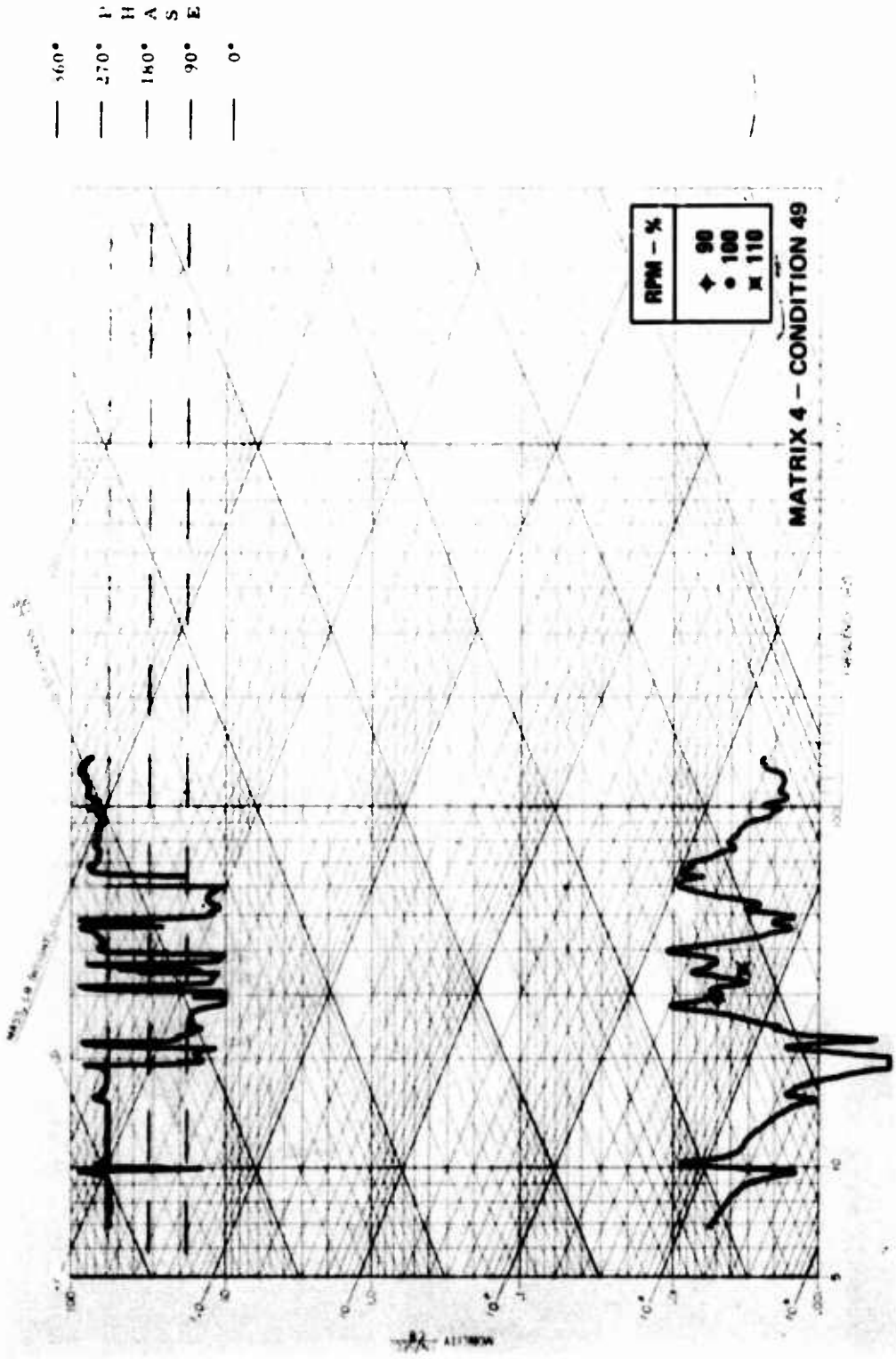


Figure 82. Direct Mobility, Main Rotor Vertical.

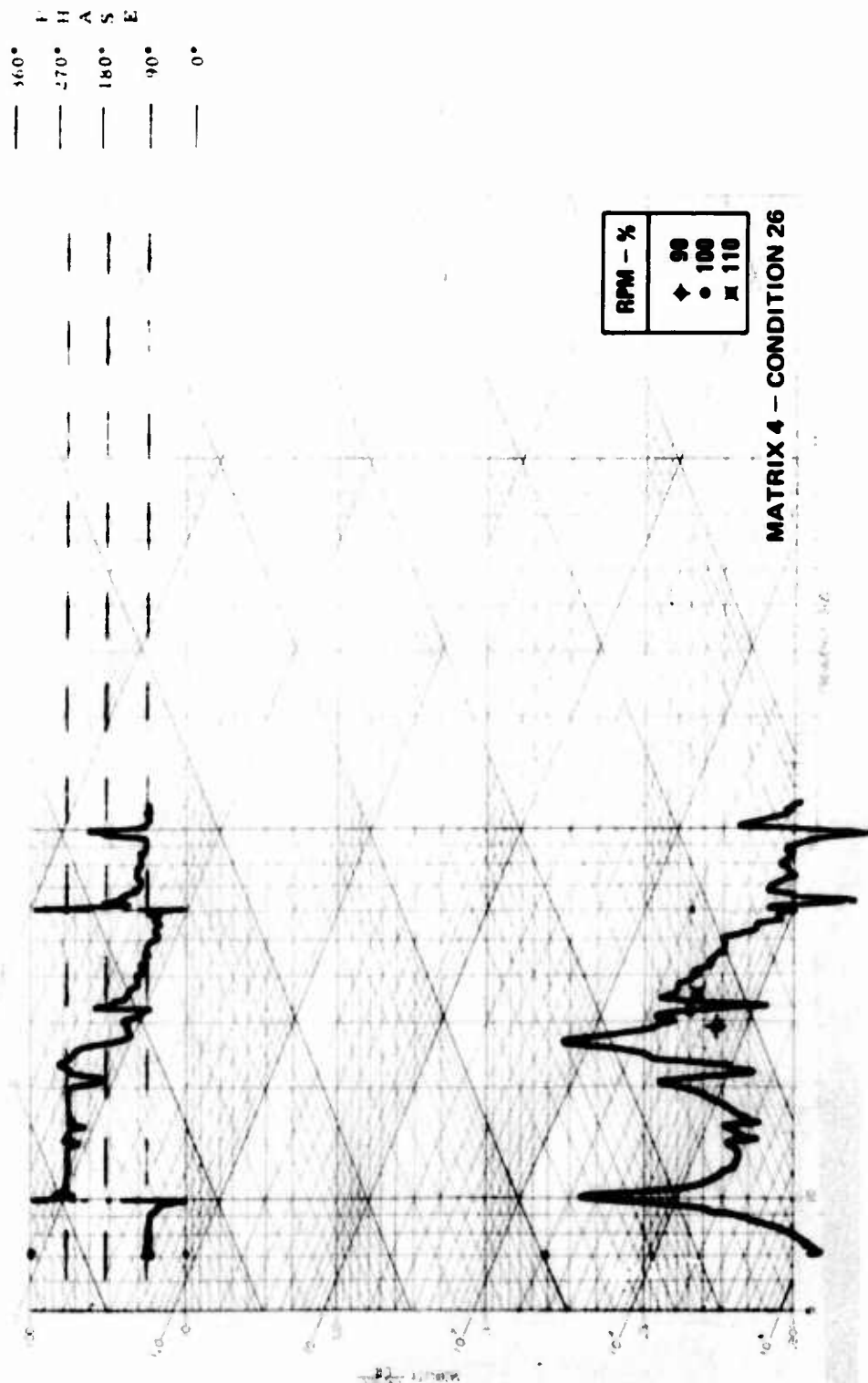


Figure 83. Cross Mobility, Main Rotor Longitudinal Due to Main Rotor Vertical.

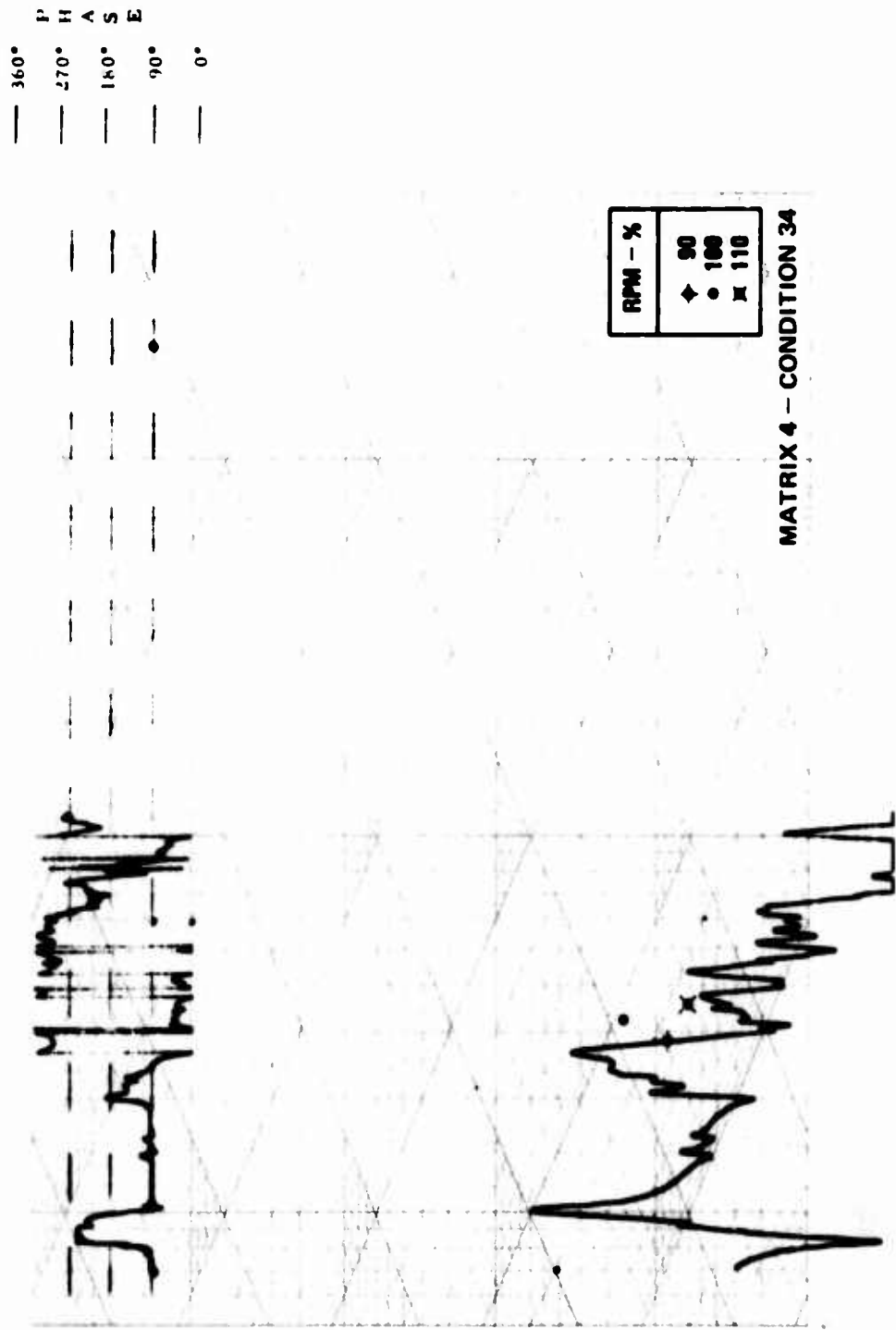
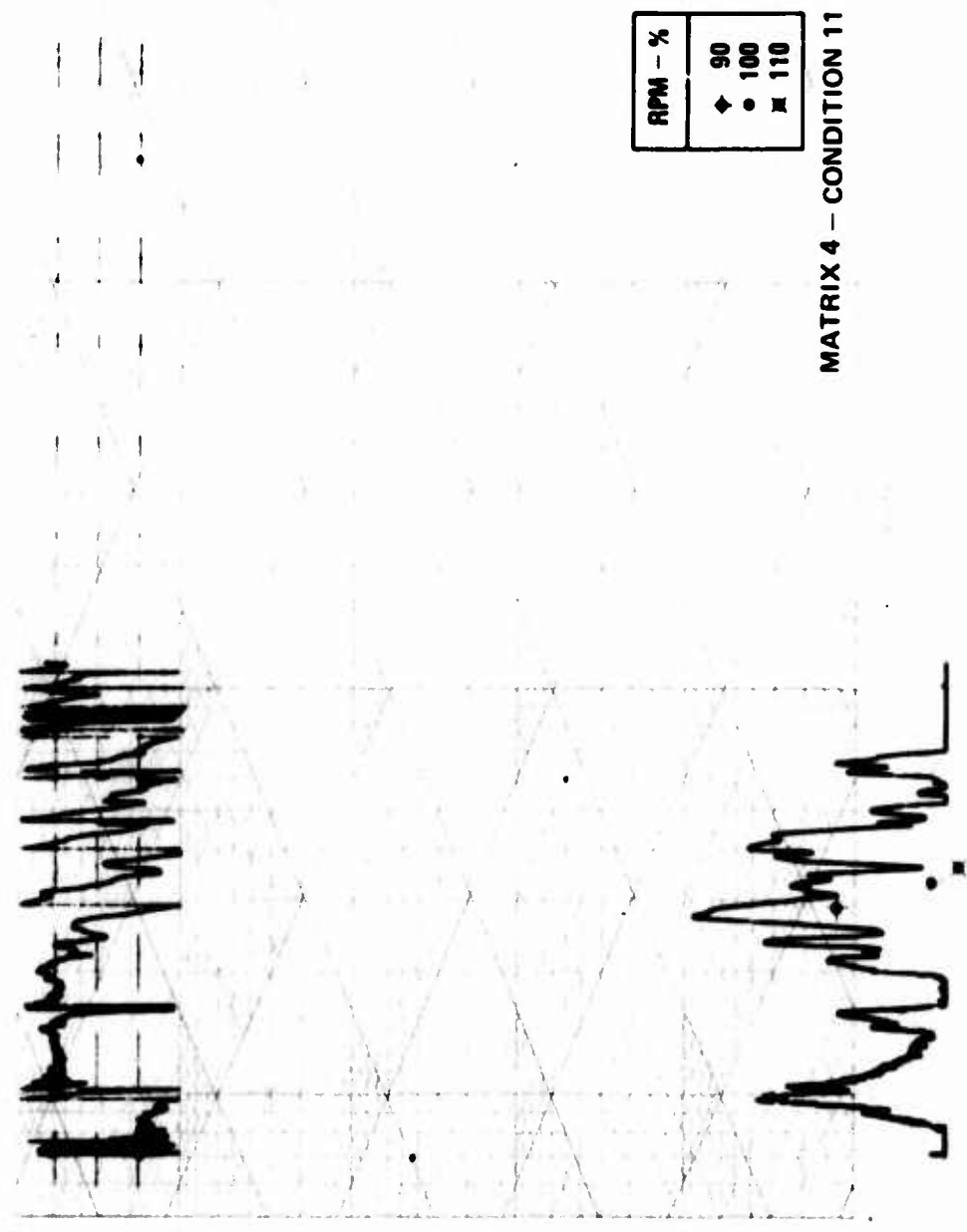


Figure 84. Cross Mobility, Center Mount Axial Due to Main Rotor Longitudinal.

— 360°
 — 270°
 — 180°
 — 90°
 — 0°



RPM - %	
◆	90
●	100
■	110

MATRIX 4 - CONDITION 11

Figure 85. Cross Mobility, Center Mount Axial Due to Main Rotor Lateral.

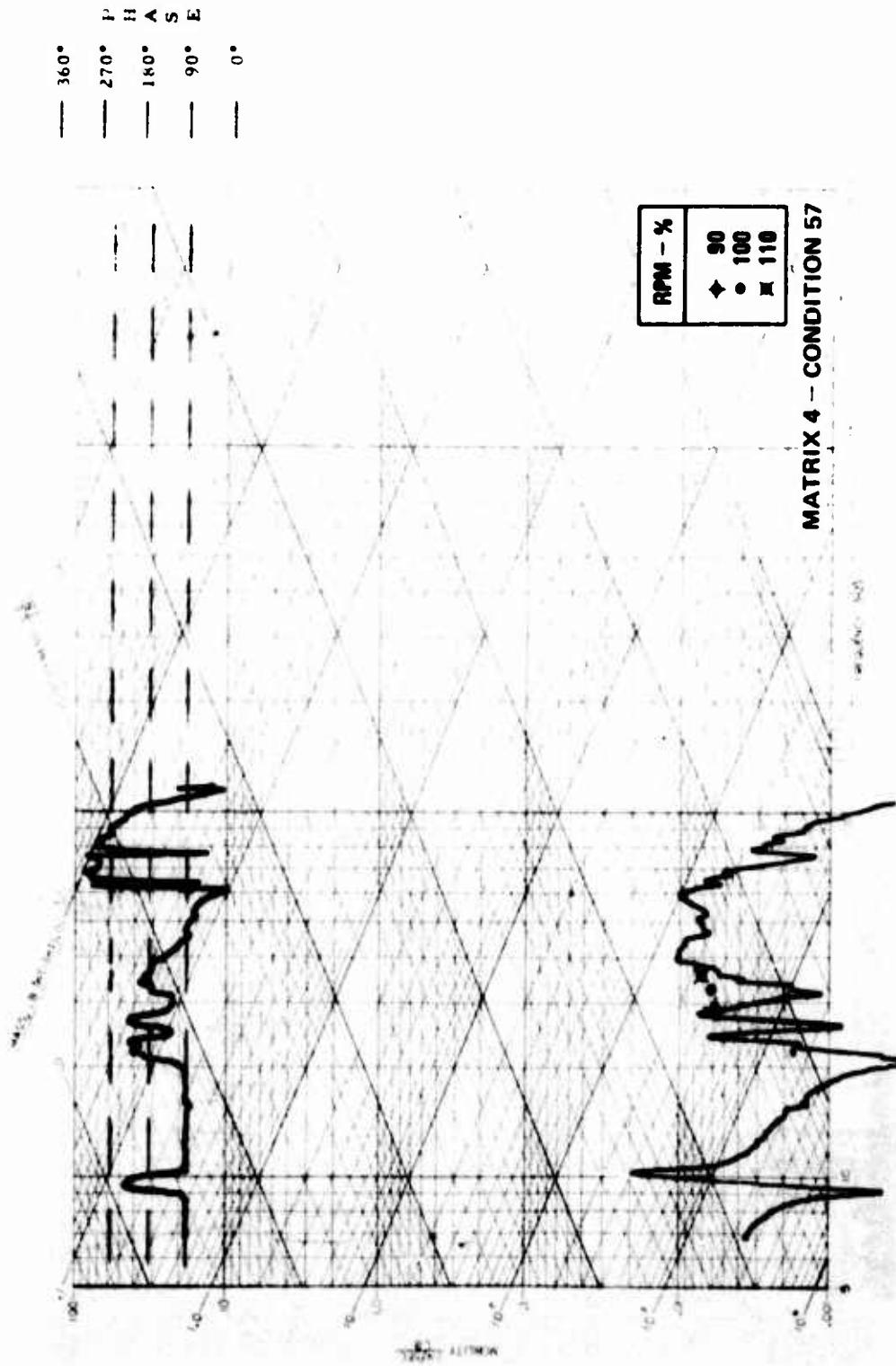
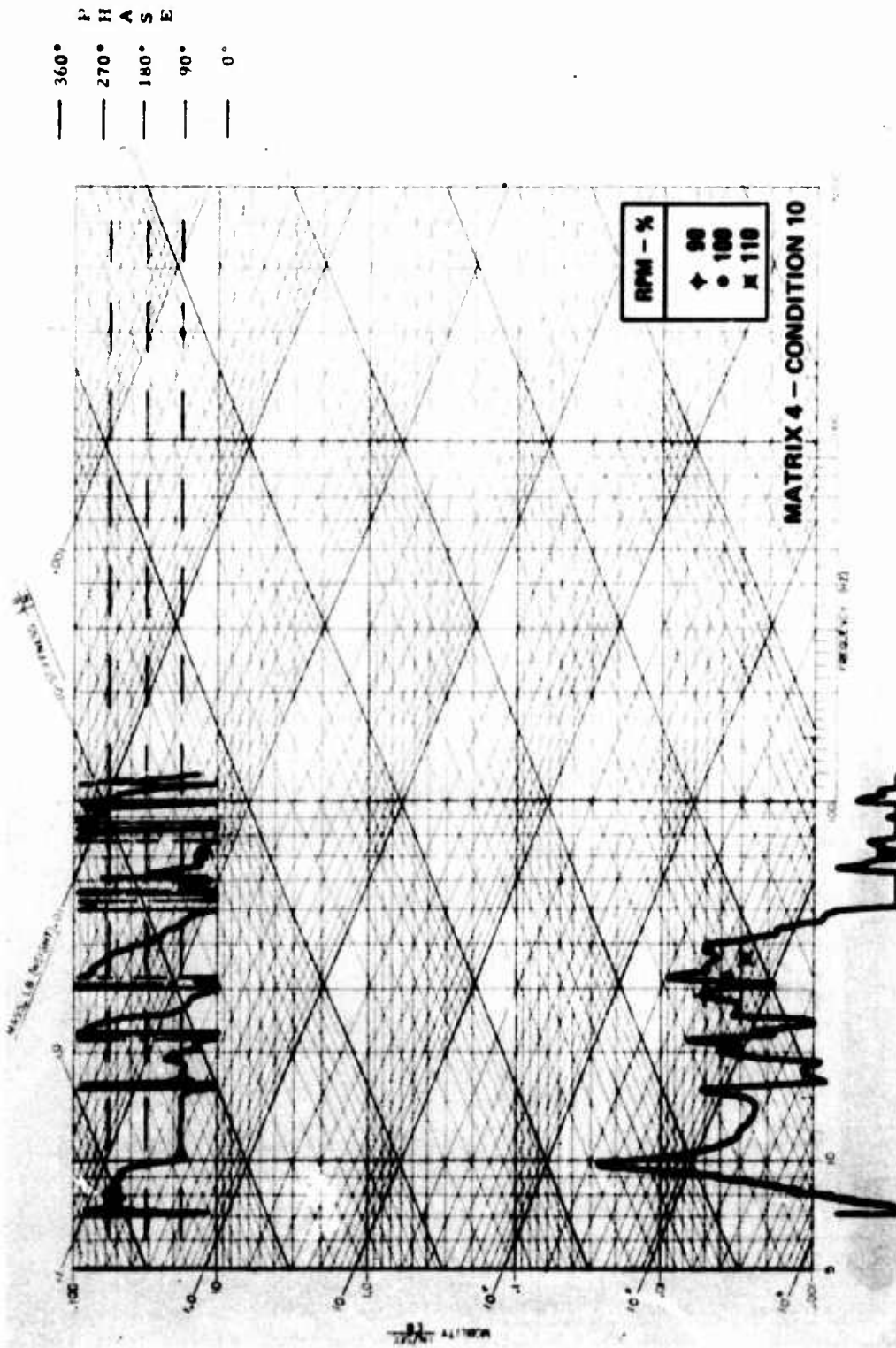


Figure 86. Cross Mobility, Center Mount Axial Due to Main Rotor Vertical.



— 360°
 — 270°
 — 180°
 — 90°
 — 0°

Figure 87. Cross Mobility, Center Mount Lateral Due to Main Rotor Lateral.

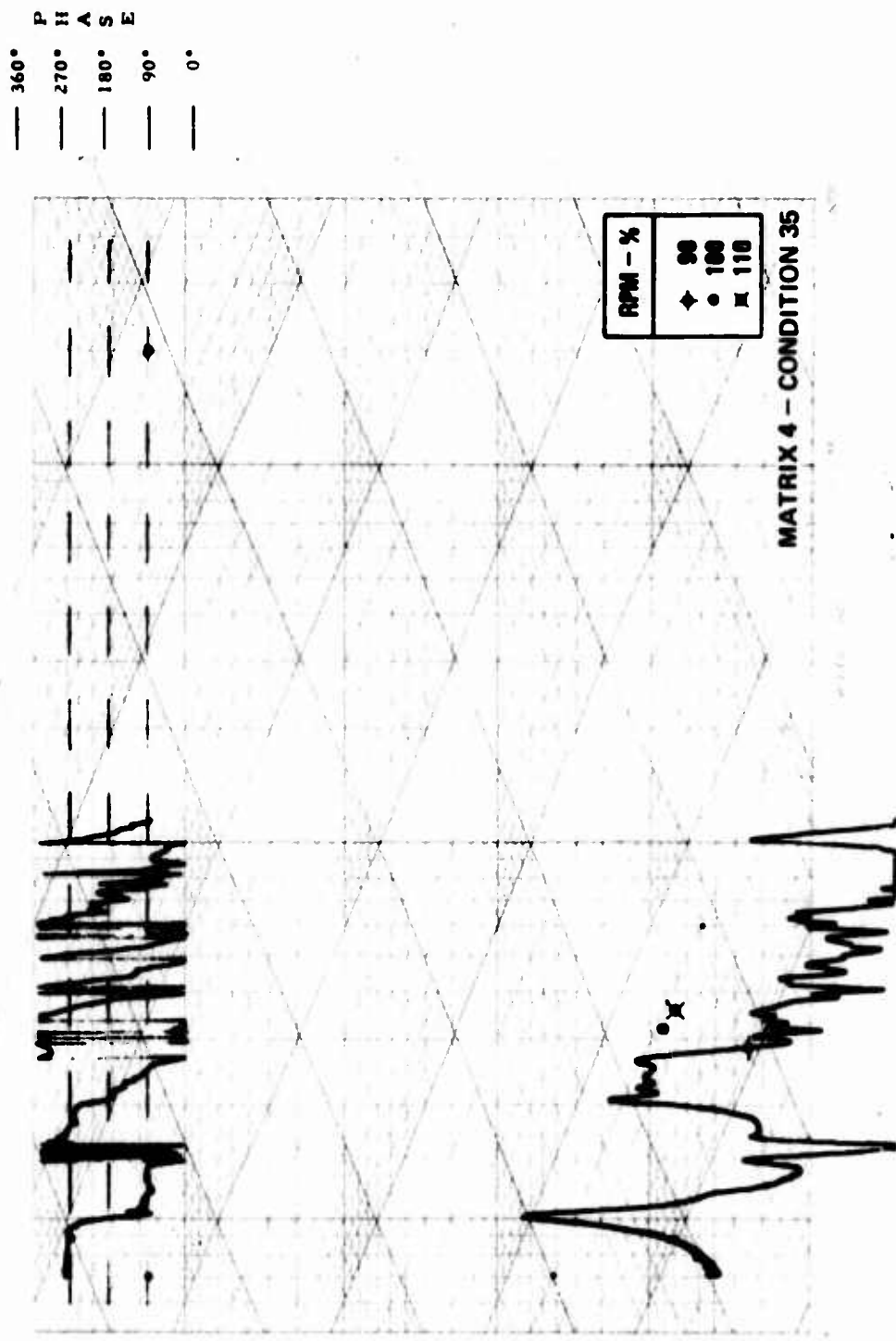


Figure 88. Cross Mobility, Center Mount Vertical (Engine Axis) Due to Main Rotor Longitudinal.

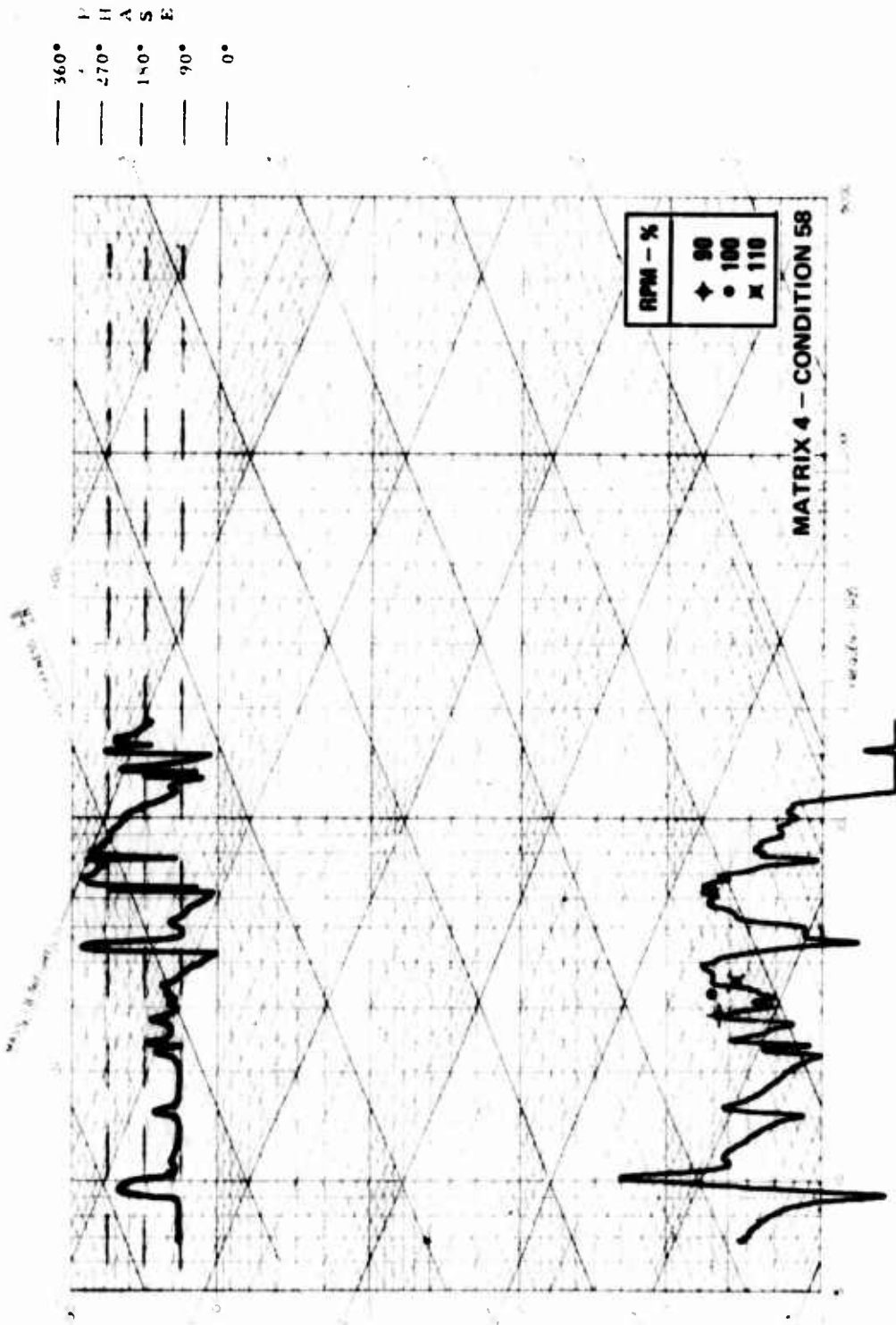


Figure 89. Cross Mobility, Center Mount Vertical (Engine Axis) Due to Main Rotor Vertical.

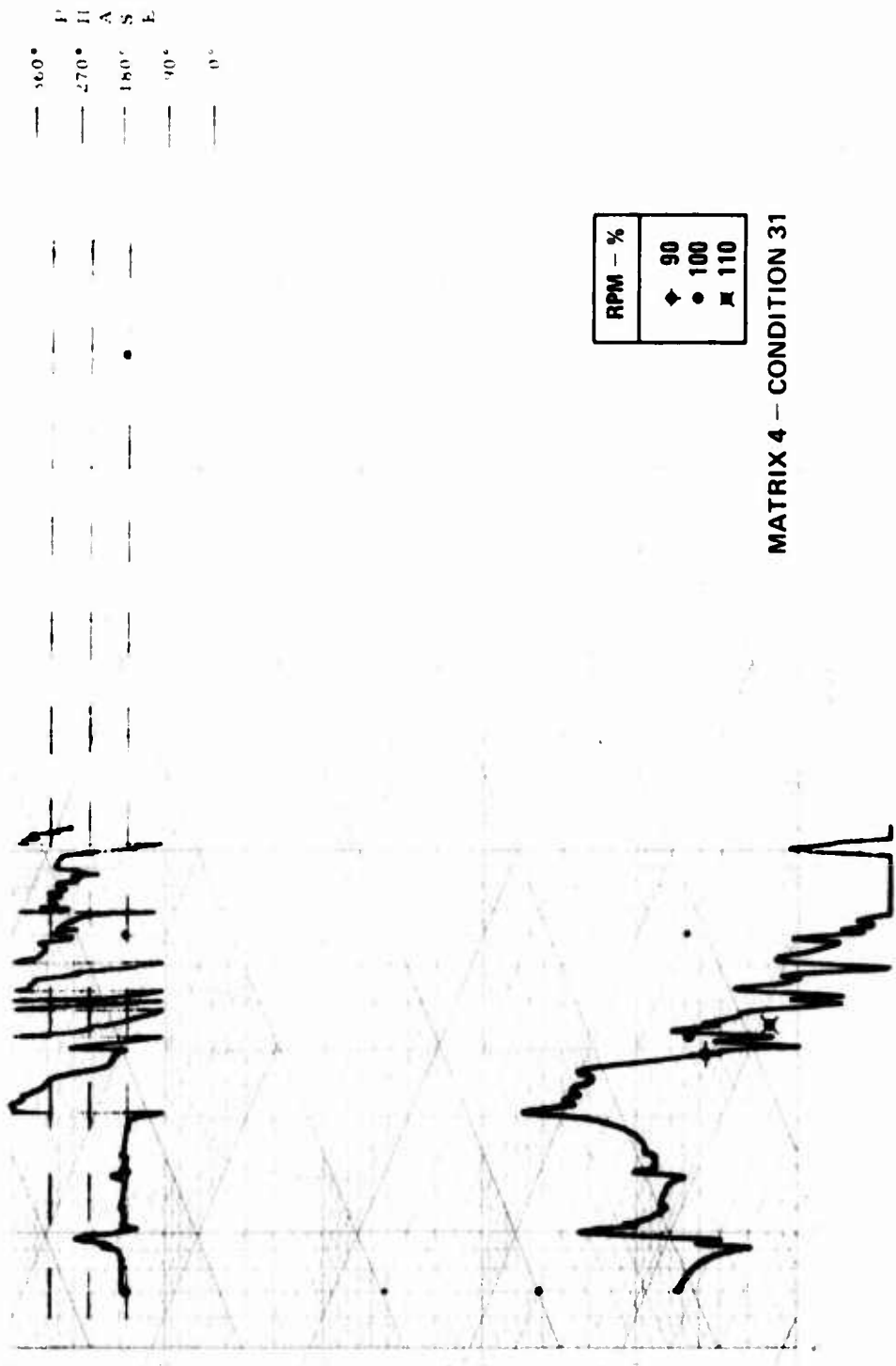


Figure 90. Cross Mobility, Right Mount Vertical Due to Main Rotor Longitudinal.

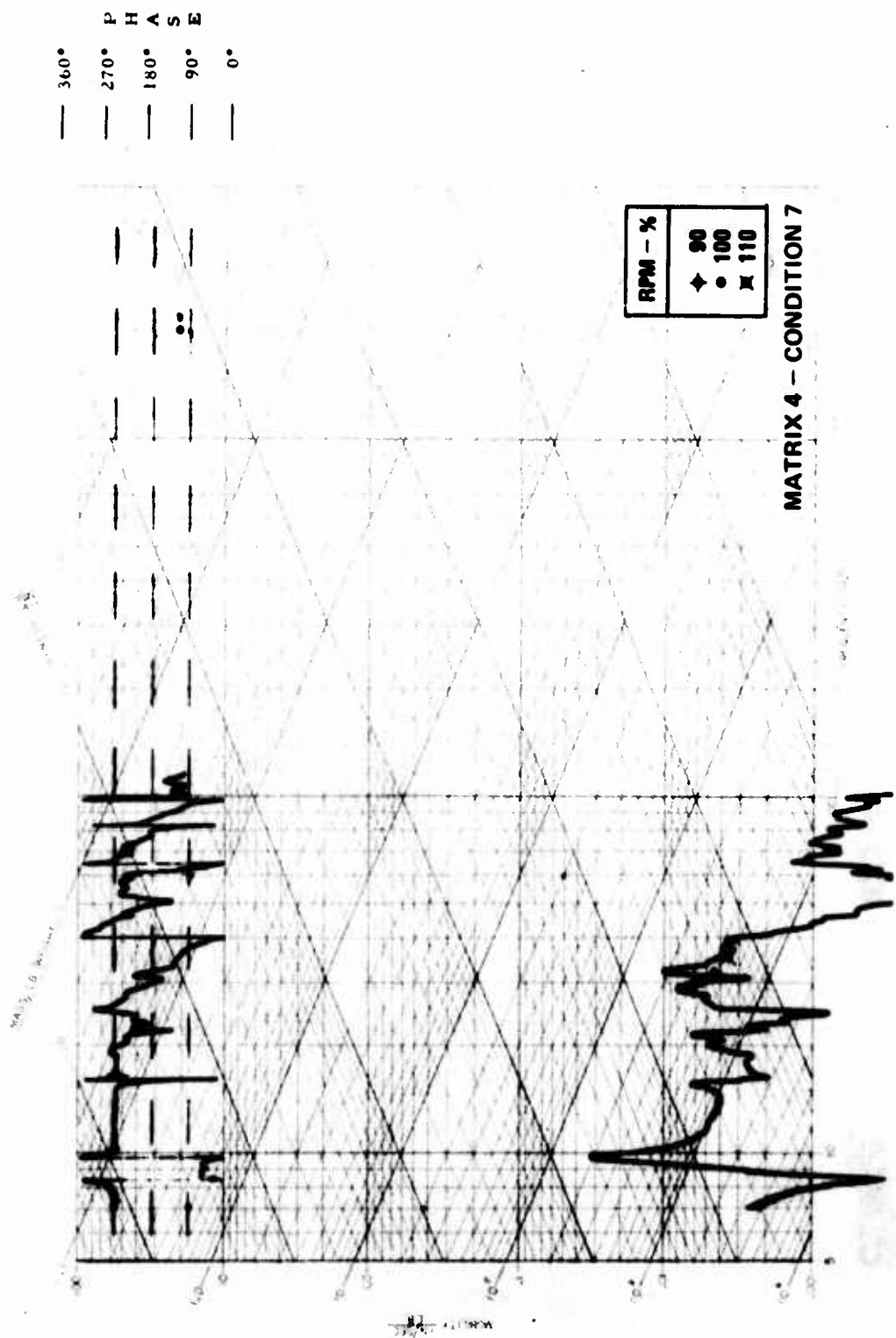
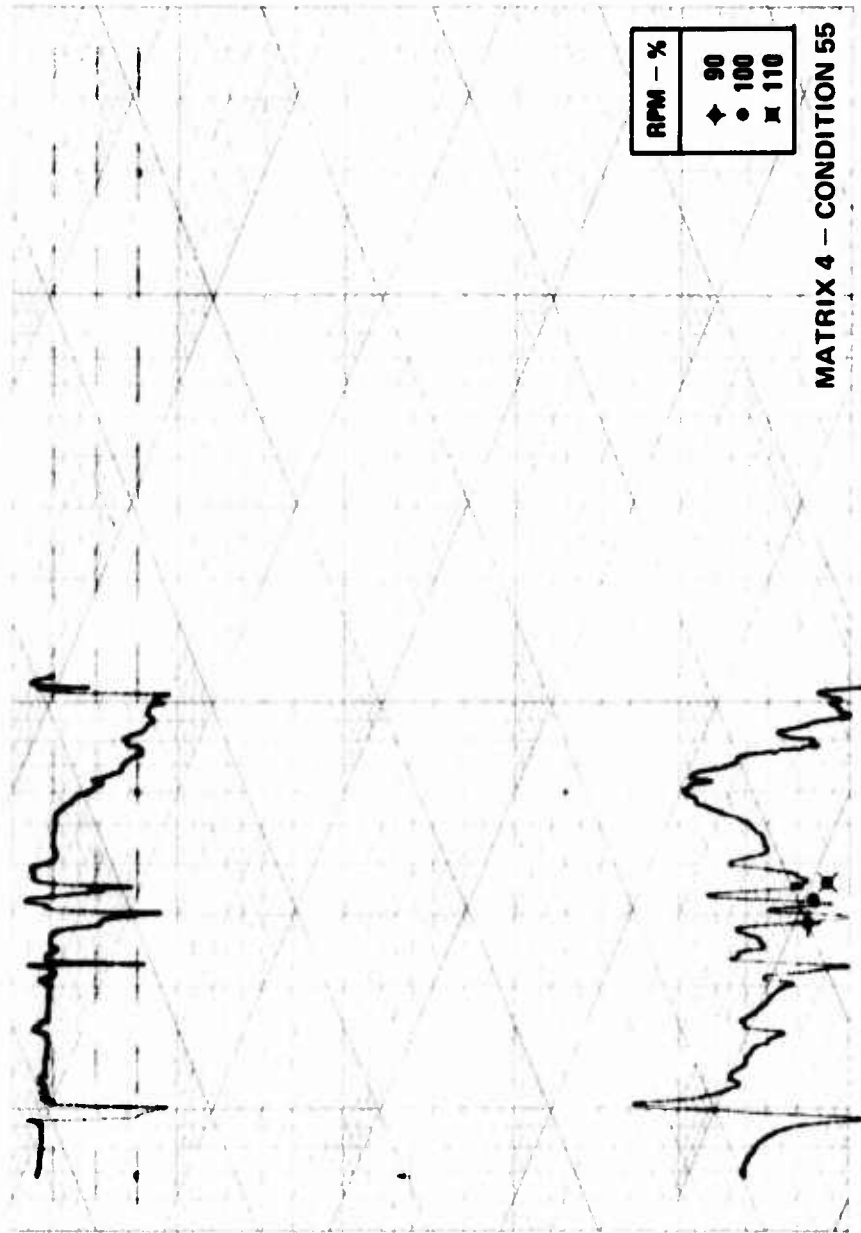


Figure 91. Cros: Mobility, Right Mount Lateral Due to Main Rotor Lateral.

— 360° P
 — 270° H
 — 180° A
 — 90° S
 — 0° E

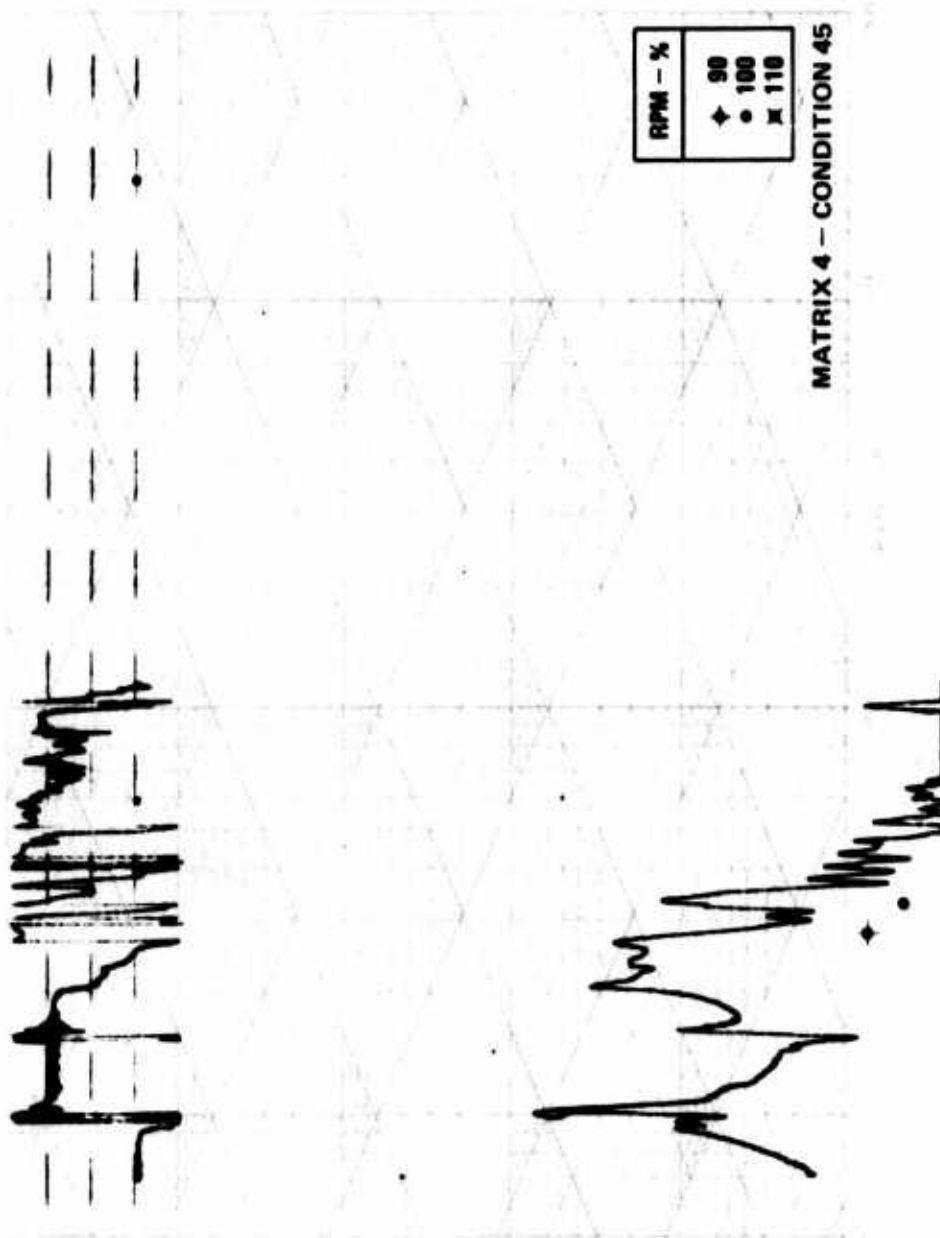


MATRIX 4 - CONDITION 55

RPM - %	
◆	90
●	100
■	110

Figure 92. Cross Mobility, Right Mount Vertical Due to Main Rotor Vertical.

— 360°
 — 270° P
 — 180° H A
 — 90° S E
 — 0°



MATRIX 4 - CONDITION 45

RPM - %	
◆	90
●	100
×	110

Figure 93. Cross Mobility, Turbine Mid-Split Lateral Due to Main Rotor Longitudinal.

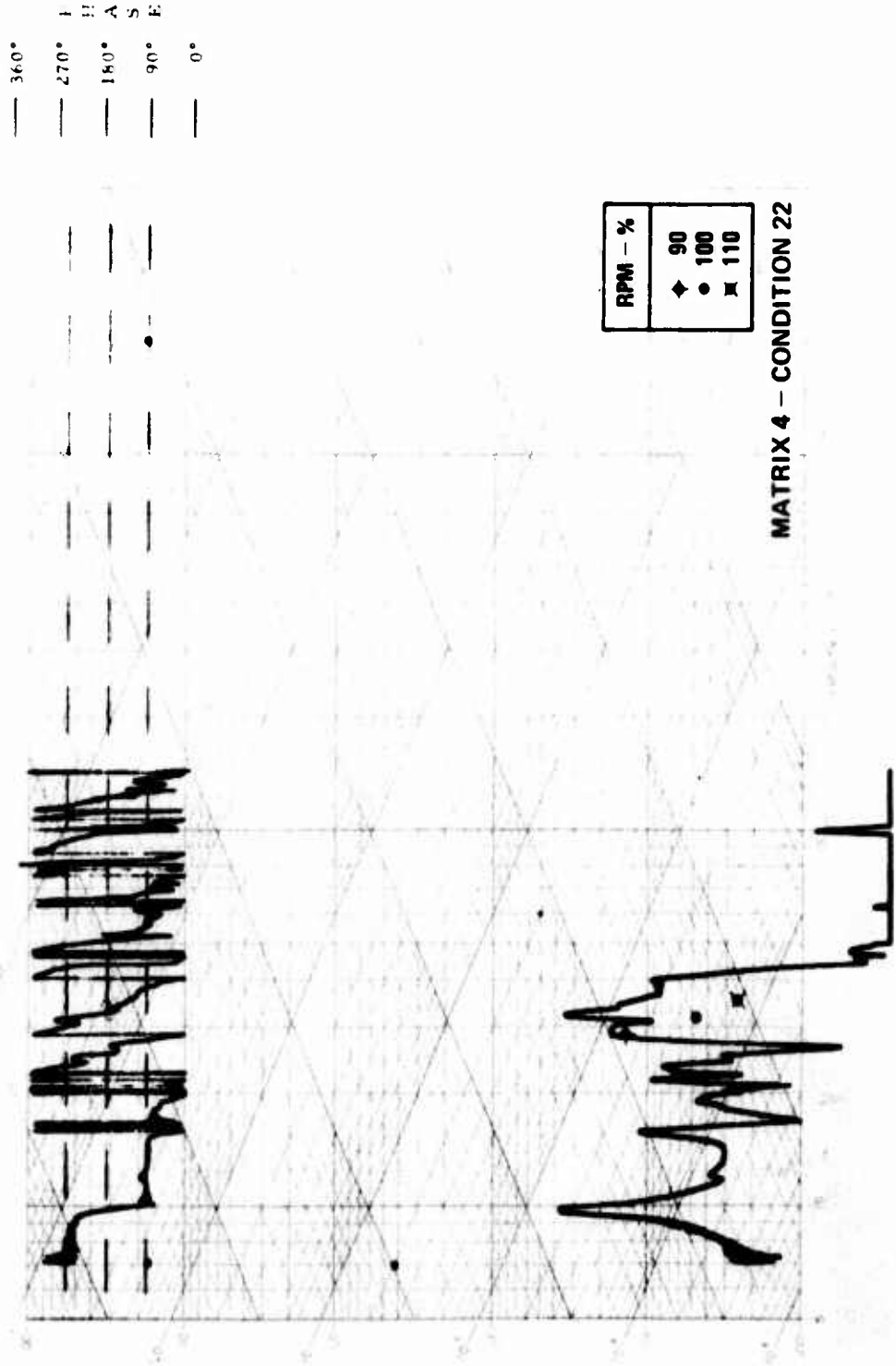


Figure 94. Cross Mobility, Turbine Mid-Split Lateral Due to Main Rotor Lateral.

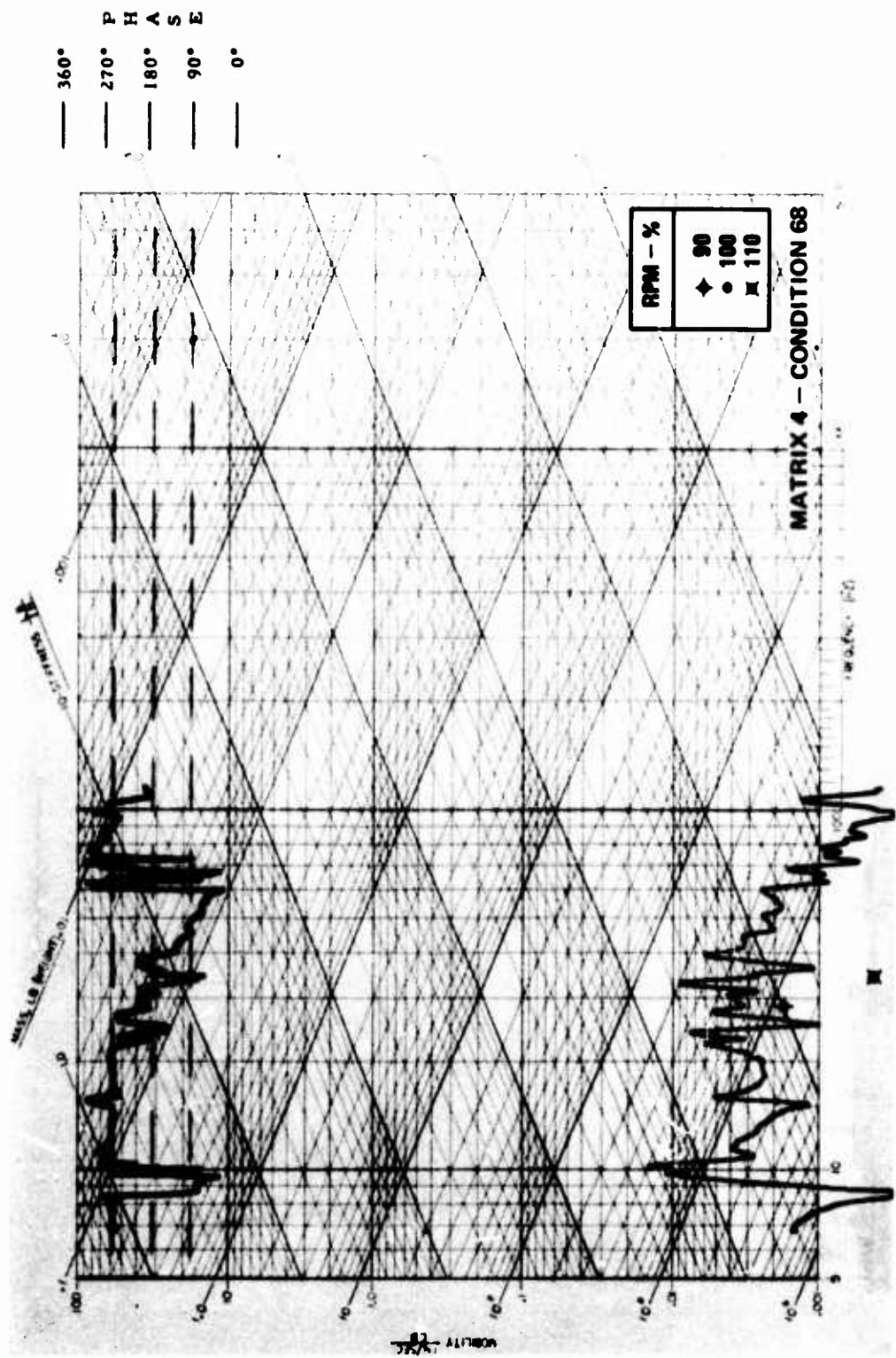


Figure 95. Turbine Mid-Split Lateral Due to Main Rotor Vertical.

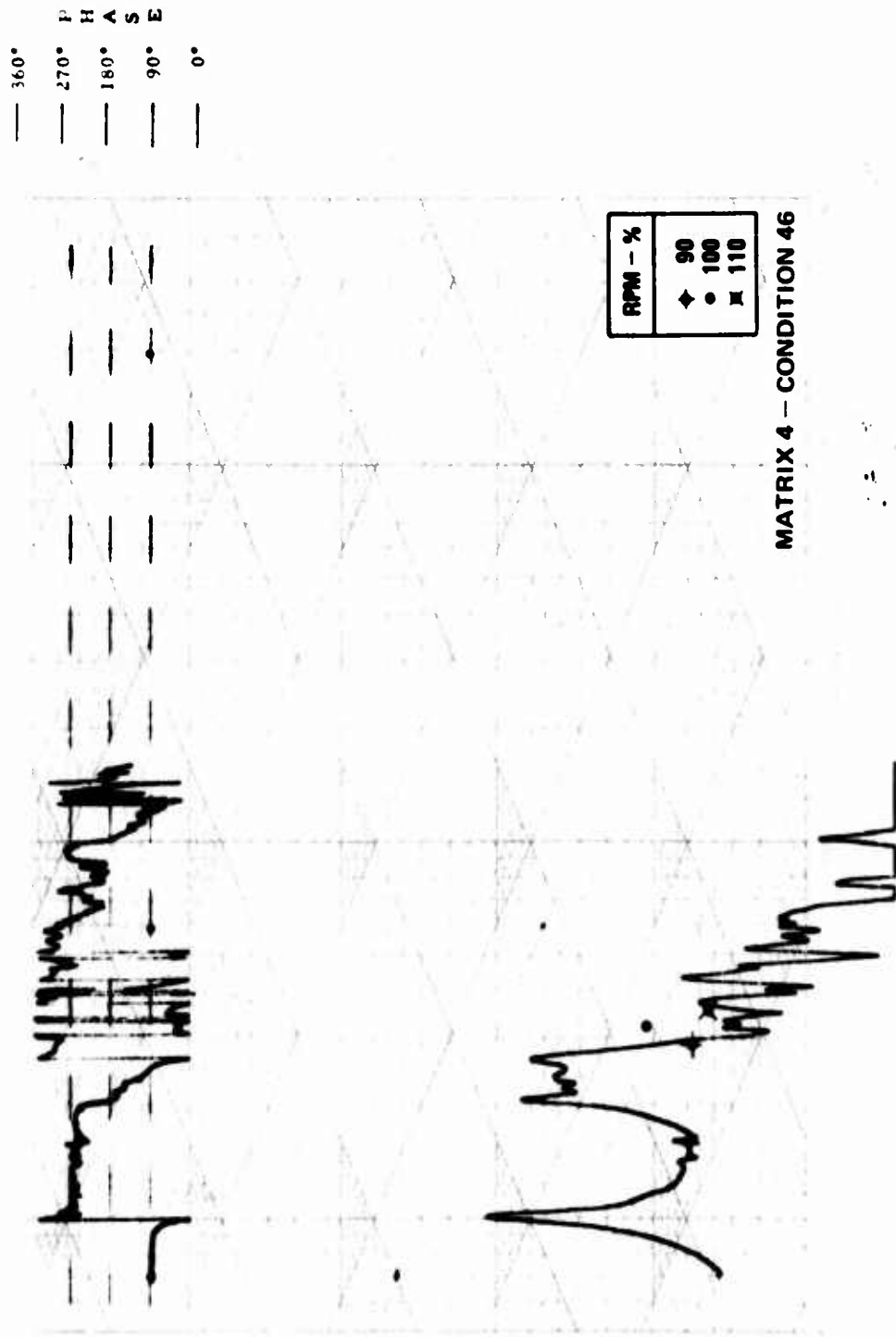
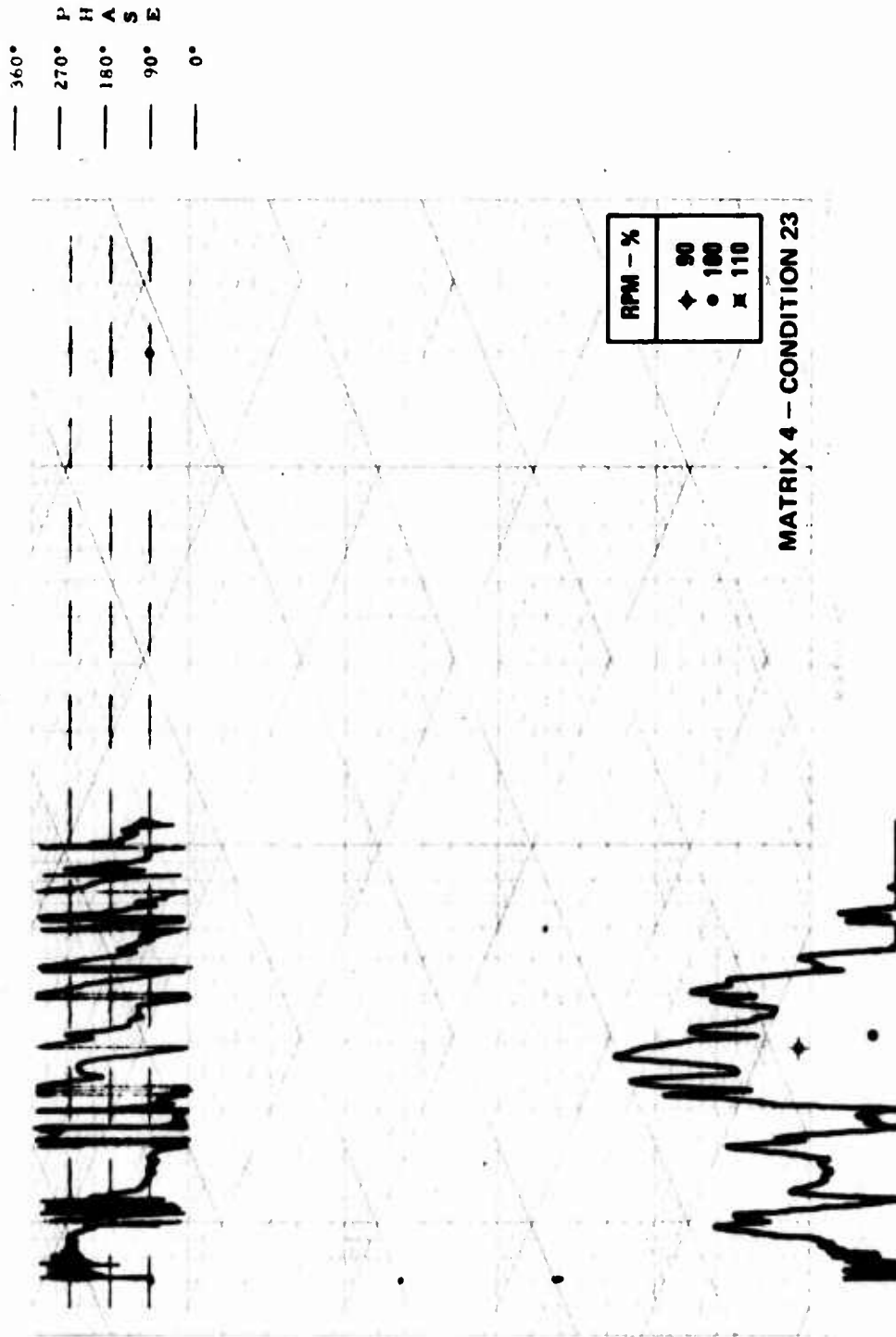
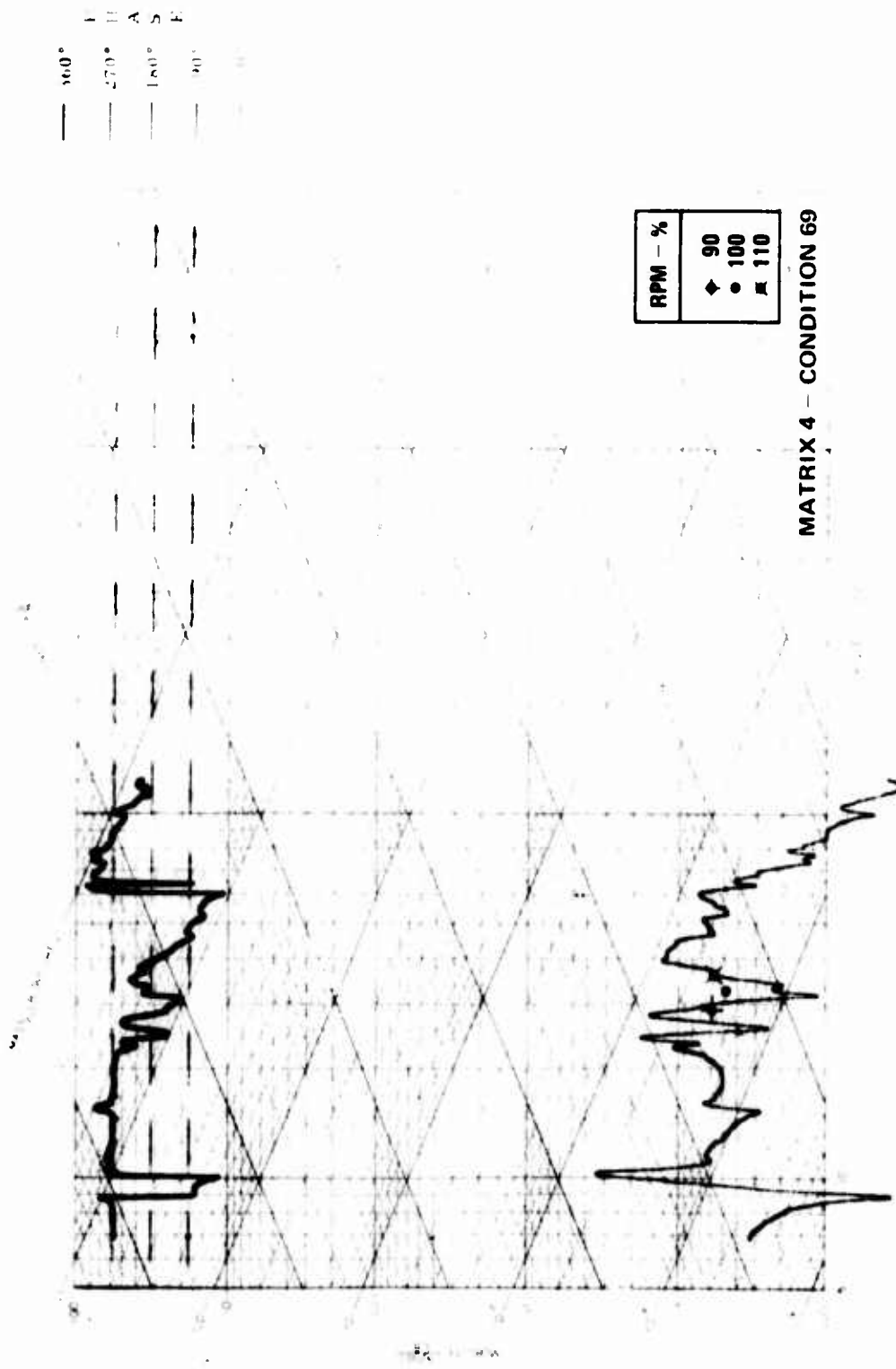


Figure 96. Cross Mobility, Turbine Mid-Split Vertical (Engine Axis) Due to Main Rotor Longitudinal.



✕ **Figure 97. Cross Mobility, Turbine Mid-Split Vertical (Engine Axis) Due to Main Rotor Lateral.**



MATRIX 4 - CONDITION 69

Figure 98. Cross Mobility, Turbine Mid-Split Vertical (Engine Axis) Due to Main Rotor Vertical.

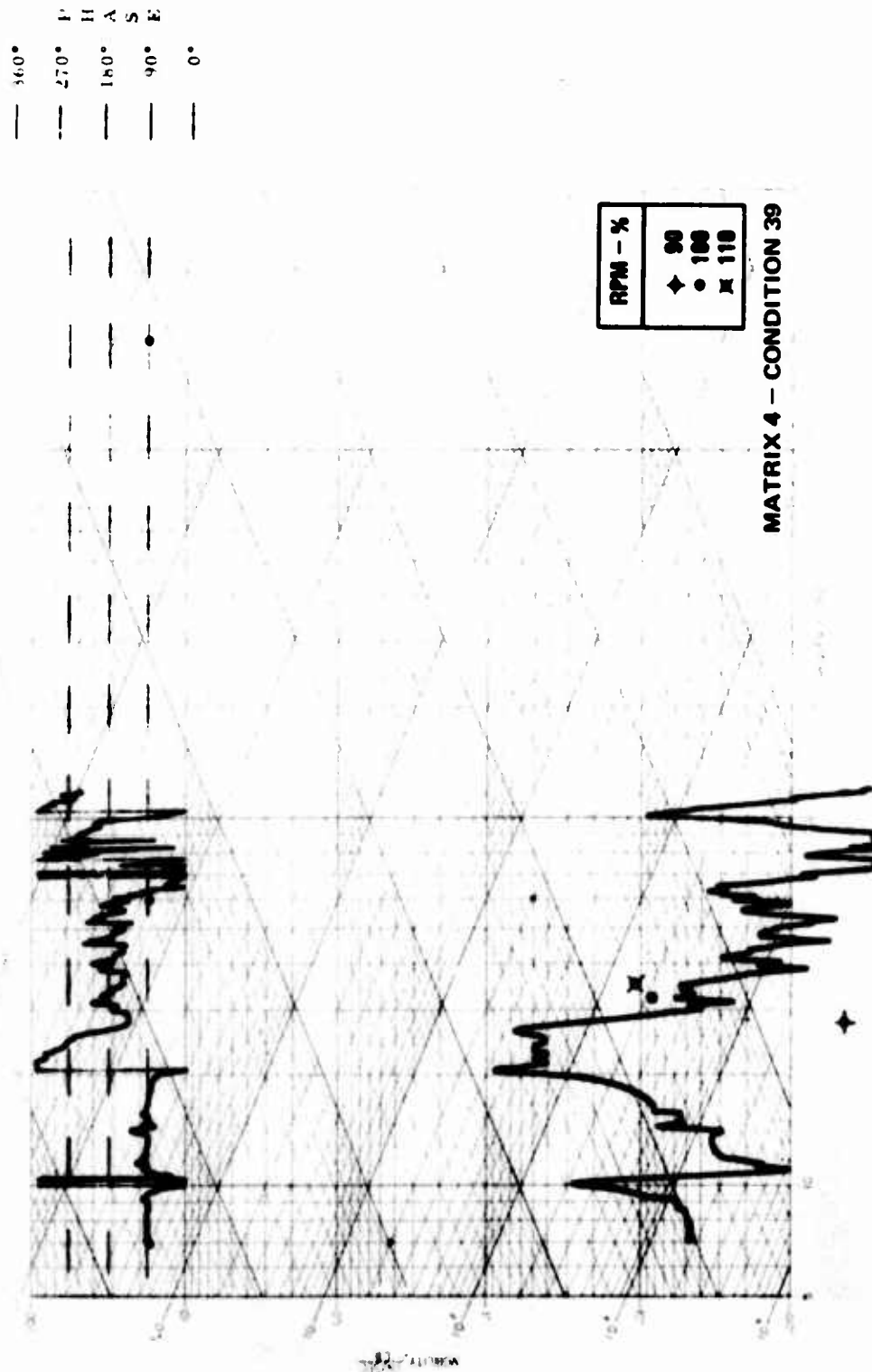


Figure 99. Forward Compressor Vertical Due to Main Rotor Longitudinal.

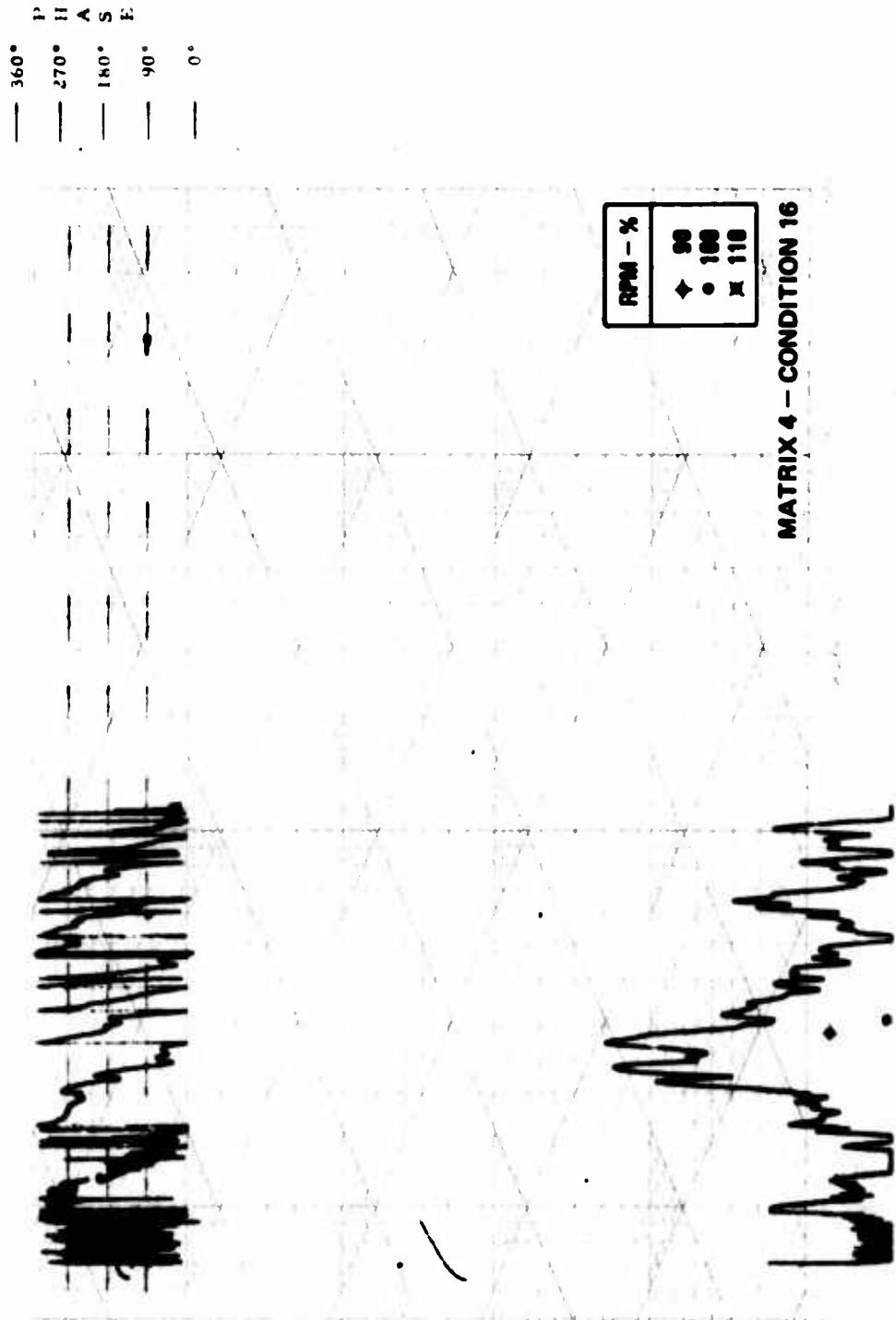


Figure 100. Front Compressor Vertical Due to Main Rotor Lateral.

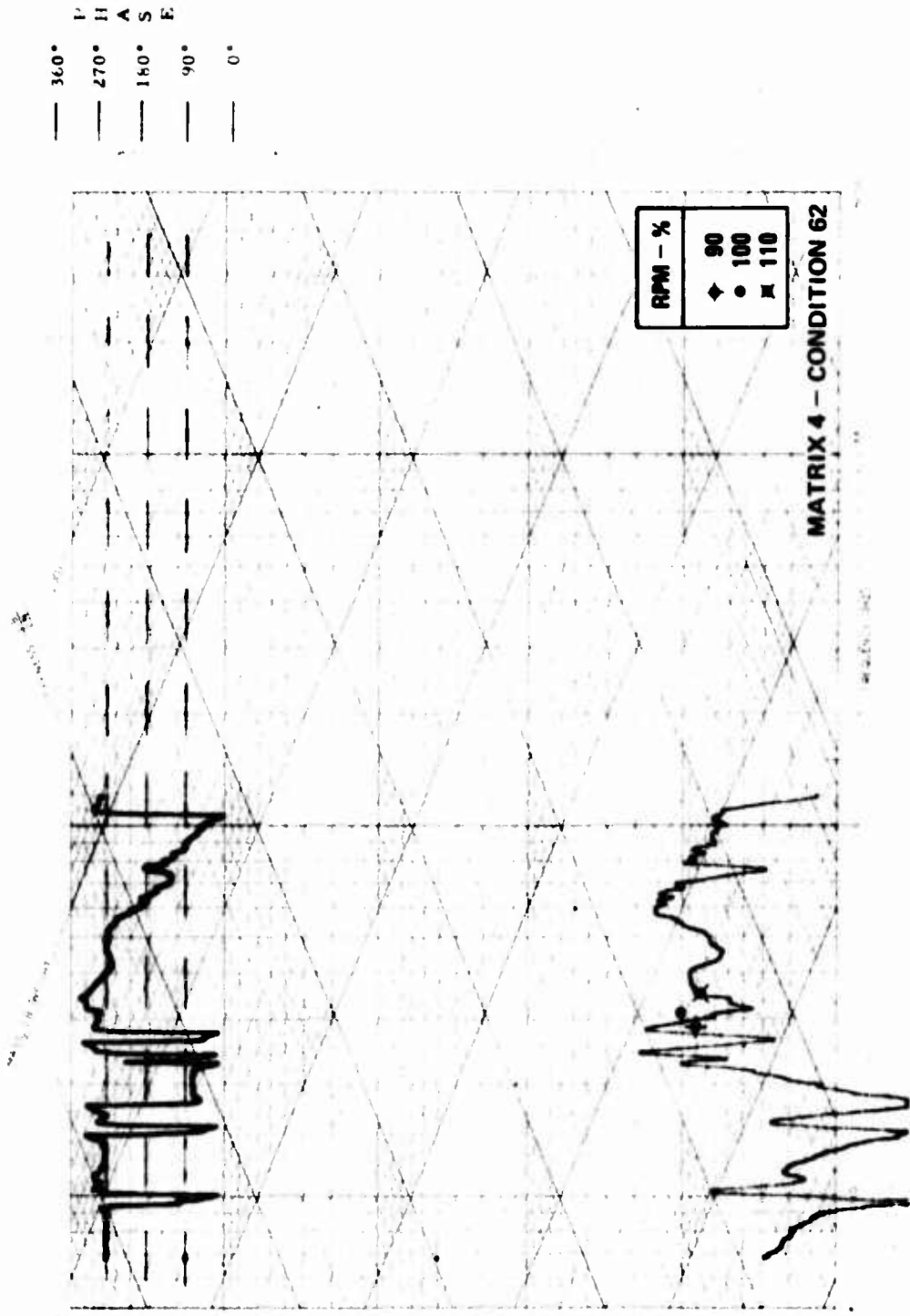


Figure 101. Front Compressor Vertical Due to Main Rotor Vertical.

NASTRAN MODEL FORCING FUNCTIONS

It is necessary to postulate forcing functions for the main and tail rotor locations of the NASTRAN model. It would be preferable if an analytical procedure were available which had been satisfactorily correlated with flight test data, but unfortunately this was not the case. Main and tail rotor n/rev loads are notoriously difficult to measure on research flights because of the presence of high steady and $1/\text{rev}$ loads and noise. Recourse is therefore made to forces based solely on aerodynamic calculations, as presented in Reference 9. Because of the uncertainty of the magnitude of the forcing functions, a range of phases was used in this study to bracket the possible phasing combinations, giving consideration to the main and tail rotors.

These phasing combinations are suggested by observing that main rotor $4/\text{rev}$ in-plane loads to the fuselage are caused by $3/\text{rev}$ and $5/\text{rev}$ in-plane shears, as measured in the rotating system. These rotating vectors describe an ellipse in the fixed coordinate system. (See Appendix C, Figure C-4.) The direction of the major axis of this ellipse has been observed in Reference 21 to change with airspeed and other flight conditions.

All main and tail rotor conditions are given for a reference condition of 126 knots, 5000 feet, corresponding to the condition shown in Figure 1.

MAIN ROTOR 4/REV LOADS

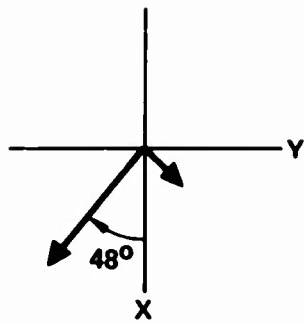
Based on Reference 9, and on scaled YAH-64 analytical data, the nine load sets shown in Figure 102 were used. The first is the most likely estimate of phasing between the three force vectors. The others are permutations on these phasings along the aircraft principal axes. (Set 1 includes phasing associated with equations 1 and 2, which were derived from Reference 9.)

TAIL ROTOR 2/REV LOADS

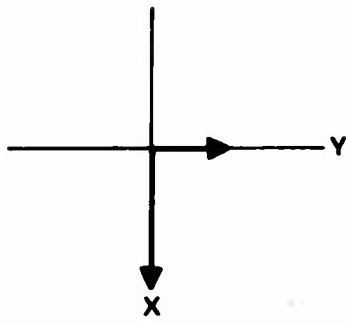
Tail rotor $2/\text{rev}$ loads are known only in magnitude, without phase information. However, lateral force (i. e., normal to tail rotor plane) dominates.

<u>Direction</u>	<u>Force (lb)</u>	<u>Assumed Phase (degrees)</u>
Vertical	3	90
Longitudinal	8	0
Lateral	50	0

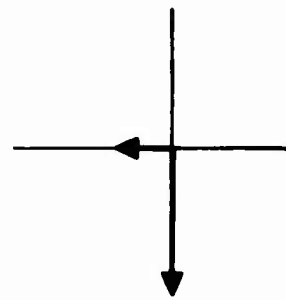
For this reason, it will be assumed that the lateral and vertical forces are in phase and that the vertical force lags the other in-plane component by 90 degrees.



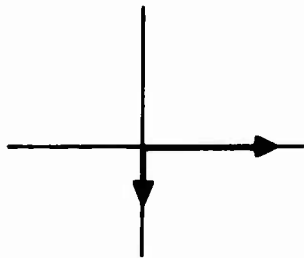
1. MOST LIKELY CONFIGURATION (SEE APPENDIX C)



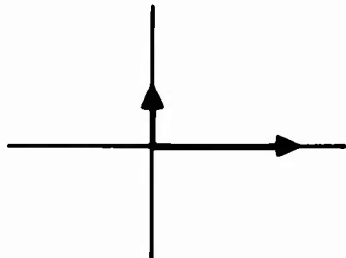
2. MAJOR AT 0° MINOR AT 90°



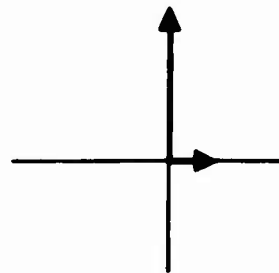
3. MAJOR AT 0° MINOR AT 270°



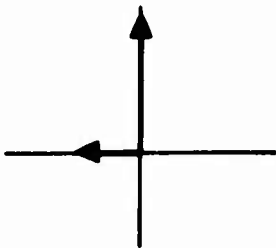
4. MAJOR AT 90° MINOR AT 0°



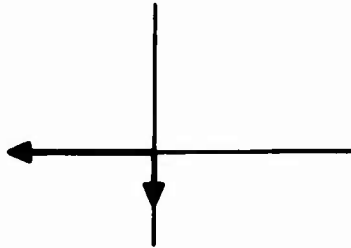
5. MAJOR AT 90° MINOR AT 180°



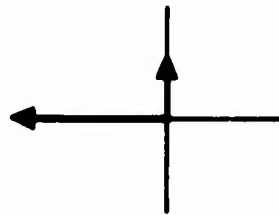
6. MAJOR AT 180° MINOR AT 90°



7. MAJOR AT 180° MINOR AT 270°



8. MAJOR AT 270° MINOR AT 0°



9. MAJOR AT 270° MINOR AT 180°

VERTICAL FORCE = 69.0 LB
 MAJOR INPLANE = 83.37 LB
 MINOR INPLANE = 33.54 LB

Figure 102. 4/Rev Load Permutations.

TRANSIENT LOAD

The rear oleo load time history was measured during a hard landing. (See Figure 10.) The ratio between oleo load and landing gear cross-tube loadings was established, and a suitably scaled transient load was applied to the aft points on both landing skids.

CORRELATION OF PREDICTED RESPONSE WITH FLIGHT DATA

The forcing functions described on page 143 are applied to the combined engine airframe model described on page 119, with the results shown below.

RESPONSE TO MAIN ROTOR 4/REV LOADS

Response at the engine center mount and turbine mid-split-line for flight test data and the calculated response for the nine load phasings are shown in Tables 12 and 13.

The calculated vertical response of the turbine mid-split-line is shown in Table 13 to be 0.87 inches per second for the first (most likely) force configuration. This calculated notion is to be compared with the turbine mid-split-line motion of 0.86 inches per second (peak) at 4/rev noted on page 63.

TABLE 12. EFFECT OF LOAD PHASING ON CENTER MOUNT 4/REV RESPONSE					
Force Configuration		Center Mount Velocity (in./sec)			
Major Axis (deg)	Minor Axis (deg)	Axial	Lateral	Vertical (Engine Axis)	
1.	Most likely	1.17	0.221	0.291	
2.	0 90	1.70	0.152	1.07	
3.	0 270	1.71	0.087	1.08	
4.	90 0	0.893	0.311	0.648	
5.	90 180	0.426	0.295	0.147	
6.	180 90	1.14	0.113	0.380	
7.	180 270	1.12	0.123	0.379	
8.	270 0	0.913	0.268	0.667	
9.	270 180	0.369	0.284	0.177	

TABLE 13. EFFECT OF LOAD PHASING ON
TURBINE MID-SPLIT 4/REV RESPONSE

	Force Configuration		Turbine Mid-Split Velocity (in./sec)	
	Major Axis (deg)	Minor Axis (deg)	Lateral	Vertical (Engine Axis)
1.	Most likely		0.33	0.87
2.	0	90	0.18	1.05
3.	0	270	0.16	1.05
4.	90	0	0.42	0.57
5.	90	180	0.40	0.41
6.	180	90	0.14	0.83
7.	180	270	0.20	0.81
8.	270	0	0.42	0.57
9.	270	180	0.43	0.36

As shown, a variation in phasing of the main rotor load components can change response from the most likely configuration by ± 50 percent. (The phases of the response points relative to one another also change radically.) This is an indication that all three components of rotor loads must be known accurately for both phase and magnitude.

Tables 14 and 15 show the variation of response with rotor rpm variations. This data confirms the trends shown in the mobility test data, where small changes in excitation frequency can cause large changes in response due to the proximity of many modes.

Table 16 lists the response of the forward compressor to unit forces and moments. After combining the unit response with the applied forces and moments, the resulting vertical compressor motion is calculated to be 0.78* inch per second at 4/rev. This calculated motion is to be compared with the measured compressor motion of 1.88 inches per second (peak) at 4/rev noted on page 63.

*Range of motion is 0.25 - 0.78 inch per second, depending on force configuration.

TABLE 14. EFFECT OF ROTOR RPM VARIATION ON CENTER MOUNT MAIN ROTOR 4/REV VIBRATION			
Most Likely Force Configuration Rotor rpm (pct)	Center Mount Velocity (in. /sec)		
	Axial	Lateral	Vertical (Engine Axis)
90	0.76	0.35	0.17
100	1.17	0.22	0.29
110	0.55	0.20	0.28

TABLE 15. EFFECT OF ROTOR RPM VARIATION ON TURBINE MID-SPLIT MAIN ROTOR 4/REV VIBRATION		
Most Likely Force Configuration Rotor rpm (pct)	Turbine Mid-Split Velocity (in. /sec)	
	Lateral	Vertical (Engine Axis)
90	1.08	0.64
100	0.33	0.87
110	0.19	0.46

As mentioned earlier, the flight data of Figure 1 was measured on a prototype helicopter. The airframe for production helicopters was modified in some areas, including the rotor mast base area. The result was to "soften" the mast base and thus reduce engine response to in-plane rotor forces. As a result, it is expected that compressor motion on production OH-6A helicopters is lower than it was on the prototype OH-6A. A review of the data in Reference 10 may validate this point.

TABLE 14. FORWARD COMPRESSOR RESPONSE DUE TO UNIT ROTOR FORCES AND MOMENTS AT MAIN ROTOR 4/REV

Main Rotor	Lateral		Vertical	
	Velocity (in. /sec)	Phase (deg)	Velocity (in. /sec)	Phase (deg)
Longitudinal force (lb)	1.05×10^{-3}	50	8.45×10^{-3}	190
Lateral force (lb)	1.23×10^{-2}	99	2.78×10^{-4}	89
Vertical force (lb)	3.50×10^{-4}	48	1.03×10^{-2}	246
Roll moment (in. -lb)	1.97×10^{-3}	275	2.86×10^{-5}	300
Pitch moment (in. -lb)	1.03×10^{-4}	47	8.72×10^{-4}	180

RESPONSE TO TAIL ROTOR 2/REV LOADS

Tables 17, 18, and 19 list engine response data due to tail rotor 2/rev excitation over a range of frequencies. Again, the response can vary greatly with nominal changes in rotor rpm.

This effect is shown in Table 19 to be very strong for compressor motion due to lateral tail rotor forces. At 90.6 percent rotor rpm (≈ 91 hertz), the compressor motion is calculated as 1.09 inches per second, which compares reasonably well with the measured compressor motion of 0.9 inch per second (average 1.41 inches per second peak) shown in Figure 4. As in the case of the main rotor response, it is expected that differences between the airframe of the prototype helicopter and the production helicopter led to the lowering of resonance by a few hertz.

TABLE 17. EFFECT OF ROTOR RPM VARIATION ON
CENTER MOUNT TAIL ROTOR 2/REV VIBRATION

Rotor rpm (pct)	Center Mount Velocity (in./sec)		
	Axial	Lateral	Vertical (Engine Axis)
90.6	0.328	0.059	0.384
97.3	0.064	0.159	0.107
104.4	0.041	0.379	0.067
112.0	0.045	0.342	0.064

TABLE 18. EFFECT OF ROTOR RPM VARIATION ON
TURBINE MID-SPLIT TAIL ROTOR 2/REV VIBRATION

Rotor rpm (pct)	Turbine Mid-Split Velocity (in./sec)	
	Lateral	Vertical (Engine Axis)
90.6	0.019	0.069
97.3	0.035	0.045
104.4	0.109	0.022
112.0	0.080	0.034

TABLE 19. EFFECT OF ROTOR RPM VARIATION ON
FORWARD COMPRESSOR VIBRATION

Rotor rpm (pct)	Velocity (in./sec)	
	Lateral	Vertical
90.6	0.222	1.09
97.3	0.242	0.368
104.4	0.238	0.232
112.0	0.140	0.306

RESPONSE TO HARD LANDING LOADS

The hard landing forcing function was applied, with a time step of 0.01 second. Predicted acceleration response at the compressor and at the ignitor is shown in Figures 103 through 105, where response without gyroscopic effects considered is plotted over response with gyroscopic effects. Response in the vertical plane does not change appreciably for this symmetric loading condition, but in the lateral direction there is a higher response in the high-frequency components when gyroscopic effects are modeled.

Figure 103 shows a peak vertical transient acceleration on the compressor of 1360 inches/sec² or about 3.5g; Figure 105 shows a peak vertical acceleration on the ignitor of 1960 inches/sec² or about 5g. Both of these calculated responses are in excess of the transient 2g limit shown in Figure 9. No data was available for comparison. As mentioned earlier, Reference 10 could be studied concerning possible additional data, including a landing transient.

It should also be noted that the frequency of the calculated engine response is 12-15 hertz.

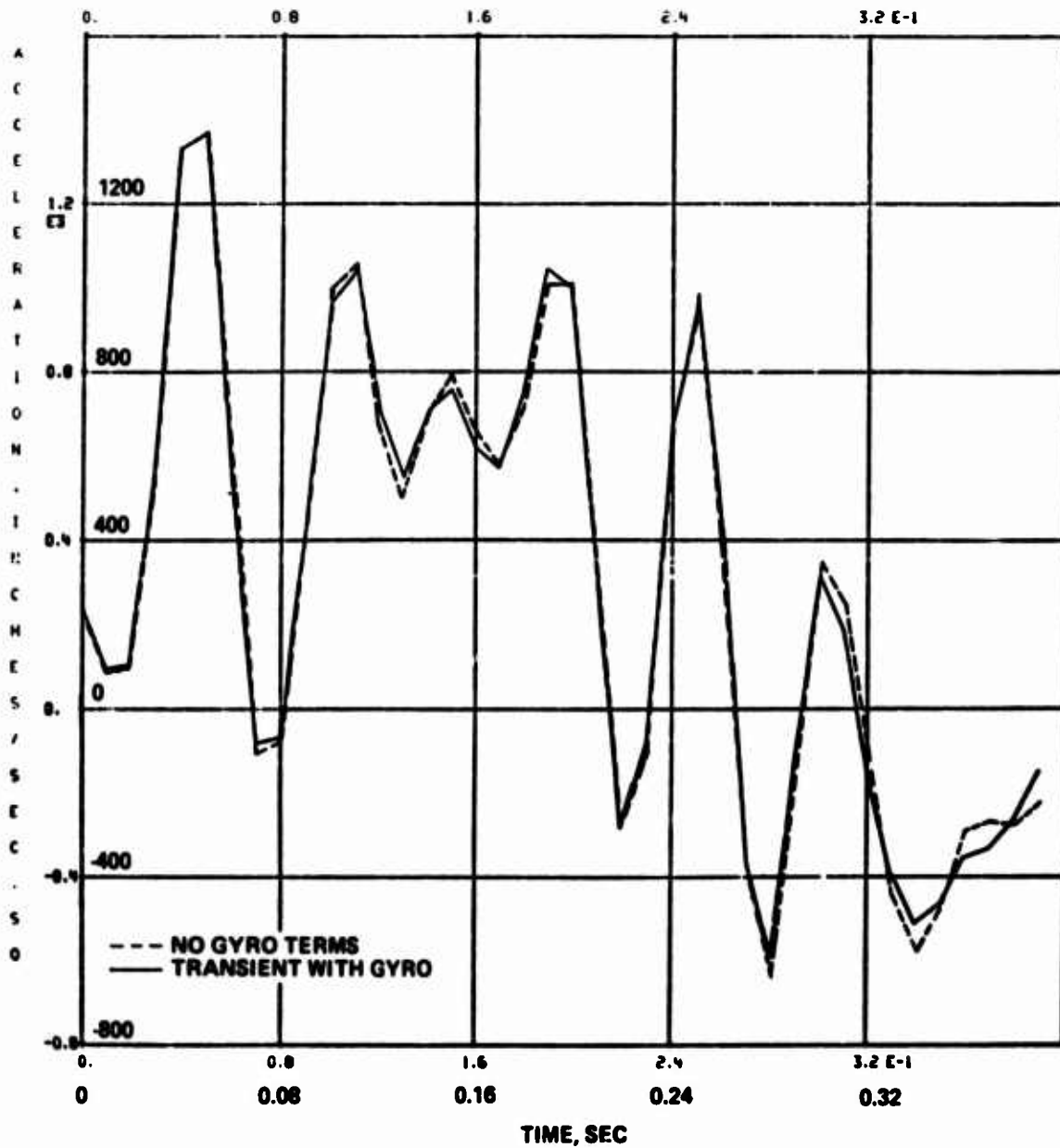


Figure 103. Forward Compressor Vertical Response (Engine Axis) Due to Hard Landing Load.

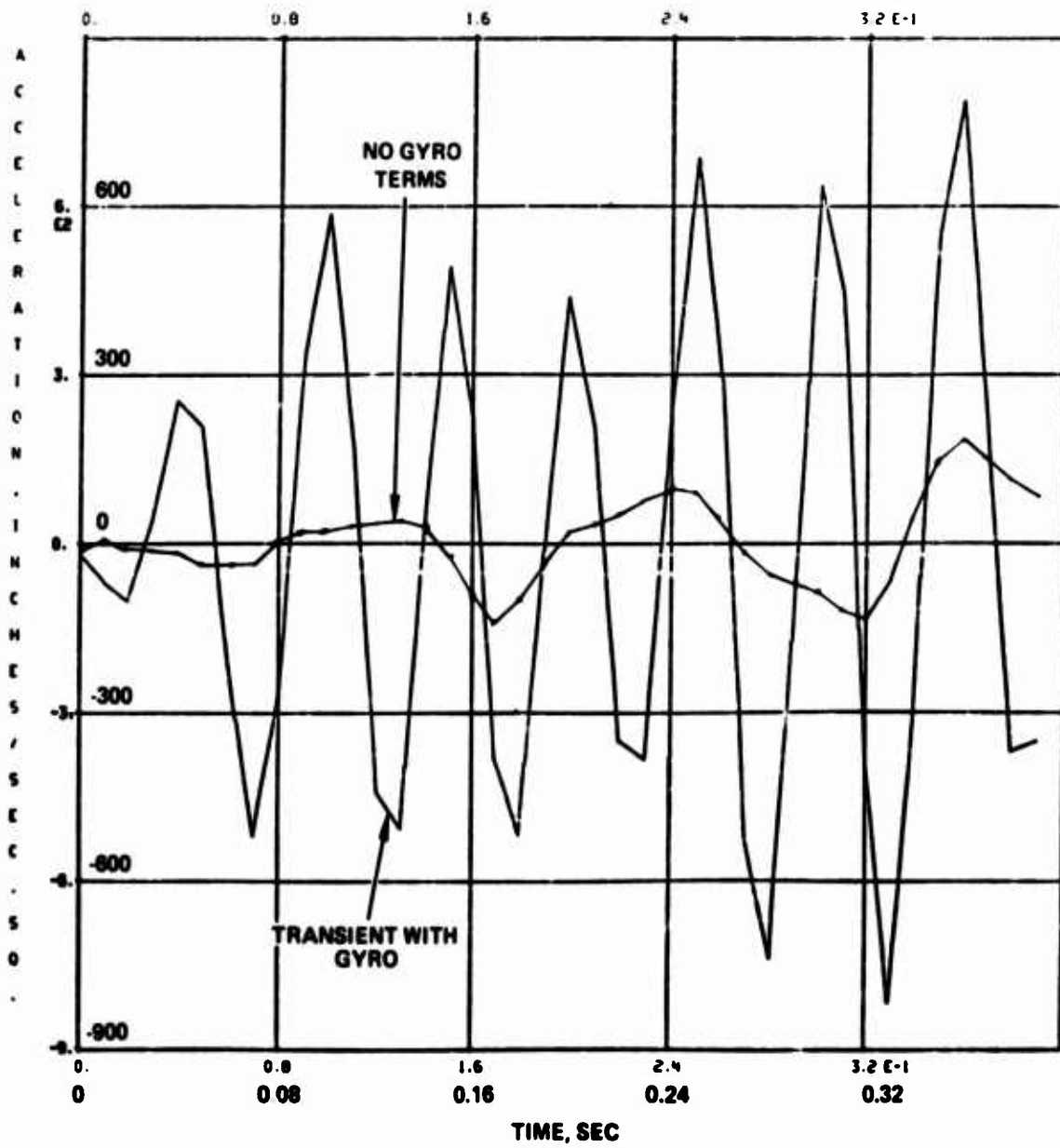


Figure 104. Ignitor Lateral Response Due to Hard Landing Load.

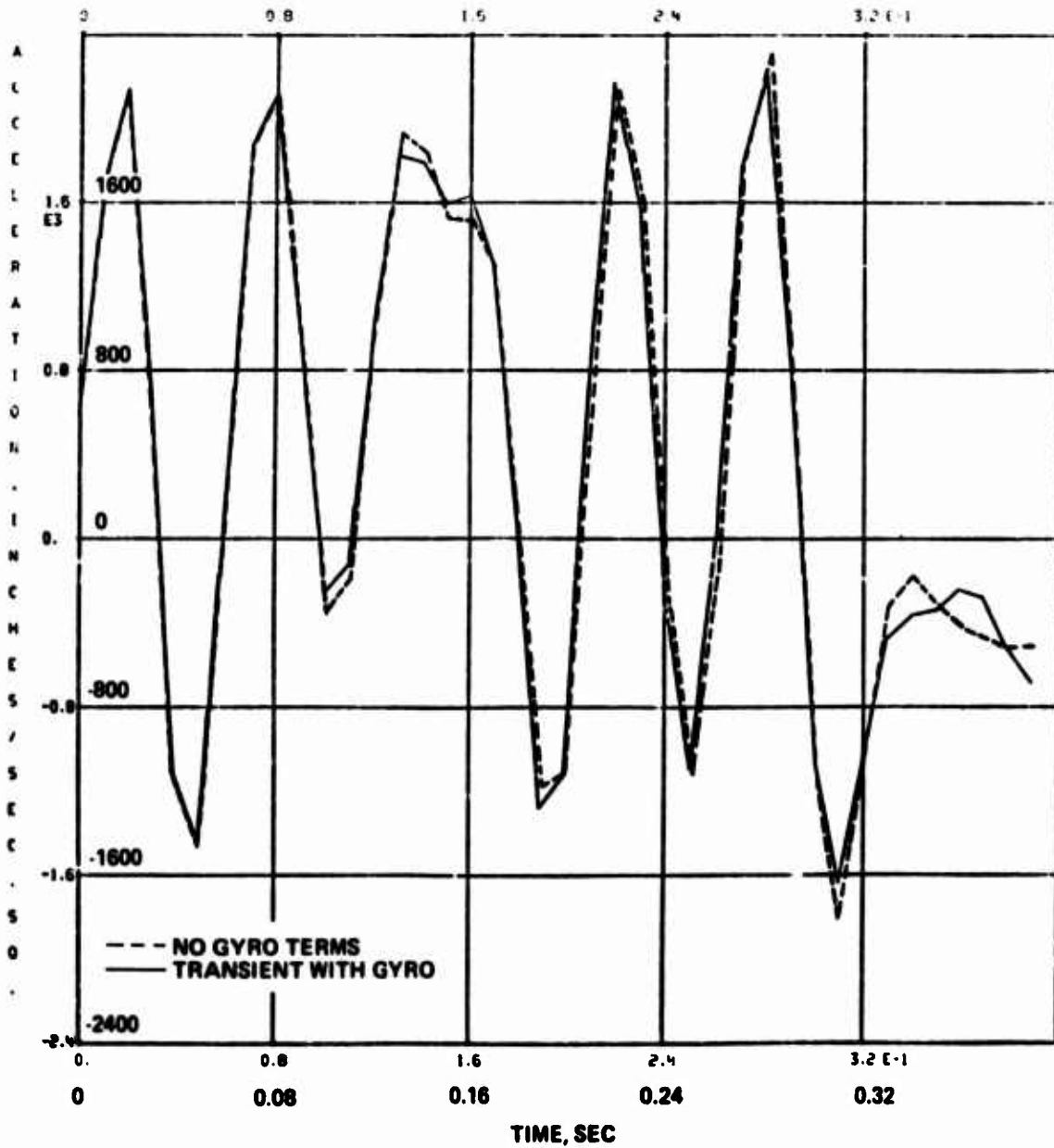


Figure 105. Ignitor Vertical Response Due to Hard Landing Load.

ENGINE VIBRATION LIMITS AND METHODS OF DATA ANALYSIS

References 3 and 4 present a review of the engine installation vibration limits for seven different engines, and the wide variation in those limits is seen in Figure 1 of Reference 3. These seven engines were available in the time period around 1970, and the limits are expressed in terms of displacement, velocity, and acceleration as particular functions of frequency. In addition, at least three methods of recording, processing, and interpreting the vibration data are involved: discrete frequency, bending angle, and overall limits.

The discussion of these vibration parameters and data handling in References 3 and 4 presents reasons for favoring one parameter or procedure over others. However, no clear statement is forthcoming as to why the engine limits are what they are, in general. Reference 3 states that bending angle limitation has been applied only when the engine had a relatively flexible section. Reference 4 substantiates that if engine vibration limits are based on bending flexure (i. e., case bending), then a constant vibratory velocity criterion would be applicable. However, Reference 4 then points out that when vibration velocity did not involve bending flexure, but, rather, rigid-body displacements, "vibratory velocity alone would not be a sufficient measure of the destructure potential of vibration."

Reference 4 also points out that the location of vibration transducers required by paragraph 3.17.3 of Reference 22* implies that external detection of bearing whir (or rotor whirl) is sought. However, an analysis is presented which shows that measurements of vibration at external locations may not be representative of the vibratory response of rotors. This conclusion, in turn, is restrained by the possibility that use of squeeze film bearing dampers (chosen to control rotor frequencies in the most recent engine designs -- see Reference 24) may render the conclusion about external measurements of internal motions invalid.

No easily understood discussion of the reasons for engine vibration limits seems to be available for the airframe designer. To the airframe designer, some understanding of what the engine designer has in mind when setting engine vibration limits would be helpful, though proficiency in engine dynamics is neither necessary nor wanted. But the helicopter engine

*It is believed that this paragraph should properly be ascribed to Reference 23.

manufacturers have no requirement to disclose the elements they consider in setting vibration limits (see Reference 23). Clearly, important proprietary considerations are involved, and there is no wish presented here to compromise competitive information.

However, the helicopter airframe manufacturers are required to comply with general airframe vibration specifications, such as paragraphs 3.7 through 3.7.3 of Reference 25. (Recent military programs involve considerably lower allowable vibration limits at the crew station and in the cabin than presented in Reference 25.) With this experience in mind, the desirability of standardizing engine vibration limits, as expressed in References 3 and 4, is understandable, and likely welcomed by all airframe manufacturers.

In any case, for reasons which are not clear, perhaps such standardization is coming. During this study, a review was made of engine vibration limits. The specifications for six engines currently in production or under development were reviewed as well as that for the T63 in the OH-6A. All seven of these engines specified an acceleration as a vibration limit in part of the frequency region from 15 hertz to approximately 300 hertz, which can roughly be considered the airframe excitation region. The acceleration (or g's) related to these specifications varied from 1 to 5g, which, while not constituting standardization, is at least a creditable beginning.

These vibration limits are shown on Figure 106, together with the first free-free bending frequency presented in the associated specification (usually paragraph 3.15.2, "Engine Stiffness," of Reference 23). The surprisingly consistent use of an acceleration (g) vibration limit may be related to the following statement taken from Section 4, "Limits," of Reference 26:

At frequencies below the engine fundamental bending mode frequency, the tolerance of the engine to a vibratory mode may be better defined by a "g" loading limit than by an "average velocity" limit.

NOTE: In the above LIMITS example, the optional discrete frequency limit was selected as a "g" limit below 40 Hz to better match the engine vibration input tolerance in this low frequency range. The 40 Hz frequency was selected as being sufficiently below the engine fundamental bending mode frequency to ensure the engine's responding as a rigid body to a vibratory input.

In other words, the first free-free bending frequencies of the several engines shown on Figure 106 are generally above 100 hertz, which is considerably above all significant main rotor excitation. For this reason, perhaps, these engines are subjected only to rigid-body motions. Therefore, their environment can be completely described by an acceleration parameter.

It is of interest to note that, in Reference 3, Figure 7 presents a vibration criterion reflecting VTOL aircraft environment. This criterion, labelled "hypothetical limits," corresponds to the envelope of a great amount of Bell flight test data. The lowest of these limits -- level flight, V_{cruise} and below -- corresponds almost identically to a 5g limit from 15 to 250 hertz. This hypothetical limit is also shown in Figure 106.

SURVEY OF ENGINE MANUFACTURERS

As part of this present study, Hughes Helicopters was required to examine and evaluate the results obtained to establish means of defining engine characteristics, parameters, and limitations so that improved engine-airframe vibratory compatibility will be ensured. A letter (Reference 27) was therefore prepared which presented major points suggested by Figure 106 and other parts of this study. The letter was sent to six helicopter engine companies, and replies were received from five companies within the available time frame.

Comments on the following points were solicited by Reference 27:

1. It is proposed that Reference 23 be amended as follows:
 - a. 3.15.2 Engine Stiffness. The first free-free lateral and vertical bending modes shall be at frequencies greater than 150 Hz.
 - b. 3.17.3 Engine Shaft Power Absorber Vibration. The maximum permissible displacement(s) of the engine case throughout the complete operating range of the engine shall be specified on the installation drawing, and shall not be less than those corresponding to 2g accelerations for harmonic motion for frequencies from 15 to 150 Hz for **steady-state** conditions.
2. It is suggested that an acceleration parameter (2g) is the best vibration parameter.
3. It is suggested that the engine manufacturer continue to specify the locations for measurement of vibration (or acceleration), but that the number of vibration pickups on the installation drawing be expanded to permit identification of mode shapes and phase data.
4. It is suggested that the best method of data reduction is to perform discrete frequency analysis.

RESULTS OF SURVEY

The results of the survey are given below, taken out of context for brevity and edited as necessary to preserve proprietary information.

1. a. First Free-Free Bending Frequency >150 Hz

- [A]* "We believe that the MIL spec should not be changed from the current wording and not require that the engine have bending mode frequencies greater than 150 Hz. ... engines ... can have the first free-free bending mode frequency below 150 Hz. Thus specifying a minimum bending mode frequency would be unduly restrictive.... The first bending mode frequency should be well above 50 Hz."
- [B] "The limit of 150 Hz seems arbitrary and may give rise to unnecessary stiffness and weight penalties."
- [C] "Because of the nature of the dynamic relationship between an engine and an aircraft, no detailed vibration limit requirements can be determined which will apply to all applications; i. e., the variables are many, and each application must be treated individually. Any arbitrary specification limit such as you have proposed would tend to apply an unnecessary constraint."
- [D] "Under the assumption that this spec is intended to ensure that engine bending modes are not excited by helicopter rotor frequencies, a criterion of 150 Hz would probably unduly penalize engine weight."
- [E] "We should agree to standardizing an airframe-induced vibration specification in the range of airframe excitation frequencies.... In general we do comply with the proposed changes to AV-E-85(3B since our engines ... have free-free bending modes in excess of 150 Hz."

* [] designates the several engine manufacturers.

1. b. 2g Vibration Limit From 15 to 150 Hz

2. Acceleration Parameter Is the Best Vibration Parameter

- [A] "Because we do not agree with the 150-Hz bending mode frequency, we cannot agree with specifying a minimum of 2g up to 150 Hz. . . . We are in agreement with the SAE AIR 1289 (Reference 26). In the case of AIR 1289, limits are suggested in the 15 to 40 Hz band and in the 40 to 2000 Hz band. At this point, I'm not sure whether the dividing point should be 40, 50, 60, or 70 Hz. . . . It seems to me that if we can get engine manufacturers to agree to present limits as suggested in AIR 1289, there would be no need of specifying a 2g minimum in the MIL spec for the low-frequency band."
- [B] "I support recommendation 1. b as a reasonable requirement, although the necessity of the 2g has not been established."
- [C] "We do not agree that g accelerations are the preferred parameters for defining limits. The forthcoming tri-service specification refers to velocity; this would get our vote in certain ranges and g's in others. We do accept the definitions contained in proposed SAE AIR 1289."
- [D] "It is assumed that the 2g acceleration is double amplitude. Again, the 150-Hz criterion appears severe. It is suggested that the vibration criterion apply only for airframe frequencies that are specified for the particular installation. . . . The measurement of airframe- and engine-induced vibration should be consistent. Generally, we favor a displacement parameter (mils) since vibratory deflection is the parameter used in engine design to evaluate engine sensitivity to rotor unbalance (mils/oz-in.)."
- [E] "Recently we have used an acceleration parameter in the airframe-induced frequency regime. . . . Also, 2g is a reasonable level to accept as airframe-induced."

3. Engine Manufacturers Specify Transducer Location and Identify Mode Shape and Phase

Only manufacturer [A] agreed to the mode shape proposal without change. Manufacturer [E] pointed out that for an engine meeting proposal 1. a (bending frequency >150 Hz), two axial stations should be sufficient to describe a rigid-body mode. No comments were received on phase measurements.

4. Discrete Frequency Is Best Method of Data Reduction

Manufacturers [A], [B], and [D] agreed with this proposal; manufacturers [C] and [E] made no direct comment.

EVALUATION OF SURVEY

The comments above generally indicate disagreement by the majority of the engine companies with the proposed specification changes in the case of item 1. a (bending frequency above 150 hertz) (four disagree, one agrees) and item 1. b (2g vibration limit from 15 to 150 hertz (three disagree, two agree). Three out of five agree with item 2 (best vibration parameter is acceleration), at least implicitly, and two disagree. Limited agreement was given to item 3 (transducer location for mode shape definition) (two manufacturers were favorable, three did not comment, and no comments were made on phase measurement). Three engine companies agreed with item 5 (discrete frequency as choice of data reductions), and two made no comment.

Overall, it would appear that the engine manufacturers do not accept the idea of specification changes involving engine design (items 1. a and 1. b), even though Figure 106 and the engine companies' own specifications show that some current and development engines already meet the proposed specification changes. There was generally more agreement than disagreement on items 2, 3, and 4, but these are concerned with selection of best vibration parameter, mode shape and phase definition, and data reduction and do not influence engine design directly and strongly, as do items 1. a and 1. b.

It should be pointed out that the arguments against a bending frequency greater than 150 hertz and an ability to withstand 2g vibration from 15 to 150 hertz generally focus on the possible adverse effect on engine weight. On the other hand, not one comment was received on the possible adverse effect on airframe weight if the proposed specification changes are not followed. Clearly, the use (the Army or other operator) could be forever buying a system (the whole aircraft) in which one component weight (the engine) is always optimized (i. e., lightened) at the expense of the airframe. The price to the user is therefore perhaps not the lowest possible, from the point of view of either first cost or life-cycle cost, including possible maintenance of engine isolators.

The traditional viewpoint of the engine manufacturer is to retain maximum specification flexibility for design; this is understandable, and airframe manufacturers have operated the same way. The airframe companies

and the engine companies have been consulted concerning specification development, but the Army and the other services clearly retain responsibility for specification content. However, in instances such as this present study, when interfaces are involved which affect the whole aircraft, the case can be presented for acceptance of a proposed change which might appear to favor the airframe manufacturer over the engine manufacturer. It is the responsibility of the procuring service (or services) to make the decision about the engine specification.

It is important to point out that a spirit of negotiation can be introduced to this subject of engine interface vibration specification. The minimum bending frequency of 150 hertz introduced by Hughes Helicopters was based on a review of twice tail rotor frequency (100 hertz) and the relative closeness of the lowest bending frequency of the T63 engine (127 hertz -- see Figure 74). Based on this particular situation, 150 hertz was selected arbitrarily, and a lower value could be negotiated. The same idea could be deduced by reading the comment in "Results of Survey -- 1. a," by manufacturer [A], who implies a bending frequency less than 150 hertz, but "well above 50 hertz" is appropriate.

With respect to the proposed vibration limit value of 2g (aside from the range from 15 to 100 hertz), experience by Hughes Helicopters in this study indicates that 1g might not be high enough to provide margin for the cruise environment; but, as mentioned above, Balke indicates (implicitly at least) in Figure 7 of Reference 3 that the cruise vibration limit (i. e., steady state) should be 5g from 15 to 250 hertz. Therefore, the airframe industry could be consulted profitably to obtain a suggested compromise vibration criterion.

In conclusion, a point of view is given here that directs the results of the survey toward giving the user the best operation and/or cost of the whole aircraft system.

SUITABILITY OF IMPEDANCE/MOBILITY COUPLING AND MODAL COUPLING METHODS

A significant aspect of this present study was to evaluate two sets of parameters, or methods, for coupling the airframe model to the engine model. The two methods, called impedance/mobility coupling (in Reference 4) and modal coupling, are now defined and evaluated for suitability for the specific case of the T63-OH-6A combination and for the general case of any engine-airframe combination.

COST-EFFECTIVE INTERFACE DYNAMIC MODELING

The reductions in cost of both dynamic testing and analysis in the last 15 years are curiously parallel. Finding the modes of a 10th-order system was a major technical achievement in the late fifties, whereas today the modes of a 1000th-order system can be found for less cost and with much less technical skill required. Conversely, the cost to produce one of the test mobility plots shown in this report to the same level of quality by the test equipment of 15 years ago (typically a meter for recording magnitude and a dual-beam oscilloscope for measuring phase, with data hand-plotted) would have taken literally orders of magnitude more test time and man-hours than required by the automated test gear in use today. In addition to being more economical, these modern test and analysis tools are in widespread use in the industry, so that a project can expect their use as a routine matter, without excessive method development costs.

Now that it is possible to analyze large, complex models, and produce large amounts of high-quality test data, the problem is how to use these powerful tools effectively.

OBJECTIVITY VERSUS RELIABILITY OF TEST DATA

There are two broad classes of methods for predicting vibratory response of two components when coupled, using test or analysis data measured when the components are not coupled. The first will be labeled "impedance/mobility coupling" herein. Matrices of impedance/mobility measurements at one frequency for each component can be inverted and summed, and the summed matrix inverted, to predict dynamic impedance/mobility of the coupled system. The second method will be labeled "modal coupling." One or more of the components can be defined in terms of an idealized modal model derived from analysis and/or test data, as was done in this report.

The impedance/mobility coupling method has the apparent virtue of objectivity. Actual test data, not idealized parameters derived from test data, can be used directly to predict coupled system response without relying on the skill or diligence of a modeler in deriving an abstract set of parameters for a modal model.

The modal coupling method, by contrast, requires that test data be reviewed and processed and decisions made on which data to match and which to ignore. There are several reasons for ignoring test data. First, the problem is overdetermined in the sense that there is an infinite number of modes, and only a finite number will be modeled. More important, the analyst may find implausible aspects to some of the data, requiring that the data be either repeated and verified or discarded. This automatic review is a feature not present in the impedance/mobility coupling technique, where the large volumes of numbers generated prevent review for other than gross implausibilities.

The modal coupling technique also offers the ability to determine the effects of design changes on an installation, whereas impedance/mobility coupling predicts only how the tested configurations will respond when coupled. The modal data is then more concise. (For this report, the modal data of Figures 74 and 75 was adequate, and more useful than the several hundred mobility plots transmitted by the engine manufacturer.) Impedance/mobility coupling is then more of a concept validation tool, while modal coupling can be used as a design tool.

CHOOSING BETWEEN IMPEDANCE/MOBILITY COUPLING AND MODAL COUPLING FOR THE OH-6A

When deciding between impedance/mobility coupling and modal coupling for adding the T63-A-5A engine to the OH-6A airframe, the choice for modal coupling was straightforward. The Allison tabulated mobility data in Reference 5 covered the range from 10 to 110 hertz in 10-hertz increments. Over the lower range of frequency, the mobility points were asymptotic to a constant acceleration line (see Figure 107), indicating that only rigid-body modes were relevant except in the 100-hertz region, where the validity of the airframe model was poor.

The impedance/mobility coupling technique would be more appealing for cases where many engine flexible modes are in a frequency range that could be excited by main-rotor-induced vibratory forces. Here, the volume of data transmitted to define the modal parameters of the component might approach the number of digitized mobility points needed for impedance/mobility coupling.

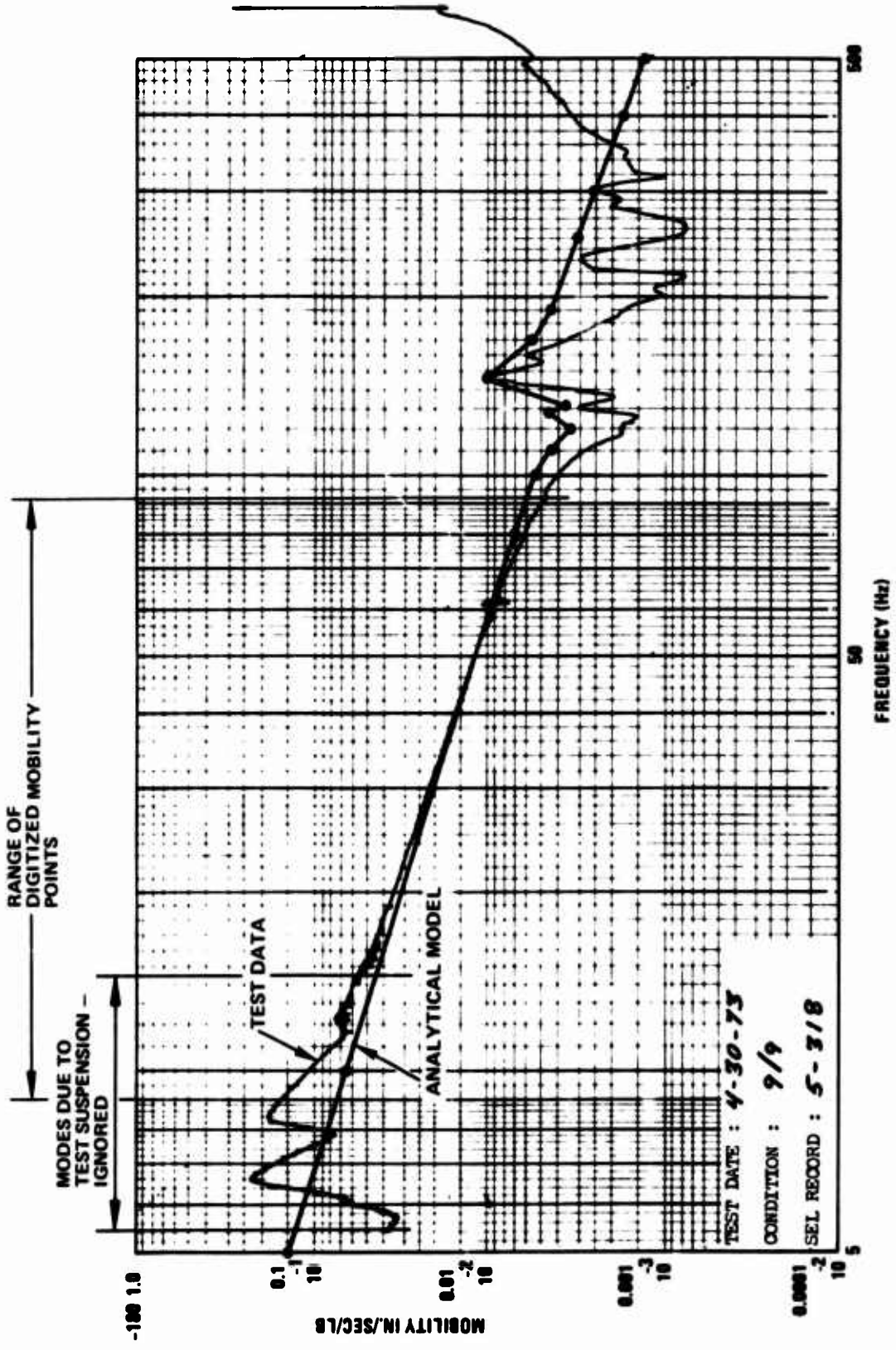


Figure 107. Typical Engine Test Data.

CHOOSING BETWEEN METHODS FOR THE GENERAL CASE

The main criterion for choosing between impedance/mobility and modal coupling is the degree of quality control each offers. If impedance/mobility coupling is chosen, the following steps are recommended:

1. An analytical model of the component should be developed before testing begins and used to generate mobility curves in the format to be output by the test gear. The test data should be plotted directly onto the analytical results.

This technique gives a much better chance of obtaining test data free of calibration errors, mislabeling, or the many other kinds of mistakes possible when taking large volumes of data rapidly.

When presenting the complex numbers typical of response plots, the so-called "Co-Quad" format, where real and imaginary components of the complex signal are used rather than magnitude and phase, has the advantage of avoiding ambiguity in phase when phase passes through a multiple of 360 degrees, which causes a "folding effect." The Co-Quad format for digitized data is also more readily useful for digital calculations.

2. The organization generating the test data, and the organization which will analyze the test data, should have complete agreement on sign conventions, phase conventions, and units of measure before analysis or testing commences. This is especially true for an engine installation such as the OH-6A, where the engine axes are canted from the airframe axis. It was convenient in testing to allow positive velocity to the left when measured on the left side of the engine and positive velocity to the right when measured on the right side of the engine, as it allowed use of the same transducer bracket. However, it complicated reduction of the test data.

If modal coupling is chosen, the following steps are recommended:

1. Again, the analytical model to be verified should be developed before testing.
2. Test and analysis conventions should agree, as in the steps recommended for impedance/mobility coupling.

Both steps above will automatically be satisfied if:

3. The organization generating the test data is also responsible for deriving the modal representation of that component. The delivered product from this test should be the raw mobility curves, with mobility as predicted by the analytical model superimposed, plus a full set of generalized masses, springs, damping values, and mode shapes used in deriving the analytical data. In this manner, the organization which manufactures the component being modeled, and which therefore understands it better than anyone else, will also be the organization that decides what assumptions are relevant in the art of modeling.

DEVELOPMENT OF IMPEDANCE/MOBILITY COUPLING TECHNIQUE

As mentioned earlier, a requirement of this study was the evaluation of the parameters and methodology of an impedance/mobility analysis of the type presented in Reference 4. That report discussed a one-dimensional application of the impedance/mobility technique and recommended that the same technique be applied to a realistic multidimensional airframe - engine interface. It has already been stated that consideration of the voluminous data handling required for use of multidimensional impedance/mobility coupling led to the choice of the modal coupling technique for the OH-6A/T63 combination. To provide guidance for those cases where impedance/mobility coupling is considered to be more suitable than the modal coupling, additional explanation is presented here.

In a conceptual way the impedance/mobility approach is very attractive. The direct mobilities and cross mobilities are measured by the engine manufacturer for the mount and drive shaft interfaces and for other points of interest on the engine. The direct and cross mobilities of the airframe at the engine mount and drive shaft interfaces and at the main and tail rotor excitation locations are calculated (or measured) by the airframe manufacturer. Then the two sets of mobility information are combined to find, for example, the cross mobility for vertical motion of the front of the engine compressor due to rotor head longitudinal unit force. Then, after all such cross mobilities at the same engine location are determined for all rotor head forces and moments, the overall vertical response of the front of the compressor is calculated. By comparison with the flight test data given in Figure 1, an evaluation of the impedance/mobility method can be made.

The impedance/mobility approach for coupling the airframe and the engine was described on page 164 as involving the sum of two inverted matrices, and the inversion of the summed matrix.

In the general case, the motion or velocity at a point on a structure due to an excitation force can be expressed as

$$\{\dot{u}\} = [M(\omega)] \{F\} \quad (22)$$

where

$M(\omega)$ = mobility, ft/sec/lb force

F = oscillating excitation force

At selected frequencies ω_1 , the mobility for the airframe and for the engine are measured:

$$[M(\omega_1)]_{\text{engine}} \quad \text{and} \quad M(\omega_1)_{\text{airframe}} \quad (23)$$

Typically, the mobility of the engine will be measured relative to natural engine axes, namely, parallel and perpendicular to the engine centerline. The mobility of the airframe will be measured relative to the principal axes of stiffness of the engine mount system. Because engine-oriented results are sought, and because the T63 engine in the OH-6A is installed with the drive shaft facing forward and upward, it is necessary to perform geometric manipulation of the airframe data in order to combine it with the engine data. Therefore, a transformation matrix $[T]$ is derived as follows:

$$\begin{array}{l} \{u\} \text{ airframe dis-} \\ \text{placement in} \\ \text{engine center-} \\ \text{line coordinates} \end{array} = \begin{array}{c} [T] \\ \text{Geometric} \end{array} \times \begin{array}{l} \{u'\} \text{ airframe dis-} \\ \text{placement in} \\ \text{engine mount} \\ \text{principal axes} \end{array} \quad (24)$$

which relates displacements in engine centerline coordinates to displacement in engine-mount coordinates.

Airframe motion in engine-mount coordinates at an interface due to forces acting at the interface is given by

$$\{\dot{u}'\} = M'(\omega)_{\text{airframe}} \times \{F'\} \quad (25)$$

Then airframe motion in engine coordinates is

$$\{\dot{u}\} = [T] \{\dot{u}'\} = [T] [M'(\omega)]_{\text{airframe}} [T^t] \{F\} \quad (26)$$

Equation (26) shows that airframe mobility in the engine coordinate system is

$$M(\omega)_{\text{airframe in engine coord system}} = [T] [M'(\omega)]_{\text{airframe in airframe coord system}} [T^t] \{F\} \quad (27)$$

Thus the two matrices to be combined are now available:

$$\left[M(\omega) \right]_{\text{engine (Allison test data)}} \quad \text{and} \quad \left[M(\omega) \right]_{\text{airframe (Hughes data, manipulated)}} \quad (28)$$

It is useful to define an inverse of the mobility matrices in Equation (28) as

$$\left[Z(\omega) \right] = \left[M(\omega) \right]^{-1} \quad (29)$$

Then, from Equations (28) and (29), the first step in using the impedance/mobility technique for coupling the airframe and engine is to find the sum of the inverse mobility matrices:

$$\left[Z(\omega) \right]_{\text{system}} = \left[M(\omega) \right]_{\text{engine}}^{-1} + \left[M(\omega) \right]_{\text{airframe}}^{-1} \quad (30)$$

and then the direct interface mobility of the coupled engine - airframe system is

$$\left[M(\omega) \right]_{\text{system}} = \left[Z(\omega) \right]_{\text{system}}^{-1} \quad (31)$$

Equations (22) through (31) lead to the coupled mobility of airframe - engine due to excitation forces applied at the several interface points. For the case being considered here, there are three engine mount points (left, right, and bottom) and one shaft connection (engine to main transmission coupling). At each of these four interface points, mobility was measured in three directions. Therefore, there are $4 \times 3 = 12$ coupled interface points resulting from the application of equations (22) through (31).

The first goal of the impedance/mobility technique is to predict system response; that is, to predict motion at a point on the engine due to excitation elsewhere on the airframe, such as excitation at the main rotor or at the tail rotor. Therefore, one must visualize that the response of the coupled-airframe engine has characteristics as follows:

$$\begin{Bmatrix} \dot{u}_{MR} & (6) \\ \dot{u}_{TP} & (3) \\ \dot{u}_{\text{interface}} & (12) \\ \dot{u}_{\text{engine}} & (8) \end{Bmatrix} = \begin{bmatrix} M_{\text{uncoupled}} \\ (29 \times 29) \end{bmatrix} \begin{Bmatrix} F_{MR} \\ F_{TR} \\ F_{\text{interface}} \\ F_{\text{engine}} \end{Bmatrix} \quad (32)$$

where the $(M_{\text{uncoupled}})$ matrix in Equation (32) consists of test data taken for direct mobility of the airframe at the main rotor and at the tail rotor, and cross mobility from the main rotor and tail rotor to the 12 interface points treated in equations 22 through 31, as well as to the 8 engine locations given on Figure 1. As noted in parentheses in the left-hand term of equation 32, there are six possible rotor head force and motion directions (x, y, z, pitch, roll, and yaw) and three tail rotor directions (x, y, z). Therefore, the matrix in Equation 32 is a 29×29 term matrix ($29 = 6 + 3 + 12 + 8$).

The total problem of determining engine response is then to solve Equation 32. All of the mobilities come from the test data and are used unchanged or are combined in using equations 22 to 31, as applicable. The forces in equation (32) are the same excitation forces used earlier with the modal coupling technique.

The solution of Equation (32) will involve a process of elimination. It must be recognized that the 12 points involved in the interface (3 mounts and the shaft, with 3 directions for each of those 4 locations) involve a redundant system. Only 6 interface points are involved in a statically determinate system. It may be necessary to apply engineering judgment to smooth the data, or it may be necessary to ignore some of the data.

There are also other practical problems involved in application of the impedance-mobility technique. First, the mobility data $M(u)$ may be ill-conditioned. This characteristic is related to "observability" - the data can be taken reliably perhaps to three digits. Also, there may well be poor quality data (bad points) in voluminous test data.

The second practical problem is related to the large quantity of data required. As a result, it is easy for errors to occur involving transcription, computer keypunching, etc. As an example, the number of data points per excitation is as follows:

$$\begin{aligned} \text{No. points/excitation} &= (\text{No. frequencies}) \times (\text{No. coordinates})^2 \\ &\times 2 \text{ (i.e., airframe + engine)} \\ &\times 2 \text{ (i.e., real and imaginary complex elements)} \end{aligned} \quad (33)$$

Specifically, for the airframe-to-engine interface, the data involve:

$$\begin{aligned} \text{No. of frequencies} &= 6 && (4/\text{rev main rotor } \pm 10\%) \\ & && (2/\text{rev tail rotor } \pm 10\%) \\ \text{No. of coordinates} &= 12 && (3 \text{ mounts + shaft, 3 directions}) \end{aligned}$$

Applying Equation (33),

$$\text{No. of points} = 6 \times 12^2 \times 4 = 3456$$

For the second type of excitation, namely, at the main and tail rotors, the quantity of points is:

No. of frequencies	6
No. of coordinates	9 (main rotor and tail rotor)
	12 (interface)
	8 (engine)
No. of points	$= 6 \times 9^2 \times 4 = 1944$ (rotors)
	$= 6 \times 12^2 \times 4 = 3456$ (interface)
	$= 6 \times 8^2 \times 4 = \underline{1536}$ (engine)
	6936 Total

Therefore, the use of the impedance/mobility technique leads to much detailed work, which may lead to bad results without extensive quality control. It was the recognition of the size of effort involved here which led to the selection of the more promising alternate method, namely, the modal coupling technique described earlier in this report. It also appears that automatic data handling must be employed if the impedance/mobility technique is used.

Based on the discussion above, it is suggested that if a complete impedance/mobility coupling is to be attempted, a sample case must be performed first. An analytical model should be prepared, involving the same number of degrees of freedom (i. e., interface points) but with much simpler geometry and with a finite number of modes. The sample case will be used to test the computational scheme for plausibility and for its sensitivity to measurement accuracy.

ADVANTAGES OF ACCELERATION AS A VIBRATION PARAMETER

The question of whether frequency response data should be presented in the format of vibratory displacement, velocity, or acceleration versus force has been endlessly argued, as noted in the survey discussed above. Use of velocity and force as the dependent and independent variable has aesthetic appeal because their product has the dimensions of power, as do

voltage and current, so that analogies between electrical circuits and mechanical devices can be made directly.

Units of acceleration have the following practical advantages for the rotary-wing industry:

1. Most modern transducers suitable for helicopter vibration measurements produce an electrical signal proportional to acceleration. The use of acceleration also avoids the added costs and lowered reliability introduced if velocity is specified for engine vibration monitoring. When velocity monitoring is specified, an acceleration signal must be converted to velocity. Converting this acceleration signal to velocity requires the added cost of one signal conditioning module per channel and increases the chance of erroneous measurements due to calibration error, phase shift with frequency, etc.
2. Direct velocity/force readings become asymptotic to a $1/\omega$ slope line at high frequencies, while acceleration/force is asymptotic to a zero slope line. Plotting acceleration tends to reduce the dynamic range needed for measurement and increases resolution of the peaks in the high-frequency ranges where a higher degree of coupling between modes makes resolutions more critical for interpretation of results.

For reason 1, the best course may be to present the measured transducer signal, in engineering units, versus frequency. Today, that means acceleration. If another transducer breakthrough occurs tomorrow, it may mean displacement or velocity, depending on the principle of its operation. For reason 2, the use of acceleration/force is desirable no matter what the measurement device.

In summary, each organization should have the freedom to choose the format best suited to its facilities and technology.

DEFINITIONS/RECOMMENDATIONS FOR
VIBRATION SPECIFICATION METHODOLOGY

1. The modal coupling technique is recommended when there are only a few engine flexible modes in the frequency range that could be excited by main-rotor-induced vibratory forces.
2. The impedance/mobility coupling technique should be considered where many engine flexible modes are in the frequency range that could be excited by main-rotor-induced vibratory forces.
3. The engine manufacturer should be encouraged to generate relevant dynamic information on his engine to permit coupling with finite-element airframe structural models. The engine manufacturer should be encouraged to understand recommendations 1 and 2 above to classify his engine. An engine analytical model should then be prepared, and mobility test data should be plotted directly onto the analytical results. If modal representation is considered proper, the engine manufacturer should prepare a modal model and plot test data on the analytical results.
4. For future helicopter engine development programs, it is recommended that applicable specifications be modified to include the following:
 - a. The first free-free lateral and vertical engine bending modes shall be at frequencies greater than 100 hertz.
 - b. The installed engine vibration limit shall correspond to 2g for harmonic motion from 15 to 100 hertz.
5. In accordance with 4. b, it is suggested that the best vibration parameter is acceleration.
6. The engine manufacturer should specify enough locations for vibration transducers on the installation drawing to identify engine mode shapes and phase data; if the engine is sufficiently stiff, a few locations will identify the rigid-body modes.
7. It is suggested that the best method of data reduction is to perform discrete frequency analysis.
8. Methods should be developed to improve methods for reliable calculating rotor excitation forces at n/rev and $2n/\text{rev}$.

CONCLUSIONS

1. Available data showed that the T63 engine in the prototype OH-6A was vibrating in cruise flight in a rigid-body mode that was essentially pitch, with an amplitude at 4/rev (32 hertz) nearly equal to the current 1g limit applicable to the T63 engine.
2. Production OH-6A helicopters have different and softer dynamic characteristics, probably leading to lower engine vibration in cruise flight. Recently acquired engine vibration data should be evaluated to check this conclusion.
3. A finite-element NASTRAN model of the OH-6A was prepared which was reasonably correlated with the test data; further tuning of the model by assuming a higher degree of skin effectivity would improve the model's accuracy.
4. A modal description of the T63 engine was prepared and mated to the airframe-only model. Reasonable correlation of the combination was obtained.
5. Use of the impedance/mobility coupling technique is indicated where the engine has flexible modes near the forcing frequencies of the helicopter rotors and drive shafts. This sophisticated method is, perhaps, unnecessarily elaborate for cases where the engine is essentially rigid with respect to forcing frequencies. For this simpler case, the modal coupling technique is suggested.
6. Engine vibration response during landing transients can be calculated with a NASTRAN airframe-engine model, including effects of engine rotation.
7. Most -- but not all -- of the engine manufacturers surveyed disapproved of the recommendation made here concerning minimum free-free bending mode frequencies (i. e., greater than 100 hertz. The objections to this point (and indirectly to the suggested minimum 2g vibration limit) centered chiefly on the probable impact on engine weight. No comment was made on the probable impact on airframe weight if those recommendations were not followed.

REFERENCES

1. Mard, K. C., and P. W. von Hardenberg, "Turbine Engine Dynamic Compatibility With Helicopter Airframes," Shock and Vibration Bulletin 39, Part 3, January 1969, pp 17-30.
2. Frederickson, C., "Engine/Airframe Interface Dynamics Experience," AHS/NASA Specialists Meeting on Rotorcraft Dynamics, Ames Research Center, February 1974.
3. Balke, R. W., "A Review of Turbine Engine Vibration Criteria for VTOL Aircraft," Joint Symposium on Environmental Effects on VTOL Designs, American Helicopter Society Preprint No. SW-70-18, November 1970.
4. Vance, J. M., Dynamic Compatibility of Rotary-Wing Propulsion Components, USAAMRDL Technical Report 73-10, Eustis Directorate, U. S. Army Air Mobility Research and Development Laboratory, Fort Eustis, Virginia, January 1973, AD 761100.
- 5a. "T63 Test Mobilities," Detroit Diesel Allison letter 73-AW-238 to Hughes Helicopters, 18 July 1973.
- 5b. "T63 Mode Shapes," Detroit Diesel Allison letter 73-AW-258 to Hughes Helicopters, 7 August 1973.
6. MacNeal, R. H. (editor), The NASTRAN Theoretical Manual (Level 15), NASA Report No. SP-221 (01), National Aeronautics and Space Administration, Washington, D. C., April 1972.
7. Faulkner, W. R., Installation Survey of YT63-A-5 Engine Installed in Hughes OH-6A Aircraft, Allison Division, General Motors Corporation, Report No. 64B19, 21 April 1964.
8. Currier, E. J., and S. P. Cammack, Model 369 Helicopter T.I. A. Flight Vibratory Test Report, Hughes Tool Company - Aircraft Division Report No. 369-FT-8003, revised 21 April 1964.
9. Combined Final Report on Analytical Study of Rotor Vibration Characteristics and Elimination of External Mechanical Pendulum Dampers, Hughes Tool Company - Aircraft Division Report No. 369-V-1001, 1 June 1967.

10. Laing, E. T., Vibration and Temperature Survey, Production OH-6A Helicopter, USAASTA Final Report No. 70-15-4, U. S. Army Aviation Systems Test Activity, Edwards Air Force Base, California, August 1973.
11. "Installation Assembly, T63-A5A, Allison Model 250-C10," Allison Division, General Motors Corporation Drawing No. 6850000, Change AM, 22 October 1971.
12. McCormick, C. W. (editor), The NASTRAN User's Manual (Level 15), NASA Report No. SP-222(01), Scientific and Technical Information Office, National Aeronautics and Space Administration, Washington, D. C., June 1972.
13. Analytical Study of Fuselage Vibration, Hughes Tool Company - Aircraft Division Report No. 369-V-8005 (HTC-AD 67-8), 27 January 1967.
14. Flannelly, William G., Alex Berman, and Nicholas Giansante, Research on Structural Dynamic Testing by Impedance Methods, Volume I - Structural System Identification From Multipoint Excitation, USAAMRDL Technical Report 72-63A, Eustis Directorate, U. S. Army Air Mobility Research and Development Laboratory, Fort Eustis, Virginia, November 1972, AD 756389.
15. Flannelly, William G., Alex Berman, and Nicholas Giansante, Research on Structural Dynamic Testing by Impedance Methods, Volume II - Structural System Identification From Single-Point Excitation, USAAMRDL Technical Report 72-63B, Eustis Directorate, U. S. Army Air Mobility Research and Development Laboratory, Fort Eustis, Virginia, November 1972, AD 756390.
16. Flannelly, William G., Alex Berman, and Nicholas Giansante, Research on Structural Dynamic Testing by Impedance Methods, Volume III - Free-Body Response, USAAMRDL Technical Report 72-63C, Eustis Directorate, U. S. Army Air Mobility Research and Development Laboratory, Fort Eustis, Virginia, November 1972, AD 765391.
17. Flannelly, William G., Alex Berman, and Nicholas Giansante, Research on Structural Dynamic Testing by Impedance Methods, Volume IV - Subsystems, USAAMRDL Technical Report 72-63D, Eustis Directorate, U. S. Army Air Mobility Research and Development Laboratory, Fort Eustis, Virginia, November 1972, AD 765392.

18. Collins, J. D., G. C. Hart, T. K. Hasselman, and B. Kennedy, "Statistical Identification of Structures," AIAA Journal, Vol. 12, No. 2, February 1974, pp 185-190.
19. Kennedy and Pancu, "Use of Vectors in Vibration Measurement and Analysis," Journal of Aeronautical Science, November 1947.
20. Joseph, J. A., MSC/NASTRAN Application Manual, MacNeal-Schwendler Corporation Report No. MSR-35, Revised 10 October 1973.
21. Paul, W., "Development and Evaluation of the Main Rotor Bifilar Absorber," 25th Annual National Forum of the American Helicopter Society, Washington, D. C., May 1969.
22. Engine, Aircraft, Turboprop, General Specification for, Specification No. MIL-E-8593, 3 September 1954.
23. Engines, Aircraft, Turboshaft, General Specification for, Specification No. AV-E-8593B, 13 October 1972.
24. Trent, R., and W. R. Lull, "Design for Control of Dynamic Behavior of Rotating Machinery," ASME Preprint No. 72-DE-39, 8 May 1972.
25. Helicopter Flying and Ground Handling Qualities, General Requirements for, Specification No. MIL-H-8501A(1), April 1962.
26. "Helicopter Turbine Engine Linear Vibration Environment," SAE Proposed AIR No. 1289.
27. "Recommendations for Engine Vibration Specification Methodology," Hughes Helicopters letter to six helicopter engine companies, 25 March 1974.

APPENDIX A

TEST PROGRAM

This appendix gives a more detailed description of the test program described in general in the "Mobility Tests" section of this report.

TEST DETAILS

The objective of these tests was to obtain point and transfer mobility data for the airframe and engine interfaces of the OH-6A helicopter. The data was obtained automatically from a mechanical impedance system that continuously recorded the varying ratio of velocity to force as the specimen under test was driven through a specified frequency range. In addition to the mobility value, the system continuously recorded the phasing between velocity and force. The data was measured for later comparison with similar information obtained from a computerized mathematical model of the helicopter structure.

The shake test was conducted in two phases with excitation sweeps from 8 through 2000 hertz:

- Phase I Testing with engine removed
- Phase II Testing with engine installed

Initially, tests were made only for vibratory force inputs in the longitudinal and lateral directions at the main rotor hub and at the tail rotor hub, in two mutually perpendicular directions in the plane of each engine mount, and in three mutually perpendicular directions at the input to the transmission. Part way through the program the scope of work was increased to include vertical force inputs at the main rotor hub, three mutually perpendicular force inputs at the tail rotor hub, and force inputs to the engine mounts perpendicular to the plane of the mounts. At the same time the extent of the frequency sweeps was reduced to cover only 8 to 600 hertz, considered to be more representative of the range of interest.

EQUIPMENT CALIBRATION

The equipment used for the tests was capable of making dynamic measurements at rated accuracy between 5 and 10,000 hertz. The following procedure was used to obtain calibrations of both force and acceleration that could be traced to National Bureau of Standards (NBS) criteria.

A steel bar approximately 29.5 inches long and 2 inches in diameter was fitted with transducer attachment screw holes, and its weight was adjusted to 20.00 ± 0.005 pounds on precision-calibrated measuring equipment traceable to NBS records. This bar was suspended in a horizontal position by steel wires located approximately at the first free-free bending mode positions to make it act as a ballistic pendulum. Figure A-1 shows a typical setup for mass calibration with the impedance head attached in series with the electrodynamic exciter at one end of the bar and the moving accelerometer attached at the other end.

The shaker was energized at a frequency of 11.00 hertz, and the amplitude of excitation increased until the displacement of the bar (ballistic pendulum) was observed to be 0.0404 inch peak-to-peak. The accelerometer and force signals were observed on an oscilloscope and found to be sinusoidal with very little distortion. The amplitude of the pendulum was measured using a binocular microscope mounted on a micrometer slide table. The 40-power microscope was used to observe the amplitude of the pendulum motion to an accuracy of 0.0005 inch peak-to-peak, or 0.00025 single amplitude. Therefore, a peak-to-peak amplitude of 0.0404 inch represents a maximum percentage error for pure sine motion:

$$\frac{0.0005}{0.0404} \times 100 = 1.24 \text{ percent}$$

Since frequency is as important for accuracy as amplitude, a digital counter was used for frequency measurements. A Hewlett-Packard counter capable of clocking the count for 1 minute at 11 hertz would give $11 \times 60 = 660$ counts ± 1 count ambiguity. Therefore, 659 - 661 counts could be the reading for 1 minute, and the error could be

$$\frac{1}{600} \times 100 = 0.167 \text{ percent}$$

The mass error could be 0.005 pound out of a total of 20 pounds, so the error could be

$$\frac{0.005}{20} \times 100 = 0.025 \text{ percent}$$

The total possible error could then be 1.24 percent (amplitude) + 0.167 percent (counter accuracy) + 0.025 percent (for mass accuracy) = 1.43 percent.

The probability exists of a small amount of harmonic distortion of the signal. This was judged to be less than 0.1 percent. Therefore, the basic calibration input parameters were accurate within ± 1.5 percent.

At this point in the calibration, the transducer conditioning modules were normalized to read the correct value of the parameter being conditioned. The technique of using the physical calibration from known properties of a mass is obviously superior to a purely electrical calibration from transducer records.

The equipment was calibrated using the ballistic pendulum before the test program started, and again after each major group of tests.

MEASURING EQUIPMENT

To achieve reliable high-frequency measurements, special attention was paid to the measuring equipment located between the electrodynamic shaker and the specimen. This equipment included the following items:

- Linkage between the shaker and the impedance head transducer. The linkage which was used for all of the shake tests may be seen in Figure 14. It consisted of a stainless steel rod with spherical ends that fitted into a pocket at the shaker, and another at the transducer. The rod was enclosed by a coaxial aluminum tube with an 0.020-inch wall and a diametral clearance of 0.032 inch. The gap between the rod and tube was filled with Aero Shell 14 grease. This complex arrangement minimized as much as possible the natural bending modes of the drive linkage. Ordinary heavy-duty elastic bands (office variety) preloaded the rod in compression to 20 pounds. The tension force was limited to 10 pounds by the shaker control. This system is shown in mockup in Figure 14 and during an actual test in Figure A-2.
- Roving transducers. An accelerometer for measuring local velocity was mounted at each point of interest around the helicopter, one location for each input force frequency sweep. Figures 17, A-3, A-4, A-5, and A-6 show the transducer in place.
- Impedance head transducer, force and acceleration. The force and acceleration transducer, generally known as an impedance head, had to be as stiff as possible to transmit valid data about the structure, especially at high frequencies. For a given set of physical conditions, such as effective mass and stiffness, there was a

limiting frequency at which data could be taken within an accuracy of the specified percentage of error. The same transducer used at different locations on a structure that has other stiffness and mass characteristics could experience a different set of limiting frequencies.

The data taken for these tests was checked using two different effective mass calibrations: one was 20 pounds, and the other was the effective mass of the transducers themselves. Representative mass calibrations are given in Appendix B.

- Linkage between impedance head and aircraft structure. The fitting that adapts the transducer to the aircraft was made as stiff and as lightweight as practicable to ensure a high degree of reliability that the data recorded would be the data at the point of interest, and that the data would be valid to the frequency limit of the plot.

DIFFICULTIES EXPERIENCED

The first problem with the test equipment was a mechanical failure in the impedance head transducer that was determined to be a manufacturing defect. The manufacturer of the transducer supplied an exchange transducer, but this replacement unit also showed some temporary difficulties. A properly calibrated replacement was eventually located and delivered for test.

The second problem was recognition that the mounting technique for the impedance transducer could have a 10-to-1 influence on the reported mobility; specifically, the transducer clamp-up force was most significant. This effect of clamp-up force was identified because the apparent rotor head mass associated with transverse shake and measurement at the rotor head was only about 1/10 of the proper value. The proper apparent mass was obtained after correcting the transducer fastening procedure.

The third problem came to light during a data review that showed that the mobility phase angle for the apparent mass response was not the required 90 degrees. An investigation of the instrumentation showed that an accelerometer signal conditioner (amplifier) had a mode that was not labeled as having a low-frequency (8 to 80 hertz) phase roll-off. Using a correct signal conditioner solved the problem.

The fourth and final problem asserted itself when a prominent resonance found earlier near 35 hertz was absent, and a new prominent resonance was observed near 50 hertz. This difference was traced to the fact that the main rotor blade straps and pitch housings which were in place for these tests drooped down and outward from the rotor head; in actual flight, the blade pitch housings cone upward and do not contact the droop straps. Recognizing this difference, the actual rotor head, blade retention straps, and blade pitch housings were replaced with a steel disc that represented the proper equivalent mass. With this change, the resonances correlated with previous data.

TEST PROCEDURES

The procedures that were followed in conducting the mobility tests were as follows:

- Attach the drive point instrumentation to the special adapter fitting installed at the desired shake location. (The fitting was made so that a single screw connection exactly aligned the instrumentation in the desired attitude and position.)
- Position the electrodynamic shaker at the desired location and make fine adjustments for alignment. (See Figures 12, 13, A-2, A-7, A-8, and A-9.)
- Make all electrical connections and mechanically connect the shaker to the drive point instrumentation.
- Install the mobility graph paper on the plotter and set the controls to the internal calibration at 2000 hertz. On internal calibration, the pen drove to a predetermined set of X-Y coordinates; at any frequency, the pen fell on the 20-pound mass line.
- At 2000 hertz and 60 hertz, locate the paper on the plotter for an exact match with the precalibrated electronic sensitivities. Careful inspection of the data plots in Appendix B shows a black dot printed as a reference check at 2000, 60, and 7 hertz along the 20-pound mass line.
- Begin the excitation and observe the force and accelerometer signal waveforms for abnormalities. If the signals appear satisfactory, start the sweep.

- Observe on the plot the force and acceleration levels and signal shape for proper indication.
- Repeat steps as required for each plot.
- After each major group of tests is completed, perform a check calibration using the ballistic pendulum.

MEASUREMENT AXES AND INDICATED POLARITIES

These tests were performed with data taken along three basic sets of measuring axes:

- The principal axes of the airframe (waterline, butt line, station line).
- The three principal axes of the engine as installed in the airframe.
- The axes of the engine mounts (for the engine-removed tests). These axes are shown in Figure A-10. In each case, consider the engine mount as a plane defined by the two points where it attaches to the airframe and the third point where the engine attaches. The "parallel" measurement axis is in this plane along the bisector of the two strut centerlines; the "perpendicular" measurement is in the plane of the mount and at right angles to the "parallel" axis. The "normal" measurement is at right angles to the other two axes, and all pass through the center of the engine attachment bolt.

The force/response directions for all the points evaluated are shown in Table 6.

CONCLUSIONS AND RECOMMENDATIONS

Although the electronic recording equipment provides a high degree of sophistication and reliability, the answers it produces are not better than the accuracy of the basic transducers used in converting the physical parameters of force and velocity to proportional electrical parameters.

In addition to the mechanical/electrical transformation, the practical problem of physically attaching the transducers to the specimen is very important. Of paramount importance is the necessity of making the physical connection as stiff and tight as possible. It is impossible to have zero mass between the specimen, the transducer, and the force generator.

Therefore, the frequency to which a given assembly can be operated without inducing the dynamics of the measuring equipment into the results is limited.

Before an arbitrary upper frequency cutoff point is established, consideration should be given to just how high a frequency is really necessary. On airframes for helicopters, for example, it is very doubtful that frequencies over 200 to 300 hertz are justified, since an examination of the stiffnesses and the masses will show that two or three resonances have been passed in reaching these values and that higher frequencies are unlikely to be generated by the airframe rotors.

Future tests of this kind should use a different type of main rotor excitation. The easiest way to instrument the OH-6A rotor mast is to measure lateral and longitudinal bending, so the preferable way to excite the mast is through bending inputs rather than through force inputs. In this way, the problem of correlation would be eliminated. The NASTRAN structures model can be programmed to accept mast bending moment, so here, too, the correlation would be direct.

The complete set of experimental data discussed here is contained in Volume II (see page 51).

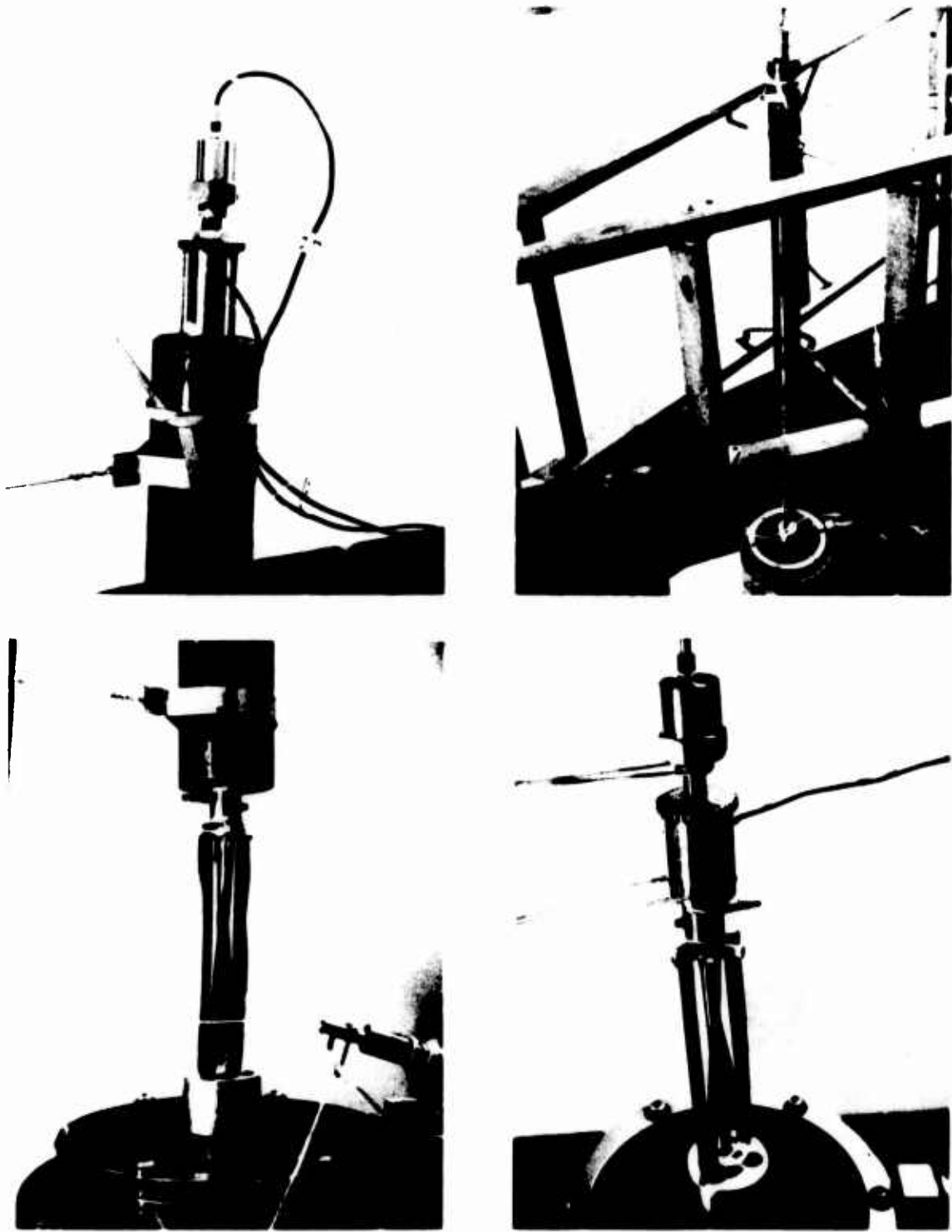
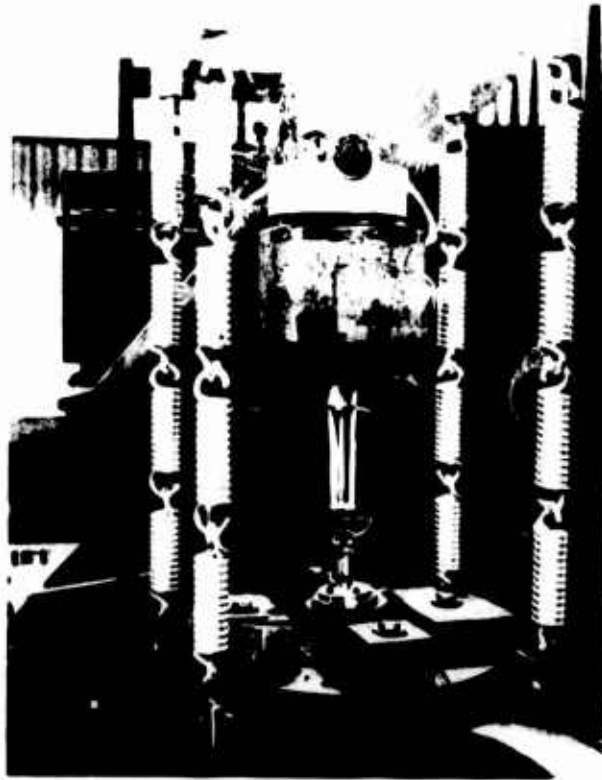


Figure A-1. Mass Calibration of a 20-Pound Steel Bar Suspended as a Ballistic Pendulum.



**Figure A-2. Suspension and Shaker Arrangement -
Main Rotor Vertical Excitation.**

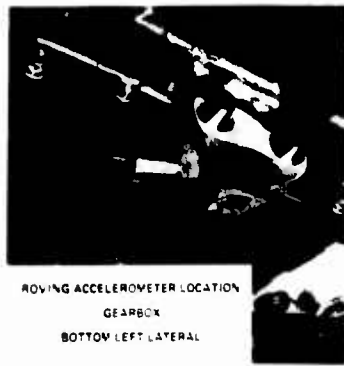


Figure A-3. Transducer Locations on Engine.

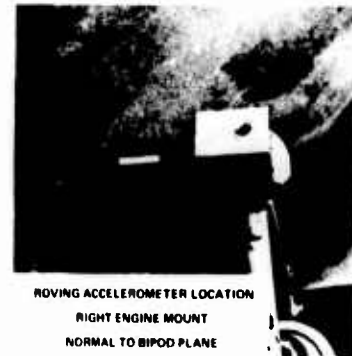
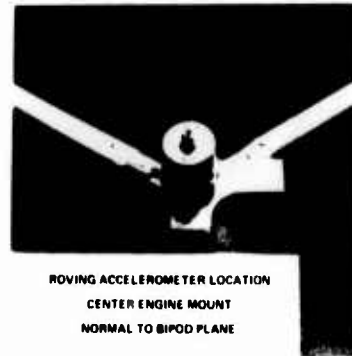
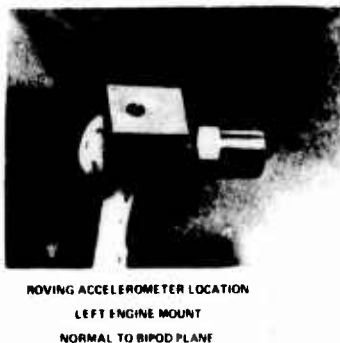
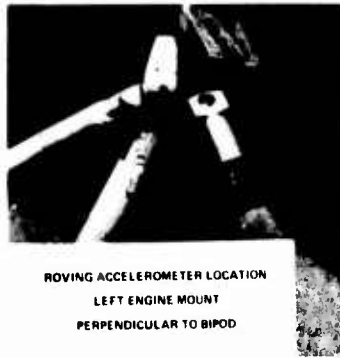


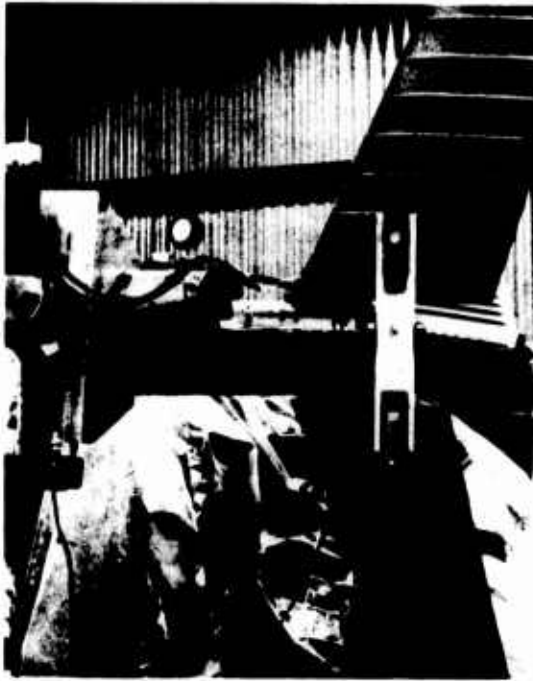
Figure A-4. Transducer Locations on Engine Mount Bipods With Engine Removed - Coincide With Shaker Input Force Positions.



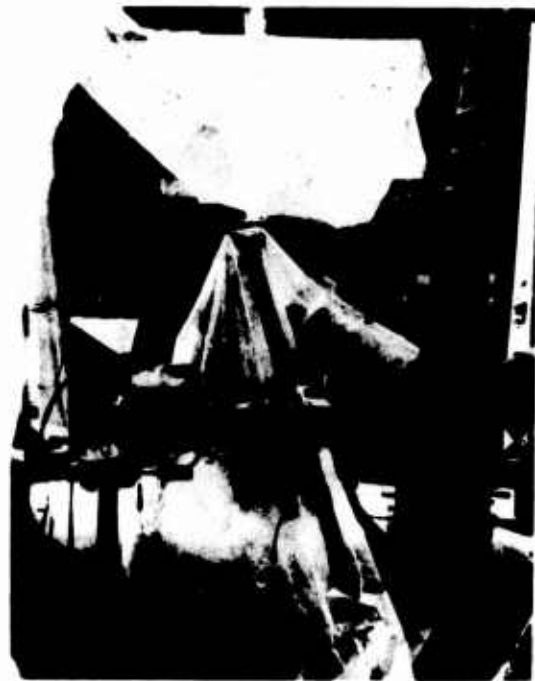
Figure A-5. Transducer Locations on Engine Mounts as They Were Located With Engine Installed - Photograph Taken With Engine Removed for Clarity.



Figure A-6. Transducer Locations on Engine Shaft at Transmission - Coincide With Shaker Input Force Positions.



LONGITUDINAL



LATERAL

Tail Rotor



LONGITUDINAL



VERTICAL

Main Rotor

Figure A-7. Shaker Locations for Rotor Excitation.

LATERAL



VERTICAL



(Left Exhaust Duct Removed for Photo)

Engine Mid-Turbine-Split Line

AXIAL



LATERAL



Engine Shaft at Transmission

Figure A-8. Shaker Locations at Engine and Transmission.



Center Mount, Perpendicular to Bipod Bisector



Left Mount, Perpendicular to Bipod Bisector

Figure A-9. Shaker Locations at Engine Mounts.

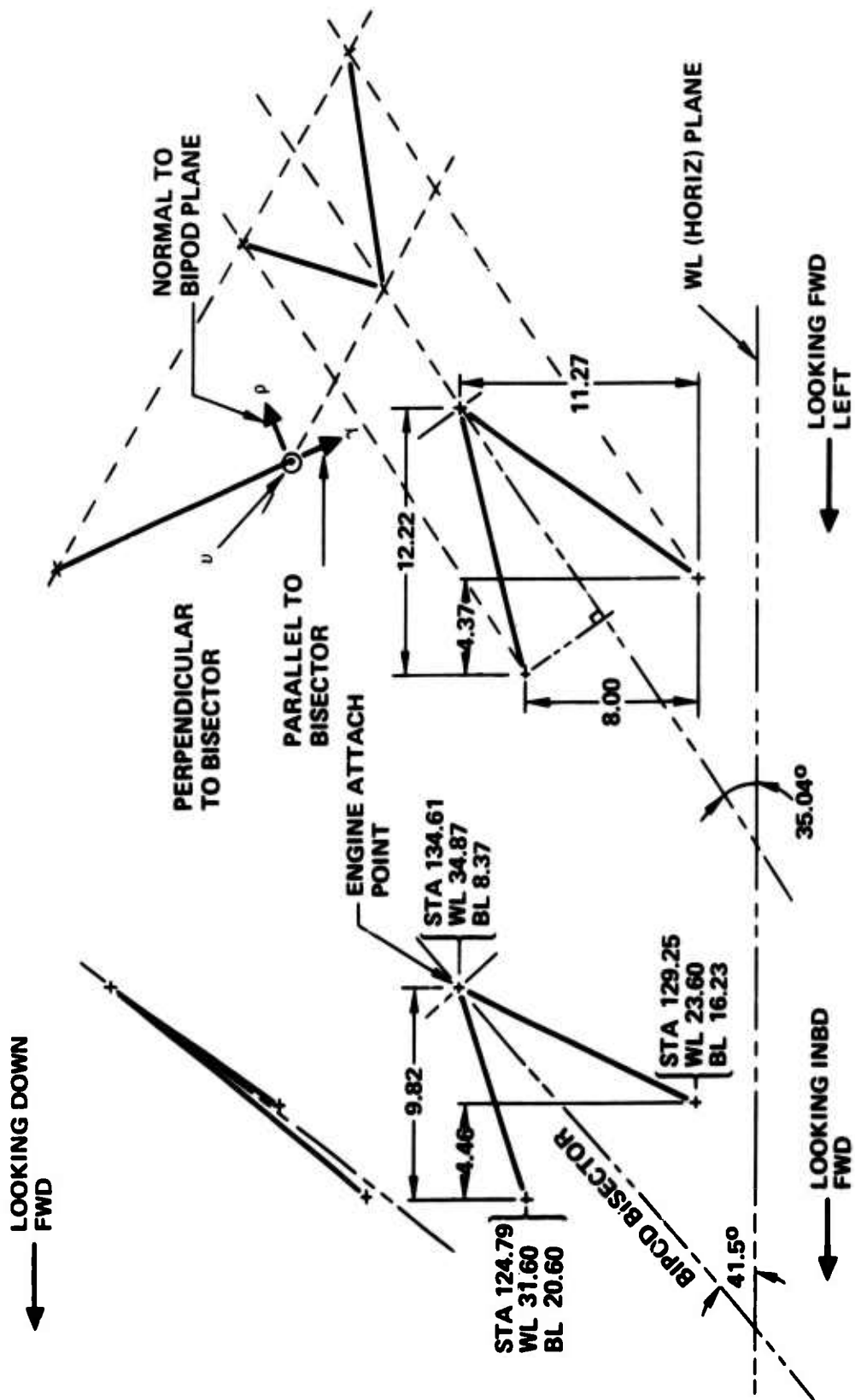


Figure A-10. Side Engine Mount Geometry.

APPENDIX B

DESCRIPTION OF UNIQUE MacNEAL-SCHWENDLER CORPORATION/NASTRAN FEATURES USED

NASTRAN and its related manuals are in general usage in the rotary-wing industry. Modeling and analysis techniques used that are available in standard COSMIC level 15.5 user's and theoretical manuals are only mentioned in the text of this report, they are not rederived.

As MSC/NASTRAN is a proprietary item; features unique to it that were used in this project are described in this appendix. Included are descriptions of a new "rigid element" capability, and of alterations to the standard NASTRAN rigid formats that decrease the cost of computation.

RIGID ELEMENTS AND MULTIPOINT CONSTRAINTS

The multipoint constraint (MPC) included with standard NASTRAN provides the capability to model rigid bodies as well as to represent other relationships which can be treated as rigid constraints. The MPC provides all the generality that will ever be required, but it lacks user convenience. Specifically, the user must supply all the coefficients in the equations of constraint defined through the MPC.

To provide increased user convenience, five new rigid-body elements are introduced in MSC/NASTRAN. These new elements limit the user's responsibility to the specification of the degrees of freedom that are involved in the equations of constraint. All coefficients in these equations of constraint are calculated internally in MSC/NASTRAN.

The five new rigid-body elements, in addition to the existing MPC, are described in Table B-1.

Any combination of the above elements may be used in an MSC/NASTRAN analysis in any of the structural rigid formats. The five new rigid elements are ignored in the heat transfer rigid formats.

RIGID FORMAT ALTERATIONS

Rigid format alterations are modifications to standard NASTRAN solution techniques that can reduce the cost of solutions for special cases.

TABLE B-1. RIGID-BODY ELEMENTS

Name	Description	m = Number of Equations of Constraint Generated
RROD	A pin-ended rod which is rigid in extension.	m = 1
RBAR	A rigid bar with 6 degrees of freedom at each end.	$1 \leq m \leq 6$
RTRPLT	A rigid triangular plate with 6 degrees of freedom at each vertex.	$1 \leq m \leq 12$
RBE2	A rigid body connected to an arbitrary number of grid points. The independent degrees of freedom are the six components of motion at a <u>single</u> grid point. The dependent degrees of freedom at the other grid points all have the same user-selected component numbers.	m = Number of dependent degrees of freedom
RBE1	A rigid body connected to an arbitrary number of grid points. The independent and dependent degrees of freedom can be arbitrarily selected by the user.	m = Number of dependent degrees of freedom
MPC	Rigid constraint that involves user-selected degrees of freedom at both grid points and scalar points. The coefficients in the equation of constraint are computed and input by the user.	m = 1

- RF3/16 This alteration function limits data recovery to the analysis set ("a set") in real eigenvalue analysis. The values of dependent degrees of freedom will not be recovered and will be replaced in the eigenvector by zero. Although the zero values assigned to these dependent coordinates in the eigenvector printout is incorrect, substantial savings in computer time may be realized through the use of this alteration.
- RF11/12 This alteration function limits data recovery to those physical set degrees of freedom specified on SDISPLACEMENT, SVELOCITY, and SACCELERATION case control deck output request cards. Substantial savings in computer time may be realized through the use of this alteration.
- RF11/15 Heretofore, SPCFORCE has been automatically calculated in rigid format 11 irrespective of the presence of an SCPFORCE request in the case control deck. These calculations, which can involve a considerable amount of computer time, are unnecessary if the user has no interest in the forces of constraint. The user may eliminate these calculations by including this alteration in the executive control deck.
- RF12/12 This alteration function limits data recovery to those physical set degrees of freedom specified on SDISPLACEMENT, SVELOCITY, and SACCELERATION case control deck output request cards. Nonlinear loads on the specified degrees of freedom may be requested through the NLLOAD case control deck card. Substantial savings in computer time may be realized through the use of this alteration.
- RF12/15 Heretofore, SPCFORCE has been automatically calculated in rigid format 12 irrespective of the presence of an SPCFORCE request in the case control deck. These calculations, which can involve a considerable amount of computer time, are unnecessary if the user has no interest in the forces of constraint. The user may eliminate these calculations by including this alteration in the executive control deck.

APPENDIX C

ENGINE MODELING

The basic data for this modeling was taken from Reference 5b. The first two modes are modeled here.

A list correlating the NASTRAN model variables with the Allison test stations is given in Table C-1. A sketch of the bipods is given in Figure C-1, and the test-aligned coordinate systems for engine-out and engine-in airframe models are given in Figures C-2 and C-3.

The test mode shapes of Reference 5b were renormalized to test station 9 (center mount vertical) and are listed in Table C-2.

The rigid-body masses were obtained from Reference 5b, and the flexible masses were obtained from the mode shape tabulations of mobility in Reference 5b.

$$b_i = \frac{1}{\text{mobility}} \quad \text{at resonance}$$

$$m_i = \frac{b_i}{2 \zeta w_i}$$

$$m_7 = \frac{1}{0.00188} \quad \times \quad \frac{1}{2 \times 0.03} \quad \times \quad \frac{1}{(127 \times 2\pi)} = 11.1098 \frac{\text{lb-sec}^2}{\text{in.}}$$

$$m_8 = \frac{1}{0.00860} \quad \times \quad \frac{1}{2 \times 0.03} \quad \times \quad \frac{1}{(145 \times 2\pi)} = 2.12717 \frac{\text{lb-sec}^2}{\text{in.}}$$

Note that all masses in the NASTRAN listing are in weight units (pounds) because the WTMASS parameter was used, with a value of $1/g$ (seconds squared per inch). (See Table C-3.)

The engine drive shaft consists of a uniform steel tube weighing 1.13 pounds and two couplings weighing 0.46 pound each. The equations in the text describe the drive shaft mass matrix in the x direction as the sum of two submatrices:

$$\left[M_{DS} \right]_x = M_S \begin{bmatrix} \frac{1}{3} & \frac{1}{6} \\ \frac{1}{6} & \frac{1}{3} \end{bmatrix} + M_C \begin{bmatrix} 1 & 0 \\ 0 & 1 \end{bmatrix} \quad (C-1)$$

TABLE C-1. ENGINE VARIABLE LIST

External Sequence Number	Name	Direction, Allison Test	
		Engine Coordinate	Station Number
12232, 1	Center mount	T1	7
12232, 2	Center mount	T2	8
12232, 3	Center mount	T3	9
13310, 1	Right mount	T1	4
13310, 2	Right mount	T2	5
13310, 3	Right mount	T3	6
13311, 1	Left mount	T1	1
13311, 2	Left mount	T2	2
13311, 3	Left mount	T3	3
29011, 0	Drive shaft	T2	11
29012, 0	Drive shaft	T3	12
29013, 0	Turbine mid-split	T2	13
29014, 0	Turbine mid-split	T3	14
29015, 0	Forward compressor	T2	15
29016, 0	Forward compressor	T3	16
29017, 0	Ignitor	T2	17
29918, 0	Ignitor	T3	18
30000, 1	Rigid-body mode	T1	-
30000, 2	Rigid-body mode	T2	-
30000, 3	Rigid-body mode	T3	-
30000, 4	Rigid-body mode	R1	-
30000, 5	Rigid-body mode	R2	-
30000, 6	Rigid-body mode	R3	-
30007, 0	Flexible mode (127 Hz)		
30008, 0	Flexible mode (145 Hz)		

Notes:

1. Directions in coordinate system 5, engine aligned (see Figure C-3).
2. T_i is translation along the i axis, and R_i is rotation about the i axis.
3. 12232, 2 means translation at grid point 12232 in the 2 direction; 4, 5, and 6 are the rotations R_1 , R_2 , and R_3 , respectively.
4. A variable followed by a zero (i. e., 29011, 0) represents a NASTRAN scalar variable.

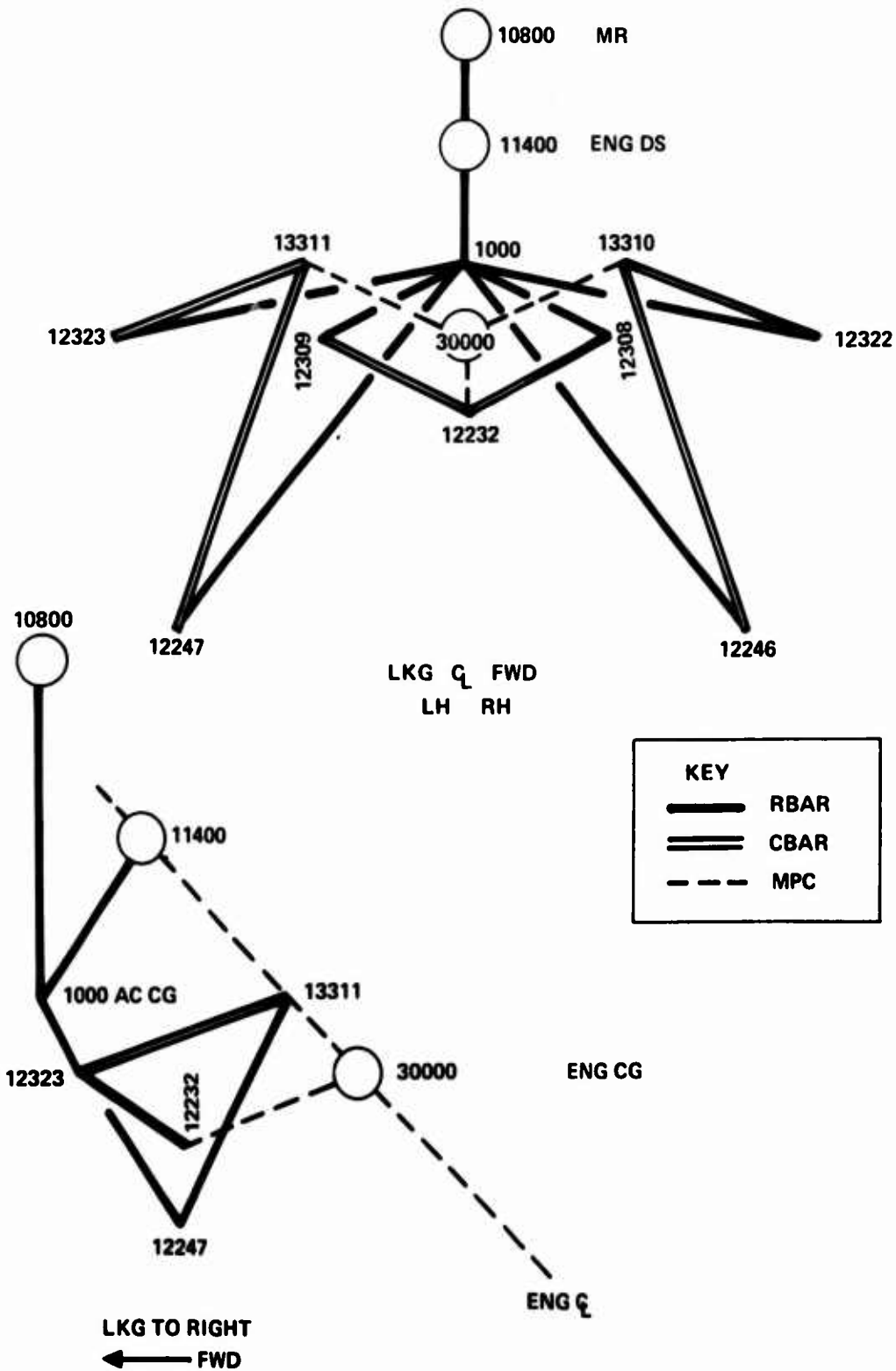
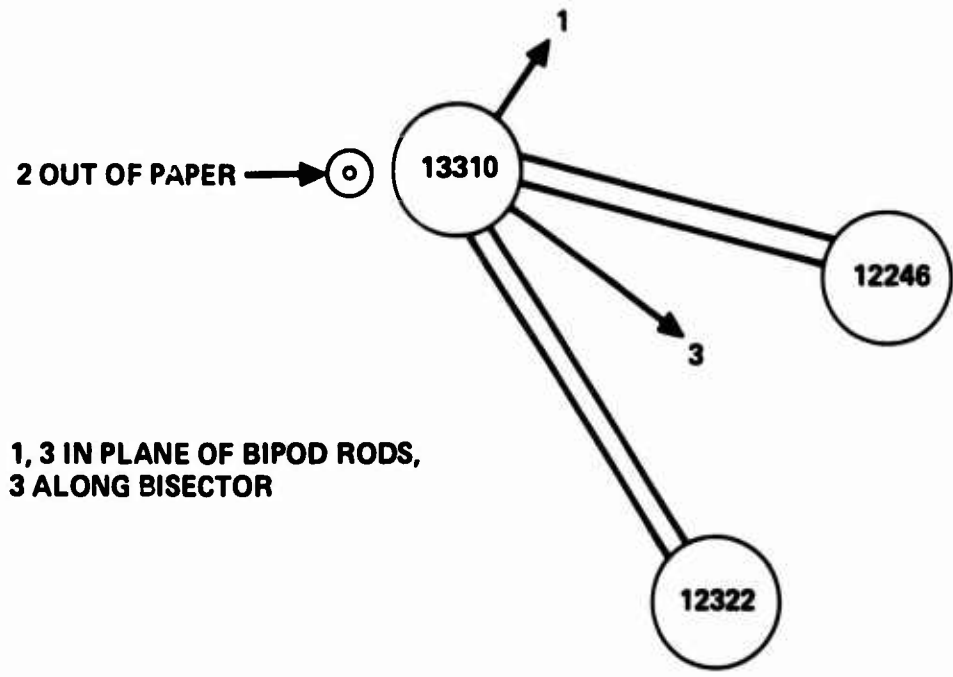
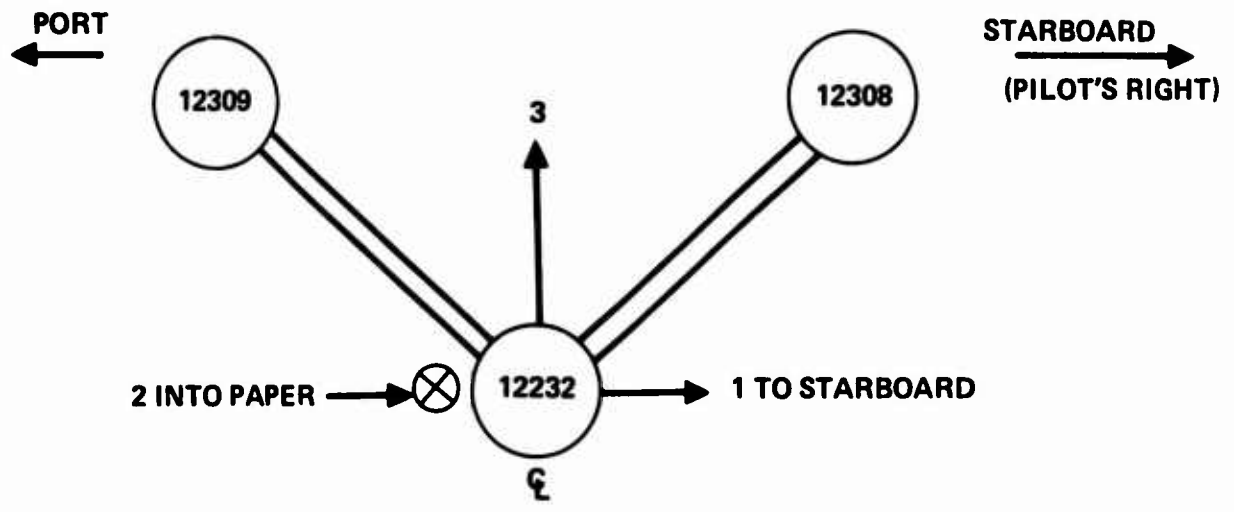


Figure C-1. Engine, Mount, and Rigid Airframe Model.

CENTER MOUNT



RH MOUNT – LH MOUNT MIRROR IMAGE ABOUT CENTER PLANE

SEE GRID CARD LIST FOR GRID POINT LOCATIONS

Figure C-2. Test Coordinate Systems - Engine Out.

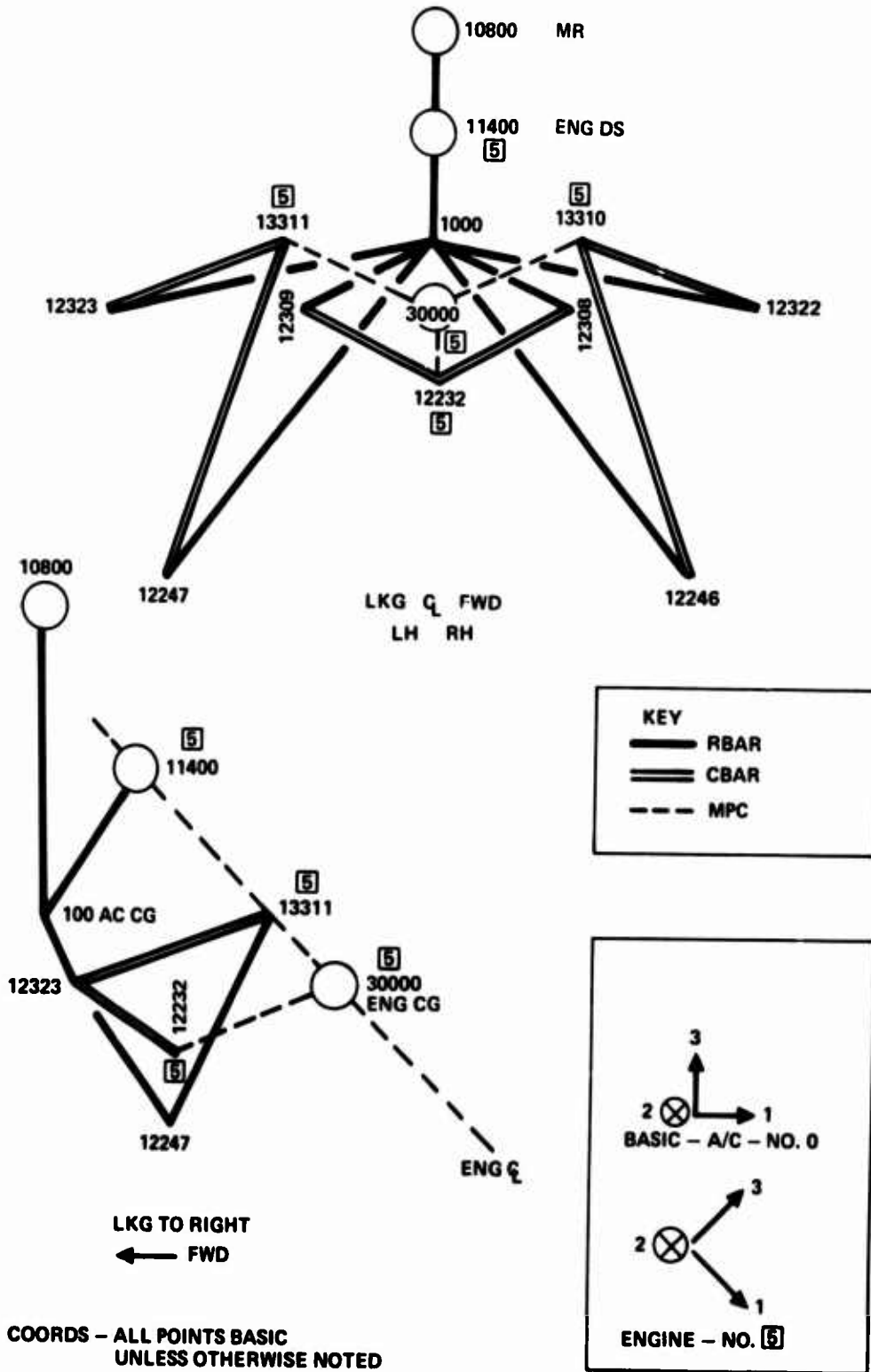


Figure C-3. Test Coordinate Systems - Engine In.

TABLE C-2. RENORMALIZED MODE SHAPES

Variable Name	Rigid T1	Rigid T2	Rigid T3	Rigid R1	Rigid R2	Rigid R3	Flexible 1	Flexible 2
Variable Number	30000, 1	30000, 2	30000, 3	30000, 4	30000, 5	30000, 6	30000, 7	30000, 8
Center mount	1.0				-10.5962			
Center mount		1.0		10.5962		-5.14105	0.037	-0.593
Center mount			1.0		5.14105		1.0	1.0
Right mount	1.0				-0.271614	-7.75		
Right mount		1.0		0.271614		-5.14105	-0.431	-0.620
Right mount			1.0	7.75	5.14105		1.20	0.376
Left mount	1.0				-0.271614	7.75		
Left mount		1.0		0.271614		-5.14105	-0.361	-0.643
Left mount			1.0	-7.75	5.14105		1.058	1.924
Drive shaft T2		1.0		4.957		-7.045	0.83	0.698
Drive shaft T3			1.0			7.045	0.745	1.232
Turbine mid-split T2		1.0		-4.418		7.56	-1.755	0.755
Turbine mid-split T3			1.0		-7.56		-5.1444	0.465
Forward compressor T2		1.0		-2.418		-15.627	-1.415	-4.893
Forward compressor T3			1.0		15.627		-9.144	-7.55
Ignitor T2		1.0		-2.418		20.628	2.011	-2.118
Ignitor T3			1.0		-20.628		10.17	-1.116

Notes: 1. T2 values were changed in sign to account for conversion between test data in the left-hand coordinates and the right-hand coordinates of the model.

2. The sign on 13311, 2 (Allison test point 2) was changed again to account for the change in orientation of the Allison transducer when changed to the opposite side.

TABLE C-3. ENGINE MODEL CHARACTERISTICS

```

$ ENGINE POINTS
ABEY1 30007 30008
ABEY1 123456 30000
$ ENGINE MODE GENERALIZED SPRINGS
CELAB2 40007 7.0741e+30007
CELAB2 80008 1.7656e+30008
$ ENG. MODE GENERALIZED MASSES
CHASS2 30007 4292.82 30007
CHASS2 30008 821.938 30008
$ DRIVE SHAFT
CHASS2 110002 -1.1883 11000 2 29011 0
CHASS2 110003 -1.1883 11000 3 29012 0
CHASS2 110012 1.025 11000 2
CHASS2 110022 1.025 29011 0
CHASS2 110013 1.025 11000 3
CHASS2 110023 1.025 29012 0
$ CHANGE MASS CHANGES
/
CONM2 727 720
CONM2 15 10100 3.0
/
CONM2 730 710
CONM2 20 10100 10.7
CONM2 21 10100 10.7
$ ENGINE MASS
CONM2 30000 30000 4 138.2
$ CHENG
$ CHENG 14000.
EIGN 3 GIV 703H. 1.0A $FIGH3
$ EIGN3 MAX
$ CHANGE TO ENGINE AXIS
/
2153
/
2190 2190
GRID 12232 127.05 0.0 27.04 5
GRID 13310 130.61 07.75 30.07 5
GRID 13311 130.61 -07.75 30.07 5
$ BASIC POINTS FOR FORCES
GRID 13312 130.61 07.75 30.07 0
GRID 13313 130.61 -07.75 30.07 0
$ ENGINE P.C.
GRID 10000 130.3 0.0 31.28 5
$ ENGINE MODE SHAPES
MPC 1000 12232 1 -1.0 30000 1 1.0 $MP1
$MP1 30000 5 -10.5962
MPC 1000 12232 2 -1.0 30000 2 1.0 $MP2
$MP2 30000 0 +10.5962 30000 0 +5.14105 $MP2A
$MP2A 30007 0 -0.37 30000 0 -5.501
MPC 1000 12232 3 -1.0 30000 3 1.0 $MP3
$MP3 30000 5 +5.14105 30000 0 0.0 $MP3A
$MP3A 30007 0 1.0 30000 0 1.0
MPC 1000 13310 1 -1.0 30000 1 1.0 $MP4
$MP4 30000 5 -0.271018 30000 0 -07.75
MPC 1000 13310 2 -1.0 30000 2 1.0 $MP5
$MP5 30000 0 +0.271018 30000 0 +5.14105 $MP5A
$MP5A 30007 0 -0.331 30000 0 -0.620
MPC 1000 13310 3 -1.0 30000 3 1.0 $MP6
$MP6 30000 0 +07.75 30000 5 +5.14105 $MP6A
$MP6A 30007 0 1.20 30000 0 1.76
MPC 1000 13311 1 -1.0 30000 1 1.0 $MP7
$MP7 30000 5 -0.271018 30000 0 +07.75
MPC 1000 13311 2 -1.0 30000 2 1.0 $MP8
$MP8 30000 0 +0.271018 30000 0 +5.14105 $MP8A
$MP8A 30007 0 -0.301 30000 0 -0.604
MPC 1000 13311 3 -1.0 30000 3 1.0 $MP9
$MP9 30000 0 +07.75 30000 5 +5.14105 $MP9A
$MP9A 30007 0 1.050 30000 0 1.924
MPC 1000 29011 0 -1.0 30000 0 -07.045 $MP16
$MP16 30007 0 0.03 30000 0 0.608 $MP17
$MP17 30000 2 1.0 30000 0 0.957
MPC 1000 29012 0 -1.0 30000 0 0.045 $MP18
$MP18 30007 0 0.705 30000 0 1.232 $MP19
$MP19 30000 3 1.0
MPC 1000 29013 0 -1.0 30000 0 0.756 $MP20
$MP20 30007 0 -1.755 30000 0 0.755 $MP21
$MP21 30000 2 1.0 30000 0 -0.418
MPC 1000 29014 0 -1.0 30000 5 -07.56 $MP22
$MP22 30007 0 -5.1444 30000 0 0.405 $MP23
$MP23 30000 3 1.0
MPC 1000 29015 0 -1.0 30000 0 -15.627 $MP24
$MP24 30007 0 -1.415 30000 0 -0.003 $MP25
$MP25 30000 2 1.0 30000 0 -0.410
MPC 1000 29016 0 -1.0 30000 5 15.627 $MP26
$MP26 30007 0 -0.144 30000 0 -07.55 $MP27
$MP27 30000 3 1.0
MPC 1000 29017 0 -1.0 30000 0 20.628 $MP28
$MP28 30007 0 2.011 30000 0 -02.118 $MP29
$MP29 30000 2 1.0 30000 0 -02.410
MPC 1000 29018 0 -1.00 30000 5 -20.629 $MP30
$MP30 30007 0 10.17 30000 0 -1.116 $MP31
$MP31 30000 3 1.0
MPCADD 2 1 1000
$ COUPLE ENGINE-BASIC AXES
RBAR 1300 13310 13312 123050
RBAR 1301 13311 13313 123050
$ ENGINE FREE POINTS
$ POINT 29011 THRU 29018
$ MODAL DISPLACEMENTS
$ POINT 30007 30008
ENDDATA
    
```

where M_S is the shaft mass and M_C the coupling mass. There is a similar equation for mass in the y direction.

These values are input via the CMASS2 bulk data card, which has the format

$$[M] = M \begin{bmatrix} 1 & -1 \\ -1 & 1 \end{bmatrix} \quad (C-2)$$

if two variables are listed on the card, or only one term on the diagonal if one variable is listed on the card. The drive shaft mass terms are then input as

$$[M_{DS}] = M_1 \begin{bmatrix} 1 & -1 \\ -1 & 1 \end{bmatrix} + M_2 \begin{bmatrix} 1 & 0 \\ 0 & 0 \end{bmatrix} + M_3 \begin{bmatrix} 0 & 0 \\ 0 & 1 \end{bmatrix} \quad (C-3)$$

where

$$M_1 = -\frac{M_S}{6}$$

$$M_2 = M_3 = M_C + \frac{3}{6} M_S$$

and each product on the right-hand side represents one CMASS2 element. See elements 14002 through 14023 in Table C-3.

$$M_S = 1.13$$

$$M_C = 0.46$$

$$M_1 = \frac{-1.13}{6}$$

$$M_2, M_3 = 0.46 + \frac{1.13}{2}$$

INPUT OF ROTOR 4/REV FORCES

The rotor force data was available in the format:

$$F_{\text{longitudinal}} = 61 \sin(4\psi + 106^\circ), \text{ lb}$$

$$F_{\text{lateral}} = 66 \sin(4\psi + 330^\circ), \text{ lb}$$

$$F_{\text{vertical}} = 69 \sin(4\psi + 231^\circ), \text{ lb}$$

where ψ is measured from a point over the tail in an advancing direction.

NASTRAN allows input of frequency response forces in the format

$$p(f) = A \times [C(f) + iD(f)] e^{i\theta + 2\pi f\tau} \quad (C-4)$$

(Reference 12, p 214-245). There are many ways to implement this equation.

The NASTRAN cards for input of this forcing function are shown in the attached listing. For the case above (subcase 1), for $F_{\text{longitudinal}}$ for example,

$$\begin{aligned} D(f) &= 0.0 \\ \tau &= 0.0 \\ A &= 61.0 \quad (\text{DLOAD card}) \\ C(f) &= 1.0 \quad (\text{TABLED1 card}) \\ \theta &= 106^\circ \quad (\text{DPHASE card}) \end{aligned}$$

The longitudinal and lateral components can be shown to result from a 3ψ force in the rotating system, which becomes an advancing 4ψ force in the fixed system, and a 5ψ force in the rotating system, which becomes a regressing 4ψ force in the fixed system. (See Figure C-4.)

The known fixed system forces, measured at the 0- and 90-degree azimuths, can then be equated to these rotating vectors to find their coefficients.

Given:

$$X_{\text{fixed}} = X_0 \sin(4\psi + \phi_x)$$

$$Y_{\text{fixed}} = Y_0 \sin(4\psi + \phi_y)$$

with X_0 , Y_0 , ϕ_x , ϕ_y known

$$X_{\text{fixed}} = A_3 \cos(4\psi + \phi_3) + A_5 \cos(-4\psi + \phi_5)$$

$$Y_{\text{fixed}} = A_3 \sin(4\psi + \phi_3) + A_5 \sin(-4\psi + \phi_5)$$

Find

A_3 , A_5 - Magnitude of rotating vectors

ϕ_3 , ϕ_5 - Azimuth of rotating vectors at $\psi = 0$

VERTICAL FORCE = 69 LB AT PHASE OF 231°

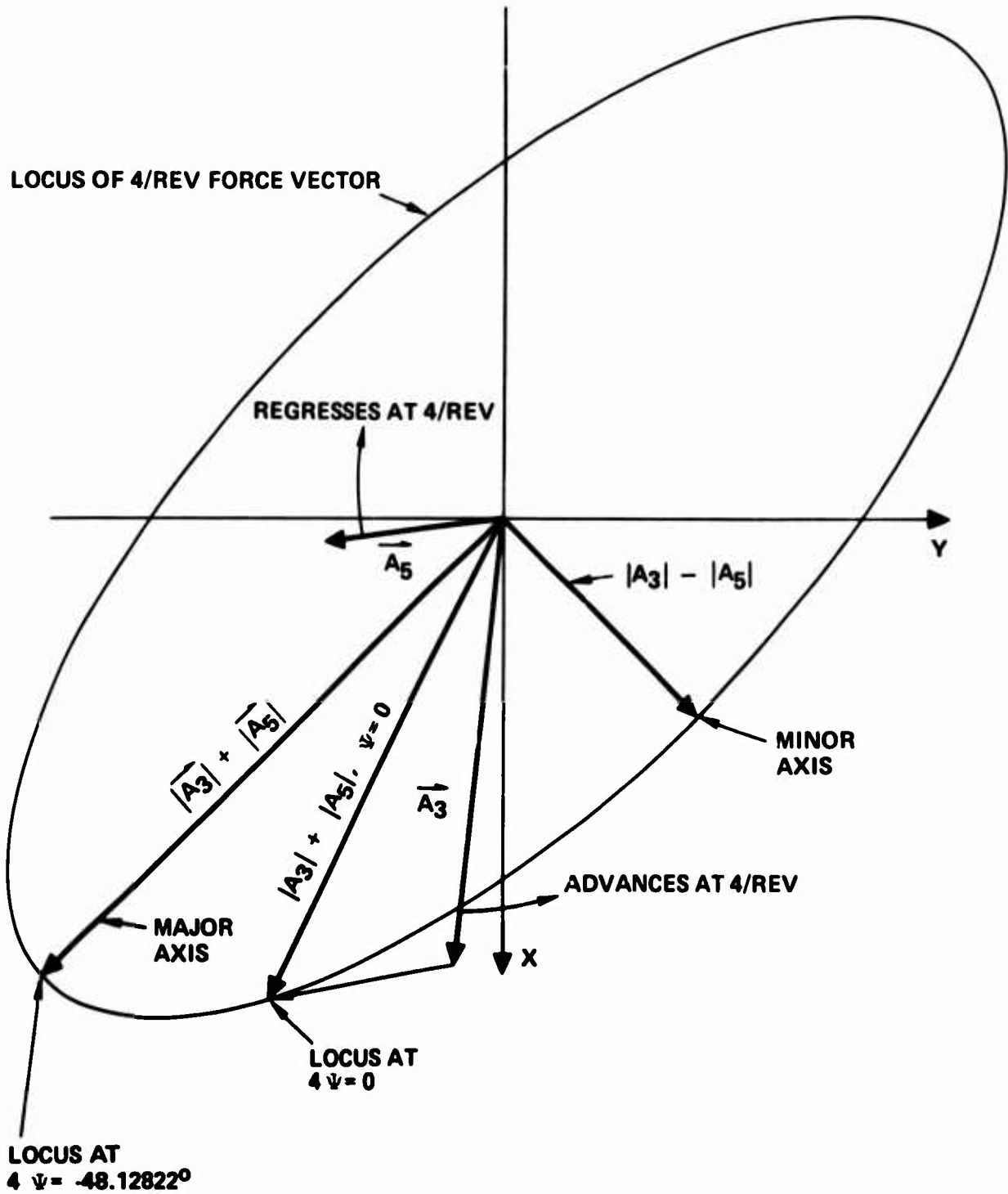


Figure C-4. Most Likely 4/Rev Rotor Force Configuration.

After performing the indicated algebra, the resulting components are as follows:

$$A_3 = 58.4602 \text{ lb}$$

$$A_5 = 24.9179 \text{ lb}$$

$$\phi_3 = -7.95742 \text{ deg}$$

$$\phi_5 = -88.2990 \text{ deg}$$

$$\text{Semimajor axis} = 83.3781 \text{ lb}$$

$$\text{Semiminor axis} = 33.5423 \text{ lb}$$

LIST OF SYMBOLS

- A_3, A_5 = magnitude of rotating 3/rev and 5/rev horizontal force vectors, lb
- b_i = damping coefficient, lb-sec/in.
- F_1, F_2 = transverse inertia force at engine end and transmission end of engine drive shaft, lb
- f_{ck} = force on the cth mode acting at the kth station
- F_x, F_y = calculated rotor head shear in longitudinal and lateral directions, lb
- I_{pi} = polar moment of inertia of components on shaft i, in. -lb/sec²
- K = spring constant, lb/in.
- K_1 = modal spring constant for mode 1, lb/in.
- k_i = modal spring constant for ith mode
- M = mass, lb-sec²/in.
- M_1 = modal mass for mode 1, lb-sec²/in.
- M_x, M_y = calculated rotor head moments in roll and pitch directions, in. -lb
- M = mobility, in./sec-lb, in./sec-in. -lb
- m_c = mass of drive shaft coupling, lb-sec²/in.
- m_s = mass of drive shaft, lb-sec²/in.
- m_7, m_8 = engine modal mass at 127 and 145 Hz, respectively, lb-sec²/in.
- p = differential operator
- u_c = displacement variable at interface between components

- u_i = vector of ζ_i variables
- u_{cj} = displacement at the cth station due to the jth mode
- V = velocity, in./sec
- V_{cj} = velocity component at the jth station due to the cth mode
- x_0 = magnitude of x-vector in fixed system, lb
- χ_1, χ_2 = motion of engine end and transmission end of engine drive shaft, in.
- y_0 = magnitude of y-vector in fixed system, lb
- ζ_i = modal damping factor
- $\dot{\theta}_{pitch}$ = rigid-body angular motion of engine rotor, rad/sec
- ξ_i = modal displacement variable
- ϕ_{ci} = mode shape at the cth station in the ith mode
- ϕ_3, ϕ_5 = azimuth of rotating vector at $t = 0$
- ψ = rotor azimuth angle, deg
- Ω_i = angular velocity of ith shaft, rad/sec
- ω = natural frequency, rad/sec
- ω_1 = natural frequency for mode 1, rad/sec